UNIVERSITAT DE BARCELONA

Caenorhabditis elegans as animal model to investigate the cellular mechanisms of resistance for the chemotherapeutic agent cisplatin

Francisco J. García Rodríguez

Caenorhabditis elegans as animal model to investigate the cellular mechanisms of resistance for the chemotherapeutic agent cisplatin

Memòria presentada per
FRANCISCO JAVIER GARCÍA RODRÍGUEZ
per optar al grau de
Doctor per la **Universitat de Barcelona**

Tesi adscrita al Departament de Genètica Molecular
Programa de doctorat en Genètica
Facultat de Biologia, Universitat de Barcelona

Treball realitzat a l'Institut d'investigació Biomèdica de Bellvitge (IDIBELL), Laboratori de Recerca Translacional
Barcelona 2016

Alberto Villanueva Garatachea
Director de tesi

Julián Cerón Madrigal
Co-director de tesi

Bru Cormand Rifà
Tutor

Francisco J. García Rodríguez
Doctorand

Acknowledgements

Resulta muy difícil tratar de resumir en unas pocas líneas todo lo que me gustaría agradecer a tanta gente durante los cinco años que ha durado este período, el cual considero, sin ninguna duda como el más importante de mi vida. Durante este tiempo, he madurado personal (un poco sólo) y científicamente (de esto algo más), pero si considero esta etapa como la mejor de mi vida es sobre todo por la gente que he conocido y me ha acompañado, dentro y fuera del laboratorio, durante todo este tiempo.

En primer lugar me gustaría dar las gracias a las dos personas que han hecho este proyecto posible. Dos grandes “coaches” que confiaron en mí para dar el salto desde la regional andaluza a toda una primera división. Dos maneras de entrenar y de entender la ciencia que me han permitido aprender el doble. Al primero de ellos, Julián, le tengo agradecer muchas cosas, dentro y fuera del lab. Científicamente hablando gracias por tu interés, paciencia (mucha) y tiempo gastado en mí durante toda la tesis, aunque especialmente estos últimos meses de escritura. Siempre te has preocupado por nuestro aprendizaje, sacando dinero de debajo de las piedras para que participáramos en congresos, y eso es de agradecer. Y fuera del lab, siempre te has preocupado por cómo me marchaban las cosas, me has escuchado y ayudado cuando ha sido posible. Por eso, más que un jefe, te considero un amigo. Ha sido toda una suerte haber podido hacer la tesis contigo, eres un míster de los que dejan huella, como Bielsa. En segundo lugar, y no menos importante, le estoy enormemente agradecido a la otra cabeza visible de este proyecto, Alberto, un míster con unos métodos de entrenamiento radicalmente diferentes, pero también efectivos. Gracias tu interés y dedicación durante este tiempo, a pesar de llevar dos millones de cosas para adelante como llevas, siempre has tenido

tiempo para mí. Gracias también por tu búsqueda incansable de financiación y sobre todo por tu preocupación y apoyo cuando las cosas no me han ido bien.

También me gustaría dar las gracias a los compañeros de equipo, pasados y presentes por el trato recibido en los vestuarios en estos cinco años que han dado para mucho. Junto a las grandes jugadoras locales que el equipo siempre ha presentado, el JC lab (a.k.a Rayo Vallecano), gracias a la gran labor de "international scouting" de la secretaría técnica, incorporó también a grandes promesas foráneas que pronto demostraron su valía dentro y fuera de los terrenos de juego, como quedó demostrado en congresos, tesis y artículos...pero también en calçotadas, en el bando de las huertas de Murcia o en los innumerables bares que frecuentaron juntos. Gracias por todo esto así como por vuestro apoyo en los momentos de fritura científica. También quiero dar las gracias a las cuatro integrantes de mi otro equipo, el AV team por todos los momentos que hemos compartido juntos así como su alegría y ayuda. Sé que me perdonáis mis misteriosas desapariciones cuando me tocaba a mí ir a por los tumores a anatomía patológica.

Gracias también a todo el LRT1 y en general, a toda la gente que he conocido en el hospital por todo este tiempo pasado juntos. Trabajas con otra alegría si estas rodeado de amigos y de buena gente. Con ellos he vivido innumerables viajes, algunos muy absurdos, como cuando fuimos a ver el Ecce homo de Borja o a Palamós, para ver un Llagostera-Betis bajo un diluvio increíble. Con ellos he pasado también muchas horas en la Flama, Salamandras, fiestas de Sants, barbacoas en áticos, cenas de rabos, rutas de bares o por supuesto, en el mítico oliverar. No sé como ha

pasado, pero parece imposible que haya coincidido tanta buena gente en el mismo sitio al mismo tiempo. Es como si el Betis fichara a Romario, Ronaldinho, Maradona, Mágico González, Higuita y Prosinecky al mismo tiempo. Muchas gracias a todos. No puedo irme sin declarar mi amor incondicional a la Comunidad de la Amistad y al Camallo Vallecano.

También me gustaría dar las gracias al resto de personas que han contribuido en el proyecto de una u otra forma. Thanks to Mike Boxem's group, especially to him for everything that I learned in that lovely six-month period I spent in Utrecht, así como a Antonio por toda su predisposición y aporte en el tema de las tioredoxinas.

Gracias también a toda esa gente que ha estado a mi lado durante la tesis, familias (la sevillana y la catalana) y amigos de siempre que con sus visitas han hecho que vivir fuera de tu casa sea algo más sencillo.

Y para el final dejo a las personas más importantes, a las que les debo mucho y me gustaría dedicar este trabajo. Gracias Marta por tu apoyo y cariño durante todo este tiempo y también por tu paciencia en estos últimos meses. Ah y por la portada! Toca poner fin a un periodo de cinco años, abrir nuevos caminos y alcanzar nuevas metas, y lo que más me gusta es que seguiré haciéndolo a tu lado…empezando por Asia. Y por supuesto muchísimas gracias a mis padres, mi hermano y mi tía. Muchísimas gracias por todo lo que me habéis dado y por no cuestionar el tipo de vida que he querido llevar, aunque os cueste alguna preocupación que otra. Aunque es duro tener a la familia lejos, sobre todo en los momentos más difíciles que hemos pasado estos años, como cuando, que

paradoja, el cisplatino también empiezan a tomarlo en tu familia, siempre os he sentido cerca. Espero que algún día estéis tan orgullosos de mí como yo lo estoy de vosotros. ¡Se os quiere a todos!

Index

List of tables

List of figures

Introduction

I.1. Cisplatin in the treatment of cancer

Cancer is a leading cause of disease and mortality worldwide. In 2012, about 14.1 million new cases produced 8.2 million of deaths (Ferlay J. 2013). Despite of the complexity and variety of tumors, as usual, the standard clinical procedure to treat cancer commonly includes a combination of three different clinical practices: (I) surgical removal of solid tumors and adjacent tissues, (II) radiation therapies and (III) chemotherapeutic treatments.

Since the FDA (Food and Drugs Administration) approved the use of cisplatin as chemotherapeutic agent in 1978, this agent was one of the most widely prescribed drug and an effective treatment for many cancer types. As example, testicular cancer was previously fatal but treatment with cisplatin provided cure for 96% of the patients (Jemal et al. 2008; Maluccio et al. 2007). Currently, cisplatin, and other platinum-based compounds such as oxaliplatin or carboplatin are still front-line clinical therapies. In fact, approximately half of all patients undergoing chemotherapeutic treatment receive a platinum-based drug (Galanski 2006). Particularly, cisplatin exert clinical activity against a wide spectrum of solid neoplasms, including testicular, bladder, ovarian, head and neck, breast, lung or brain cancers (Dasari & Bernard Tchounwou 2014).

I.2. Mode of action and side effects of cisplatin

Cisplatin, also called cisplatinum, cis-diamminedichloroplatinum(II) or CDDP is a square planar platinum-based molecule. Chemically is composed by a double charged platinum ion surrounded by four ligands: forming a strong interaction with two amines on a side and leaving groups with two chlorides on the other side which allows to the platinum ion to bind its targets (Goodsell 2006) (Figure 1A).

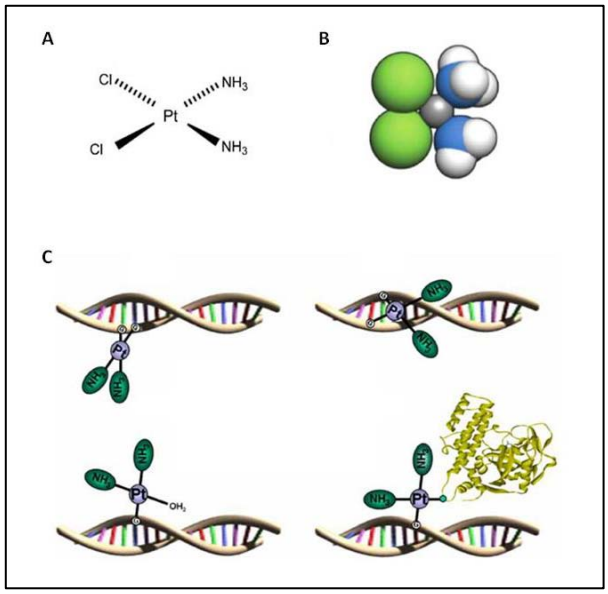

Figure 1. Chemical structure and DNA binding of cisplatin.
(A) Cisplatin is composed by a central atom of platinum surrounded by two chlorides (Cl) and two amines (NH3). (B) Computational molecular structure of cisplatin. Color code: Grey (Pt), green (Cl), blue (N) and white (H) (Modified from Dasari & Bernard Tchounwou, 2014). (C) Main adducts formed by cisplatin-DNA binding: intrastrand crosslink (upper left), interstrand crosslink (upper right), monoadduct (lower left) and protein-DNA crosslink (lower right) (Extracted from Cepeda et al., 2007).

In the cytoplasm, cisplatin chloride groups are replaced by water molecules. This hydrolyzed product is a potent electrophile that can react with any nucleophile, including the sulfhydryl groups on proteins and nitrogen donor atoms on nucleic acids (Kelland 2007). In the nucleus, cisplatin primarily binds to DNA at the nitrogen 7 reactive center on purine residues promoting DNA-DNA adducts (intra- and interstrand crosslinks) but also DNA-protein adducts (Figure 1C) This adduct-induced DNA damage hinders both transcription and replication, blocks cell division, to finally provoke apoptotic cell death (Kelland 2007).

Although DNA-damage induced apoptosis is considered the first cause of cell death produced by cisplatin, only a 5-10% of intracellular cisplatin interacts with DNA while the rest binds to other nucleophilic sites at RNA, proteins, membrane phospholipids or thiol-containing molecules like glutathione (Cepeda et al. 2007). These unspecific interactions increase the levels of reactive oxygen species (ROS) and consequently, alter the oxidative stress state of cells. Accordingly, cisplatin-induced oxidative stress is also capable to trigger apoptosis or necrosis independently of DNA damage (Wang & Lippard 2005) (Mandic et al. 2003), being one of the most important cytotoxic effects of cisplatin (Figure 2).

Due to this unspecific mode of action, cisplatin hits non-tumor cells also. Among cisplatin secondary-effects have been reported nephrotoxicity (de Jongh et al. 2003), hepatotoxicity (Al-Majed 2007), cardiotoxicity, neurotoxicity or ototoxicity (Hartmann & Lipp 2003). Still, the major obstacle in the clinical use of cisplatin as anticancer drug is the chemoresistance developed by tumors rather than its toxicity in normal cells.

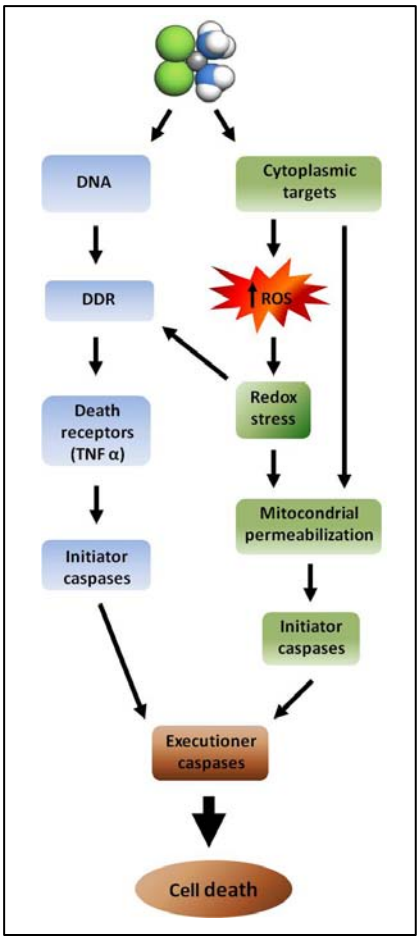

Figure 2. Simplified mode of action of cisplatin.
Once inside the cell, activated cisplatin can bind a plethora of nucleophilic molecules both in nucleus and cytoplasm. In the nucleus, cisplatin produces DNA adducts. Exceeded DNA insults triggers the activation of a DNA damage response (DDR) that frequently involves the ATR kinase and P53. As consequence, P53 transactivates several genes whose products facilitate mitochondrial outer membrane permeabilization, thereby triggering apoptosis. As well as genes that encode for components of the TNFα-dependent apoptotic pathway. Mitochodrial permeabilization sets off the caspase cascade that eventually turns out in cell death. In the cytoplasm, the interaction between cisplatin and glutathione or metallothioneins results in the depletion of reducing equivalents and/or directly sustains the generation of reactive oxygen species (ROS). ROS can directly trigger apoptosis or exacerbate cisplatin-induced DNA damage, thereby playing a dual role in cisplatin cytotoxicity (Modified from Galluzzi et al., 2012).

I.3. Molecular mechanisms of cisplatin resistance

Despite its effectiveness, many patients are intrinsically resistant to cisplatin-based therapies (Beyer et al. 1996). Moreover, an important fraction of tumors eventually develop chemoresistance (Ozols 1991; Giaccone 2000; Köberle et al. 2010).

Cisplatin resistance acquisition is multifactorial. The mechanisms of tumor cells becoming resistant to the action of cisplatin have been classified in three types: (i) Pre-target mechanisms: reducing intracellular accumulation of cisplatin or increasing cisplatin sequestration by nucleophilic scavengers like glutathione (GSH) or metallothioneins; (ii) On-target mechanisms: acquiring the ability to repair adducts or becoming tolerant to unrepaired DNA lesions; and (iii) Post-target mechanisms: hampering the execution of apoptosis in response to DNA damage (Dasari 2014) (Figure 3).

I.3.1. Pre-target mechanisms

Reduced intracellular accumulation and inactivation of cisplatin are two frequent strategies to develop resistance to this drug. A reduced accumulation of cisplatin has been reported in many different cell lines resistant to cisplatin (Kelland 1993). Thus, inactivation of copper transporters (CTRs) limits cisplatin uptake and leads to develop resistance *in vitro* and *in vivo* (Ishida et al. 2010). In parallel, the overexpression of cisplatin cellular-efflux transporters ATP7A/ ATP7B and MRP2 contributes to resistance. Therefore, the expression levels of these

transporters might predict the responsiveness of tumors to cisplatin-based therapies (Aida et al. 2005; Yamasaki et al. 2011).

In the cytoplasm, nucleophilic 'scavengers' such as glutathione (GSH), methionine, metallothioneins and other cysteine-rich proteins are capable to bind activated cisplatin limiting the amount of reactive cisplatin and facilitating its removal. In addition, redox systems such as GSH-dependent redox pathways tend to balance the oxidative stress induced by cisplatin. Accordingly, high levels of GSH, or GSH-related enzymes such as γ-glutamylcysteine synthetase (GCS) and glutathione S-transferases (GSTs) have been observed in the context of cisplatin resistance, both *in vitro* and *ex vivo* (Chen & Kuo 2010; Peng, Xu & Elias S. J. Arnér 2012).

I.3.2. On-target mechanisms

Inter- and intrastrand DNA adduct recognition and the consequent generation of an apoptotic signal is often impaired in cisplatin-resistant cancer cells because of diverse reasons. Thus, a downregulation in Mismatch Repair (MMR) complexes, implicated in cisplatin-induced DNA adduct recognition and apoptosis activation has been related to cisplatin resistance (Shachar et al. 2009). Moreover, cisplatin resistant cells achieve the ability to repair adducts and tolerate unrepaired DNA lesions. Therefore, upregulation of Nucleotide Excision Repair (NER) related components, or the activation of Translesion Synthesis Polymerases (TLS) are recurrent (Olaussen 2009; Kamal et al. 2010).

I.3.3. Post-target mechanisms

Post-target resistance to cisplatin arises from defects in the signal transduction pathways that triggers apoptosis after DNA damage and also from defective cell death executioner machinery (Galluzzi et al. 2012). One of the most predominant mechanisms associated to post-target resistance implicates the inactivation of TP53 (Vousden & Lane 2007), which occurs in approximately half of all human neoplasms (Kirsch & Kastan 1998). In addition, the inhibition of other pro-apoptotic signaling genes, like several MAPK members, might contribute to the cisplatin-resistant phenotype (Brozovic et al. 2004). Moreover, between the factors that regulate and execute apoptosis a huge variety of them have the potential role of modulating the response to cisplatin (BAX-like, BCL-2-like, caspases) being several of them capable to predict cisplatin responsiveness as well (Tajeddine et al. 2008; Jain & Meyer-Hermann 2011).

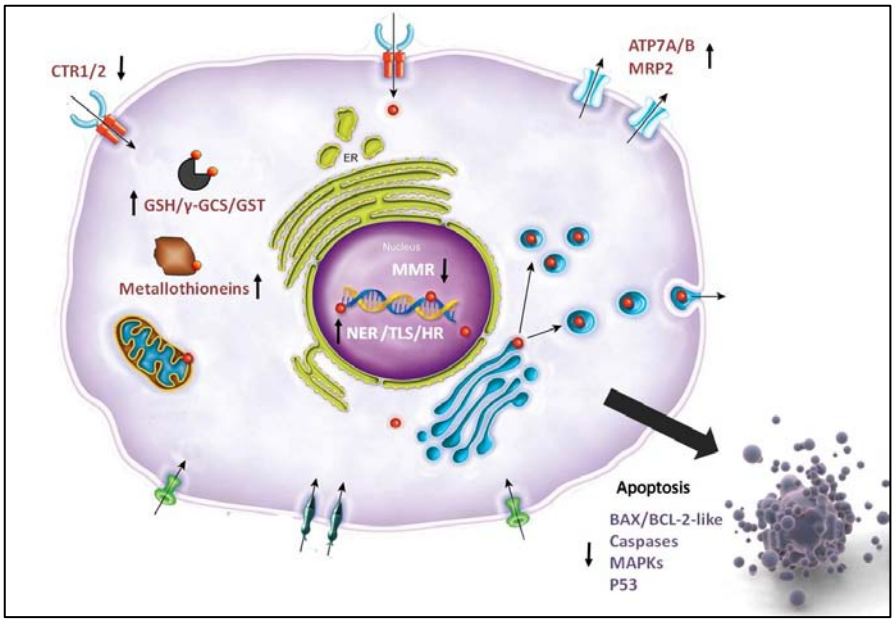

Figure 3. Cellular mechanisms involved in cisplatin resistance acquisition. Pre-target mechanisms (represented in red) include influx (CTRs) and efflux (ATP7A/B and MRP2) cisplatin transporters, action to glutathione (GSH) metabolism (γGCS and GST enzymes) and metallothioneins. On-targets mechanisms (white) have effects in nucleotide excision repair (NER) machinery, translesion synthesis (TLS), homologous recombination (HR) or mismatch repair (MMR). Post-target mechanisms (purple) consist in inhibiting apoptosis. Arrows indicate the activity, high or low, of distinct mechanisms in a cisplatin resistant cell.

I.4. *C. elegans* as a model to study cancer-chemotherapy response

The nematode *Caenorhabditis elegans* was proposed as model organism in the seventies by Sydney Brenner, who published a seminal paper about the genetics of *C. elegans* (Brenner 1974) presenting a simple model to unravel the genetic basis of the development of metazoan systems.

In the last three decades, the use of *C. elegans* as model organism has grown exponentially. This worm was the first fully sequenced animal (Anon 1998). The worm anatomy is known in detail and its cell lineage is invariant (Sulston & Horvitz 1977). In addition, an extensive knowledge exists about its behavior, development or its cellular and molecular biology (Girard et al. 2007). Moreover, *C. elegans* field rapidly benefited from the combination of powerful genetics and modern functional genomics approaches to study gene function like RNAi gene mediated interference or the yeast two-hybrid system (Kamath & Ahringer 2003; Vidalain et al. 2004).

In addition, the computational tools and the rise to high throughput studies in *C. elegans* fueled up the appearance of open-access databases as (I) Wormbase (www.wormbase.org), which is used as a repository of genomic information and curation, providing data regarding the biology of worms including genomes, gene models, allelic variations, mutant phenotypes or expression patterns, or (II) Wormbook (www.wormbook.org), a collection of original peer-reviewed chapters covering topics related to the biology of *C. elegans.*

The possibilities in *C. elegans* to perform a wide variety of genetic analysis linked to the knowledge of its invariant development have proven valuable in many research disciplines. Accordingly, many essential human genes and pathways are highly conserved between humans and worms making possible to model *C. elegans* to get insights in molecular and cellular basis of human diseases in worms. For example, the characterization of genes controlling programmed cell death in *C. elegans* supposed a landmark in medicine, making possible to identify related genes with similar functions in humans (Yuan et al. 1993) opening new challenges in cancer research.

In cancer-chemotherapy research, worms provide an excellent platform to study the effect of many different antitumor agents, as revealed studies on the mechanism of action of different chemotherapeutics such as 5-fluorouracyl (5-FU), farnesyltransferase inhibitors or cisplatin (S. Kim et al. 2008; Lackner et al. 2005; Kratz et al. 2010). Focusing on cisplatin, as we summarized in Table 1, previous studies revealed the capacity of *C. elegans* research to respond to cisplatin. Thus, new cisplatin-induced DNA-damage response pathways involved in DNA inter-strand crosslinks repair (van Haaften et al. 2006) or the role of endoplasmic reticulum stress in altering the response to cisplatin (Hemmingsson et al. 2010; Natarajan et al. 2013) have been uncovered using worms. However, still there are not comprehensive studies in *C. elegans* describing the global response of the animal to cisplatin.

Gene(s)	Function	Consequences of inactivation	Reference
fcd-2	**NER**	**Sensitivity (to cisplatin)**	(Collis et al. 2006)
rpa-2	**DSB**	**Sensitivity**	(van Haaften et al. 2006)
mus-101	**DSB**		
drh-3	**DSB**		
emb-4	**DSB**		
rad-51	**DSB**		
pqn-85	**Chromatin cohesion**		
npp-15	**RNA trafficking**		
nola-3	**RNA processing**		
F32D1.5	**Signaling**		
helq-1	**ICL**	**Sensitivity**	(Muzzini et al. 2008)
polq-1	**ICL**		
lem-3	**DDR**	**Sensitivity**	(Dittrich et al. 2012)
polh-1	**TLS**	**Sensitivity**	(Roerink et al. 2012)
asna-1	**ER stress**	**Sensitivity**	(Hemmingsson et al. 2010)
enpl-1	**ER stress**	**Sensitivity**	(Natarajan et al. 2013)
xpf-1	**NER**	**Sensitivity**	(Meier et al. 2014)
parp-1	**DSB**	**Sensitivity**	(Crone et al. 2015)

Table 1. Previous studies on cisplatin in *C. elegans*.
Abbreviations: NER: Nucleotide Excision Repair, DSB: Double Strand Break, ICL: Interstrand crosslink, DDR: DNA Damage Response, TLS: Translesion Synthesis, ER: endoplasmic reticulum**.**

I.4.1. *C. elegans* biology

C. elegans is an ubiquitous small nematode of about 1mm. As free-living organism is frequently found in soil, feeding on different bacteria present in decomposing plant material (Frézal & Félix 2015). In laboratory, *C. elegans* is commonly maintained, between 15ºC and 25ºC, on agar plates seeded with *E. coli* as source of food. Among the most relevant biological features that make these worms a powerful tool for biomedical research and drug discovering are:

- A short life cycle

After hatching, *C. elegans* development consists in four main larval stages (L1 to L4) before reaching the adult stage (Figure 4). This life cycle is temperature dependent and can be completed in three days at 20°C. After a reproductive period of about three days at 20ºC, wild type worms can live up to 20-25 days at that temperature.

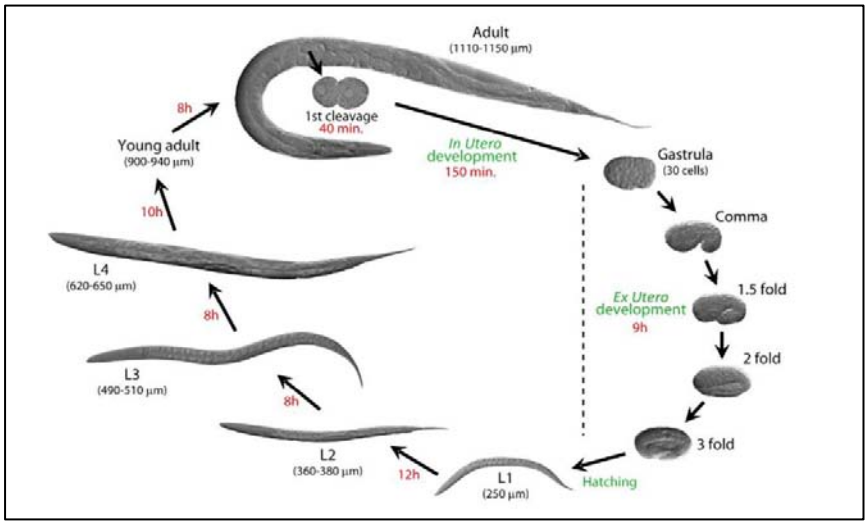

Figure 4. *C. elegans* life cycle and development.
Simplification of an unperturbed worm life cycle at 22°C. Numbers in red indicate the approximate length of time spent by the animals at each specific stage (modified from Altum and Hall 2009).

- Easy maintenance

C. elegans strains are cheap to culture and maintain. Moreover, stocks can be kept at -80ºC for long-term storage. The Caenorhabditis Genetics

Center (CGC) keeps and distributes a collection of published mutants and transgenic strains.

- A dual mode of reproduction

C. elegans is a two-sexed diploid animal with hermaphrodites (XX) and males (X0). Under normal growth conditions, hermaphrodites are the most frequent sex. They produce both sperm and oocytes and are self-fertilized allowing easily isolating and maintaining genomic modifications through generations.

However, males appear spontaneously in hermaphrodite populations but at very low frequency rates (0.1%). They only produce sperm and mate with hermaphrodites promoting cross-fertilization and refreshing genomes in worm populations. The cross-fertilization allows to design strategies to generate new strains combining genetic modifications, for instance to uncover meaningful genetic interactions.

- An invariant cell lineage

The development and fate of somatic cells has been characterized at the single cell resolution (Sulston & Horvitz 1977; Sulston et al. 1983). These cell lineages are invariant among individuals (959 cells in hermaphrodites, 1031 in males) facilitating the detection of phenotypes caused by mutations affecting cell divisions and developmental processes (Horvitz & Sulston 1980).

- A transparent body

This feature allows the direct visualization of internal structures and cellular or subcellular phenotypes caused by genetic alterations during development as well as *in vivo* visualization of fluorescent reporters.

- Generation and maintenance of mutant strains

Exposing worms to certain chemical compounds or ionizing radiations have been used to induce mutations in the *C. elegans* genome. As mentioned above, the short life cycle and self-fertilization facilitates the propagation and isolation of detrimental mutations as homozygous strains along genetic screens (Jorgensen & Mango 2002). The Japanese National Bioresource Project (NBP) generates and distributes an ample collection of new mutant strains. Nowadays, more accurate techniques have been developed like CRISPR/Cas9 based system or MosSCI method to generate mutations "*a la carte*" in the locus of interest (Frøkjaer-Jensen et al. 2008; Waaijers et al. 2013).

- Gene silencing by RNA-mediated interference (RNAi)

The administration of a gene specific dsRNA triggers the mRNA sequence-specific inactivation producing the corresponding gene silencing. This effect is usually systemic and transgenerational. Two RNAi libraries are available and together cover about 94% of the *C. elegans* genome allowing the study of gene functions both at individual or genome wide level.

I.4.2. Inactivating gene expression by RNA-mediated interference (RNAi) in *C. elegans*

The mechanism of gene silencing by RNAi was first discovered in *C. elegans* (Fire et al. 1998) meaning a landmark in biological research and coming to be awarded with the Nobel Price of Physiology and Medicine in 2006. Based on an evolutionary conserved mechanism of defense against viruses, nowadays is used as a powerful approach to specifically modulate gene functions in worms and other systems. Briefly, once the gene-specific double-strand RNA (dsRNA) is introduced inside the cells it is recognized by the Dicer-RDE complex who cleaves the template in small RNA molecules (~20 nucleotides) also known as small interfering RNAs (siRNAs). Once the sense strand is degraded, the single antisense strand forms a complex called RNA-induced silencing complex (RISC) that allow recognizing the complementary endogenous mRNA and eventually producing its degradation in small fragments. The targeted-mRNA silencing not only takes place by mRNA degradation but siRNAs are also capable of inhibiting transcription and translation (Grishok 2005).

As is shown in figure 5, there are three different methods to administrate the desired dsRNA in *C. elegans* with different efficiency: by feeding with bacteria containing plasmids producing the dsRNA of interest, by direct dsRNA microinjection or by soaking in liquid medium containing dsRNA, although this last method is not frequently used because it is noisier and less reproducible (Tabara et al. 1998).

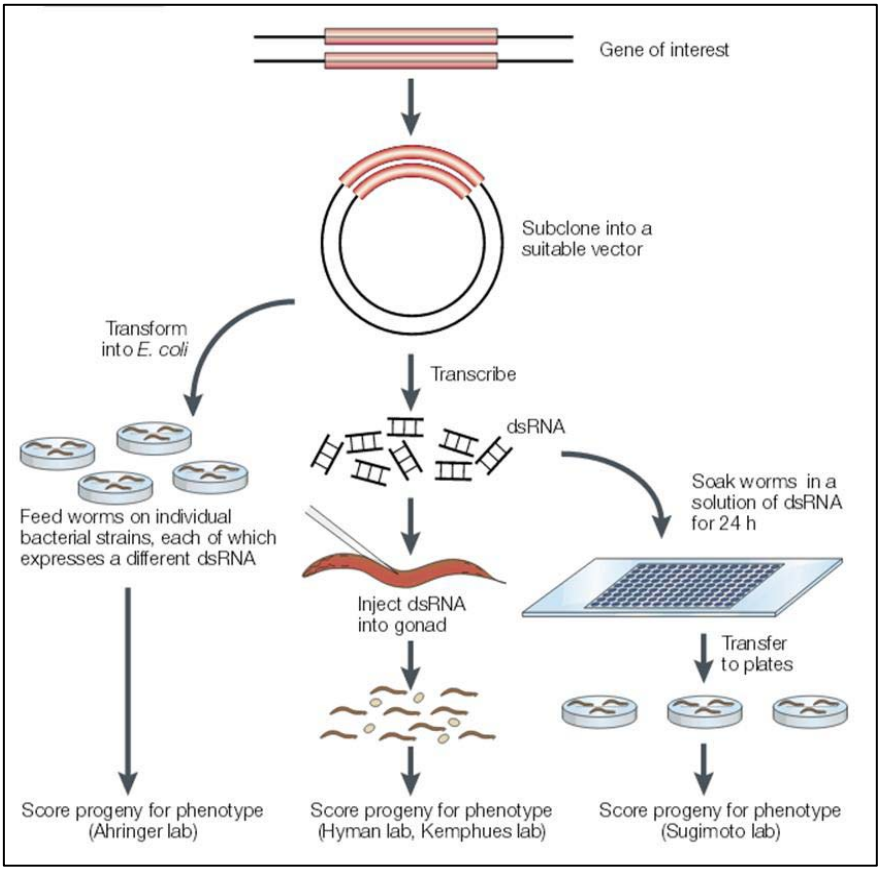

Figure 5. Different RNAi protocols used to inactivate gene function in *C. elegans*.
RNAi by feeding (left), by dsRNA microinjection (middle) and by soaking (right), extracted from (Kim 2001).

RNAi by feeding

There are two different RNAi feeding libraries available that together cover about 94% of the *C. elegans* genome. Basically both libraries are based in cloning of gene-specific fragments between two inverted T7

RNA polymerase promoters in the L4440 vector and transformation in the HT115 bacteria strain (Fraser et al. 2000; Kamath & Ahringer 2003). This vector has an IPTG inducible T7 polymerase and a non functional dsRNAseIII gene allowing the dsRNA accumulation inside the cells (Timmons et al. 2001).

The library made by Julie Ahringer's lab contains 19,762 clones and is based in cloning genomic fragments into the L4440 vector (Fraser et al. 2000; Kamath & Ahringer 2003). The library from Marc Vidal's lab contains around 12.000 clones and it was made by cloning full length open reading frames (ORF) from cDNA sequences (Rual et al. 2004). Despite that RNAi by feeding is less efficient than injecting, this method is also less arduous in terms of time, allowing both handle large worm populations and modulate the level of gene-inactivation through the feeding. Because of that, this method has been successfully used to perform large-scale RNAi screenings to find genes involved in specific processes (Gönczy et al. 2000; Piano et al.; Maeda et al. 2001; Piano et al. 2002; Kamath & Ahringer 2003; Simmer et al. 2003; Rual et al. 2004). Moreover, different RNAi clones can be combined to target different genes at the same time allowing uncovering genetic interactions (Tischler et al. 2008).

I.4.3. Engineering in *C. elegans* genome

In addition to gene inactivation by RNAi or the traditional generation of mutant strains by mutagenic agents, approaches like transgenesis have allowed to study gene functions in *C. elegans* (Chalfie et al. 1994). Moreover, more accurate techniques have been developed to generate a

directed genome editing as CRISPR/Cas9 (Friedland et al. 2013; Waaijers & Boxem 2014) or MosSCI method (Frøkjaer-Jensen et al. 2008).

Transgenesis in *C. elegans* consists in the introduction of exogenous DNA (plasmid or PCR product) directly into the germ line of the self-fertilizing hermaphrodite by microinjection or by particle bombardment. DNA microinjection is a relatively easy technique, which results in the formation of extrachromosomal arrays, consisting of multiple copies (80–300) of the exogenous DNA arranged as concatemers. These arrays behave as artificial chromosomes, as they are efficiently replicated and segregated to the progeny, often producing stable transgenic lines (Mello et al. 1991; Stinchcomb et al. 1985).

During gene bombardment, DNA-coated beads are used as vectors to introduce DNA into the animals (Wilm et al. 1999). This protocol also produces extrachromosomal arrays, but in addition, random integration of several copies of the transgene into the genome is observed (Praitis et al. 2001; Reece-Hoyes et al. 2007).
The majority of transformation markers used for *C. elegans* transgenesis are easily scorable under a dissecting scope. Most of them are based on the rescue of nonlethal mutations or in the use of dominant fluorescent markers, allowing visual identification of specific traits. Additionally, antibiotic selection has been successfully applied to *C. elegans* for an easier strain maintenance and genetic studies (Giordano-Santini & Dupuy 2011; Cornes et al. 2014).

CRISPR/Cas9 system

The development of this technique in early 2013 has supposed a new milestone in the field of genetic engineering increasing the capacity of editing genomes of model organisms, including *C. elegans*. This system is based in the *Streptococcus pyogenes* type II CRISPR system to create double strand breaks (DSB) in DNA foreign sequences in response to bacteriophages. It provides an efficient tool making the entire *C. elegans* genome accessible for engineering. In brief, this system is based in (I) the CRISPR associated (Cas) endonuclease (Cas9) and (II) two noncoding RNAs (CRISPR RNA or crRNA, and the trans-activating crRNA or tracrRNA). Target site specificity is mediated by a 20 nucleotides spacer region in the crRNA, complementary to the target region and a 3-nt motif (NGG) following the target site in the DNA [termed protospacer adjacent motif (PAM)] necessary to produce the DBS (Gasiunas et al. 2012; Jinek et al. 2012). On the contrary to MosSCI method, that requires a worm strain containing a Mos1 transposon at the target region (Frøkjaer-Jensen et al. 2008), in CRISPR/Cas9, since the only requirement is to localize the PAM sequence in the target region, a wide range of sites can be chosen. Conveniently, the system was improved by a single synthetic guide RNA (sgRNA) that fuses the 3′end of crRNA to the 5′end of tracrRNA , this sgRNA is sufficient to target Cas9 to a specific site and generate DSBs (Jinek et al. 2012) (Figure 6).

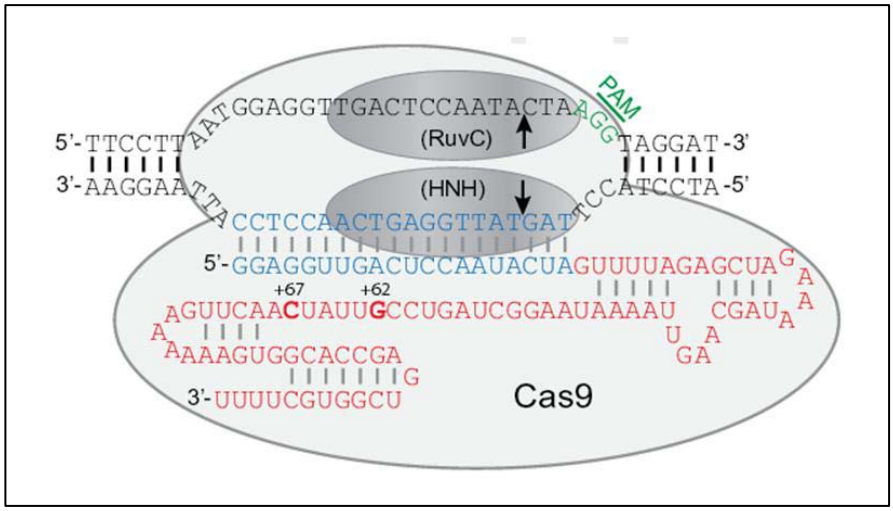

Figure 6. Cas9/sgRNA in complex with a target site.
The RuvC and HNH endonuclease domains of Cas9 together generate a double strand break. The PAM sequence in the genome is in green, the 20 nucleotide recognition sequence in blue, and the remainder of the sgRNA sequence in red (Waaijers & Boxem 2014).

In *C. elegans*, the expression of Cas9/sgRNA system in the germ line produces DBS that can be repaired by two methods: (I) non-homologous end joining (NHEJ), an error-prone process that can create insertions, deletions or mutations at the cut site, or (II) homology-dependent repair (HDR), a precise mechanism that repair the break using a homologous donor molecule to repair the break. Thus, providing a donor molecule that carries the desired edit flanked by homologous sequences to the targeted locus ("homology arms"), these edits could be integrated as part of the repair process. (Waaijers & Boxem 2014; Paix et al. 2014). Therefore, the possibilities that CRISPR/Cas9 offers in genome engineering are wide, as summarized in Figure 7, being possible to generate deletions of different lengths, endogenous tagging, single modifications or insertions anywhere on the genome.

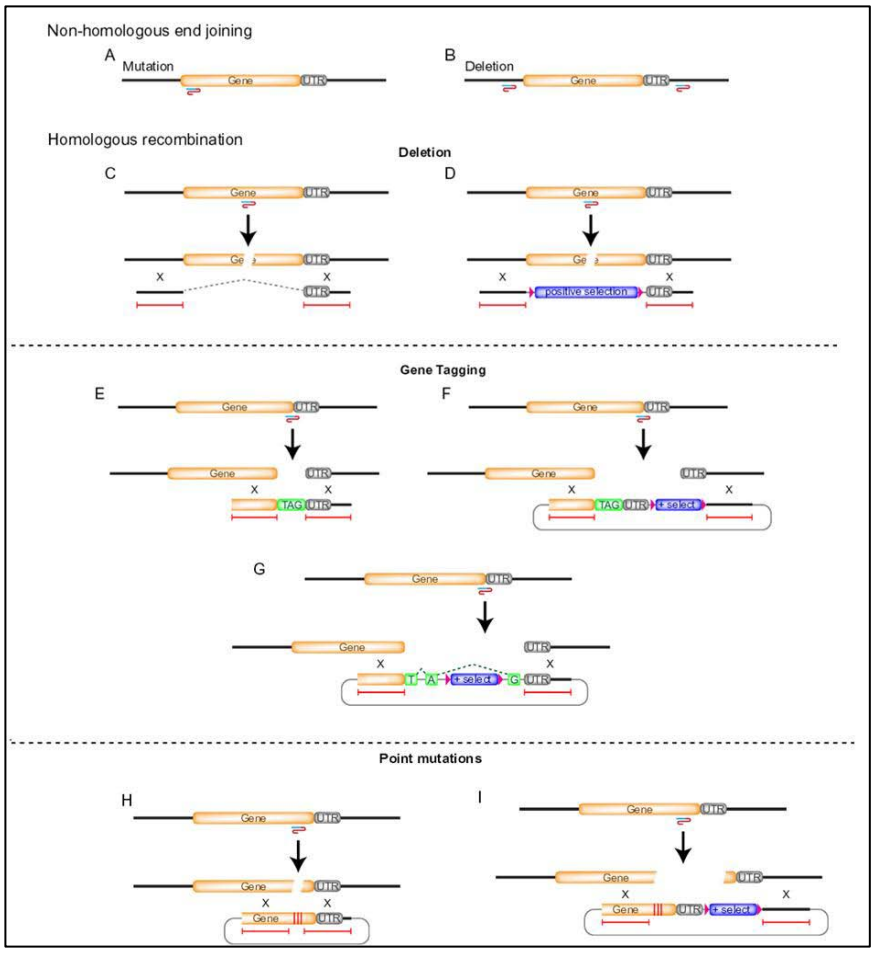

Figure 7. Different strategies of genome editing based in CRISPR/Cas9.
Target sites are indicated by the stylistic sgRNA. (A and B) Non-homologous end joining can be used to generate mutations and deletions. (C–I) Use of homologous recombination to generate deletions, insert gene tags, or engineer point mutations. Homologous regions are indicated by red lines at the repair constructs. For the introduction of templates different strategies are used (plasmids or single strand DNA), re-cleavage is prevented by simultaneously mutating the PAM sequence or target sequence in the repair template. (Modified from Waaijers & Boxem, 2014).

This technique is one of the most rapidly moving fields of research since new applications and improvements are continuously showing up. Regarding *C. elegans*, it does not exist a unique method and many different approaches are used on CRISPR/Cas9 delivery, repair template design or mutant/recombinant selection. Although these different protocols demonstrated to be efficient, the rules that dominate the efficiency are still unclear. It is likely that future studies will address some of these questions resulting in optimized canonical protocols.

I.4.4. *C. elegans* germ line

C. elegans germ line has represented an excellent system to study the effect of DNA-damaging agents because it is the only adult tissue that is maintained by stem cells that constantly replenish its population (Craig et al. 2012). The hermaphrodite *C. elegans* germ line consists of stem cells that proliferate to later enter in meiosis to produce sperm (first) and oocytes. The hermaphrodite *C. elegans* germ line is formed two U-shaped symmetric gonad arms that connect to a central uterus through the spermatheca (Figure 8.A). In the distal part of the gonad there is a syncitium where germ cells share a common core cytoplasm (rachis). Moreover, germ cells cellular state is organized into a spatiotemporal gradient along the distal-proximal axis. In the distal germ line (proliferative region), cells are continuously proliferating to produce new germ cell precursors by mitotic divisions. After this proliferative region, we can find the transition zone with nuclei in premeiotic S phase and other subsequent stages of meiotic prophase. After the transition zone, germ cells progress to pachythene, diplothene and diakinesis to complete

the oocyte maturation (Hubbard & Greenstein 2000). Mature oocytes are fertilized going through the spermatheca to produce embryos that are accumulated in the uterus. Besides the germ cells, the gonad also consists on somatic components such as Distal Tip Cells (DTCs), gonad sheath or spermatheca. DTCs are located at the end of each gonad arm being necessary to maintain the pool of stem cells. The gonad sheath is based on five pair of cells forming a single layer covering the germ line and the spermatheca is the structure containing mature sperm where fecundation takes place (Lints, R. and Hall, D.H. 2009).

The germ line of each gonad arm produces about 150 sperm during L4 (L'Hernault 1997). Spermatogenesis takes place within the proximal gonad. During this process primary spermatocytes, after meiosis, form the sperm precursors (spermatids). Spermiogenesis is the process in which the spermatids become a mature sperm (spermatozoa). *C. elegans* spermatozoa crawl using a pseudopod, which is mainly composed by major sperm proteins (MSPs), a group of sperm-specific proteins with several functions such as providing sperm motility or inducing oocyte maturation that are redistributed during the spermatogenesis process (Miller et al. 2001; Roberts & Stewart 2000) (Figure 8.B).

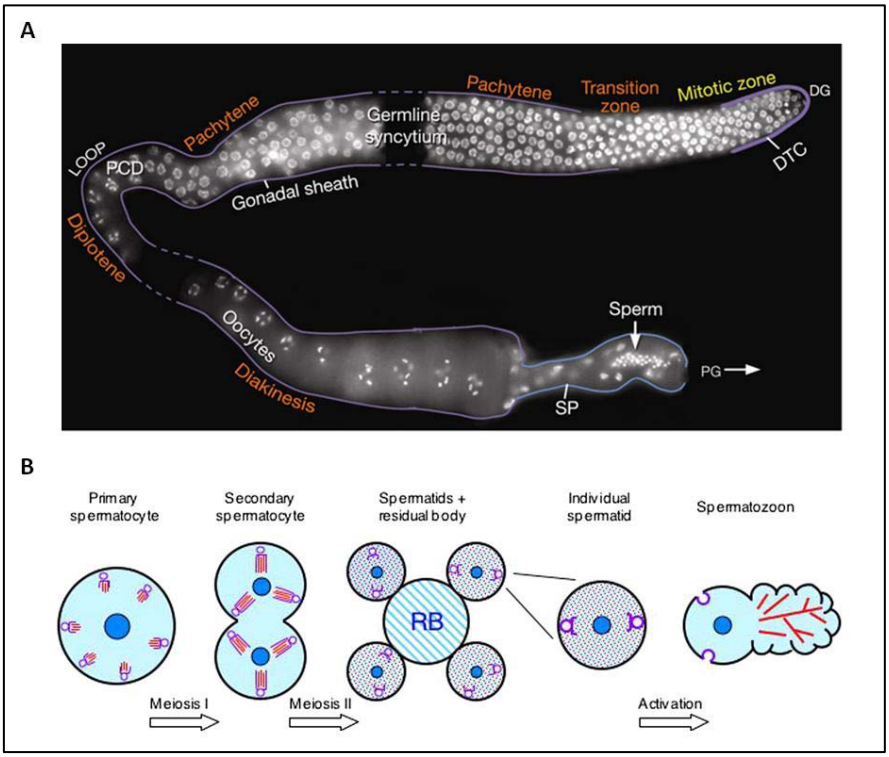

Figure 8. Structure of the germ line and process of spermatogenesis in *C. elegans*
(A) DAPI-stained adult hermaphrodite gonad arm. Distal-proximal polarity of germ line cell nuclei morphologies as they progress from mitosis through the various stages of meiotic prophase I**.** Orange text indicates different stages of meiotic prophase I. (PCD) Programmed cell death, (DG) distal germ line, (PG) proximal germ line, (SP) spermatheca (image source: J. Maciejowski and E.J. Hubbard.). (B) *C. elegans* phases of spermatogenesis. MSP (red) are assembled and associated with the membranous organelles (purple). Assembly continues through the secondary spermatocyte stage. MSP dissociates into the cytosol upon spermatozoon activation and reassembles into filamentous fibers in the pseudopod (image source from Wormbook).

I.4.5. *C. elegans* DNA damage-induced apoptosis

The wide knowledge about physiological apoptosis mechanisms in germ cells and somatic tissues prompted studies to analyze DNA damage

induced apoptosis in *C. elegans* (Gartner et al. 2000). In response to genotoxic stress worms trigger a conserved DNA-damage response consisting in the activation of DNA-repair pathways that can produce, depending on the damage, cell-cycle arrest and induction of apoptosis (Gartner et al. 2000). DNA damage induced apoptosis, in contrast to the physiological, requires CEP-1/P53 to activate the proapoptotic genes *egl-1* and *ced-13*, which are BH3-only domain proteins (Greiss et al. 2008) (Figure 9). Thus, EGL-1 is essential to activate the core executioner machinery in response to DNA damage. In the germ line, like physiological apoptosis, stress related apoptosis only takes place during pachytene stage, while no apoptosis have been observed in sperm-precursors or male germ line (Salinas et al. 2006).

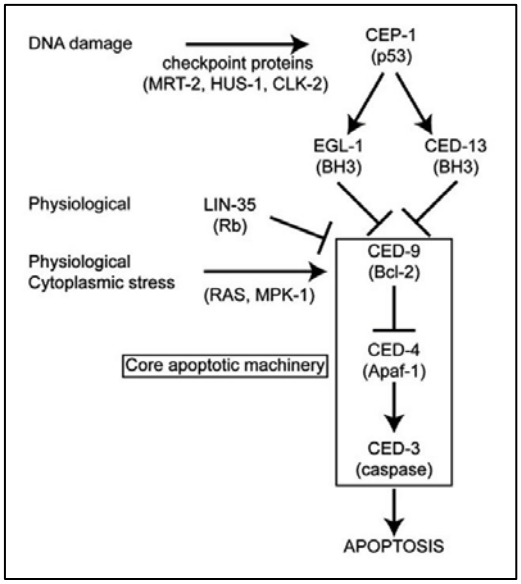

Figure 9. Apoptosis signaling pathways in *C. elegans*.
CEP-1-dependent apoptosis is induced by DNA damage or chromosomal integrity checkpoint while physiological apoptosis is *cep-1*-independent and a normal feature of oogenesis. The frequency of *cep-1*-independent germ cell apoptosis increases in response to various cytoplasmic stresses (oxidative, heat, osmotic, starvation) and it is regulated by RAS/MAP-kinase signaling (extracted from Gartner et al. 2008).

I.4.6. The Insulin/ Insulin-like grow factor-1 signaling (IIS) pathway in *C. elegans*

The evolutionary conserved IIS pathway has extensively been studied because of its role in modulating ageing or stress response (Murphy et al. 2003). Often, genetic and gene expression manipulations that increase *C. elegans* longevity also provide stress resistance; conversely, promoting stress responses in the nematode can also prolong lifespan (Zhou et al. 2011). This fact underscored the functional relation between pathways regulating both processes.

In *C. elegans*, *daf-2* encodes the only worm ortholog of insulin-like growth factor receptors (IGFs) (Baugh & Sternberg 2006). DAF-2 receptor is active by binding to its ligands (Insulin-Like Peptides), promoting a signaling cascade that results in the phosphorylation of the FOXO transcription factor DAF-16 by AKT-1 (Figure 10). As a consequence, phosphorylated DAF-16 is recognized by 14-3-3 proteins PAR-5 and FTT-2 promoting its cytoplasmic retention. On the contrary, upon reduced IIS signaling, unphosphorylated DAF-16 translocates into the nucleus regulating a subset of genes involved stress resistance, innate immunity and metabolic adaptation, which are processes that determine lifespan (Singh & Aballay 2009; Murphy & Hu 2013). Thus, genetic alterations that result in a reduced IIS signaling, like mutations in *daf-2* or *akt-1,* promote stress resistance and an extended lifespan. On the contrary, *daf-16* inactivation causes sensitivity to stress and reduces lifespan (Mukhopadhyay et al. 2006).

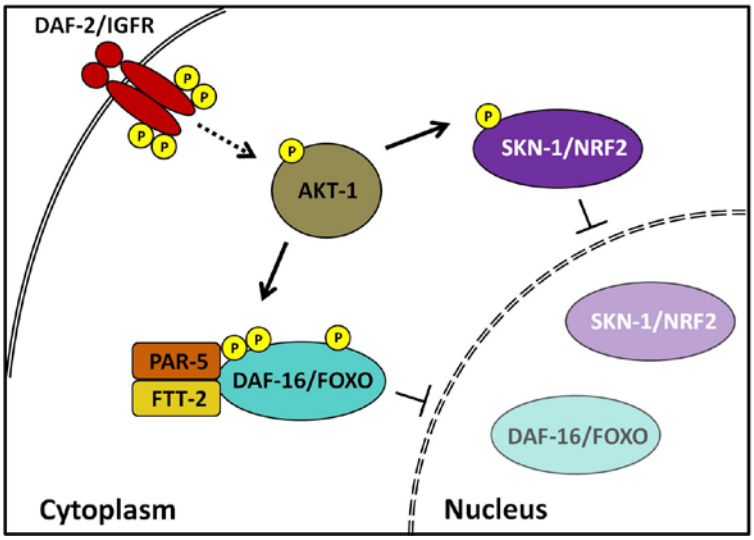

Figure 10. Simplified scheme of ISS pathway.
DAF-2 activates a signaling pathway producing DAF-16 phosphorilation by AKT-1 and the interaction with the two 14-3-3 proteins PAR-5 and FTT-2, which inhibits DAF-16 nuclear translocation. SKN-1 cytoplasmic retention is also promoted by AKT-1 phosphorilation.

The Nrf2 *C. elegans* ortholog SKN-1 is an important factor of the organismal response to oxidative stress. This transcription factor regulates expression of Phase 2 detoxification system genes in the intestine, which are genes that protect against oxidative and xenobiotic stresses, and shares common targets with DAF-16/FOXO (Oliveira et al. 2009). Accordingly, *skn-1* mutants are highly sensitive to oxidative stress and show a reduced lifespan (An & Blackwell 2003; An et al. 2005; Inoue et al. 2005). Interestingly its nuclear translocation is also mediated by IIS through *akt-1* phosphorilation (Tullet et al. 2008).

I.4.7. Role of selenoprotein thioredoxin reductase 1 (TrxR1) in the response to cisplatin

Thioredoxin reductases are NADPH-dependent oxidoreductases that, together with thioredoxins, compose the thioredoxin system (Gromer et al. 2004; Arnér 2009) (Figure 11.A). They are involved in many different cell processes such as antioxidant defense, redox regulation or deoxyribonucleotide synthesis (Arnér & Holmgren 2000). Due to these important functions, it is reasonable to hypothesize that TrxR inhibition would impose a significant stress on cells due to the resulting inhibition of thioredoxin-dependent reactions. In addition, mammalian thioredoxin reductases are selenoproteins because during translation they incorporate a residue of selenocysteine (Sec) in a conserved C terminal GCSecC motif that is essential for its Trx-reducing activity (Lee et al. 2000; Zhong et al. 2000) (Figure 11.B). The highly accessible chemically reactive Sec-containing active site of reduced mammalian TrxR1 makes this enzyme suitable to be inhibited by a broad range of electrophilic compounds such as cisplatin (Peng, Xu & Elias S. J. Arnér 2012). Therefore, the effect of cisplatin on the Sec residue may produce highly pro-oxidant forms of TrxR1, also named SecTRAPS (Selenium-compromised Thioredoxin Reductase Derived Apoptotic Proteins) that contribute to increase the intracellular oxidative stress undergoing apoptosis (Anestål et al. 2008) (Figure 11.C). Consistently, a TrxR1 variant that replaces selenocysteine for cysteine, which is formed in some in vivo conditions as selenium deficiency, causes less sensitivity to cisplatin in cell lines (Peng, Xu & Elias S J Arnér 2012). Interestingly, it has recently been demonstrated the role of human TrxR1 as a potent regulator of stress responsive transcription factor Nrf2, showing that inhibition of TrxR1 functions or selenium deficiency activates Nrf2 increasing the detoxification response (Cebula et al. 2015).

C. elegans thioredoxin system is based in two thioredoxin reductases TRXR-1 (cytoplasmic) and TRXR-2 (mitochondrial), being TRXR-1 the only selenoprotein in worms (Li, Bandyopadhyay, Hwaang, B. J. Park, et al. 2012; Gladyshev et al. 1999). This feature, together with the fact that TRXR-1 is essential in mammals but not in worms (Stenvall et al. 2011), makes *C. elegans* a convenient model to unravel the *in vivo* significance of selenocysteine residue in the response to cisplatin.

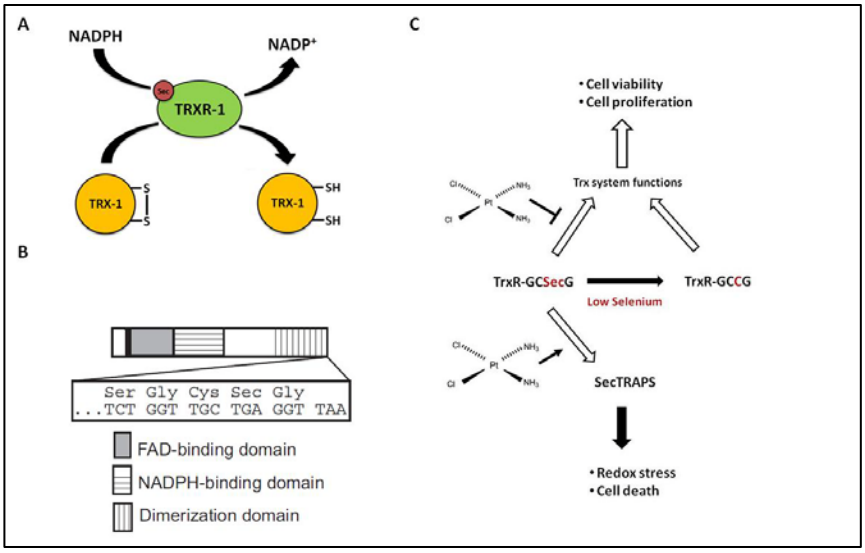

Figure 11. TrxR1, through a Sec residue, is required to the cytotoxic effect of cisplatin.
(A) The cytoplasmic thioredoxin system in *C. elegans*. Reducing potential of NADPH is used by TRXR-1 to reduce disulfide-form TRX-1 (oxidized) to the dithiol-form. (B) Domain structure of the TRXR-1 protein. In black is represented the N-terminal redox active site. The sequence of the C-terminal domain is shown below where the Sec residue is occuping the second to last position (modified from Stenvall et al. 2011). (C) Cisplatin inhibits the Trx system and induces the formation of SecTRAPs. The functions of the endogenous Trx system promoting cell viability and proliferation can potentially be sustained by both wild type and Sec-to-cysteine-variant TrxR species. Only the Sec-containing form of TrxR is susceptible to inhibition by cisplatin and can mediate some of the cytotoxicity of cisplatin, both inhibiting Trx system functions and forming toxic SecTRAPs (modified from Peng. 2012).

I.5. Patient derived orthoxenograft models to study the mechanisms of cisplatin resistance in germ cell tumors

I.5.1. Human germ cell tumors

Despite of germ cell tumors (GCTs) represent only 1% of male malignancies are the most common neoplasm among men aged 15–35 years and their incidence is increasing (Oing et al. 2015). Male GTCs are highly sensitive to platinum-based chemotherapy. In fact, surgery, in combination to platinum postchemotherapy, gets cure rates approaching 50% up to 90% even in metastatic stages. They can be classified as seminomas (SEs), which represent around 40% of cases, or nonseminomas (NSEs) (60%). While SE are radio- and chemo-sensitive tumors, and are highly curable at all stages (Germà-Lluch et al. 2002), in the case of patients with NSEs, a 10-15% of the deaths from cisplatin refractoriness are due to the absence of alternative effective resensitizing therapies (Kollmannsberger et al. 2006).

In women, epithelial ovarian cancer is the fifth leading cause of death and is the most common cause arising from gynecologic malignancies (Jemal et al. 2008). The mainstay of front-line therapy is cytoreductive surgery followed by chemotherapy. Currently, the standard first-line treatment is a platinum-taxane combined regime but its efficacy is limited; most patients show an initial response to treatment but upon relapse, the platinum response rates progressively diminish until they die. Different second-line therapies such as bevacizumab, trabectedin or olaparib are being used, but currently, none of them promises disease cure (Korkmaz et al. 2015). So, the development of effective innovative therapeutic strategies to overcome cisplatin resistance remains a high priority.

I.5.2. Patient derived orthoxenograft models

Platinum-based drugs are in the front-line of clinical therapies for epithelial ovarian cancer and testicular germ cell tumors, but many aspects of intrinsic and acquired resistance to platinum-based chemotherapy still remain unknown. Thus, the establishment of preclinical models mimicking patients' primary tumor features, which accurately reflect phenotypic, genotypic, and tumor chemotherapy response behavior, is a key step to identify novel therapeutic targets and to test novel treatments (de Plater et al. 2010; Teicher 2006). Primary orthotopic tumorgraft models are among the most recent class of preclinical cancer models and involve the direct implantation, serial transplantation and propagation of freshly excised primary human tumors into immune-deficient mice to create a primary human tumorgraft in a manner that preserves and stabilizes both the genotypic and phenotypic features of the original human tumor (Ruggeri et al. 2014). This method avoids secondary molecular and epigenetic changes caused by *in vitro* selection in models derived from tumor-cell line implantation. Importantly, this model maintains their clinical markers and histopathologies, gene expression and DNA copy number variations, while frequently recapitulating clinically relevant patterns of metastasis (Fiebig et al. 2004; Rubio-Viqueira et al. 2006).

More importantly for their utility as preclinical drug discovery models is the clinical relevance and predictability of tumorgrafts to a variety of cytotoxic and targeted therapeutic agents. Primary patient-derived tumorgrafts benchmarked against a variety of standard of care chemotherapeutic agents demonstrated that these primary tumorgrafts correctly predicted positive clinical responses and therapeutic resistance in most of the patients (Ruggeri et al. 2014; Hidalgo et al. 2014).

Importantly, this model is also a versatile tool for simulating drug resistance. As was shown in ovarian cancer, a prolonged exposure to cisplatin results in induction of resistance to this agent in a platinum-sensitive model, similar to what is observed in the clinic (Vidal et al. 2012).

I.5.3. Generation and characterization of a collection of paired resistant/sensitive orthoxenografts

Our group was capable to generate and characterize a collection of several ovarian and testicular cancer model based on orthotopic tumor implantation in nude mice which have already been used in preclinical studies (Juliachs et al. 2013; Juliachs et al. 2014; Vidal et al. 2012) (Tables 2 and 3). These engrafted tumors reproduce the histopathological characteristics of primary patients' tumors but also recapitulate in mice characteristic features of primary tumor in response to cisplatin, allowing *in vivo* development of a cisplatin resistant orthotopic tumor model. The general approach used to obtain the cisplatin-resistant engrafted tumor model is illustrated in Figure 12.A. In brief, tumor-implanted mice were initially treated with low doses of cisplatin. When tumors relapsed, they were harvested and implanted in new animals (mouse-to-mouse passage). The process was repeated up to 5 times by treating tumor-bearing mice with stepwise increasing doses of cisplatin. Then, the levels of cisplatin tumor resistance were evaluated by comparative assays between the initial tumor (OVA1X, TGT1) and each of the independent lines of resistant tumors (Figure 12.B-C).

Paried orthoxenografts (resistant vs. sensitive)	Histology
OVA1-QT#4/OVA1	SE/EN
OVA3-QT#4/OVA3	CA
OVA3-QT#5/OVA3	CA
OVA8-QT#2/OVA8	SE
OVA11-QT#4/OVA11	SE
OVA11-QT#5/OVA11	SE
OVA13-QT#1/OVA13	EN
OVA15-QT#5/OVA15	EN
OVA15-QT#6/OVA15	EN
OVA17-QT#4/OVA17	SE
OVA17-QT#5/OVA17	SE
OVA19-QT#3/OVA19	SE
OVA20-QT#3/OVA20	CA
OVA20-QT#4/OVA20	CA
OVA24-QT#3/OVA24	SE
OVA24-QT#4/OVA24	SE
OVA25-QT#3/OVA25	CA
OVA25-QT#4/OVA25	CA
OVA26-QT#2/OVA26	CC
OVA29-QT#1/OVA29	MU
OVA34-QT#3/OVA34	CA
OVA34-QT#4/OVA34	CA
OVA43-QT#1/OVA43	CC
OVA44-QT#4/OVA44	EN
OVA44-QT#5/OVA44	EN
OVA46-QT#3/OVA46	SC
OVA46-QT#4/OVA46	SC
OVA47-QT#3/OVA47	MU
OVA47-QT#4/OVA47	MU

Table 2. List of paired orthoxenograft (Resistant/Sensitive) ovary tumors used in this project.
OVA-QT mentions to cisplatin resistant tumors. Number indicates the number of cycles of chemotheraphy suffered. Tumor histology abbreviated as: SE: Serous, EN: Endometrioid, CA: Carcinosarcoma, CC: Clear Cell, MU: Mucinous tumor.

Paried orthoxenografts (resistant vs. sensitive)	Histology
TGT1-QT / TGT 1	YS
TGT12-QT / TGT12	EC
TGT21-QT / TGT21	YS, CH, EC
TGT34-QT / TGT34	EC
TGT38-QT / TGT38	CH

Table 3. List of paired orthoxenograft (Resistant/Sensitive) testicular germ cell tumors used in this project.
Five paired testicular nons seminous germ cell tumors (TGTs) showing different histologies where TGT-QT mentions to cisplatin resistant tumor and TGT to the sensitive one. Tumor histology abbreviated as: YS: Yolk Sac, EC: Embryonal Carcinoma, CH: Choriocarcinoma.

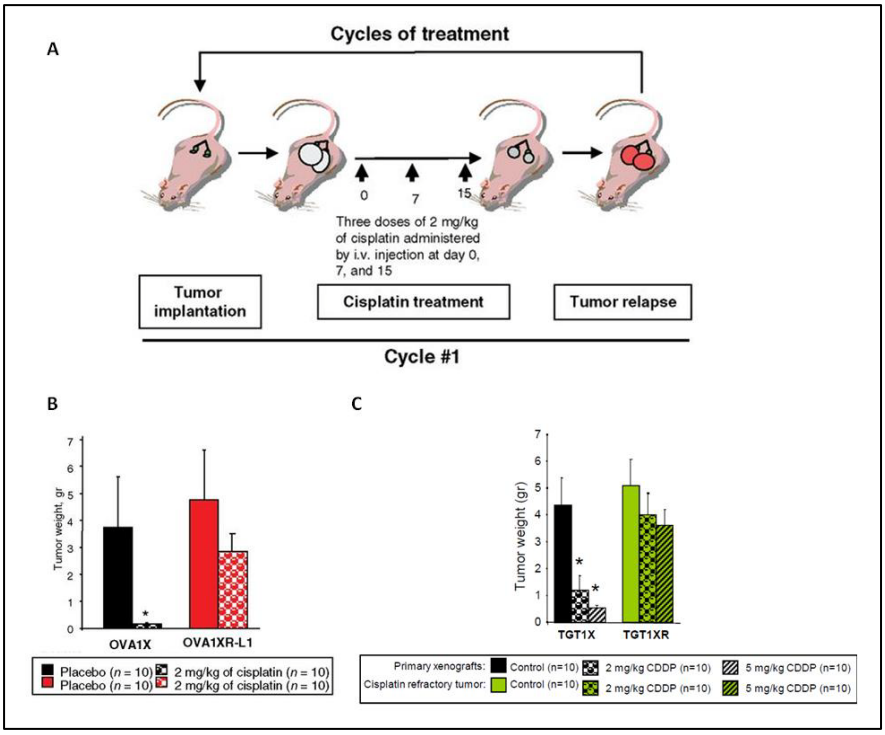

Figure 12. Generation of *in vivo* cisplatin resistant orthoxenografts.
(A) Experimental approach used for cisplatin-resistant tumor generation: after ovarian and testicular primary tumor implantation mice are treated with cisplatin (3 doses of cisplatin administered by injection). Postchemotherapy relapsed tumor is engrafted in the ovaries of other young mice, and this cycle repeated up to 5 additional times. Increased doses of cisplatin were used through the cycles. (B and C) Comparative short-time cisplatin response of the cisplatin resistant generated tumors OVA1XR-Line1 (B) and TGT-1XR compared to their respective untreated tumors. (C) (Extracted from Vidal et al. 2012, and Piulats et al. Unpublished).

This orthotopic-based preclinical tumor models are outstanding resources for the development of new drug therapies. They would also be very valuable for exploring new therapeutic applications for drugs that are currently approved for use in humans, as we recently reported with the role of lurbinectidin inhibiting cisplatin resistant ovarian tumors (Vidal et al. 2012), but also represents a system to address cisplatin refractoriness from a genetic perspective and for the preclinical development of novel targeted therapies based on overcoming cisplatin resistance.

1.5.4. Recurrent amplification in 9q32-q33.1 region in cisplatin resistant testicular germ cell tumors contains genes that respond to this drug

The group of Alberto Villanueva studied the relation between the acquisition of cisplatin resistance and the selection of specific genomic imbalances and genetic alterations against the genetic background of reference for these NSE testicular tumors. A fine-scale comparative whole-genome mapping using array-based comparative genomic hybridization (CGH) performed in four paired untreated parental engrafted tumors and their resistant counterparts resulted in few additional recurrent genomic changes that were consistently detected in resistant tumors. Among the modifications, the most recurrent was an amplification in the chromosome 9, specifically the 9q32-q33.1 region (Figure 13). Surprisingly, this region is enriched in genes previously associated to drug response.

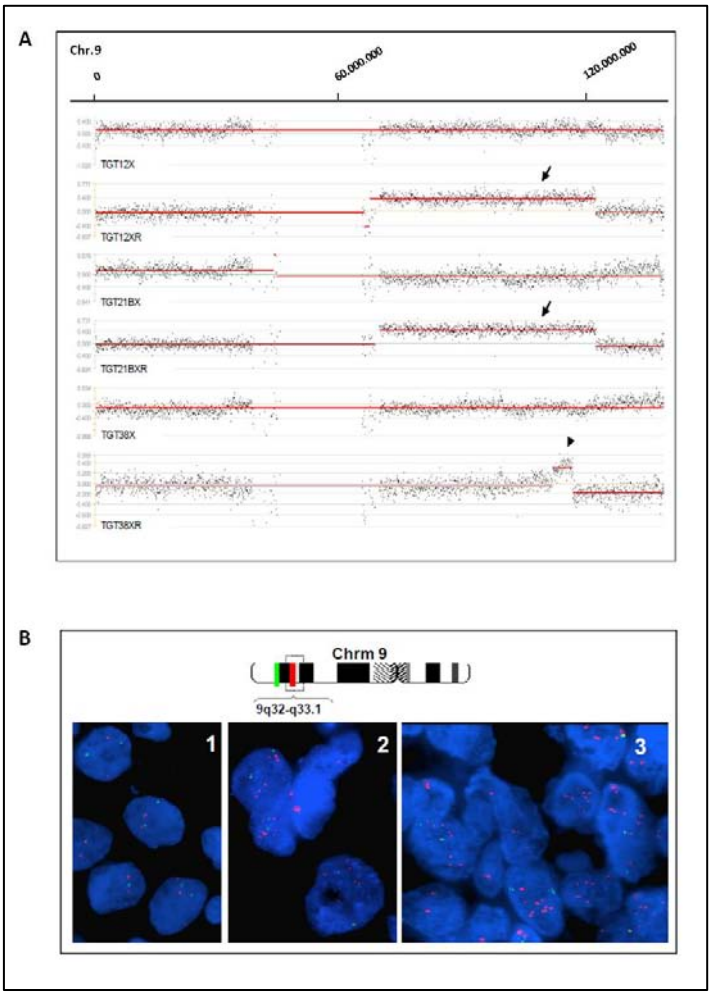

Figure 13. Recurrent gains at 9q in different refractory tumors.
(A) The long 9q21.11-q33.3 gain region (arrow) was identified in TGT12XR and TGT21BXR, while in tumor TGT38XR there was a small overlapping region at 9q32-q33.1 (arrowhead). Whole genome mapping was performed by oligonucleotide array CGH analysis. (B) Representative FISH analyses of the copy number of 9q32-q33.1 in metastatic CGT samples contained in the TMA. Interphase FISH with probes binding to 9q32-q33.1 region (red) and control region in chromosome 9 (green). Panel 1 shows the absence of amplification in control tumors, characterized by two red and two green signals in all interphase nuclei; and panels 2 and 3 show amplification of the region that displays cisplatin resistant tumors (modified from Piulats et al. Unpublished).

To further analyze if these genes at 9q region are contributing to the process of acquisition of resistance, we compared the expression profiles between the five paired-orthoxenografts (resistant vs. control). We found recurrent missregulation of several genes that can be classified in: (i) those whose expression changes correlate with 9q32-q33.1 gain status (*PAPPA*, *POLE3*, and *AKNA*), and mainly (ii) those that do not, and are associated solely with cisplatin refractoriness (*GCS*, *EDG2*, *ZNF883*, *FLJ31713*, *TNC*, *ATP6V1G1*, *CTR1*, and *CTR2*) (Figure 14).

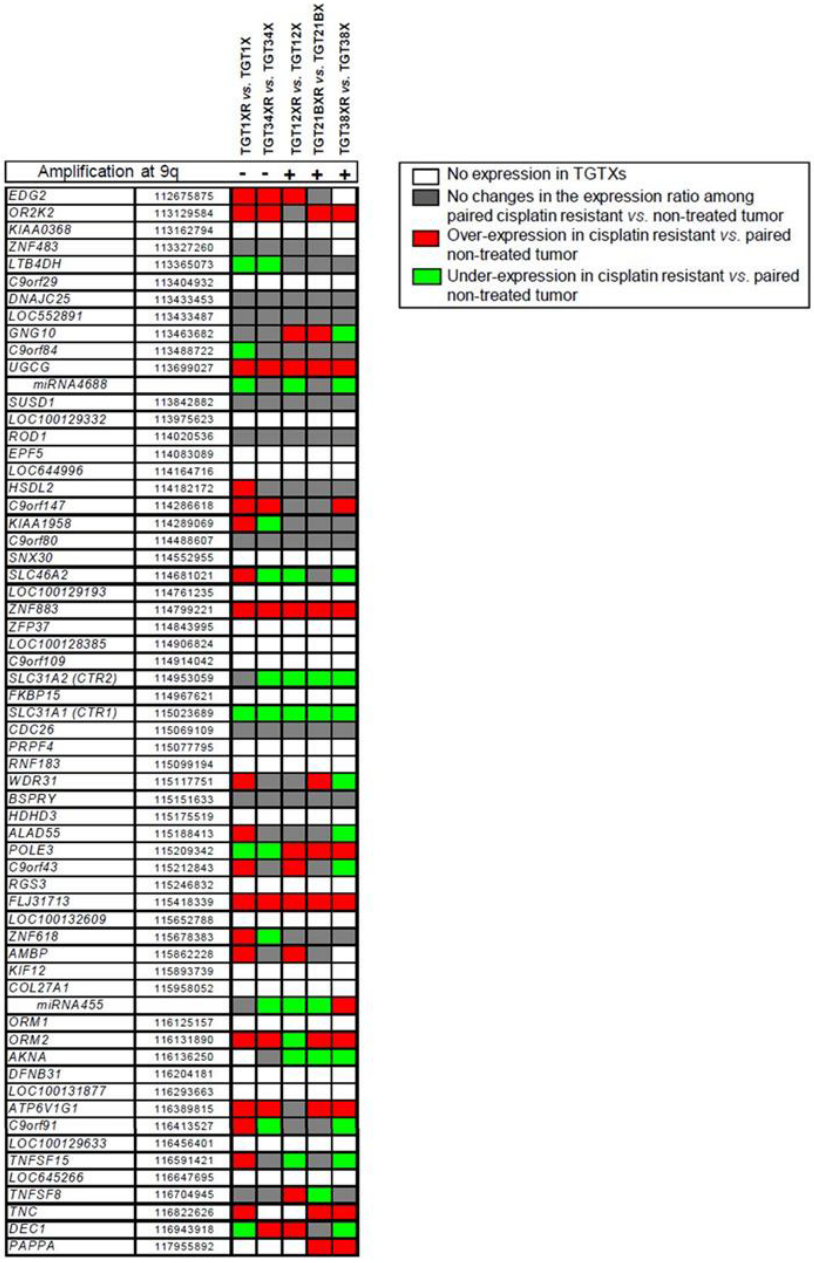

Figure 14. Differential profiling expression patterns of the 60 genes and two miRNAs annotated on 9q32-q33.1 region.

(A) Results are presented as changes in the expression levels in cisplatin refractory tumors relative to the untreated tumors, grouped by 9q32-q33.1 gain status. No expression changes (in grey), downregulation in resistant tumors (in green), upregulation in resistant tumors (in red) and no expression in engrafted tumors (in white)(extracted from Piulats et al. Unpublished).

Objectives

1. Consolidate *C. elegans* as animal model to investigate the response to cisplatin or other chemotherapeutic agents.

2. Uncover new *C. elegans* genes involved in the response to cisplatin to map cellular pathways capable of modulating such response.

3. Investigate the role of the thioredoxin reductase 1 selenocysteine amino acid in the cytotoxic effect caused by cisplatin.

4. Determine what genes at 9q32-33.1 human region are candidate to influence the tumor response to cisplatin.

Results

R.1. Effects of cisplatin in *C. elegans*

The effect of cisplatin in *C. elegans* have previously been reported in embryos, L1 larvae and adult worms (Collis et al. 2006; van Haaften et al. 2006), but still the mechanisms responsible for the cellular response to cisplatin are poorly understood. In addition, the enormous potential of *C. elegans* as model organism has not been fully exploited to understand the complex mechanisms involved in the response to cisplatin. Here, we explored the action of cisplatin in the multicellular organism *C. elegans* to establish a solid system to investigate how cells react when animals are treated with this drug.

R.1.1. *C. elegans* phenotypes associated to cisplatin exposure

We first characterized the different effects of cisplatin in worms. By performing different treatments in terms of extension and doses, we observed that this chemotherapeutic agent induces a wide variety of phenotypes in distinct developmental stages (Table 4). We noticed that low doses of cisplatin provoke germ line phenotypes and developmental effects. In contrast, higher doses of cisplatin were needed to produce phenotypes in adult worms. These observations are concordant to the DNA-damaging action of cisplatin, being the animals with active cellular proliferation more sensitive to cisplatin.

Stage	Duration (hours)	Medium	Cisplatin (µg/ml)	Phenotypes
L1	48	Solid (NGM)	40	Rbs, Emb, Pvl.
			50-100	Ste, Gro, Pvl.
			100	Lva.
L3	24	Solid (NGM)	100	Rbs, Emb, Pvl.
			200	Ste, Pvl.
L4	4	Liquid (M9)	200	Rbs, Emb.
Adult	48	Liquid (S-medium)	250	Lav.
			500	Lav, Let.

Table 4. Phenotypes observed in *C. elegans* upon different cisplatin treatments.
Phenotypes are abbreviated as follows: Rbs (Reduced brood size), Emb (Embryonic lethality), Pvl (Protruding vulva), Ste (Sterile), Lav (Locomotor activity variant), Let (lethal). Gro (Growth delay).

R.1.2. Action of cisplatin in *C. elegans* germ line

The *C. elegans* germ line has been a valuable system to study the effect of many molecules in cell-cycle regulation and DNA damage response (Gartner et al. 2004). To investigate the cisplatin effects in the germ line, we exposed L4 worms to cisplatin for 24 hours and observed a dose-dependent decrease in fertility, which was monitored scoring the brood size (Figure 15.A), and an increase in the proportion of unfertilized oocytes laid (Figure 15.B).

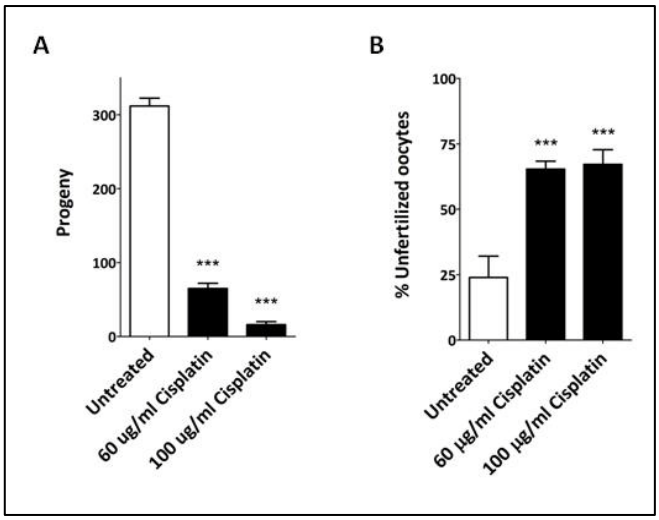

Figure 15. Cisplatin reduces the brood size and increases the number of unfertilized oocytes.
(A) Progeny of worms exposed to cisplatin from L4 for 24 hours at the indicated concentrations. Bars show mean and SEM of two different experiments (n=12). (B) Plot showing the percentage of unfertilized oocytes in the progeny of treated and untreated animals. Bars show mean and SEM of two different experiments (n=12). ****p*>0,001 compared to untreated animals by Student's t-test.

To better understand the effect of cisplatin in *C. elegans* reproductive capacity we analyzed DAPI stained germ lines of one-day adults treated with cisplatin. Cisplatin produced a decrease in the number of germ cells (Figure 16.B) and, interestingly, we also observed an increase in the size of germ cells at the proliferative region (distal part) of the gonad, which indicates arrested cell cycles upon S-phase checkpoint activation (Gartner et al. 2004) (Figure 16.A).

Worm exposure to other DNA-damaging agents such as ionizing radiation or ultraviolet C light induces cell-cycle arrest at the distal part of the proliferative region and an increase of apoptotic nuclei in the pachytene region of the gonad (Gartner et al. 2004) producing sterility and

embryonic lethality. The fact that cisplatin mimics these phenotypes suggest that is acting on the DNA (Table 4).

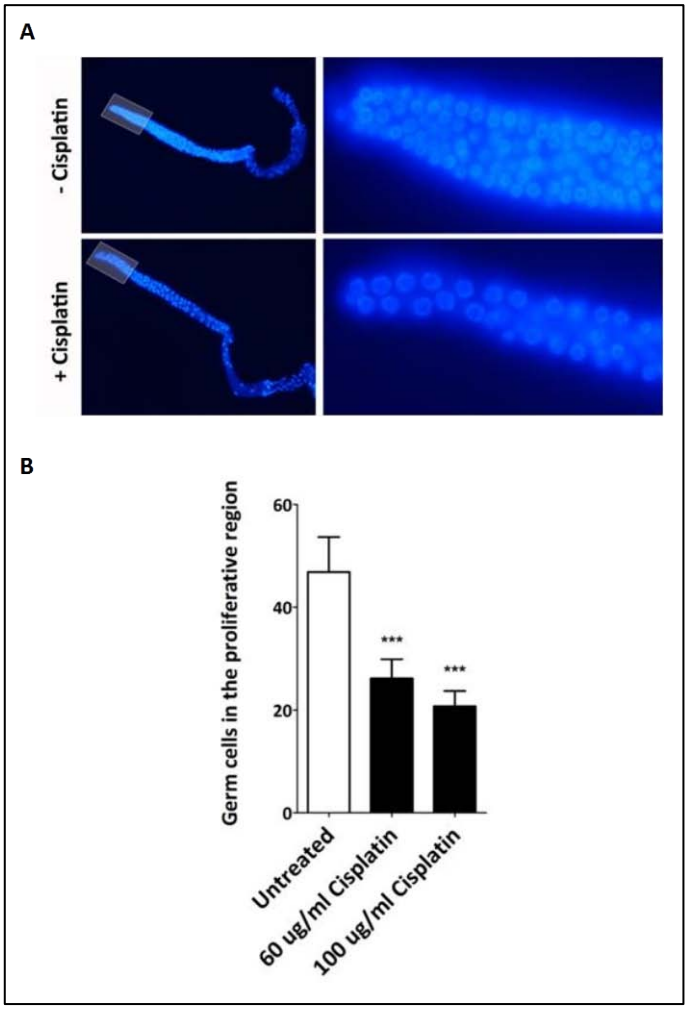

Figure 16. Cisplatin affects germ line development.
(A) Representative images of DAPI stained germ lines from 1 day-old adults after a treatment of 60µg/ml cisplatin for 24 hours. Proliferative regions (distal part) are marked in rectangles and showed at higher magnification on the right image. (B) Quantification of germ cell nuclei in one area of the proliferative region. Bars represent mean and SD of two experiments (n=15).

R.1.3. Action of cisplatin in *C. elegans* somatic cells

Since we are interested in the resistance to cisplatin as a chemotherapeutic agent, we oriented our studies towards the response to cisplatin in somatic cells. Thus, to set a reliable system to model the response of *C. elegans* to cisplatin, we established a dose-response pattern in two distinct scenarios: (i) developing larvae, where cell division occurs in somatic and germ cells; and (ii) adult worms, where somatic cells do not divide anymore.

Cisplatin hampers larval growth in a dose-dependent manner

In developing larvae, we studied the cisplatin effect by exposing a synchronized population of L1 larvae to different cisplatin doses for 48 hours. We observed a developmental delay at doses of cisplatin ranging from 25 to 75 µg/ml whereas concentrations higher than 100µg/ml produced larval arrest (Figure 17).

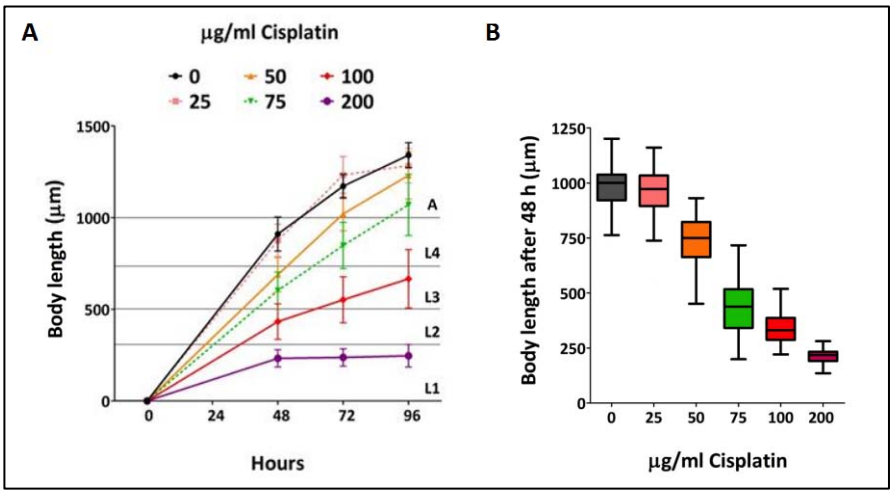

Figure 17. Cisplatin produce a dose-dependent developmental delay and arrest.
(A) Growth of a L1 synchronized population of worms treated with different doses of cisplatin for 96 hours at 20ºC. Data are represented as mean and SD (n=50). The assay was performed twice with similar results. (B) Body length of a synchronized population of wild type L1 larvae grown in agar plates containing different doses of cisplatin for 48 hours at 20ºC. The experiment was performed three times with similar results (n=50).

Cisplatin affects adult survival in a dose-dependent manner

The impact of cisplatin on DNA is expected to be higher in developing tissues than in post-mitotic cells (Hemmingsson et al. 2010). We found that larvae (enriched in somatic-dividing cells) are more sensitive to cisplatin than adults (only post-mitotic somatic cells), probably due to DNA-damage events. In adults, all somatic cell divisions have been completed and therefore somatic tissues tolerate high levels of DNA-insults. As a consequence the toxic effects of cisplatin are mainly driven by cytoplasmic events (Hemmingsson et al. 2010). Thus, a higher concentration of cisplatin was required to compromise the viability of

animals in adulthood than during development. By measuring the locomotor activity of the animals we monitored the cisplatin toxicity (Figure 18.A), and its capacity to cause lethality (Figure 18.B).

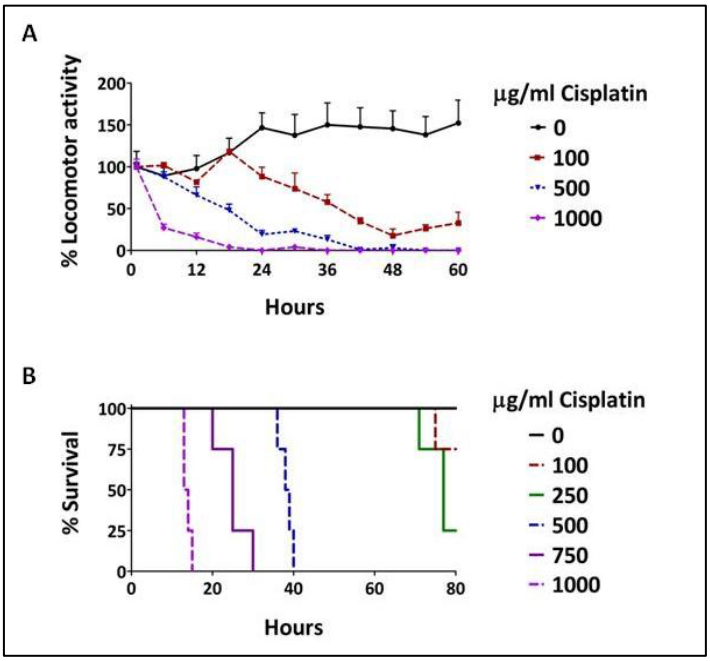

Figure 18. High concentration of cisplatin induces a progressive decrease in the locomotor activity causing lethality in adult worms in a dose-dependent manner.

(A) Plot exhibiting the locomotor activity in a synchronized population of young-adult worms, cultured in liquid media, and exposed to different doses of cisplatin. Locomotor activity is represented as percentage of variation respect to initial activity. Data are represented as mean and SD (n=4, 4 wells with 20 animals) This experiment was performed three different times with same results. (B) Survival staircase of a synchronized population of young-adult worms exposed to different doses of cisplatin in NGM plates. Death was determined by absense of movement in each replicate (n=4). Same result were obtained in three experiments.

R.1.4. *C. elegans* allows studying the somatic response to cisplatin in two scenarios

Thus, we have established in *C. elegans* the methodology to test the action of cisplatin in two contexts (Figure 19):

(i) Postembryonic development: somatic tissues with dividing cells where the cisplatin effects are mainly nuclear.
(ii) Adulthood: tissues with non-proliferating somatic cells where cisplatin effects are mainly cytoplasmic.

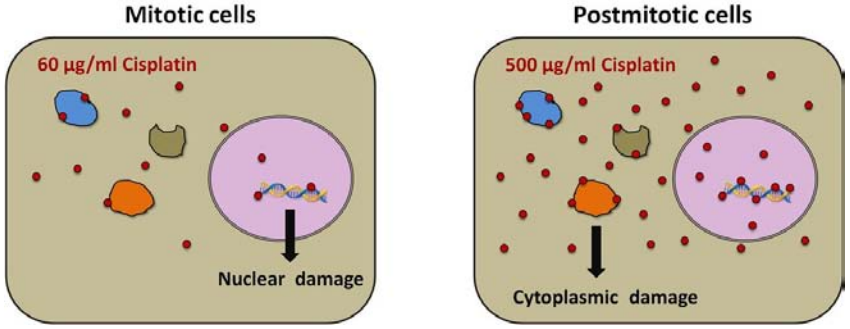

Figure 19. Schematic of cisplatin effects in mitotic and postmitotic cells.
In mitotic cell (developing larva), low levels of cisplatin are enough to induce DNA damage by nuclear events while in postmitotic tissues (adult worm), which tolerate high levels of DNA damage, higher concentrations of cisplatin are required to induce cellular damage, which is provoked by cytoplasmic events. Red spots represent cisplatin molecules. Nuclei in purple. Cytoplasmic proteins are represented in blue, orange and brown.

To support the different nature of these two scenarios, we analyzed the response to cisplatin of mutants for the translesion synthesis polymerase 1 (POLH-1). This protein has an essential role in repairing DNA damage caused by cisplatin in germ line resulting in embryonic lethality (Roerink

et al. 2012). These *polh-1* mutants showed sensitivity to cisplatin during larval development (Figure 20.A) but they did not display cisplatin sensitivity during adulthood (Figure 20.B). These results suggest that cisplatin phenotypes observed during postembryonic development probably are caused by a direct DNA-damaging effect of cisplatin in somatic mitotic cells.

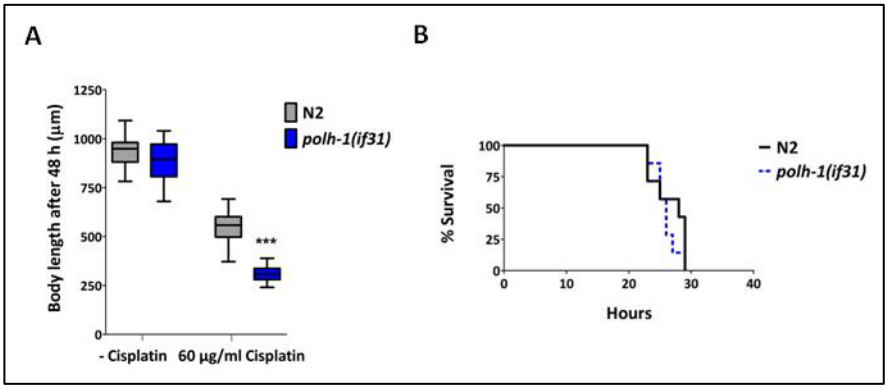

Figure 20. DNA repair is important for a response to cisplatin in larvae but not in adults.
(A) Developmental delay induced by cisplatin in control worms (N2) and *polh-1(if31)* mutants. ****p*<0,001 relative to control worms for each condition by Student's t-test. This assay was performed at least three times with similar results. For each condition, cisplatin untreated animals showed 100% survival (data not shown). (B) Survival staircase of young-adult worms treated with 500µg/ml of cisplatin. The assay was performed three times with similar results (n=8).

R.2. Transcriptional response of *C. elegans* to cisplatin

A better understanding of the *in vivo* response against cisplatin would be indeed desirable for improving therapeutic approaches to enhance the antitumor activity of this platinum-based drug. Deep sequencing technologies are allowing the study of transcriptomes on animals at high resolution. To get insights on how worms respond to this drug we analyzed the transcriptome of a mixed-stage population of worms treated with 60µg/ml of cisplatin for 24 hours. This concentration of drug, as mentioned above, produces some phenotypes but is compatible with the viability of the animals.

R.2.1. Cisplatin promotes the activation of apoptosis and stress-related genes, and diminishes the expression of sperm-specific genes

By processing two biological replicates and performing bioinformatic and statistical analyses we identified 83 genes upregulated and 78 genes downregulated by cisplatin (p>0.05) (Figure 21.A). To deeper study this set of genes we set a p-value of 0.01 as threshold, reducing the number of candidate genes to 28 upregulated and 29 downregulated. To explore the functions of these genes we used the Database for Annotation, Visualization and Integrated Discovery (DAVID) (Huang et al. 2009a; Huang et al. 2009b) and clustered them into functional categories defined by their gene ontology (GO) terms or predicted protein domains (Tatusov et al. 2003) (Figure 21B-C and Tables 5-6).

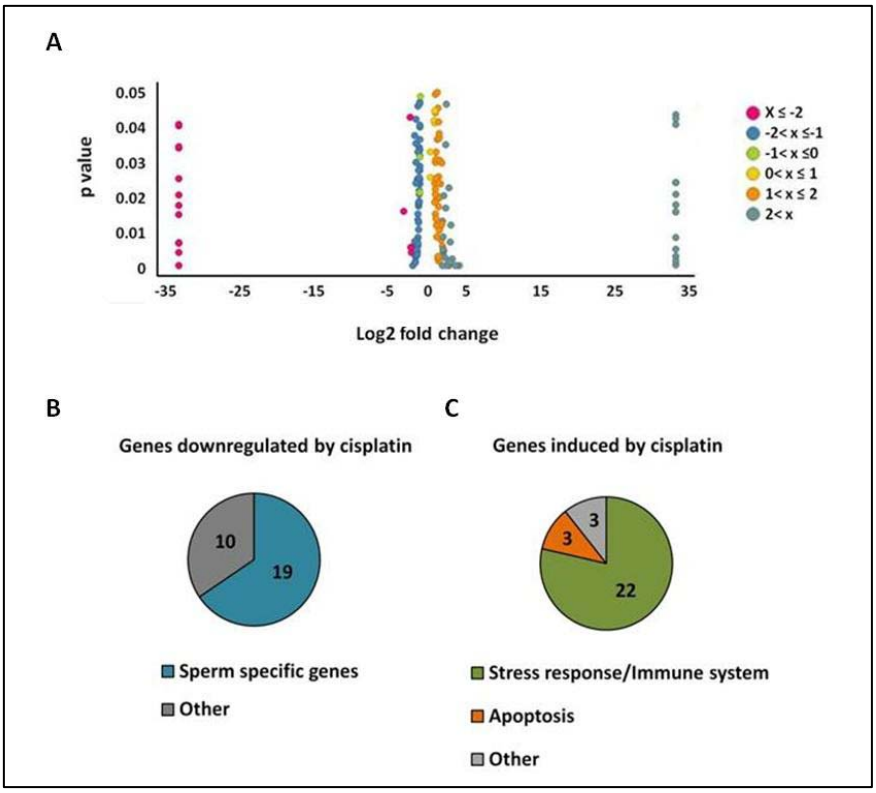

Figure 21. Transcriptomic analyses of cisplatin treated worms.
(A) Volcano plot showing genes significantly up- and downregulated (p<0,05) in a population of worms treated with 60µg/ml cisplatin (24h) compared to wild type (N2). Each dot represents a single gene. Color code represents the indicated fold change scale. (B) Functional categories of genes significantly downregulated (p<0,01) after a treatment of 60 µg/ml cisplatin for 24 hours. Genes were clustered according to DAVID the gene functional classification tool and GO terms retrieved from Wormbase.

Upregulated genes

Among the upregulated genes, we found an overrepresentation of functional categories associated to stress response and innate immune system. As example, we identified oxidoreductases belonging to phase I and II detoxification system, being the glutathione-s-transferase (GSTs) the GO category more represented (Table 5). Another group highly represented was the one composed by CUB-like domain proteins genes, whose motifs are associated to immune response and defense against pathogens (Shapira et al. 2006). Interestingly, among the cisplatin-induced genes we detected three related to apoptosis: *egl-1* and *ced-13*, involved in DNA-damage-dependent apoptosis, and *Y47G7B.2* (Greiss et al. 2008). Surprisingly, although the most relevant effect of cisplatin is to produce DNA double-strand breaks, we did not observe expression changes in genes related to DNA repair, DNA-damage checkpoints or other apoptotic genes. The fact that we were studying the transcriptome of a multicellular animal may mask the expression of these genes in specific cells. In summary, our RNA-seq experiments suggest that cisplatin in *C. elegans* induces at least the expression of DNA-damage-related apoptosis and the activation of stress response.

Sequence name	Gene name	Protein Domain	Log2 fold	Regulated by: DAF-16	SKN-1	IR
Apoptosis related genes (3)						
R09F10.9	*ced-13*	Single BH3 domain	33,33	-	-	+
F23B12.9	*egl-1*	Single BH3 domain	3,33	-	-	+
Y47G7B.2			2,12	-	-	+
Stress response/ innate immune response related genes (22)						
F55G11.6		CUB-like domain	33,33	-	-	-
Y51B9A.8		CC domain / ShKT domain	33,33	-	-	-
C41H7.7	*clec-3*	C-type lectin / CUB-Domain	4,29	-	-	-
F35E8.8	*gst-38*	Glutathione S-transferase	3,86	+	+	+
F55G11.2		CUB-like domain	3,75	+	+	+
ZK546.11	*gst-30*	Glutathione S-transferase	3,04	-	-	-
C32H11.4		CUB-like domain	2,91	+	+	+
C32H11.12	*dod-24*	CUB-like domain	2,85	+	+	+
F35E12.5		CUB-like domain	2,85	+	+	-
K08F4.7	*gst-4*	Glutathione S-transferase	2,56	+	+	-
K10C2.3	*asp-14*	Aspartic peptidase	2,41	-	+	-
W06H8.2		Aldolase-type TIM barrel	2,22	-	-	-
Y39G10AR.6	*ugt-31*	UDP-glucuronosyl/UDP-glucosyltransferase	2,16	-	+	-
C17H12.6		CUB-like domain	2,15	-	+	+
F37B1.2	*gst-12*	Glutathione-S-transferase	2,15	-	+	
K10D11.1	*dod-17*	CUB-like domain	2,06	+	+	+
Y40B10A.6	*comt-4*	O-methyltransferase family 3	1,99	+	-	-
C55A6.5	*sdz-8*	Oxidoreductase activity	1,87	-	-	
F11G11.3	*gst-6*	Glutathione-S-transferase	1,50	-	+	+
F56A4.2		C-type lectin	1,45	+	-	
K01D12.11	*cdr-4*	Glutathione S-transferase-like protein	1,42	-	-	+
F35E12.6		CUB-like domain	1,26	-	-	-
Other genes (3)						
Y108F1.4	*math-43*	Decapping exoribonuclease	33,33	-	-	-
Y54G2A.48		DUF4473	33,33	-	-	-
R09E10.2			2,96	-	-	-

Table 5. Genes induced by cisplatin.
Genes whose expression was significantly increased in two different experiments after a 60µg/ml cisplatin treatment. *p*-value<0.01.

Downregulated genes

Regarding the 29 genes downregulated by cisplatin, we found that most of those were sperm-specific genes (Ortiz et al. 2014), being the Major Sperm Protein domain (MSP) the GO category most frequent (Table 6). Therefore, the reduced brood size induced by cisplatin may be, at least partly, provoked by a specific effect of this agent in spermatogenesis or in sperm activity.

Sequence name	Gene name	Protein Domain	Log2 fold change
Sperm specific genes (20)			
F46A8.9			-33,33
C04G2.3		MSP domain	-1,74
R13H9.2	*msp-57*	MSP domain	-1,60
ZK354.1	*msp-65*	MSP domain	-1,60
ZK354.5	*msp-51*	MSP domain	-1,60
ZK354.4	*msp-113*	MSP domain	-1,58
C34F11.6	*msp-49*	MSP domain	-1,45
F32B6.6	*msp-77*	MSP domain	-1,45
C09B9.6	*msp-55*	MSP domain	-1,44
F58A6.8	*msp-45*	MSP domain	-1,41
R13H9.4	*msp-53*	MSP domain	-1,41
K07F5.2	*msp-10*	MSP domain	-1,40
ZK354.11	*msp-59*	MSP domain	-1,40
T13F2.11	*msp-78*	MSP domain	-1,38
F36H12.7	*msp-19*	MSP domain	-1,37
K07F5.3	*msp-56*	MSP domain	-1,37
ZK546.6	*msp-152*	MSP domain	-1,34
K07F5.1	*msp-81*	MSP domain	-1,28
ZK1251.6	*msp-76*	MSP domain	-1,26
R05F9.8	*msp-33*	MSP domain	-1,23
Other genes (9)			
F07C6.6			-33,33
M110.8			-33,33
Y60A9.3		Zinc finger, CCCH-type	-33,33
ZK666.6	*clec-60*	C-type lectin	-2,19
F53G12.9		Gluthatione-S-transferase	-2,13
F44C4.3	*cpr-4*	Peptidase C1A	-1,94
W03F9.4		Acyltransferase ChoActase/COT/CPT	-1,72
F09C8.1		Lipase, GDSL	-1,64
F58B3.1	*lys-4*	Glycoside hydrolase, family 25	-1,50

Table 6. Genes downregulated by cisplatin.
Genes whose expression was significantly decreased in two different experiments upon a 60µg/ml cisplatin treatment. *p*-value<0.01.

R.2.2. Cisplatin induces a dual response through the apoptotic and the IIS pathways

In addition to functional annotation clustering, we investigated the overlap between cisplatin-induced genes and published *C. elegans* datasets. According to cisplatin ability of activating DNA-damaged related apoptosis, we first explored the overlap with a set of genes induced by ionizing-radiation (IR) (Boyd et al. 2010). We found a significant enrichment of 11/29 genes (p<0,01 by Fisher's test). The list of common genes induced by IR and cisplatin includes genes involved in apoptosis and general stress response, suggesting that DNA-damaging agents as cisplatin could trigger in worms a dual response (Figure 22.A, Table 5).

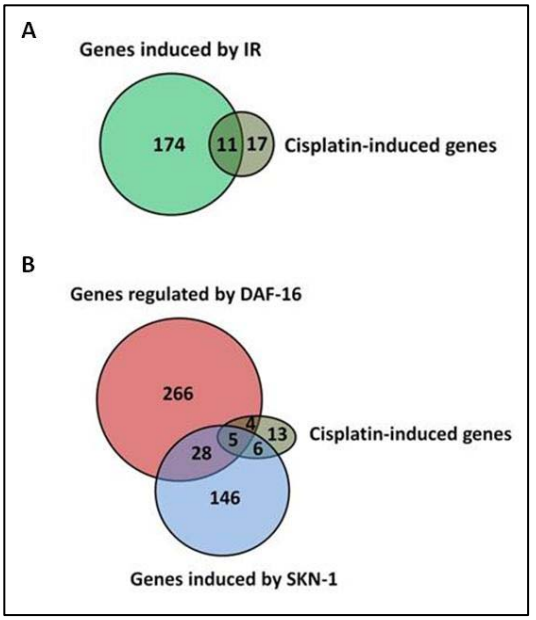

Figure 22. The transcriptional response produced by cisplatin includes DNA-damage response genes and DAF-16/FOXO and SKN-1/Nrf2 targets.
(A) Venn diagrams showing the significant overlap between genes induced by cisplatin (p<0.01 by Fisher's test) and by irradiation (genes with 2-fold increase at least) (Boyd et al. 2010). (B) Comparison between cisplatin-induced genes, DAF-16-regulated genes and SKN-1-induced genes (Tepper et al. 2013; Oliveira et al. 2009).

Since the evolutionary conserved insulin/insulin-like growth factor signaling (IIS) pathway plays a central role in the metabolic and proliferative adaptation to stress (Murphy & Hu 2013), we compared our dataset of cisplatin-induced genes with genes up and down regulated by the DAF-16/FOXO transcription factor (Tepper et al. 2013) and found a significant overlap (10 out of 28 genes, $p<0,01$ by Fisher's test) (Figure 22.B). These common genes are related to stress response and innate immune system (Table 5).

Due to the large number of cisplatin up-regulated genes belonging to phase II detoxification system, a group of enzymes that protect against oxidative and xenobiotic stresses (Blackwell et al. 2015), we also compared our dataset with genes induced by SKN-1/Nrf2 transcription factor. SKN-1 is also regulated by the IIS pathway, in parallel to DAF-16, and plays an essential role in the systemic response to oxidative stress, mainly by regulating the phase 2 detoxification system genes (Oliveira et al. 2009). We obtained a significant overlap of 11/29 genes ($p<0,01$) (Figure 22B, Table 5). Taken together, our data in *C. elegans* suggest that cisplatin induces both a DNA-damaged related apoptosis and a general stress response that would be modulated by IIS pathway through the regulation of DAF-16 and SKN-1 activities.

R.2.3. Cisplatin induces ectopic expression of the pro-apoptotic gene *egl-1* in somatic cells

We found that cisplatin induces the expression of three genes involved in the activation of apoptosis, namely *egl-1*, *ced-13*, and *Y47G7B.2*. It is known that these three genes are induced upon DNA damage and such induction is CEP-1/p53 dependent (Greiss et al. 2008). The only function described so far for *ced-13* is a modest role in promoting germ cell death after DNA damage. *Y47G7B.2* encodes a worm-specific gene without any apparent apoptosis-related phenotype (Schumacher et al. 2005; Greiss et al. 2008). However, *egl-1* is a key pro-apoptotic gene required for DNA-damage induced apoptosis in both somatic and germ cells (Gartner et al. 2000; Rubio-Peña et al. 2015). To confirm the ectopic expression of *egl-1* induced by cisplatin we used the reporter strain P*egl-1*::GFP. During larval development only 18 somatic cells of wild type worms undergo apoptosis during early L2 (Lettre & Hengartner 2006). However, a 24-hour cisplatin treatment in *C. elegans* induces ectopic P*egl-1*::GFP expression, particularly evident in hypodermal cells, which are somatic-dividing cells (Figure 23.A). In addition, the effect of cisplatin on P*egl-1*::GFP is dose-dependent in terms of number of worms, but also in terms of number of cells expressing P*egl-1*::GFP (Figure 23.B). We observed that cisplatin effect on P*egl-1*::GFP was evident at least in three larval stages (L2-L4) (Figure 23.A).

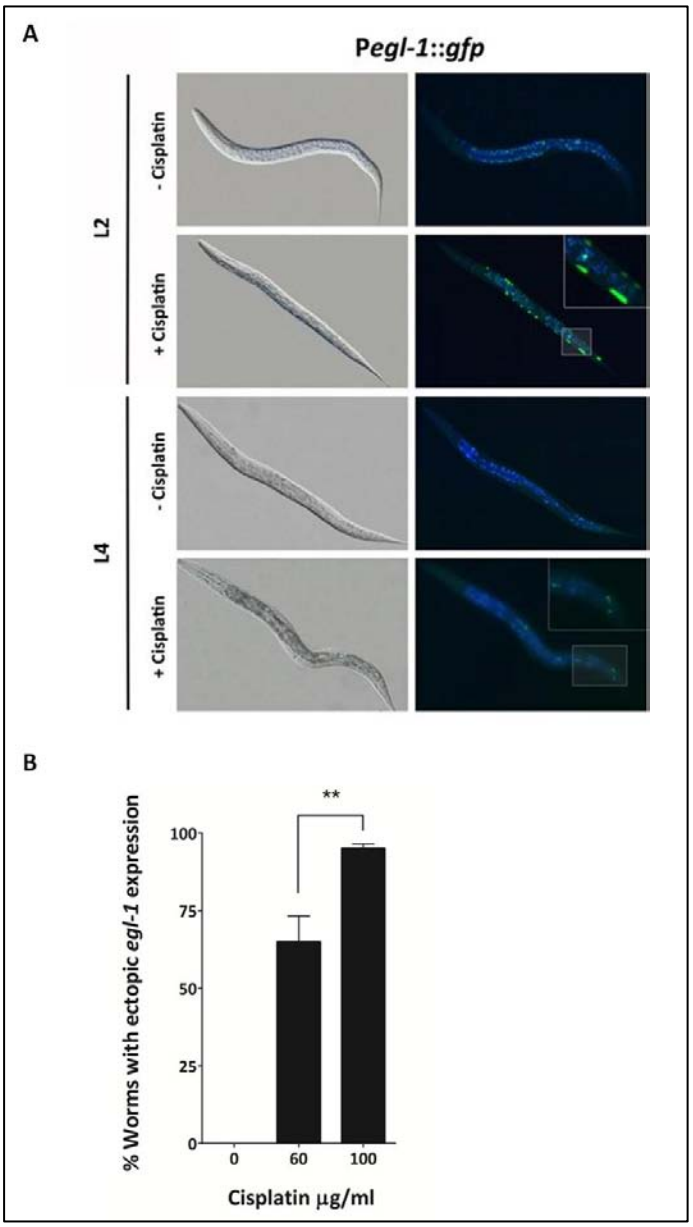

Figure 23. Cisplatin induces ectopic expression of the pro-apoptotic gene *egl-1* in somatic cells.

(A) Cisplatin induces *egl-1* ectopic expression in somatic tissues during larval development. Representative images of L2 and L4 stage worms carrying a P*egl-1::gfp* transgene upon a treatment of 60µg/ml of cisplatin for 24h. (B) Percentage of L2 worms with GFP fluorescence in somatic cells upon a cisplatin treatment. Bars represent mean and SEM of three different experiments (n=50). ** p<0,01 by Student's t-test.

R.2.4. Inhibition of apoptosis does not confer cisplatin resistance to *C. elegans*

Blockage of apoptosis is the main post-target mechanism of cisplatin resistance acquisition of tumors and, although is mainly caused by p53/*cep-1* inactivation (Vousden & Lane 2007), alterations in any factor that regulates or executes apoptosis should have the capacity to modulate the tumoral response to cisplatin. Inactivation of pro-apoptotic BCL2 protein family members (*egl-1* and *ced-1* are their *C. elegans* orthologues) results in cisplatin resistance acquisition in human cell lines (Castedo et al. 2006; Vitale et al. 2007; Tajeddine et al. 2008). To analyze whether blockage of apoptosis leads to increased resistance to cisplatin in *C. elegans* we observed the response to this drug during larval development of *cep-1(gk138)* and *egl-1(n1048n3032)* mutants, which lack all somatic apoptosis (Conradt & Horvitz 1998). No changes where observed in terms of resistance but, interestingly, *cep-1* showed even more sensitivity to cisplatin compared to control worms (Figure 24). Independently of the *cep-1* role in apoptosis, this protein takes part in other cell processes in *C. elegans* such as inducing cell cycle arrest upon DNA damage (Schumacher et al. 2001) or promoting DNA repair after some types of replicative stressors as hydroxyurea (Derry et al. 2007). Therefore, impairment of these processes could explain the increase of cisplatin sensitivity of these mutants. These results, together with evidences of cisplatin-induced necrosis in worms (Hemmingsson et al. 2010), allow to conclude that blockage of apoptosis is not the main mechanism of cisplatin resistance acquisition in *C. elegans*.

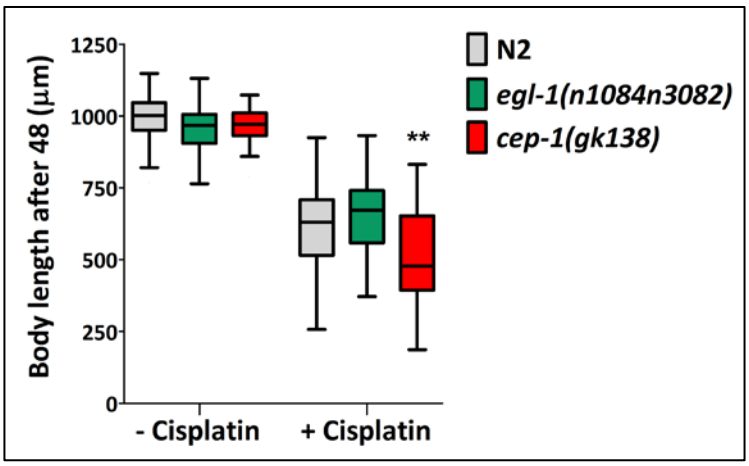

Figure 24. Blockage of apoptosis pathway does not confer resistance to cisplatin.
Inhibition of apoptosis signaling pathway by *egl-1(n1084n3082)* or *cep-1(gk138)* mutant alleles does not induce resistance to cisplatin (50µg/ml) during larval development. ** p<0,01 compared to control (N2) by Student's t-test.

R.2.5. The stress response triggered by cisplatin is mediated by the IIS pathway

As reported above, cisplatin induces the activation of some genes related to the stress response and the innate immune system, many of them being reported as downstream of the IIS pathway effector DAF-16/FOXO (Tepper et al. 2013). In *C. elegans*, the nuclear translocation of the transcription factor DAF-16 modulates the resistance to diverse stresses such as heavy metal exposure (Barsyte et al. 2001) or oxidative stress (Honda & Honda 1999).

Cisplatin promotes DAF-16 activity by inducing its nuclear translocation

To further investigate the link between the IIS pathway and cisplatin, we first studied the subcellular distribution of DAF-16 in the presence of cisplatin. We used a DAF-16::GFP reporter strain to analyze whether cisplatin was able to modify the cellular distribution of DAF-16, and therefore its activity. Under normal growth conditions, the IIS pathway is active and DAF-16 is mainly cytoplasmic. Interestingly, an exposure to cisplatin induces DAF-16 nuclear translocation (Figure 25) mimicking the effect of other stress conditions or the inactivation of the DAF-2/IGF-1-like receptor (McColl et al. 2010).

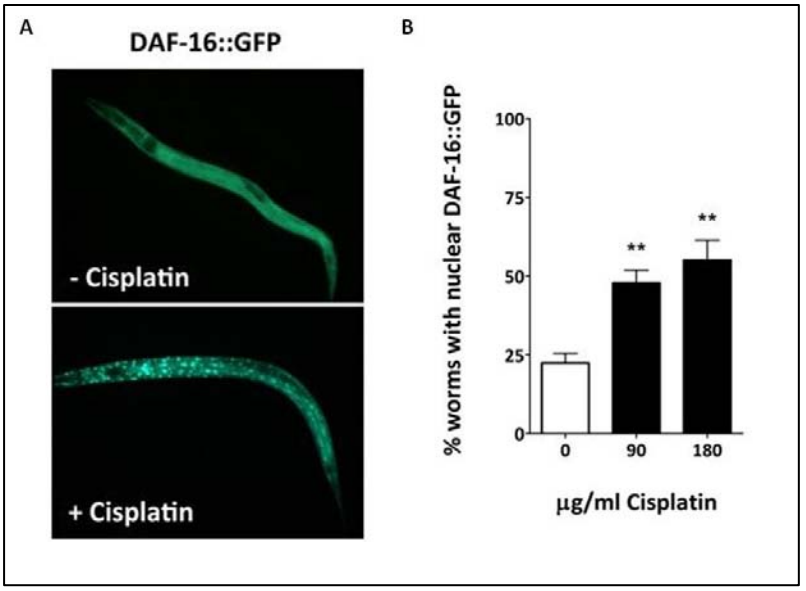

Figure 25. Cisplatin promotes DAF-16 nuclear translocation.
(A) Representative image of L2-staged worms carrying a translational reporter of DAF-16 and exposed to 90µg/ml cisplatin for five hours. (B) Graph indicating the percentage of worms with visible DAF-16:GFP nuclear fluorescence after different cisplatin treatments. Bars represent mean and SEM of three different experiments (n=50). ** $p<0.01$ relative to untreated worms by Student's t-test.

The IIS pathway is involved in the response to cisplatin

We investigated to what extent the manipulation of the IIS activity could modify the response of the organism to cisplatin. Thus, we observed that *daf-2(e1370)* mutants, which constitutively present DAF-16 in the nucleus (Lin et al. 2001), display resistance to cisplatin effects during larval development (Figure 26.A) and adult-stage worms (Figure 26.B). Consistently, *daf-16(mu86)* mutants were more sensitive to cisplatin in both larval and adult stages (Figure 26), highlighting the relevance of the nuclear activity of DAF-16 transcription factor in the cellular response to cisplatin. All together, the activity of IIS pathway key genes such as *daf-2* and *daf-16* is capable of influencing the response to cisplatin both in larvae and adult worms, underscoring the capacity of this pathway to mediate the cisplatin response through off-target mechanisms in both proliferating and postmitotic cells.

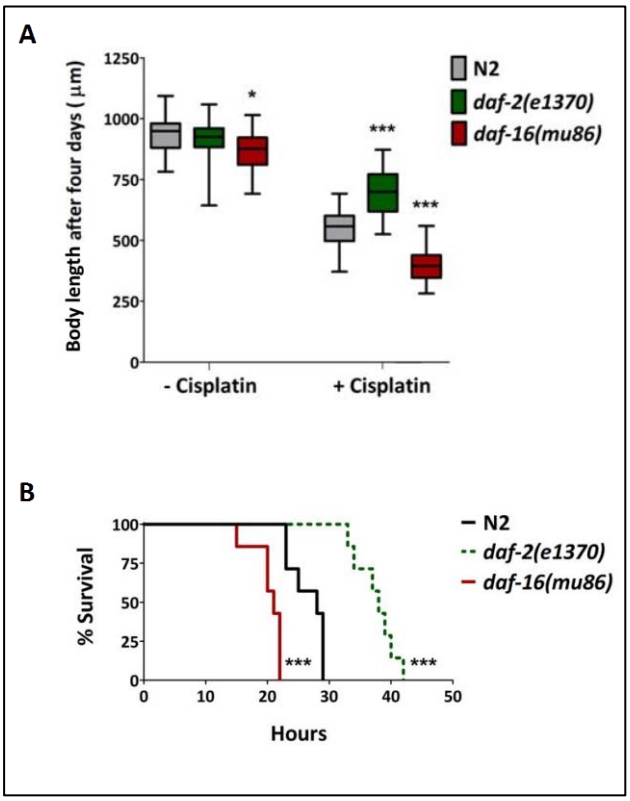

Figure 26. The Insulin/IGF-1 like signaling (IIS) pathway influences the response to cisplatin.
The inactivation of IIS pathway in *daf-2(e1370)* mutants, which keeps DAF-16 constitutively in the nucleus, produces resistance to cisplatin during larval development (50µg/ml) (A) and adulthood (500µg/ml) (B). In contrast, the lack of DAF-16 in *daf-16(mu86)* mutants makes these animals more sensitive to cisplatin. For each condition, cisplatin untreated animals showed a 100% of survival (data not shown). * $p<0.05$, *** $p<0.001$ relative to control (N2) worms for each condition.

- Levels of 14-3-3 proteins determine the response to cisplatin

As shown above, the presence of DAF-16 in the nucleus has a great impact in the cellular resistance to cisplatin. To further support this observation, we studied the 14-3-3 proteins, which regulate the nuclear localization of DAF-16. PAR-5 and FTT-2 are the two 14-3-3 existing

proteins in *C. elegans*, and the knock-down of either promotes DAF-16 nuclear translocation during larval development, mimicking *daf-2* mutant phenotypes (Berdichevsky & Guarente 2006; Li et al. 2007). Accordingly, we observed that *par-5(RNAi)* or *ftt-2(RNAi)* produce resistance to cisplatin during adulthood. Consistently, transgenic animals overexpressing PAR-5::GFP in somatic cells (Aristizábal-Corrales et al. 2013) are more sensitive to cisplatin than wild type animals (Figure 27). As conclusion, the amount of nuclear DAF-16, and therefore the capacity to resist the harmful cisplatin effects, can be regulated by the levels of cytoplasmic 14-3-3 proteins, which are conserved from worms to mammals.

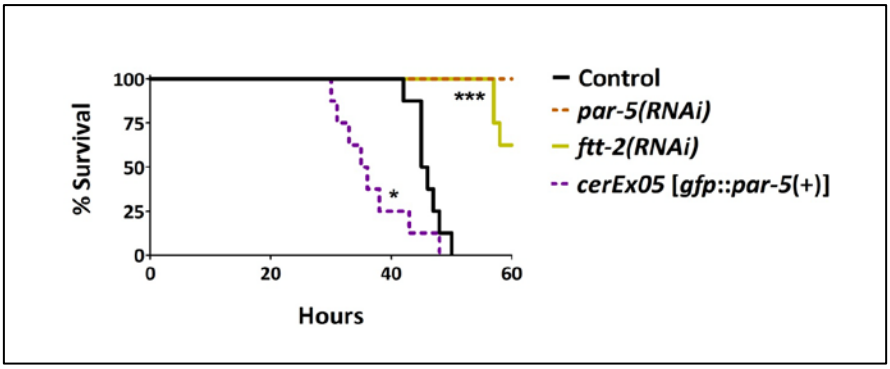

Figure 27. *C. elegans* 14-3-3 genes *par-5* and *ftt-2* influence the response of worms to cisplatin.
par-5(RNAi) and *ftt-2(RNAi)* generate resistance to cisplatin (500µg/ml) during adulthood while GFP::PAR-5 transgenic animals carrying extra copies of PAR-5 in somatic cells are sensitive. The assay was performed three times with similar results (n=8). **p*<0.05, ****p*<0.001 relative to control (empty vector). For each condition, cisplatin untreated animals showed 100% survival (data not shown).

R.2.6. Role of SKN-1/Nrf2 transcription factor in the response to cisplatin

As demonstrated above (Table 5), cisplatin upregulated genes showed a significant overlapping with genes downstream of SKN-1. The canonical role of this transcription factor in protecting worms against oxidative stress has been studied widely (Blackwell et al. 2015). Here we show the role of SKN-1 in the presence of cisplatin and the capacity of this transcription factor to modulate the response to this drug.

SKN-1/Nrf2 mediates the cisplatin-induced transcription of gst-4

Our dataset revealed that *gst-4* expression was induced in the presence of cisplatin. This gene is induced by several redox cycling compounds as paraquat (Tawe et al. 1998) or heavy metals (Roh et al. 2006). Moreover, such stress-induced transcription of *gst-4* is regulated by SKN-1 (Kahn et al. 2008; Hasegawa et al. 2008; Choe et al. 2009). We first monitored *gst-4* expression, with and without the presence of cisplatin, using a transcriptional GFP reporter (*Pgst-4*::GFP) (Link & Johnson 2002). Under control conditions, these worms showed a low GFP signal expression in longitudinal muscles and hypodermis (Figure 28). However, upon cisplatin exposure, these animals displayed an evident *gst-4* induction, being more prominent in the intestine.

To determine if SKN-1 is involved in this process, we studied the P*gst-4*::GFP signal in *skn-1(RNAi)* animals upon cisplatin exposure. Strikingly, these worms did not shown GFP induction in the presence of cisplatin (Figure 28). In contrast to *skn-1(RNAi)* worms, *daf-16(RNAi)* animals showed the same response than control worms. These results indicate that *gst-4* activation is SKN-1 dependent, demonstrating that SKN-1 participates in the response of *C. elegans* to cisplatin. Therefore DAF-16 is not the only key effector in the regulation of the stress response upon cisplatin exposure.

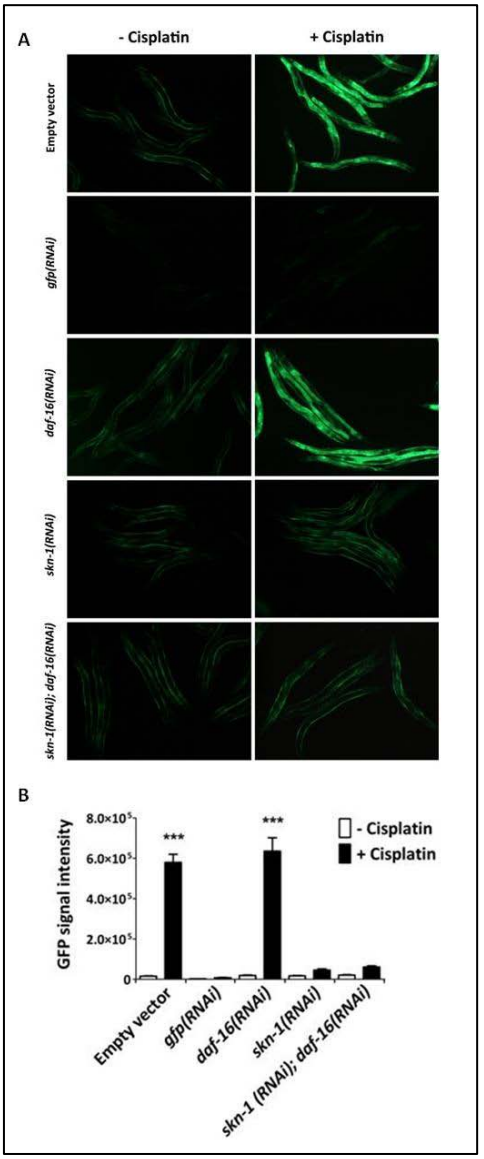

Figure 28. Cisplatin-induced activation of *gst-4* is regulated by SKN-1/Nrf transcription factor.

(A) Representative images of transgenic worms (L4/YA stage) expressing P*gst-4*::GFPand fed with *daf-16(RNAi)*, *skn-1(RNAi)* or both RNAis, with and without cisplatin (60µg/ml). The cisplatin-induced *gst-4* expression observed under control conditions (empty vector) was repressed by *skn-1(RNAi)*. Worms fed with *gfp* RNAi were used as positive control. (B) The graph shows the worm fluorescence for each condition. Bars represent the mean and error bars indicate the standard error of the mean (SEM) of two different experiments (N=30). ***p>0,001 relative to untreated animals by Student's t-test.

SKN-1/Nrf2 is required for a proper response to cisplatin

Since SKN-1/Nrf2 participates in the regulation of genes involved in detoxification and its downregulation has been associated to hypersensitivity to different stressor agents (Blackwell et al. 2015), we investigated the role of SKN-1 activity in the response to cisplatin. We observed that reduction of SKN-1 levels by RNAi in adults favors the sensitivity to cisplatin. *skn-1(RNAi)* animals present a lower survival rate in presence of cisplatin compared to wild type worms, but also to *daf-16(mu86)* mutants (Figure 29). These results suggest that although cisplatin promotes the activation of both transcriptions factors, and both are required for a proper response to cisplatin, SKN-1-associated response seems to have higher impact than DAF-16 response.

In addition, to determine the functional crosstalk between *skn-1* and *daf-16* functions in the response to cisplatin, we performed *skn-1(RNAi)* in d*af-16* mutant background. These worms showed a significant increase in the sensitivity to cisplatin compared to *daf-16* and also a weak hypersensitivity compared to *skn-1(RNAi)* alone. This experiment suggests that both proteins are involved in the response to cisplatin by activating different mechanisms.

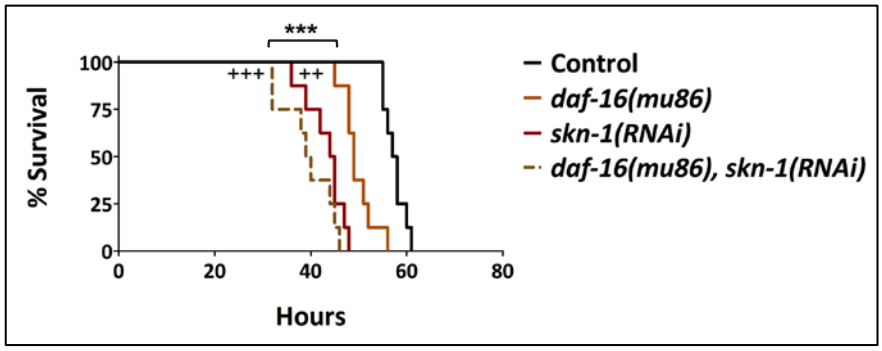

Figure 29. SKN-1 and DAF 16 cooperate in the response to cisplatin.
Survival staircase of adult worms treated with 500 µg/ml of cisplatin. Worms fed with *skn-1* RNAi or *daf-16(mu86)* mutant allele showed hypersensitivity to cisplatin, compared to control worms (*gfp* RNAi). The hypersensitivity observed in *daf-16(mu86)* was significantly increased by feeding these animals with *skn-1(RNAi)* bacteria. ***p<0.001 relative to control. ++ p<0,01, +++ p<0,001 relative to *daf-16(mu86).* For each condition, cisplatin untreated animals showed 100% survival (data not shown).

To support the hypothesis of two independent mechanisms in cisplatin response, we analyzed the role of the SKN-1-induced gene *gst-4* in the presence of cisplatin. *gst-4(RNAi)* animals showed a wild type response to cisplatin (Figure 30). Interestingly, *gst-4(RNAi)* enhances the sensitivity to cisplatin in *daf-16(mu86)* mutants but not in *skn-1(RNAi)* animals. These experiments demonstrate that, in the response to cisplatin, *gst-4* and *skn-1* are in a common pathway, but *daf-16* acts through different mechanisms.

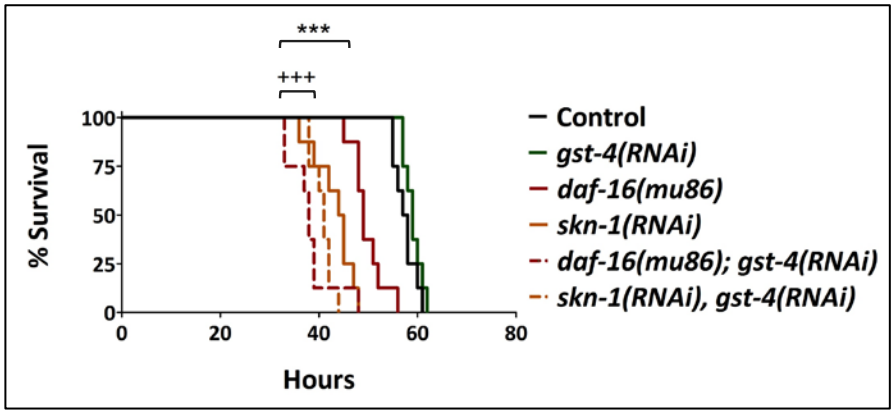

Figure 30. The GST-4/SKN-1 pathway and the DAF-16 pathway regulate the sensitivity to cisplatin by different mechanisms.
Survival staircase of adult worms treated with 500 µg/ml of cisplatin under different conditions. *gst-4(RNAi)* animals did not present alterations in the response to cisplatin while a significant increase in cisplatin sensitivity was observed in *daf-16(mu86);gst-4(RNAi)* animals compared to *daf-16(mu86)* worms. Control worms were treated with *gfp(RNAi)*. *skn-1(RNAi)* was used as negative control ***p<0.001 relative to control. +++ p<0,001 relative to *daf-16(mu86)*. For each condition, cisplatin untreated animals showed 100% survival (data not shown).

R.2.7. Cisplatin-induced genes *cdr-1* and *dod-24* confer resistance to cisplatin

The cadmium responsive gene cdr-1 promotes resistance to cisplatin toxicity

We examined if modulation of cisplatin up-regulated genes could have an effect in the response to cisplatin. Our dataset revealed that cisplatin induces the expression of several proteins containing a gluthatione S-transferase domain that is directly involved in cisplatin quelation and

detoxification (Goto et al. 1999). Elevated levels of these enzymes have been related to resistance to cisplatin in cancer cell lines both *in vitro* and *ex vivo* (Sawers et al. 2014; Abbas et al. 2015). *cdr-1* and *cdr-4* belong to a group of glutation-s-transferases related to cadmium response as detoxification genes (Cui et al. 2007). This gene family is composed of seven paralogs (*cdr-1* to *7*) but only *cdr-1* and *cdr-4* are transcriptionally induced by cadmium while the exposure to any other metal or stressor does not seem to affect their transcription (Dong et al. 2005). However, only CDR-1 inhibition results in increased sensitivity to cadmium (Dong et al. 2008; Liao et al. 2002). To determine if CDR-1 knock-down also increases the sensitivity to cisplatin in worms we analyzed response of *cdr-1* mutants to this drug. We found that *cdr-1(ok3456)* worms are sensitive to cisplatin both in larva and adulthood, compared to control animals (Figure 31.A-B). We also tested the effect of cisplatin in two different transgenic strains overexpressing *cdr-1*. As expected, these worms showed higher resistance to cisplatin compared to control animal (Figure 31.C-D) demonstrating that CDR-1 levels influence the response to cisplatin. Therefore, *cdr-1* in worms does not function exclusively in the presence of cadmium, but also has a relevant role in the response to cisplatin.

To investigate the functional crosstalk between *cdr-1* and the IIS pathway, we studied the effect of cisplatin in the double mutant *cdr-1(ok3456); daf-16(mu86)*. We observed these worms did not display a synergistic sensitivity to cisplatin. Instead, they showed similar sensitivity to cisplatin than *cdr-1* and *daf-16* single mutants. These data suggest that CDR-1functions in the response to cisplatin are not additive to the DAF-16 effect.

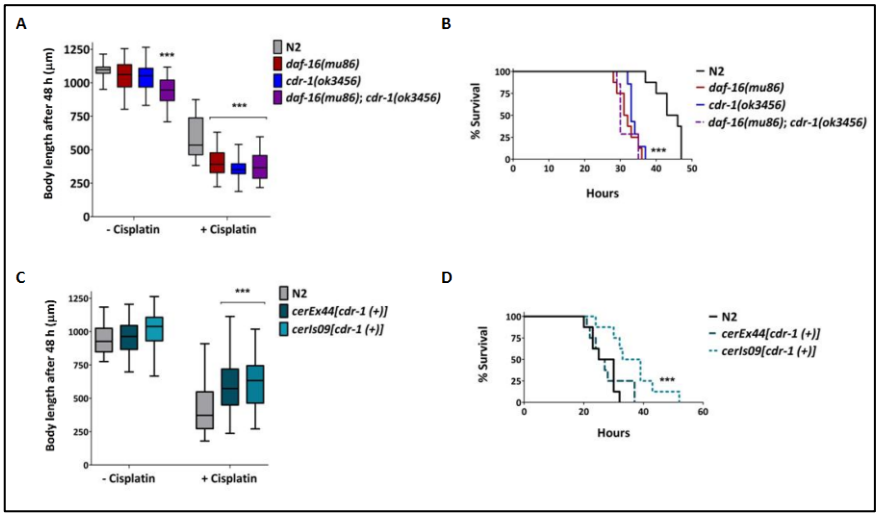

Figure 31. The cisplatin-induced gene *cdr-1* confers resistance to cisplatin in larvae and adults.
Lack of CDR-1 produces sensitivity to cisplatin during adulthood (A) and in larval development (B). Combination of *cdr-1(ok3456)* and *daf-16(mu86)* mutant alleles does not produce a synergistic effect in terms of sensitivity. Additional copies of the *cdr-1* gene, integrated in the genome (Is) or as extrachromosomal arrays (ex), provide resistance to cisplatin both in larvae and adults (C and D). *** $p<0.001$ compared to control (N2). For each condition, cisplatin untreated young-adult worms showed 100% survival (data not shown).

The CUB-like related gene dod-24 confers resistance to cisplatin

Cisplatin also induces the expression of several CUB-like domains related genes. This family comprises a group of 50–60 genes whose sequence is related to CUB domains, a group of proteins that are normally found extracellularly, including proteases and complement components of the mammalian immune system (Shivers et al. 2008). In *C. elegans* these genes participate in innate immune response against pathogens and the exposure to other DNA-damaging agents also induce their overexpression (Boyd et al. 2010). Among the upregulated CUB-like domain containing

genes we observed that some of them are "downstream of daf" as *dod-24*, and *dod-17*. Both genes are ortholog to human epoxide hydrolase, an enzyme with an important role in the inflammatory response whose inhibition is associated to cisplatin-reduced nephrotoxicity (Y. Liu et al. 2012). Additionally, *dod-24* knock-down is able to live longer (Murphy et al. 2003). Thus, to investigate if DOD-24 is related to cisplatin response, we studied the developmental delay and lethality induced by cisplatin in *dod-24(ok2629)* mutants. Interestingly, these worms resulted more sensitive to cisplatin compared to control in both developmental stages (Figure 32) suggesting that DOD-24 is required for responding to cisplatin.

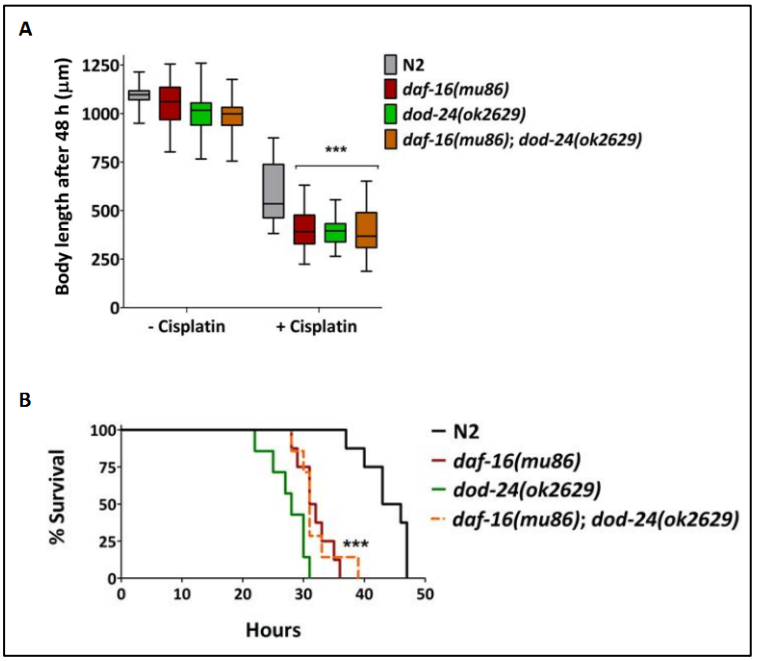

Figure 32. The cisplatin-induced gene *dod-24* confers resistance to cisplatin in adults and larvae influenced by DAF-16.
DOD-24 is required to a proper response to cisplatin during larval development (A) and in adulthood (B) while combination of *dod-24(ok2629)* and *daf-16(mu86)* mutant alleles does not produce a synergic effect in terms of sensitivity. ****p*<0,001 relative to control (N2) worms for each condition. For each condition, 100% untreated animals survived (data not shown).

Moreover, *daf-16* and *dod-24* double inactivation did not show any additive effect in cisplatin sensitivity compared to single inactivation. This result suggests that DAF-16 could also mediate in the response of DOD-24 functions upon cisplatin exposure indicating that this gene, similar to *cdr-1*, may act through the IIS pathway in response to cisplatin.

Summarizing, in this section we have reported that cisplatin-induced damage provokes in worms a systemic response promoting the activation of a set of genes whose transcription could be mediated by IIS-related transcription factors SKN-1 and DAF-16. In addition, altering both IIS-pathway-related genes and some of their targets (*cdr-1*, *dod-24*), leads to modify the response to cisplatin.

R.2.8. Several *C. elegans* cisplatin-induced genes show a functional correlation with resistance acquisition to cisplatin in human tumors

In order to investigate a connection between the response to cisplatin in *C. elegans* and its resistance acquisition process in human tumors, we analyzed in a cohort of cisplatin-resistant ovarian orthoxenografts the expression levels for the human orthologs of the genes that were upregulated in *C. elegans* upon cisplatin exposure (Table 7).

C. elegans sequence	*C. elegans* gene name	Human ortholog	Description	BLAST E-value
R09F10.9 F23B12.9	*ced-13* *egl-1*	BAD*	BCL2-associated agonist of cell death	-
C55A6.5	*sdz-8*	RDH11	Isoform 1 of Retinol dehydrogenase 11	4.3e-10
Y108F1.4	*math-43*	DXO**	Decapping exoribonuclease	Panther
K08F4.7 F11G11.3 F37B1.2 ZK546.11 F35E8.8	*gst-4* *gst-6* *gst-12* *gst-30* *gst-38*	HPGDS/ GSTP1***	Glutathione S-transferase P	2.0e-14 2.0e-17 6.0e-17 3.0e-12 3.0e-17
C17H12.6 C32H11.4 K10D11.1 C32H11.12 F55G11.2	*dod-17* *dod-24*	EPHX1**	Epoxide hydrolase 1, microsomal	Panther
Y40B10A.6	*comt-4*	COMTD1	Catechol-O-methyltransferase domain containing 1	7.0e-34
C41H7.7	*clec-3*	CSMD1 MCR1	CUB and sushi domain-containing protein 1 Mannose receptor, C type 1	2.0e-14 4.8e-12
K10C2.3	*asp-14*	PGC	Progastricsin (pepsinogen C)	8.8e-21
F35E8.11 K01D12.11	*cdr-1* *cdr-4*	FAXC	Failed axon connections homolog	8.0e-21 2.6e-18
Y39G10AR.6	*ugt-31*	UGT3A2	UDP glycosyltransferase 3 family, polypeptide A1	2.5e-38

Table 7. Human orthologs to genes induced by cisplatin in *C. elegans*.
BLAST e-value indicates the statistical significance for the alignment between *C. elegans* and human proteins. * No homology in terms of sequence but similar functions. ** Functional relation based on PANTHER (Mi H. et al 2010). ***Selected as member of the GST protein family.

Analyzing each gene expression by RT-qPCR (Figure 33), a similar tendency than in *C. elegans* was observed for MCR1/*asp-14*, FAXC/*cdr* and UGT3A2/*ugt-31* human genes and *C. elegans*. The expression levels of these genes were mostly upregulated in the cisplatin refractory tumors analyzed, but is not correlated to tumor histology. In contrast, minimal or no changes were observed in the rest of the genes. In addition, the tendency to keep these modifications during tumor passages may indicate a selective pressure over these changes in the process of resistance acquisition. We observed that, in those genes with a direct relationship with cisplatin detoxification such as FAXC (glutathione S-transferase) and UGT3A2 (UDP-glucuronsyl transferase), gene upregulation was always maintained during tumor passages, which could reveal a possible role for these two genes in cisplatin refractoriness. Thus, these results support the evolutionary conserved role of stress response genes in the cisplatin resistance acquisition.

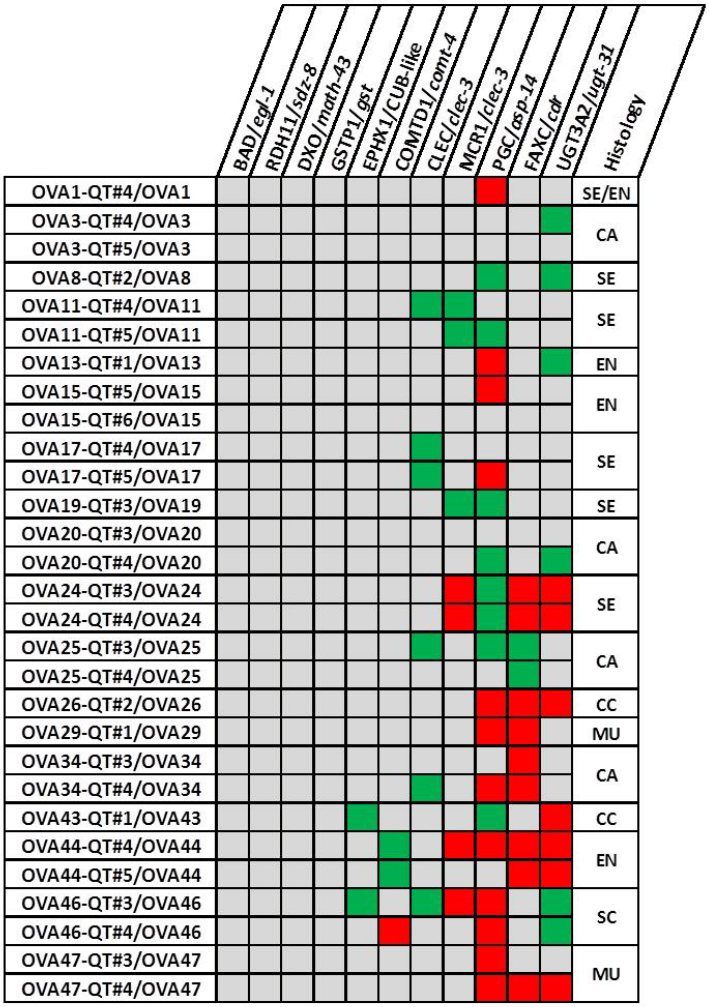

Figure 33. Differential profiling expression patterns for all human orthologs to *C. elegans* genes induced by cisplatin in cisplatin resistant ovarian tumors. **(**A) Results are presented as changes in the expression levels in cisplatin refractory tumors relative to the untreated tumors. No expression changes (in grey), > 3-fold underexpression in resistant tumors (in green), > 3-fold overexpression in resistant tumors (in red). Tumor histology abbreviated as: SE: Serous, EN: Endometrioid, CA: Carcinosarcoma, CC: Clear Cell, MU: mucinous tumor

R.2.9. Spermatogenesis is more sensitive to cisplatin than oogenesis

C. elegans germ line is a powerful tool to study the effect of a wide variety of molecules in cell-cycle regulation and DNA damage response (Gartner et al. 2004). As we described above, cisplatin produces reduced brood size, a decrease in the number of germ cells, and an increase in the cell size at the proliferative region of the gonad (Figure 16). Such increase in cell size indicates arrest upon S-phase checkpoint activation (Gartner et al. 2004). Despite all these phenotypes, to our surprise, our dataset revealed most of genes downregulated upon cisplatin treatment were sperm-specific, being the vast majority genes containing a major sperm protein domain (Table 6). Accordingly, worms treated with cisplatin displayed an increase in unfertilized oocyte laying (Figure 15.B), pointing towards a possible defect in spermatogenesis. However, cisplatin treated gonads apparently did not show any obvious phenotype in terms of sperm number or morphology.

To analyze whether the production of unfertilized oocytes is due to a failure in sperm function we crossed cisplatin treated hermaphrodites with untreated males that provided wild type sperm (Figure 34.A). These cross-fertilized worms did not lay unfertilized oocytes and the brood size was significantly higher compared to non-crossed animals treated with cisplatin, although they did not reach wild type levels. These results suggest that the production of unfertilized oocytes of cisplatin-treated animals is mainly caused by a defect in spermatogenesis.

To study the effect of cisplatin in spermatogenesis and oogenesis separately we used the *fog-2(oz40)* mutant strain, which presents two separate sexes: females (hermaphrodites that do not produce sperm) and males. Females treated with cisplatin and crossed with untreated males

showed 2-fold lower brood size compared to control animals confirming the effect of cisplatin during oogenesis, but we did not observe a phenotype related to unfertilized oocytes. On the other hand, males treated with cisplatin and crossed with untreated females produced even more reduced brood size and an increase in unfertilized oocyte laying. These results confirm that the production of unfertilized oocytes upon cisplatin exposure is exclusively provoked by a failure in sperm functionality (Figure 34.B).

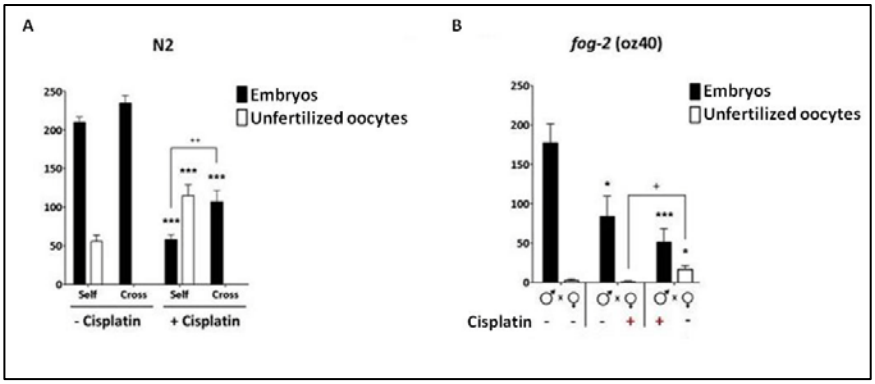

Figure 34. Spermatogenesis is more sensitive to cisplatin than oogenesis.
(A) Cisplatin reduces the progeny and increases the number of unfertilized embryos (laid oocytes) in *C. elegans* hermaphrodites. Crossing treated animals with untreated males increased the fertilized/unfertilized ratio. Self: self-fertilization progeny. Crossed: Crossed progeny. Bars show mean and SEM of two different experiments (n=12). ****p*>0,001 compared to untreated animals. ++*p*>0,01 compared to self-fertilized animals under the same conditions. (B) The increase of unfertilized embryos laid (oocytes) upon cisplatin treated animals is caused by defective sperm. *fog-2(oz40)* hermaphrodites do not produce sperm and mating is necessary for fertilization. Cisplatin-treated males crossed with untreated females produce more unfertilized embryos than cisplatin-treated females crossed with untreated males. + or - indicates cisplatin-treated or untreated respectively.

R.3. Functional studies in *C. elegans* to unravel the role of selenocysteine in the response to cisplatin

As described above, we have revealed the role of several oxidative stress responsive genes in the response to cisplatin. Since the thioredoxin system, together to the glutathione system, is fundamental in the redox defense against cisplatin (Muller 1996; Kanzok 2001; Peng, Xu & Elias S. J. Arnér 2012), we decided to study the importance of thioredoxin reductase 1 (TrxR1) in the response to cisplatin. Interestingly, it has been shown that TrxR1 selenocysteine amino acid is a direct target of cisplatin producing cytotoxic TrxR1 forms *in vivo* (Anestål et al. 2008).

C. elegans thioredoxin reductase 1 (TRXR-1) is the only selenoprotein (protein that includes a selenocysteine amino acid) in worms and, in contrast to mammals, this protein is not essential for viability (Li, Bandyopadhyay, Hwaang, B.-J. Park, et al. 2012). Inhibition of *C. elegans trxr-1* does not produce phenotypes in terms of morphology, growth, lifespan, brood size or response to oxidative stress. It is only essential for larval molting when *gsr-1* is inactivated in parallel (Stenvall et al. 2011). These features make of *C. elegans* a great pluricellular system to specifically study the role of the selenocysteine residue in the response to cisplatin.

R.3.1. TRXR-1 is required for cisplatin cytotoxicity

To analyze the role of TRXR-1 in the response to cisplatin we first observed the effect of cisplatin on the *trxr-1(sv47)* null mutant strain. These worms evidenced more resistance to cisplatin during larval development (Figure 35.A). On the contrary, no differences were observed in the response to cisplatin during adulthood (Figure 35.B). These results indicate that TRXR-1 functions are required for cisplatin cytotoxicity during larval development.

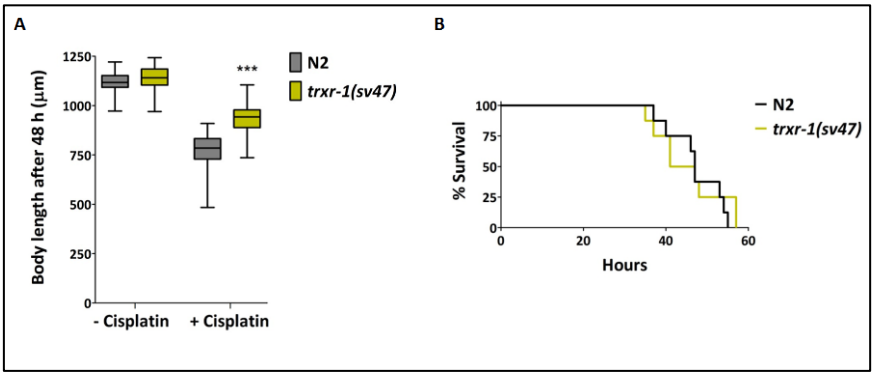

Figure 35. TRXR-1 is required for cisplatin cytotoxicity effect during larval development.
trxr-1(sv47) null allele shows increased resistance to cisplatin in developing larva (A), but wild type response in adults (B). ****p*<0,001 relative to control (N2).

R.3.2. TRXR-1 Sec amino acid influences the response to cisplatin

In human cell lines, cisplatin affects TrxR1 normal functions by binding to the selenocysteine residue and producing highly pro-oxidant forms of this enzyme, called SecTRAPs, that leads to high redox stress resulting in cell death (Anestål et al. 2008). In this process, the selenocysteine residue is essential, since TrxR1 variants that contains cysteine instead selenocysteine, formed in some *in vivo* conditions as selenium deficiency, display reduced sensitivity to cisplatin (Anestål et al. 2008; Peng, Xu & Elias S. J. Arnér 2012). In addition, it has been shown that Sec-compromised TrxR1 variants positively regulate Nrf2 transcription factor promoting better response to cisplatin.

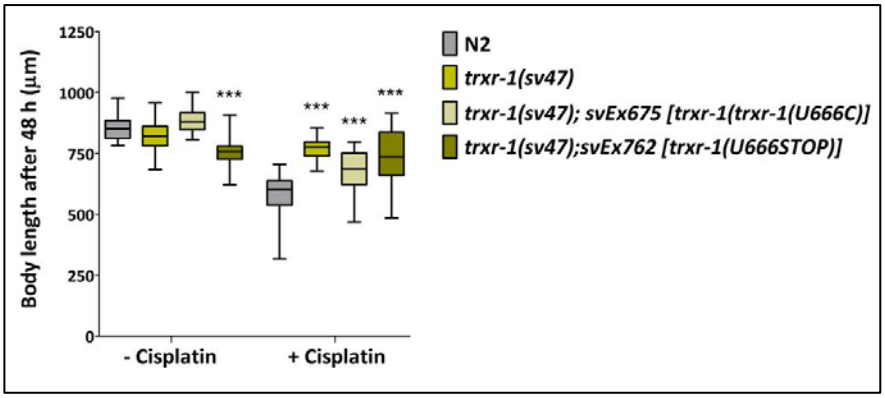

Figure 36. *C. elegans* response to cisplatin depends on a single Sec residue. Extrachromosomal transgenic lines expressing TRXR-1 variants lacking the Sec amino acid show similar increased resistance to cisplatin than the null allele *trxr-1(sv47)*. ***$p<0.001$ relative to control (N2) worms for each condition.

To investigate the nexus between selenocysteine and cisplatin in a living animal, we used two transgenic strains that carry two different TRXR-1 variants in a *trxr-1(sv47)* background: VB2155, that contains cysteine instead selenocysteine and VZ50 which carries an early stop codon producing a truncated version of TRXR-1 that lacks the last two amino acids (Sec-Cys). Both extrachromosomal arrays produce stable proteins that cannot reduce TRX-1, resulting in *trxr-1(sv47)* related phenotypes in terms of molting (Stenvall et al. 2011). These transgenic animals showed resistance to cisplatin similarly to *trxr-1(sv47)* mutants (Figure 36), indicating that a single selenocysteine residue is required to produce a normal cytotoxic effect in multicellular organisms upon cisplatin exposure.

Taking advantage of the possibilities in genome editing that the CRISPR/Cas9 system offers, we produced two endogenous TRXR-1 variants with the same substitutions: *trxr-1(cer4[U666C])* and *trxr-1(cer5[U666STOP])* (see methods for detailed info) to validate the results obtained with the extrachromosomal arrays. Similarly to VB2155 and VZ50 extrachromosomal arrays and the null mutant *trxr-1(sv47)*, these genetically engineered worms showed larval arrest, due to molting defects, in combination with *gsr-1(RNAi)* (Figure 44.A) and resistance to cisplatin (Figure 37.B) confirming the significant relevance of the selenocysteine amino acid in promoting cisplatin cytotoxicity. Thus, both the developmental role and the capacity to promote cytotoxicity in presence of cisplatin rely on a single amino acid.

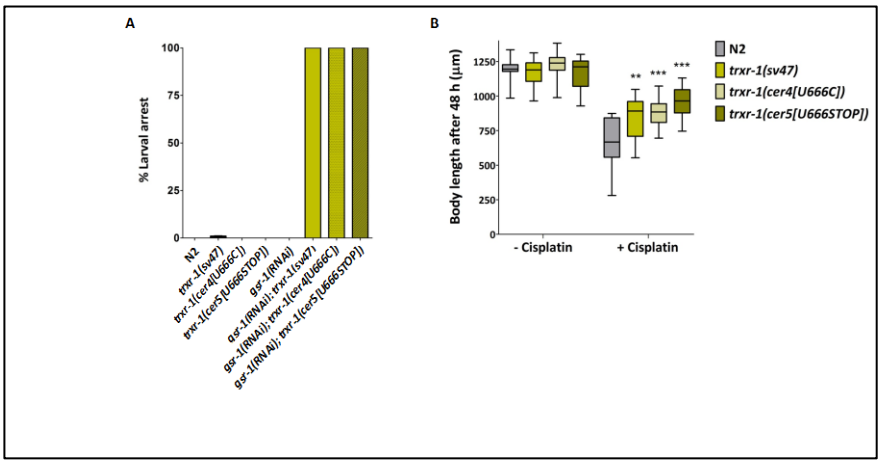

Figure 37. Sec amino acid is required for the TRXR-1 activity and for cisplatin cytotoxicity.
(A) Sec deficient *trxr-1* alleles cause the molting-associated growth arrest displayed by *gsr-1(RNAi);trxr-1(sv47).*(B) TRXR-1 variants lacking the Sec residue show resistance to cisplatin similarly to the null allele *(sv47).* ***p<0,001 relative to control (N2) worms for each condition.

R.4. From mammals to worms: *C. elegans* as tool to validate genes involved in the resistance/sensitivity to cisplatin

Our research group was able to generate a representative collection of paired orthotopically transplantable patient-derived cisplatin-sensitive/resistant testicular tumors in nude mice (orthoxenografts) (Figure 13). Such approach allows the study of genetic alterations related to tumor resistance to cisplatin in the same genetic background. As a result, our laboratory found several recurrent genetic imbalances that were present in distinct resistant tumors, being the most recurrent the amplification in the 9q32-q33.1 region of the human genome (Piulats et al., to be submitted). Consistently, this region contains genes whose expression has been described as altered in cisplatin resistant tumors and genes previously associated to the response to this agent such as the copper transporters CTR1 and CTR2 or the glucosylceramide transferase (GCT) (Gouazé et al. 2005; Burger et al. 2011) (Figure 14).

To further analyze the individual contribution of genes present at the 9q32-q33.1 region, we assayed the response to cisplatin of the corresponding *C. elegans* orthologs. To do so, we decided to test the function of these genes on the cytotoxic effect of cisplatin by using RNAi.

R.4.1. A RNAi-based approach uncovered a role in cisplatin response for several *C. elegans* orthologs of genes present at the 9q32-q33.1 region

The 9q32-q33.1 region contains 62 genes. First we filtered out those genes that were not expressed in the collection of testicular germ cell tumors, to get a list of 37 genes. Then, BLAST analyses reduced our list of genes of interest to 16 *C. elegans* orthologs (Table 8). To investigate the individual contribution to the response to cisplatin of these genes, we first performed the RNAi of these 16 genes and we exposed them to cisplatin in young-adult stage to avoid RNAi phenotypes during larval development. Interestingly, we found that RNAi of six genes were capable to modify the response to cisplatin in *C. elegans* (Table 8, Figures 38-40)

Human gene	*C. elegans* ortholog	*C. elegans* gene name	Description	BLAST E-value	Cisplatin response
AKNA	-	-	-	-	
ALAD	-	-	-	-	
AMBP	C37C3.6	*mig-6*	Thrombospondin, type 1	6e-20	None
ATP6V1G1	F46F11.5	*vha-10*	Vacuolar proton-translocating ATPase, subunit G	7e-18	Sensitive
BSPRY	-	-	-	-	
C9orf147	-	-	-	-	
C9orf43	-	-	-	-	
C9orf80	-	-	-	-	
C9orf84	-	-	-	-	
C9orf91	-	-	-	-	
CDC26	-	-	-	-	
CTR1 CTR2	F27C1.2		Copper ion transmembrane transporter activity	5e-15 3e-08	Resistant
DEC1	Y54G2A.1	*lin-22*	Helix-loop-helix (bHLH)-containing protein	7e-03	-
DNAJC25	B0035.2	*dnj-2*	Protein containing a DnaJ domain	2e-62	Sensitive
EDG2	AC7.1	*tkr-3*	G protein-coupled receptor, rhodopsin-like	6e-11	None
FLJ31713	-	-	-	-	
GCS	T06C12 F20B4.6 T06C12.10	*cgt-1* *cgt-2* *cgt-3*	Ceramide glucosyltransferase	9e-88 3e-93 1e-93	Sensitive
GNG10	K02A4.2	*gpc-1*	Heterotrimeric guanine nucleotide-binding protein	7e-09	None
HSDL2	C17G10.8	*dhs-6*	Short-chain dehydrogenase/reductase SDR	4e-46	None
KIAA1958	-	-	-	-	
LOC552891	-	-	-	-	
LTB4DH	M106.3		Alcohol dehydrogenase superfamily, zinc-type	5e-29	Non tested
OR2K2	Y39A3B.5	*ckr-2*	Cholecystokinin receptor	7e-07	Sensitive
ORM2	-	-	-	-	
PAPPA	-	-	-	-	
POLE3	T26A5.8		Polymerase (DNA directed), epsilon 3, accessory subunit	5e-08	None
ROD1	D2089.4	*ptb-1*	Polypyrimidine tract binding protein PTB.	1e-120	None
SLC46A2	Y4C6B.5		Major facilitator superfamily domain	1e-05	None
SUSD1	F47C12.2	*clec-78*	C-type lectin	1e-09	-
TNC	R13F6.4	*ten-1*	Teneurin	1e-43	None
TNFSF15	-	-	-	-	
TNFSF8	-	-	-	-	
WDR31	T05A8.5		WD40-repeat-containing domain	7e-31	None
ZNF483	-	-	-	-	
ZNF618 ZNF883	Y55F3AM.14		Zinc finger, C2H2-like	8e-08 2e-53	None

Table 8. Tumor-expressed genes within the 9q32-9q33.1 region of the human genome and their corresponding *C. elegans* ortholog.
BLAST e-value reveals the statistical significance for the alignment between nematode and human proteins. "Cisplatin response" indicates the differential response to cisplatin of RNAi-treated animals compared to wild type worms.

R.4.2. *dnj-2*/DNAJC25, *vha-10*/ATP6V1G1 and *ckr-2*/OR2K2 are required for a proper response to cisplatin

dnj-2/DNAJC25

DNAJC25 is a heat shock induced chaperone that belongs to HSP40 subfamily, a group of proteins with an important role in protecting cells not only against heat but other environmental and metabolic stimuli, including UV exposure, being relevant in cancer progression and anticancer drug resistance (Stope et al. 2015). Although little is known about DNAJC25, its downregulation has been related to cancer progression (T. Liu et al. 2012). Our study revealed that the expression of this gene is not altered in cisplatin resistant orthoxenografts (Figure 14). However, *dnj-2(RNAi)* adult worms, showed increased sensitivity to cisplatin compared to control worms indicating that this gene is indeed capable to regulate the response to cisplatin (Figure 38.A).

vha-10/ATP6V1G1

Previous results showed that drug resistance of cancer cells is related to pH changes in the extracellular environment and the cytoplasm (Sasazawa et al. 2009). Vacuolar-H ATPase ATP6V1G1 is a proton pump that promotes the acidification of cellular microenvironments. In fact, high expression levels of vacuolar-H ATPase have been related to tumor survival (Di Cristofori et al. 2015) and cisplatin resistance in several tumor lines (Lu et al. 2013). According to these results, our analysis revealed that all the cisplatin resistant orthoxenograft tumors also tend to

overexpress this gene. Concordantly, analyzing the response of cisplatin in the *C. elegans* ortholog, *vha-10(RNAi)* worms showed an increase of sensitivity supporting a conserved role of this protein for a proper response of cisplatin (Figure 38.A).

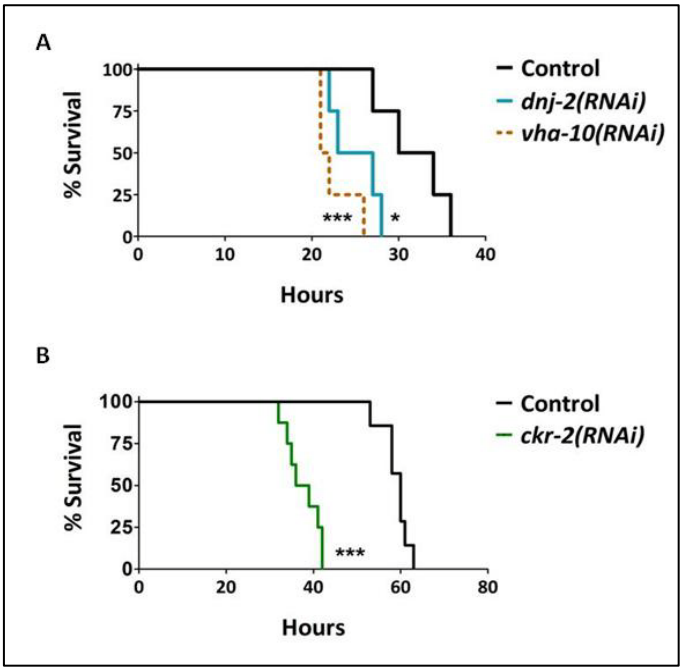

Figure 38. Inactivation of *dnj-2, vha-10* and *ckr-1* by RNAi induces sensitivity to cisplatin.
Survival staircase of young-adult animals fed with (A) *dnj-2, vha-10* or (B) *ckr-2* RNAi clones and treated with 500µg/ml cisplatin. *gfp*(RNAi) was used as control. **p*<0,05, ****p*<0,001 relative to control by the log-rank (Mantel-Cox) test. For each condition, cisplatin untreated animals showed 100% survival (data not shown).

ckr-2/OR2K2

The human OR2K2 olfactory receptor gene is member of the large family of G-protein-coupled receptors that, in principle, do not have any relationship to cancer or cisplatin. Surprisingly, this gene is expressed in testicular tumors and also upregulated in those that are resistant to cisplatin (Figure 14). *ckr-2* is the closest *C. elegans* gene in terms of homology, and this gene codifies a receptor that is only expressed in motor neurons (McKay et al. 2007). Interestingly, we observed that *ckr-2(RNAi)* animals are more sensitive to cisplatin (Figure 38.B), which is in agreement to the upregulation that we detected in cisplatin-resistant tumors.

R.4.3. Simultaneous depletion of ceramide glucosyltransferase 1(*cgt-1*) and 3(*cgt-3*) confers sensitivity to cisplatin

Several studies reported *in vitro* the correlation between high levels of the human glucosylceramide synthase (GCS) and multidrug resistance, inhibition of apoptosis and cancer progression (Liu et al. 2001; Ichikawa et al. 1996). In addition, GCS blockade by gene silencing or drugs leads chemoresistant cancer cells to enter in apoptosis (Gouazé et al. 2005; Liu et al. 2011). Accordingly, we observed a tendency of GCS to be highly expressed in cisplatin resistant orthoxenografts independently of 9q32-9q33.1 amplification (Figure 14).

Worms have three functional GCS genes (*cgt-1*, *cgt-2* and *cgt-3*) that present high homology to the single mammalian GCS gene. These genes show redundant functions and only combining either inactivation of all three *cgt* genes, or both *cgt-1* and *cgt-3* is possible to reduce GCS enzymatic activity to cause L1 larval arrest (Marza et al. 2009). As expected, single inactivation of *cgt-1* by a null mutant or *cgt-3* by RNAi resulted in a normal response to cisplatin (Figure 39). However the double inactivation, performing RNAi by feeding in late L3 to skip larval arrest, caused cisplatin hypersensitivity, demonstrating the important role of GCS activity in cisplatin response.

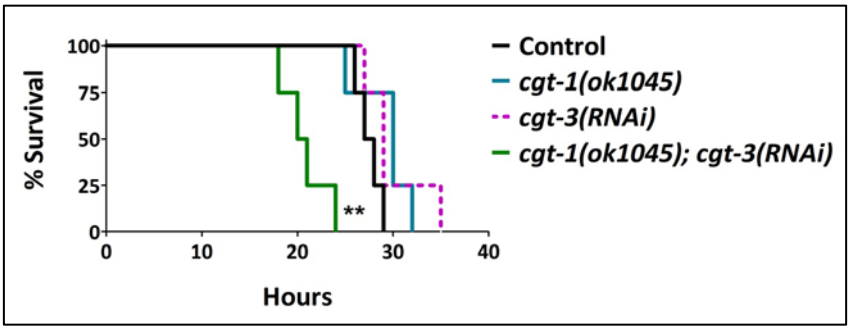

Figure 39. Simultaneous inactivation of *cgt-1* and *cgt-3* genes induces sensitivity to cisplatin.
Survival staircase of young adult animals treated with 500µg/ml cisplatin and fed with and without *cgt-3(RNAi)* bacteria. RNAi against *gfp* was used as control. ***p*<0,01 relative to control (N2) by the log-rank (Mantel-Cox) test. For each condition, 100% untreated animals survived (data not shown).

R.4.4. Copper transporter ortholog *F27C1.2* influences the cellular response to cisplatin in *C. elegans*

The contribution and importance of copper transporters to the cellular accumulation of cisplatin has extensively been reported (Ciarimboli 2012; Ishida et al. 2010). In addition, it is known that CTR1 and CRT2 human copper transporters mediate the influx of cisplatin, being a major determinant of sensitivity to cisplatin both *in vitro* and *in vivo* (Blair et al. 2009; Larson et al. 2009). According to these results, both copper transporters were downregulated in the cisplatin refractory orthoxenografts (Figure 14).

Sequence name	Chrom.	Operon	E-value		RNAi phenotype
			CRT1	CRT2	
F27C1.2	I		9e-09	3e-08	Ste, Gro, Sma
F01G12.1	X	-	8e-08	1e-05	Wt
F31E8.4	II	-	5e-07	7e-07	Wt
F58G6.3	IV	CEOP4332	3e-07	2e-02	Wt
F58G6.7	IV	CEOP4332	3e-04	2e-03	Wt
F58G6.9	IV	-	5e-06	5e-01	Wt
K12C11.3	I	-	6e-05	-	Wt
K12C11.6	I	CEOP1962	8e-06	3e-03	Ste, Gro, Pvu, Lva, Sick
K12C11.7	I	CEOP1962	3e-02	2e-04	Wt
Y58A7A.1	V	-	4e-07	4e-03	Wt

Table 9. Family of *C. elegans* orthologs to human CRT1 and CRT2 copper transporters.
Chrom (Chromosome). RNAi phenotypes according to wormbase. Phenotypes are abbreviated as follows: Ste (Sterile), Gro (growth delay), Sma (Small), Pvl (Protruding vulva), Lva (Larval arrest), Wt (Wild type).

BLAST analysis revealed that F27C1.2 was the *C. elegans* protein that shared higher homology to human CRT1 and CRT2. F27C1.2 has a copper transporter domain and belongs to a family of genes with at least ten different paralogs known presenting distinct homology to human

CTR1 and CTR2 (Table 9). Although little is known about expression or distribution of these proteins in *C. elegans*, it has been reported some interactions among them (Zhong & Sternberg 2006). Whereas copper transporters form homotrimers in human cells, worm copper transporters may have a more complex composition according to the higher number of subunits. As a first approach, we analyzed whether single *F27C1.2* inactivation is capable to modify the response to cisplatin. Thus, we found that *F27C1.2(RNAi)* animals treated with cisplatin showed higher tolerance to cisplatin than control worms (Figure 40).

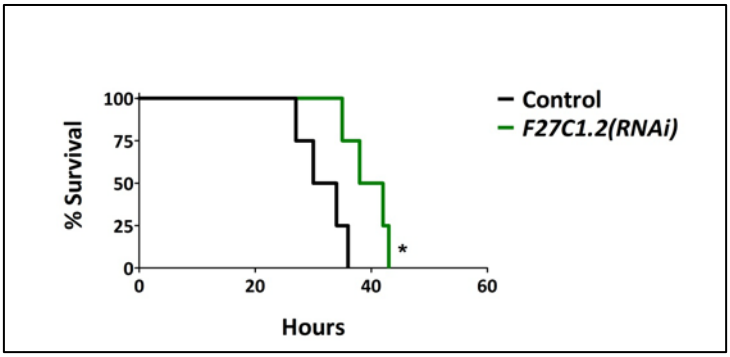

Figure 40. RNAi inactivation of F27C1.2, one of *C. elegans* copper transporter gene, produces cisplatin resistance.
Survival staircase of young adult animals fed with RNAi bacteria against F27C1.2, treated with 500µg/ml cisplatin. *gfp(RNAi)* was used as negative control. **p*<0,05 relative to control by the log-rank (Mantel-Cox) test. For each condition, 100% untreated animals survived (data not shown).

To analyze if this transporter is also capable to modify the cisplatin response in a mitotic scenario we tested the response to cisplatin in the *F27C1.2(tm5909)* mutant strain. This allele consists of a 251bp deletion affecting two coding exons (Figure 41). Accordingly, we observed that *F27C1.2* mutants showed more resistance to cisplatin during larva development (Figure 42). However, whereas *F27C1.2(RNAi)* inactivation

produced sterility, *F27C1.2(tm5909)* animals did not show any reproductive defect, probably because this mutant produces a truncated protein that could retain a partial activity.

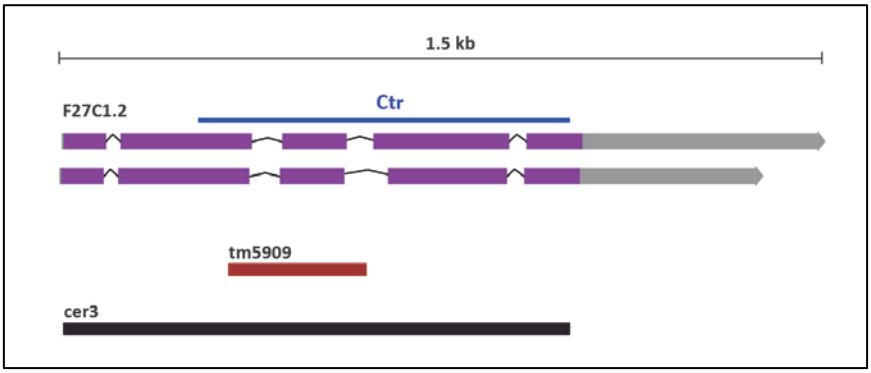

Figure 41. Scheme of *F27C1.2* gene.
Purple boxes represent exon while grey connecting lines introns. Blue line represents the localization of copper transporter domain. Red and black boxes represent deletion alleles

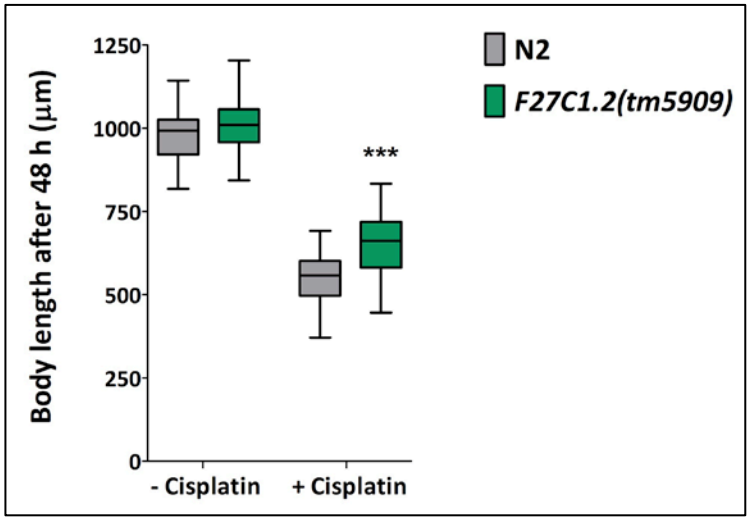

Figure 42. *F27C1.2(tm5909)* deletion allele protects *C. elegans* larvae from cisplatin.
Developmental delay induced by cisplatin in control worms (N2) and *F27C1.2(tm5909)* mutant strain grown from L1 for 48 hours. ****p*<0,001 relative to control worms for each condition by Student's t-test.

R.4.5. Generation of tools to study the role of F27C1.2 in cisplatin resistance

Generation of a new F27C1.2 mutant allele by CRISPR/Cas9

To solve the inconsistency between the RNAi and the mutant phenotype, taking the advantages that a directed mutagenesis the CRISPR/Cas9 system offers, we generated a new *F27C1.2* deletion allele showing a 1kb deletion that completely disrupts both transcripts (Figure 41, 43). According to the *F27C1.2(RNAi)* phenotype, homozygous animals for this new allele displayed sterility. In contrast, *tm5909* worms do not present any reproductive deffect, indicating that the small deletion of the *tm5909* allele may produce a truncated protein whose partial function is sufficient to avoid the sterility but not for promoting the wild type response to cisplatin.

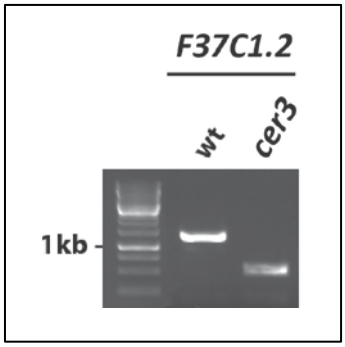

Figure 43. F27C1.2(cer3) produces a deletion of around 1kb.
PCR products from genomic DNA of wild type worms and homozygous worms carrying *F27C1.2(cer3)* deletion allele.

Making a translational reporter for F27C1.2

In order to investigate the expression pattern of this gene we generated, by using the Gateway cloning system, an extrachromosomal transgenic strain, CER185, expressing F27C1.2 protein fused to mCherry, under the control of its own promoter. At one-day adult stage, we observed that F27C1.2 is broadly expressed in the plasmatic membrane of different somatic tissues (Figure 44). Its expression seems to be more prominent in the nervous system (nerves around the head and ventral cord) but also in hypodermal cells and excretory system. On the contrary, no expression was observed in intestine or germ line, probably because of the tendency of this tissue to silence high-copy extrachromosomal arrays.

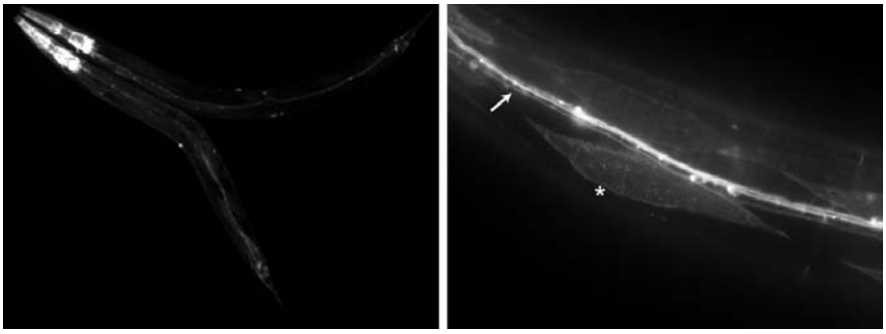

Figure 44. F27C1.2::mCherry expression pattern.
Representative images of adult worms expressing extrachromosomal F27C1.2::mCherry transgene. This construct is highly expressed in pharynx, excretory system, hypodermic cells and neurons. The right image shows seam cells (asterisk) and excretory cells channel (arrow) at higher magnification.

Discussion

D.1. *C. elegans* is a system suitable to investigate the action of cisplatin in animals

Platinum-based chemotherapy is widely used and is increasingly important in the treatment of cancer. Despite three decades of clinical use and intense research, greater knowledge about the cellular responses to platinum compounds is necessary to figure out the molecular basis of inherited and acquired resistance. Model organisms are prosperous platforms to study the cellular response to chemotherapy but also to screen for new treatments. Our study intends to consolidate *C. elegans* as a pluricellular model to better understand the biological response to cisplatin-based chemotherapy. We demonstrated the capability of this model system to dissect the functional pathways involved in cisplatin response. In addition, we confirmed the translational value of this model, which could fill a gap between *in vitro* studies and preclinical models.

Impact of cisplatin in germ line and sperm

A strong effect of cisplatin on germ line development and fertility is somehow expected because germ cells present an active proliferation and DNA-damage induced by adduct formation is considered the major cytotoxic effect of cisplatin (Dasari & Bernard Tchounwou 2014). Thus, our phenotypic analyses showed that cells with proliferative activity are more sensitive to cisplatin, causing germ line and developmental defects. In *C. elegans*, germ line has been used to study the effect of a wide variety of molecules and genes in cell-cycle regulation and DNA damage response (Gartner et al. 2004). We observed that the effect of cisplatin in

fertility and cell cycle arrest in the germ line is similar to that produced by other DNA-damaging agents as ionizing or ultraviolet C radiations (Gartner et al. 2004), suggesting a direct action of cisplatin on DNA. This fact makes of *C. elegans* germ line a model for studies focused on DNA-damage response associated to cisplatin, as shown by several publications (van Haaften et al. 2006; Meier et al. 2014; Roerink et al. 2012).

However, the use of *C. elegans* germ line as a model to predict a tumor response to chemotherapy presents limitations. As example, the syncytial nature of the distal germ line hampers the study of the cytoplasmic damage caused by cisplatin. Moreover, *C. elegans* germ line contains mitotic cells, meiotic cells, mature oocytes and sperm, and therefore the cellular context is quite diverse.

We concluded that sperm defects are the main cause of the reduced fertility observed upon cisplatin exposure. One possibility is that cisplatin affect the spermatogenesis reducing the sperm reservoir, but we did not observe a dramatic reduction in sperm in treated animals. Another option is that cisplatin affect the proper spermatogenesis making dysfunctional sperm. Supporting this former option, spermatid activation it is altered upon heat stress (Aprison & Ruvinsky 2014). At any case, it seems evident that sperm and oocytes are different in term of response to cisplatin. Patients with testicular tumors that has been treated with cisplain present a drastic effect on spermatogenesis and sperm, but such harmful effect seems to affect primarily to chromatin and it is reversible (Bujan et al. 2013). In females with ovarian cancer cisplatin also affect gametogenesis producing a reduction of the ovarian reserve (Chang et al. 2015). Detailed experiments need to be performed to better understand at what step the gametogenesis is hampered in the presence of cisplatin. In this sense, the hermaphrodite condition of *C. elegans* is a clear advantage

to study the effect of certain cisplatin dose on oogenesis and spermatogenesis in the same organism.

Two biological contexts to study the cellular response to cisplatin in animals

Since our scientific interest is the study of cisplatin as chemotherapeutical agent, given the somatic nature of most of the tumors we rather focused on how somatic cells response to cisplatin. Based on cisplatin capability to alter worm development but also adult survival we have established two systems to study the systemic response to this agent in two different somatic scenarios:

- Larval development (presence of proliferating cells)

In *C. elegans*, a wide variety of agents with different toxic mode of action are able to cause developmental defects (Cui et al. 2007; Helmcke et al. 2009; Kumar et al. 2010). We hypothesized that cisplatin growing-related phenotypes observed in larvae were mainly provoked by a direct action of cisplatin on DNA in somatic-dividing cells. Consequently, a failure in DNA-damaging repair, as happens in *polh-1* mutant worms (Roerink et al. 2012), enhances cisplatin sensitivity during development but not in adulthood. Moreover, we reported that cisplatin induces the activation of the proapoptotic gene *egl-1* only during postembryonic development.

Accordingly, other DNA damaging agents such as HU or 5-FU produce similar effects than cisplatin during larval development (Rubio-Peña et al. 2015; S. Kim et al. 2008). The anticancer drug 5-FU produces in *C. elegans* vulva development defect, smaller body size and, at high concentrations, arrest in larval stage (Kumar et al. 2010). Moreover, DNA repair pathway defects sensitize the response to 5-FU. Interestingly, a recent paper published by our group demonstrated that HU-induced replicative stress in *C. elegans* larvae produces *egl-1*-induced apoptosis in hypodermal cells causing L3 larval arrest (Rubio-Peña et al. 2015). Taking advantage of tissue-specific reporters, future studies could take the study of cisplatin effect in *C. elegans* development to cell-type resolution.

- Adulthood (post-mitotic cells only)

We demonstrated that adult worms tolerate higher concentration of cisplatin and the cytotoxicity of this drug is not driven by its action on DNA. Differently to other animals that present adult somatic stem cells, all adult somatic cells are post-mitotic in *C. elegans*. This feature makes *C. elegans* adult cells capable to tolerate high levels of DNA. Exposed to the same level of DNA-damage, differentiated somatic cells neither undergo apoptosis nor show DNA-repair activation, but germ cell do (Vermezovic et al. 2012). This post-mitotic scenario is very convenient to investigate and characterize cytoplasmic-specific mechanisms of response to cisplatin (Hemmingsson et al. 2010; Natarajan et al. 2013).

Cisplatin is neurotoxic and nephrotoxic and it is thereby affecting differentiated somatic cells also in human patients (Yao et al. 2007). Ototoxicity and peripheral neuropathy are common side effects to cisplatin treatment (Rybak et al. 2009; Bobylev et al. 2015). We believe that our model system could be used to find coadjuvant treatments to

reduce cisplatin-induced cytoplasmic damage that may be behind the side-effects produced by this drug in human differentiated cells, which are hampering the use of cisplatin in chemotherapy.

D.2. Cisplatin induces a stress response

The number of genes deregulated and the activation of DAF-16 in distinct somatic cell types upon cisplatin exposure suggest that cisplatin-damaging effect could induce a coordinated systemic response in *C. elegans*, involving stress-related reactions and the innate immune response. Bioimaging of cisplatin determined that the uptake of this drug is dose and time dependent, and that cisplatin is predominantly located in the intestine although it should reach all cell types (Crone et al, 2005). Thus the effect of cisplatin on the organism could be understood through (i) non-autonomous mechanisms (the effect in certain cells influence other distant cells), or (ii) cell autonomous mechanisms (all cells have an individual response to cisplatin uptake).

Non autonomous mechanisms: DNA damage as origin of systemic response

As mentioned above, DNA damage responses have been well characterized with regard to their cell-autonomous checkpoint functions leading to cell cycle arrest and apoptosis (Bartek & Lukas 2007). Our transcriptomic study showed that, despite of DNA-damage dependent apoptosis related genes, the vast majority of genes induced by cisplatin are

mainly related to general stress responses and the innate immune system, which could indicate a possible crosstalk between DNA damaged-proliferative cells and non-proliferative tissues. According to this, similar pattern of response was showed in the transcriptomic profile of worms exposed to IR or UVC (Boyd et al. 2010; Schumacher et al. 2005). Following this rationale, it has recently been discover that germ line specific DNA damage induces a systemic stress response indicating a non-cell autonomous response to genome instability. Moreover, this response have been reported as reaction to different types of DNA insults such as UV-induced bulky lesions, IR-induced DNA strands breaks, HU-induced replication stalling or meiotic double strand breaks (Ermolaeva & Schumacher 2013). Although these studies were focused in adult germ cells, our *in vivo* experiments using the *egl-1::gfp* reporter in larval somatic cells demonstrated that cisplatin-induced DNA damage-related apoptosis is not constrained to germ cells. Thus the non-autonomous mechanisms could be triggered from either somatic or germ cells.

Interestingly, immune and stress reactions upon DNA damage are common in mammals (Ermolaeva & Schumacher 2013). As example, UV irradiation induces complex immune reactions in human skin (Schwarz & Schwarz 2011). Moreover, the systemic response induced by IR-related DNA damage do not increase IR sensitivity (Schumacher et al. 2005) but leads to an enhanced resistance to heat and oxidative stress (Ermolaeva et al. 2013). In addition, in thymic epithelial cells, DNA damage provokes p53-induced cytokine release resulting in both innate and adaptive immune response leading to tumor cell death (Kang et al. 2011) . Accordingly, attenuate this non-autonomous systemic response triggered by cisplatin-induced DNA damage could provide a path to reduce the effect of cisplatin in non-dividing tissues, thus, reducing side-effects such as nephrotoxicity or ototoxicity (Yao et al. 2007; Rybak et al. 2009).

The direct link between cisplatin-induced DNA damage and SKN-1 and DAF-16 activation has not been investigated in this work but, interestingly, a recent work exposes that radiation-induced DNA damage in germ cells leads the induction of putative secreted immune peptides, via ERK MAP kinase MPK-1 activation, which promotes a somatic systemic response (Ermolaeva et al. 2013). Therefore, to study the role of this protein in altering the response to cisplatin could represent and exciting point to be explored in the future.

Cell autonomous mechanisms: DAF-16 and SKN-1 are key effectors in the cisplatin-induced response

Cisplatin induces the nuclear translocation of the DAF-16 homolog FOXO3A in human cell lines (Fernández de Mattos et al. 2008). Therefore, individual cells have the capacity to activate cellular mechanisms in response to cisplatin. In this study we demonstrated that activation of the IIS-related transcription factors DAF-16 and SKN-1 is required to promote the systemic response to cisplatin.

DNA damage-induced systemic response does not require DAF-16 (Ermolaeva et al. 2013). Therefore although germ line deficient worms shows a constitutive DAF-16 nuclear localization and an elevated baseline stress resistance (Arantes-Oliveira et al. 2002), DAF-16 seems to be more implicated in the cell autonomous response to cisplatin.

The Nrf2 *C. elegans* ortholog SKN-1 is an important factor in the animal response to oxidative stress that positively regulates the expression of Phase 2 detoxification system genes in the intestine to protect the animal against oxidative and xenobiotic stresses (Blackwell et al. 2015), while

DAF-16 activation positively regulates a wider spectrum of processes such as stress resistance, innate immunity or metabolic adaptation (Singh & Aballay 2009; Murphy & Hu 2013). We demonstrated a correlation between cisplatin-exposure and increased expression of genes regulated by both transcription factors. Moreover, we found that despite of they share some common targets, both are essential for a proper response to cisplatin in a non-redundant manner.

DAF-16 target genes have been classified as class I or class II. While class I are directly related to stress response and are positively regulated by DAF-16, Class II genes are required for normal development and dauer recovery and are negatively regulated by DAF-16 (Murphy et al. 2003; Tepper et al. 2013). Our results do not suggest a strong correlation between cisplatin and the expression of any class of DAF-16 genes. However, it is clear that cisplatin promotes DAF-16 nuclear location in the animal and missregulates the expression of DAF-16 targets.

However, we observed a direct correlation between cisplatin-induced genes and genes positively regulated by SKN-1. Moreover cisplatin promotes SKN-1 dependent activation of *gst-4* supporting a key role of this transcription factor promoting the response to cisplatin. A remarkable difference between DAF-16 and SKN-1 upon cisplatin exposure is that cisplatin induces SKN-1 activation (via *gst-4*) in almost all worm population, but only 50% of the worms showed DAF-16 activation (see Figure 25). These observations, together with the fact that *skn-1(RNAi)* animals showed higher sensitivity to cisplatin than *daf-16(-)* animals, may denote the prevalence of SKN-1 over DAF-16 in activating the cisplatin-induced systemic response targets in *C. elegans*.

D.3. Relevance of targeting redox homeostasis modulators for tumor development and chemoresistance

Both carcinogenesis and chemoresistance are frequently related to increased oxidative stress and activation of redox metabolism (Polimeni & Gazzano 2014). Oxidative levels are controlled by specific intracellular enzymes, such as superoxide dismutase, glutathione peroxidase, catalase, glutathione-S-transferase and thioredoxin reductase (Glasauer & Chandel 2014). Regarding carcinogenesis, the US Food and Drug Administration (FDA) has approved 132 cancer chemotherapy drugs, of which 56 have been reported to cause oxidative stress (Chen et al. 2007). Concerning chemoresistance, redox balance modulators could be promising molecules as coadjuvant treatments in prevention of resistance acquisition for cisplatin. This study reveals the importance of redox homeostasis in the resistance to cisplatin, and the role of Nrf2/SKN-1 and FOXO/DAF-16 as modulators of cisplatin resistance acquisition through this mechanism, which is conserved from worms to mammals.

FOXO proteins

Human FOXO proteins are crucial regulators of a multitude of cellular functions. In addition to their role in inducing the stress response, these proteins also modulates genes involved in differentiation, proliferation, survival, apoptosis or DNA repair (Yang & Hung 2009). This wide-range regulation makes that FOXO activity has not only been related to drug resistance. In fact, these proteins can also act as tumor suppressors and even as oncogenes (Tzivion et al. 2011). Thus, FOXOs inactivation seems

to be important in carcinogenesis and increasing their activity could represent a therapeutic strategy for tumor suppression (Myatt & Lam 2007; Yang & Hung 2009). On the contrary, in terms of drug chemotherapy, upon continuous stress, FOXOs constitutive activation promotes an antioxidant defense inducing drug resistance (Goto et al. 2008; Zhu 2014). Therefore, the same molecules may have therapeutical interest to kill the tumor in an initial treatment, but later they also may be targets to modulate the resistance to drugs. Paradoxically, given the complex regulation of these proteins, FOXO activation also resensitizes chemotherapy-resistant cell lines, but this effect is mainly produced by its proapoptotic role (Fernández de Mattos et al. 2008). Thus, the effect of FOXOs on tumor progression and drug resistance needs to be experimentally determined in each tumor type.

-14-3-3 proteins as FOXO regulators

In this study we have demonstrated that 14-3-3 levels can modulate the response to cisplatin altering the stress response presumably by retaining DAF-16 in the cytoplasm. As in *C. elegans*, human 14-3-3 proteins bind to AKT phosphorilated FOXO inducing its cytoplasmic retention. 14-3-3 proteins are a family of evolutionary conserved modulator proteins that regulate multiple signaling pathways (Tzivion et al. 2011). It is known their roles in cancer-related processes, both in cancer progression and in the regulation of the sensitivity to chemotherapeutic agents. 14-3-3 levels are relevant to the resistance or sensitivity to chemotherapies, and interestingly, this is a mechanism that seems to be conserved from worms to humans (Aristizábal-Corrales et al. 2013). Several studies have shown a correlation between high 14-3-3 levels and drug resistance. For instance,

overexpression of 14-3-3σ makes certain cell lines more resistant to chemotherapeutic drugs, such as cisplatin or gemcitabine (Li et al. 2009; Neupane & Korc 2008). Conversely, 14-3-3σ depletion is correlated with increased sensitivity of colorectal cancer cells to doxorubicin-induced apoptosis (Chan et al. 2000). The contribution of 14-3-3 proteins in the resistance to DNA-damaging drugs has been mainly associated with their function in suppressing cell death pathways, such as by regulating the pro-apoptotic protein BAD (She et al. 2005; Porter et al. 2006) or to its role in regulating the cell cycle checkpoint upon DNA damage (Li et al. 2009). This study supports the therapeutic potential of 14-3-3 proteins to modify the chemotherapeutic response to cisplatin through regulating FOXO/DAF-16 activity.

Nrf2 transcription factor

SKN-1 human ortholog Nrf2 regulates the expression of stress responsive genes as SOD, catalases or phase II detoxification enzymes (Kaspar et al. 2009). Nrf2 overexpression or hyperactivation provokes a direct effect in acquisition of resistance to a wide-spectrum of anticancer drugs in many cancer types (Gañán-Gómez et al. 2013)(S. K. Kim et al. 2008; Kaspar et al. 2009). Accordingly, increased nuclear Nrf2 expression have been shown in cisplatin resistant bladder human cancer samples (Hayden et al. 2014). On the contrary, inhibition of Nrf2 sensitizes cisplatin-resistant A549 cells (Huo et al, 2015). These observations are concordant to our findings in *C. elegans* showing that targeting SKN-1, direct or indirectly, should be explored for cisplatin-combined therapeutic intervention.

-TrxR1 as possible Nfr2 regulator

Thioredoxin system proteins are key players in many important cellular processes (Arnér 2009; Lu & Holmgren 2014). Regarding their function in presence of cisplatin, in mammalian cells have been shown a delicate balance exists between the protective pathways propelled by the functional TrxR1/TRX system, the cytotoxic effects produced by the direct interaction between cisplatin and a selenocysteine residue, and protective effects due to Nrf2 activation after TrxR1 targeting (Anestål et al. 2008; Peng, Xu & Elias S. J. Arnér 2012; Cebula et al. 2015).

In mammals, the thioredoxin and glutathione systems are the most important redox machineries against reactive exogenous and endogenous molecules and complementarities of their *in vivo* functions have been suggested by many studies (Muller 1996; Kanzok 2001; Peng, Xu & Elias S. J. Arnér 2012). In *C. elegans*, TRXR-1 and GSR-1 only share overlapping functions during molting and, while *gsr-1* is essential for worm viability and determines the tolerance to redox stress (Lüersen et al. 2013), worms lacking *trxr-1* display no obvious developmental defects under laboratory growth conditions and are not hypersensitive to acute oxidative stress (Stenvall et al. 2011). Thus, TRXR-1 may play minor roles in protecting against acute oxidative stress or supporting cell proliferation in *C. elegans*. These features allow studying the other TRXR-1 roles separately to their protective function in *C. elegans*. According to this, we demonstrated that the single TRXR-1 Selenocysteine (Sec) amino acid is essential for the cytotoxic effect of cisplatin. Some studies in cell lines suggest that cisplatin cytotoxicity in wild type cells is promoted by a direct interaction between cisplatin and

Sec amino acids leading to the consequent formation of SecTRAPS (Anestål et al. 2008). Moreover, the absence or reduction of TrxR1 positively regulates Nrf2/s*kn-1* promoting cisplatin resistance (Cebula et al. 2015) Still, further experiments need to be done to finally demonstrate that the resistance to cisplatin of animals with compromised TRXR-1 functions that we observed is produced by SKN-1 activation in *C. elegans.* These facts would reveal TrxR1 as a new potential target to regulate the Nfr2/SKN-1 activity, and hence cisplatin responsiveness, in pluricellular organisms.

- Alternative modificators of redox homeostasis

In addition, many other factors altering FOXO/DAF-16 and/or Nrf2/SKN-1 activities could reveal as putative targets for new therapies. In this way, we demonstrated the reduced insulin signaling by *daf-2*/IGFR1 also contribute to modify the response to cisplatin. In line with this, metabolic changes promoted by fasting has been demonstrated to selectively protect normal cells and mice by FOXO activation, but not cancerous cells against oxidants and common chemotherapeutic agents (Raffaghello et al. 2008). Accordingly, we suggest that the modulation of other players involved in the IIS pathway such as SIR-2, AKT-1 or JNK-1, antioxidant enzymes as SOD, catalases, GSR-1 or mitochondrial alterations could also represent a strategy to regulate the response to cisplatin through changes in redox homeostasis. In any case, due to the complexity underlying drug resistance, it could be necessary to perform antioxidant profiling of tumor cells to identify clinically relevant therapeutic targets. In line with this, the manipulation of these pathways in non-proliferating tissues could be also useful to decrease cisplatin side effects. Given the increased ROS levels of cancer cells, a further increase of oxidative stress could be toxic to these

cells and potentially induce cell death via oxidative stress while normal cells could tolerate it.

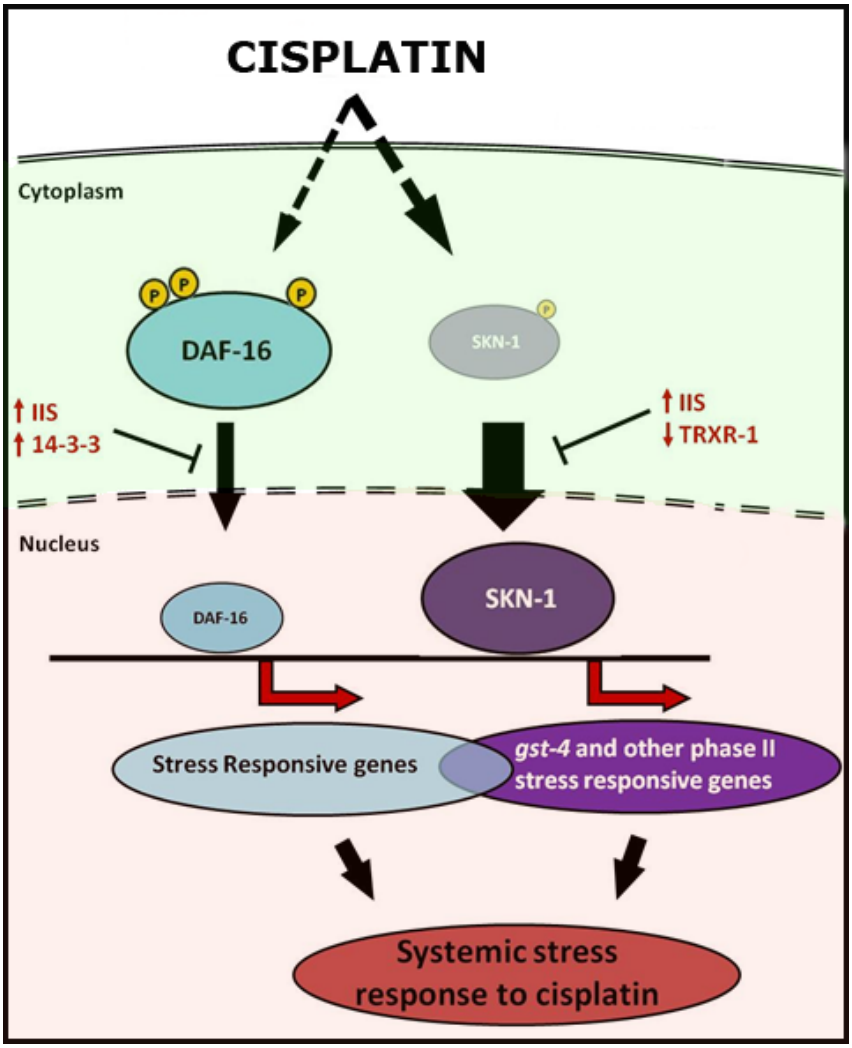

Figure 45. Mode of action of DAF-16 and SKN-1 in the presence of cisplatin. Cytotoxic effect of cisplatin in somatic cells promotes DAF-16 and, mainly, SKN-1 nuclear translocation. Both factors activate a battery of genes related to immune system and stress responsive genes that act in the direct inactivation of cisplatin and reduce the high redox levels produced by cisplatin in the cytoplasm. Red arrows indicates the activity, high or low, of distinct proteins or mechanisms able to alter the DAF-16 or SKN-1 activation and, hence, the normal response to cisplatin.

D.4. Towards the clinic: *C. elegans* as translational tool to discover cisplatin-combined therapies that decreases cisplatin refractoriness in orthotopic tumors

Our RNAi approach to inactivate all *C. elegans* ortholog genes within 9p32-p33.1 human region showed that five genes (*gst-1*,*gst-3*/GCS, *dnj-2*/DNAJC25, *vha-10*/ATP6V1G1, *ckr-2*/OR2K2 and *F27C1.2*/CRT1/2) take part in the response to cisplatin. In addition, for three of them, *cgt*, *vha-10* and *F27C1.2*, there is a coincidence between up or downregulation in cisplatin resistant tumors and resistance or sensitivity response to cisplatin in worms. In other words, genes upregulated in cisplatin-resistant tumors also promote resistance to cisplatin in worms. This functional results obtained in *C. elegans* strongly suggest that targeting GCS, ATP6V1G, CTR1/2, should be underscored to study the unresponsiveness in cisplatin tumors.

Glucosylceramide synthase (GCS)

Our group paid special attention to GCS, due is central role in the glycosphingolipid synthesis pathway and its emerging relevance for treating metabolic diseases such as Gaucher, Niemann-Pick or diabetes (Messner & Cabot 2010; Vanier 2015; Chaurasia & Summers 2015). In this context, several GCS inhibitors are in clinical use or under development, including Miglustat, PDMP or EXEL-0346 (Richards et al.

2012; Venier & Igdoura 2012; Huang et al. 2011). Based on our previous results and after confirm the increased GCS activity in cisplatin refractory tumors (Fig 46.A), an in vivo experiment was carried out to evaluate the effect of inhibiting GCS in these resistant tumors. Thus, engrafted animals with cisplatin-refractory TGT1XR and TGT38XR orthoxenografts, which exhibit increase GCS expression and enzyme activity (Fig 46.A), were treated with PDMP, which is a competitive inhibitor of GCS (Figure 46.B). Single treatment with PDMP or cisplatin did not reduce the tumor mass. Nevertheless, a treatment combining cisplatin and PDMP produced a significant reduction of tumor weight.

With this study, we demonstrated the relevance of the GCS activity as a biological mechanism that mediate tumor cell protection against cisplatin exposure, highlighting the relevance of targeting GCS as a novel approach to resensitize tumors to cisplatin. Moreover, we reinforced the translational value of *C. elegans* in the field of cisplatin chemotherapy, beside its amenability to study the DNA damage caused by this agent.

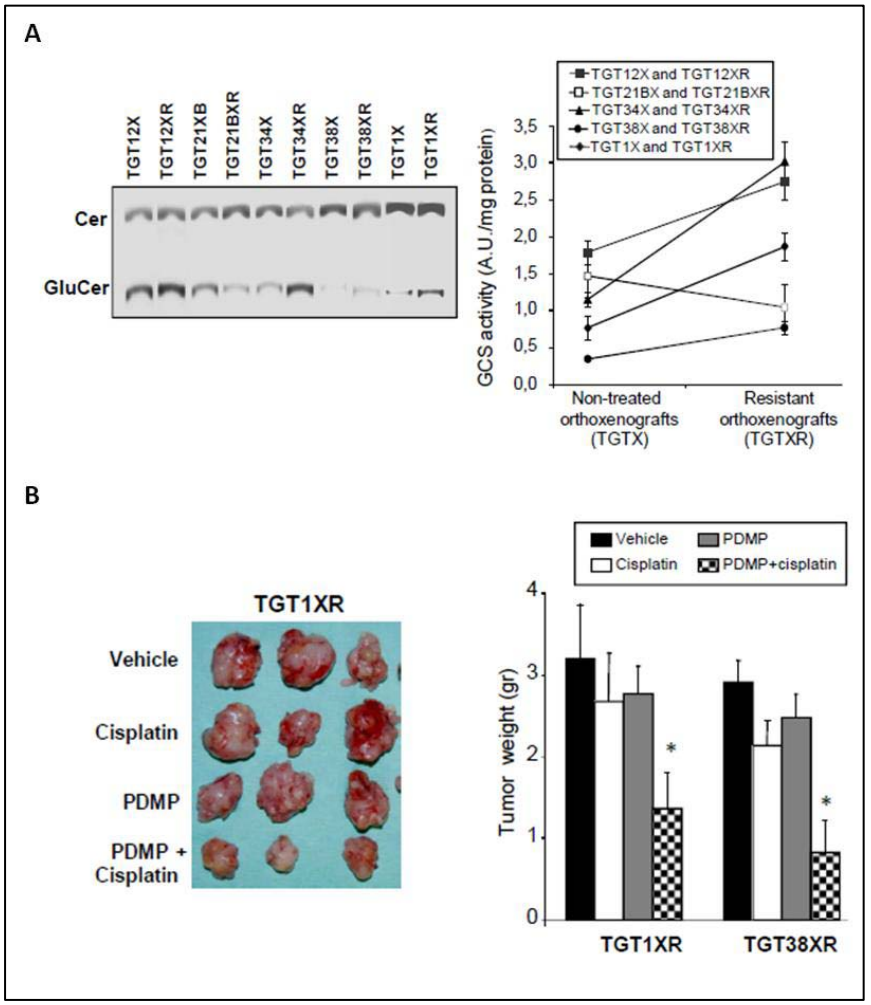

Figure 46. Effect of targeting GCS for the resistance to cisplatin in testicular germ cells tumors.
(A) GCS activity is increased in cisplatin resistant tumors. Left panel shows the levels of NBD-labeled ceramide or glucosylceramide formation, which is the readout for GCS activity, in each testicular germ cell tumor. Right panel compares the GCS enzymatic activity for each pair of control/resistant tumors. (B) Response of cisplatin-refractory engrafted TGT1XR and TGT38XR tumors to treatment with the GCS inhibitor PDMP. Tumors were implanted in mouse testicle and when homogeneous tumor sizes were detected they were randomized to tour treatment groups (n=6-8 mice/group): (i) vehicle, (ii) cisplatin (iii) PDMP and (iv) PDMP + cisplatin. Left picture shows the tumor mass after treatment of one of the cisplatin resistant tumor. Right panel shows the effect of the tumor weight of two different cisplatin resistant for each treatment (Extracted from Piulats et al. Unpublished).

Copper transporters (CRT1/2)

There are multiple evidences in cell lines indicating that copper transporters, mainly CTR1, affect cisplatin cytotoxicity by affecting drug uptake (Ciarimboli 2012). Moreover cisplatin resistant cells tend to negatively regulate CTR-1 (Larson et al. 2009; Holzer et al. 2006). Accordingly, several lines of investigation are focused on hampering CTR1 degradation. For instance, the proteosome inhibitor bortezomib in combination with carboplatin is currently in phase I trial for patients with recurrent ovarian cancer (Ramirez et al. 2008). Interestingly, new liposomal drugs as lipoplatin, make possible the delivery of platinum drugs into the cytoplasm to overcome the resistance caused by low levels of CRT1 (Zalba & Garrido 2013). Our results in *C. elegans* support these findings. We demonstrated the role of one of the *C. elegans* copper transporters in the response to cisplatin. Copper transporter shows in *C. elegans* a higher complexity that needs to be explored. There are ten paralogs, but only two of them present RNAi phenotypes. We have generated the necessary tools to study F27C1.2 copper transporter in *C. elegans*, such as an *F27C1.2* null mutant and a F27C1.2 translational reporter. First, we need to characterize these tools to understand the role and dynamics of this gene upon cisplatin exposure, to finally perform chemical or genetic screenings to functional validate modulators of copper transporter activity using *C. elegans*.

D.5. Perspectives of new platinum based therapies and concluding remarks

Despite cisplatin effectiveness, different strategies have been carried out to improve the platinum-based pharmacology, mainly focused in minimizing platinum secondary effects and overcoming the resistance acquisition. These strategies can be classified in three groups: (I) development of new platinum-based compounds, (II) improvement of platinum drug delivery and (III) platinum-combined therapies

Development of new platinum-based drugs

Several thousand of cisplatin analogues have been synthesized and tested for properties that would enhance its therapeutic effectiveness. About 13 of these analogues were evaluated and 9 were further considered to clinical trials (Dasari & Bernard Tchounwou 2014). In 1989, the FDA approved carboplatin, which is, broadly speaking, equally effective to cisplatin and causes a more acceptable side-effect profile. Other analog, oxaliplatin, displays a different spectrum of activity, low cross-resistance with cisplatin and a different pattern of cellular responses. In fact is the only platinum compound effective in colorectal cancers (Goldstein et al. 2015). More recently, satraplatin was developed as the first orally administered platinum drug. The action of this drug is promising in patients with prostate cancer. In addition, picoplatin retains activity against a wide range of cisplatin and oxaliplatin-resistant tumors (Kelland 2007). The search of new platinum-based compound does not stop currently, as example, platinacycle 6a is capable of induce FOXO3a nuclear translocation and inhibit lung cancer cells synergistically with cisplatin (Cortés et al. 2014).

Apart from cisplatin, there are not studies in *C. elegans* using or developing platinum-drugs. We performed a preliminary experiment analyzing the effect of carboplatin and oxaliplatin in *C. elegans* resulting in both drugs were capable to alter worm development (Figure 47). Interestingly, higher dose of carboplatin was necessary to induce same effects than cisplatin. This mimics the effect in mammals where carboplatin shows less toxicity than cisplatin.

In conclusion, *C. elegans* could also be used to study the functional differences between these platinum drugs but also as a platform to screen for more effective cisplatin analogues.

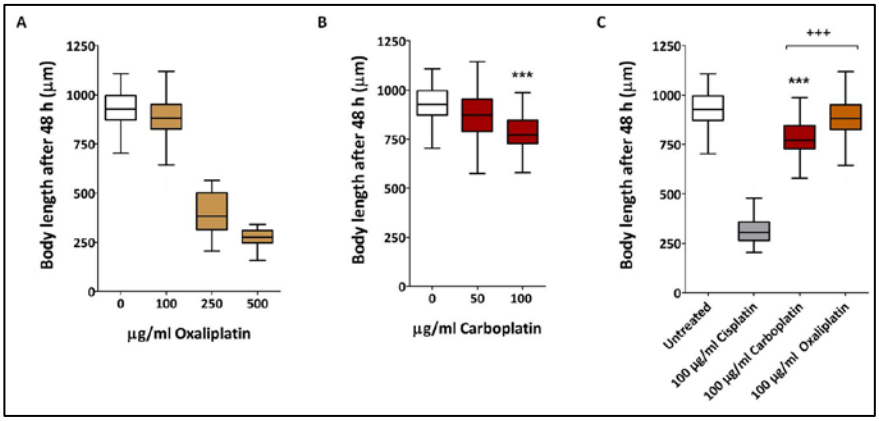

Figure 47. Comparison between the effects of three different platinum drugs in *C. elegans*.
Oxaliplatin (A) and carboplatin (B) alter the larval development in a dose dependent manner. (C) The cytotoxic effect of cisplatin is higher than carboplatin and oxaliplatin at same concentration. ***p<0,001 relative to untreated worms +++p<0,001 relative to cisplatin treated worms by Student's t-test.

Improving drug delivery

In the recent years, new site-specific delivery systems are being explored, which would allow to improve the effectiveness and avoid side-effects of platinum drugs. Thus, different nanoparticles are currently being used in cancer therapeutics including liposomes, lipids, dendrimers or metallic nanoparticles (Apps et al. 2015). As example, liposomal cisplatin, "lipoplatin", shows same efficacy than cisplatin but a significant reduction of side-effects (Stathopoulos & Boulikas 2012). Similar results were obtained *in vitro* evaluating the effect of "cisplatin-magnetic fluid" nanocomposites (Chekhun et al. 2013). Another strategy is a localized administration of cisplatin, like the intraperitoneal administration of cisplatin or carboplatin in patients with ovarian cancer (Armstrong et al. 2006). In this area, worms represent an excellent model for improving new systems of delivery, in fact there is an emergent field using *C. elegans* as an alternative model to *in vivo* test new nanocomposites toxicity and efficacy of delivering drugs that could be applied in platinum-based chemotherapy (Miyako et al. 2015; Charão et al. 2015).

Develop of cisplatin-combined therapies

Because of cisplatin resistance is multifactorial, most of the efforts in the field of the platinum-based chemotherapy are focused in unraveling the mechanisms of resistance of platinum drugs and develop new combined therapies (Dasari & Bernard Tchounwou 2014). In fact, in the clinic, this is currently the most recurrent and effective strategy to overcome cisplatin associated resistance and tumor relapse. As summarized in Table 10, its use is widely extended for the treatment of many different cancers.

Combination Drug(s)	Cancer type
Paclitaxel	Ovarian, breast, lung, melanoma, head and neck carcinoma
Paclitaxel and 5-FU	Gastric and esophagogastric adenocarcinoma
UFT	Non small lung carcinoma
Doxorubicin	Diffuse malignant pleural mesothelioma
Cyclophosphamide and doxorubicin	Salivary gland advanced carcinoma
Gemcitabine	Biliary cancer
Osthole	Lung cancer
Honeybee venom	Ovarian cancer
Anvirzel	Breast, colon, lung, prostate, melanoma and pancreatic cancer
Bevacizumab	Non small lung carcinoma
Vinbalstine and bleomycin	Metastatic granulosa cell tumors in ovary
Methotrexate and bleomycin	Advanced squamous cell carcinoma of the male genital tract
Everolimus	Urothelial bladder cancer
Fluorouracil, doxorubicin and cyclophosphamide	Salivary gland carcinoma
Metformin	Lung adenocarcinoma
Oxaliplatin, quercetin and thymoquinone	Ovarian cancer
Olaparib	PTEN deficient Lung cancer
Tetra arsenic oxide	Cervical cancer
Vindesine	Non small lung carcinoma
β-galactosyl-pyrrolidinyldiazeniumdiolate	Glial cells of brain, human cervical cancer gliosarcoma cell lines

Table 10. List of cisplatin based combined therapies used in cancer treatment (Extracted from Dasari 2014).

Despite of the progress has been notorious in the last years, new advances in research allow to better dissecting the cisplatin mechanism of action. Thus, analyses of tumor cell resistance against cisplatin are aiming to develop more efficient and targeted drugs that hit defined molecular pathways. Moreover, previous tumor characterization would allow of individualized and targeted treatments. In line with this, recent advances in *C. elegans* such as the CRISPR/Cas9 technology could fast and easily reproduce in worms same genetic alterations allowing screening for better alternative individualized therapies (avatar worms).

Conclusions

1. *C. elegans* is an optimal animal model with translational capability to investigate the action of cisplatin in two different somatic scenarios allowing discriminating between cytoplasmic and nuclear events caused by this drug.

2. Cisplatin activates the *egl-1*-dependent apoptosis pathway in specific somatic cell lineages.

3. Cisplatin-damaging effect promotes in *C. elegans* a transcriptional response where the IIS transcription factors SKN-1/Nrf2 and DAF-16/FOXO are involved.

4. Both DAF-16 and SKN-1 are required for the response to cisplatin.

5. IIS pathway outcomes, regulated by *daf-2*/IGFR1 or the 14-3-3 proteins PAR-5 and FTT-2, are able to alter the response to cisplatin in a *daf-16* and *skn-1* dependent-manner.

6. The cisplatin-induced stress responsive genes *cdr-1*/FAXC and *dod-24*/EPHX1 are required for a proper response to cisplatin.

7. Cisplatin reproductive defects in *C. elegans* are mainly caused by a failure in spermatogenesis.

8. The TRXR-1 selenocysteine amino acid is required for protein activity and cisplatin cytotoxicity in *C. elegans.*

9. The 9q32-q33.1-related *C. elegans* ortholog genes *dnj-2*/DNAJC25, *vha-10*/ATP6V1G1, *ckr-2*/OR2K2, *cgt-1;cgt-3*/GCS and *F27C1.2*/CRT1 are required for a proper response to cisplatin.

Materials and methods

M.1. Worm strains and general methods

The N2 (Bristol) strain was used as wild type in all experiments. Mutant alleles and transgenic strains used in this study are summarized in Table 11.

Strain	Genotype	Source
XF132	*polh-1(if31)*	CGC
CB1370	*daf-2(e1370)*	CGC
CF1038	*daf-16(mu86)*	CGC
TJ356	zIs356 (DAF-16::GFP)	CGC
RB2496	*cdr-1(ok3456)*	CGC
RB1994	*dod-24(ok2629)*	CGC
BS553	*fog-2(oz40)*	CGC
WS1973	*opIs56*(P*egl-1::gfp*)	CGC
CER9	*cerEx05*(P*par-5::gfp::par-5*_ORF_3'UTR)	JC
CER176	*cerIs09*(P*cdr-1::cdr-1::gfp*::*cdr-1*_3'UTR, *unc-119*(+); *prps-0*::HygR_CeOPT::*gpd-2/gpd-3::mCherry::unc-54* 3'UTR)	JC
CER177	*cerEx44*(P*cdr-1::cdr-1::gfp*::*cdr-1*_3'UTR,*unc-119*(+); *prps-0*::HygR_CeOPT::*gpd-2/gpd-3::mCherry::unc-54* 3'UTR)	JC
CER174	*daf-16(mu86), cdr-1(ok3456)*	JC
CER175	*daf-16(mu86), dod-24(ok2629)*	JC
VB1414	*trxr-1(sv47)*	CGC
CER170	*trxr-1(cer4*[U666C]*)*	JC
CER171	*trxr-1(cer5*[U666Stop]*)*	JC
VB2155	*rrf-3 (pk1426); trxr-1(sv47); svEx779* [pCC (P*unc-122::gfp*); *trxr-1(Sec-to-Cys)*)]	ST
VZ50	*trxr-1(sv47); svEx761*[pCC(*Punc-122::gfp*);*pPD49.78*(*trxr-1 (Sec-to-Stop)*)]	AMV
	F27C1.2(tm5909)	NBP
CER184	*F27C1.2(cer3)*	JC
CER185	P*F27C1.2::F27C1.2* ORF*::mCherry::unc-54* 3'UTR	JC
VC693	*cgt-1(ok1045)*	CGC
CL2166	*dvIs19[pAF15*(P*gst-4::gfp*::NLS)]	CGC

Table 11. List of strains used in this study.
CGC: *Caenorhabditis* Genetics Center (Minnessota, USA), NBP: National Bioresource Project (Tokyo, Japan). ST: Simmon Tuck. AVC: Antonio Miranda-Vizuete. JC: Julián Cerón's Lab.

Standard methods were used to culture and manipulate worms (Stiernagle 2006). Thus, worms usually were grown at temperatures between 15ºC and 25ºC in NGM (Nematode grow medium) agar plates seeded with *Escherichia coli* strain OP50. Worm synchronization was carried out by hypochlorite treatment (Porta-de-la-Riva et al. 2012). To genotype mutant alleles from CGC and NBP reference primers were used (Table 12). *daf-2(e1370)* genotyping was performed by PCR/restriction digest phenotyping using NcoI enzyme (Zhang, P. 2012).

Gene		Sequence
daf-2(e1370)	**F**	CGGGATGAGACTGTCAAGATTGGAGATTTCGG
	R	CAACACCTCATCATTACTCAAACCAATCCATG
daf-16(mu86)	**F**	CGCCTTTGTCTCTCTATCG
	R1	GGTTGGTAGAAGAACGAGTG
	R2	CAGGAATCGAGAGGTTCG
cdr-1(ok3456)	**Ext. F**	TGCTCGCGAATTGAAGTATG
	Ext. R	GAACTGTCCGAACTTGTCCC
	Int. F	AAAACGTAAAACACCACGTAAAA
	Int. R	TTTCTGCATGAAAATCGAGA
dod-24(ok2629)	**Ext. F**	GGTTAACCTCCCCAATTCGT
	Ext. R	TTCCGTGATCACAATTGACC
	Int. F	ATTGTCGTCACTTTTCGGCA
	Int. R	TGTGTCCCGAGTAACAACCA
F27C1.2(tm5909)	**Ext. F**	AGCGCATTTGGTGCTGCAAT
	Ext. R	TCATCGACCCGCAGGAGAGA
	Int. F	GTTGCGTATAAAAGGTCGCA
	Int. R	CTAAGGTCGATTAGTGAGGA
trxr-1(sv47)	**Ext. F**	CAGCTCAAACTTTCGAACAC
	Ext. R	GCTTACGAATTCGTTCAGCC
	Int. F	CACTATCTTGTATTTCCGTCC
	Int. R	CCACGAAGTAGAATAGAACG

Table 12. Primers used in this study to genotype mutant alleles.
F: Forward primer. R: Reverse primer. Ext: External primer. Int: Internal primer.

M.2. RNA sequencing analyses

A mixed population of worms representing all stages and growing under control conditions was exposed to 60µg/ml of cisplatin for 24 hours at 20ºC. After 24 hours treated worms, and untreated control animals, were washed with M9 buffer to remove bacteria and pellet frozen in TRIzol. Total RNA purification was performed using the mirVana miRNA isolation kit (Ambion) and mRNA was purified by poly-A capture.

Library construction was performed following manufacturer instructions, and paired and RNA sequenced by Illumina's HiSeq technology. More than x millions of reads (100bp length) were processed and aligned using Tophat software to the *C. elegans* reference genome, version WBcel235.74, to produce BAM files. These BAM files were analyzed using the SeqSolve software, which use Cufflinks/Cuffdiff for differential gene/transcript expression analyses (Trapnell et al. 2012).

M.3. RNAi mediated interference

In this study, RNAi-mediated knockdown was carried out by feeding *C. elegans* with bacterial clones producing dsRNA targeting the desired gene. The RNAi clones used in this study were obtained mainly from the ORFeome libray (Rual et al. 2004) but also from the Ahringher library (Kamath & Ahringer 2003). All RNAi clones were verified by sequencing using L4440 forward and reverse primers.

To perform RNAi by feeding, standard NGM plates were supplemented with 50µg/µL ampicillin, 12,5µg/µL tetracycline and 3mM IPTG. For each experiment, the corresponding RNAi clones were picked from the

corresponding RNAi library or from a previously validated glycerol stock. Colonies were grown overnight at 37ºC in LB medium supplemented with 50μg/μL ampicillin and 12,5μg/μL tetracycline. After seeding bacteria on the RNAi plates, plates were let dry overnight at RT to allow dsRNA production induced by IPTG. RNAi plates were used to feed synchronized L1 worms, unless otherwise stated.

In experiments using *gsr-1(RNAi)* bacteria, five L4 worms of the corresponding genotype were transferred to plates containing *gsr-1(RNAi)* bacteria for 24 h. Then worms were transferred to new fresh *gsr-1(RNAi)* plates, allowing to lay eggs for 12 hours and then removed. After 3 days at 20ºC larval arrest was analyzed only in these day-2 plates.

M.4. Cisplatin assays

Cisplatin powder (Sigma, 15663-27-1) was used to perform all experiments. To prepare NGM agar plates containing cisplatin, 1 ml of this drug previously dissolved in water at the desired concentration was added to the surface of NGM agar plates containing fresh OP50. Once dried, these plates were used before than 24 hours to avoid cisplatin degradation. No differences were observed, in terms of cisplatin activity, using death or alive OP50 on plates with cisplatin (data not shown). In carboplatin (Paraplatin™) and oxaliplatin (Eloxatin™) assays NGM agar plates were prepared 1 ml of each drug, diluted in physiological serum was added to the surface of agar plates containing fresh OP50. Plates with 1ml of serum were added as control.

M.4.1. Cisplatin assay during larval development

A synchronized population of L1 larvae was cultured on NGM plates containing fresh OP50 and cisplatin at different concentrations. After 48 hours at 20ºC, the body length of more than 50 worms for each condition was measured using a stereomicroscope and the NIS-Elements 3.2 software. Most of the comparative studies were performed at 60µg/ml of cisplatin. Experiments containing *daf-2(e1370)* animals were performed at 15ºC and body length measured after four days of incubation. Each assay was performed three independent times, using two biological replicates (plates with worms) at least. Similar procedure was used in carboplatin and oxaliplatin assays. Non-parametric t-student test (GraphPad Prism 5) was used to determine the significance of differences in the mean.

M.4.2. Cisplatin assay in adult animals

To study the effect of cisplatin in adulthood, a synchronized population of young-adult animals growth in NGM plates with fresh OP50 were transferred to a flat 96-well plate containing the indicated doses of cisplatin diluted in S-medium containing OP50 (0,5 ml of pelleted culture in each ml of S-medium). Cisplatin-induced toxicity was evaluated by measuring worm locomotor activity by using an automatized tracking system (WMicrotracker-One) (Simonetta & Golombek 2007). The activity of about 30 worms/well was tracked in a minimum of 4 replicates for each condition. Death was determined when locomotor activity decreased to the level of the negative control (free-worm medium). For RNAi experiments, L1 synchronized larvae were fed with the desired RNAi clone using the standard protocol described above. Then, at the young-

adult stage, worms were transferred to a flat 96-well plate containing S-medium and the corresponding RNAi clone (0,5 ml of pelleted culture in each ml of S-medium), 50 μg/ml ampicillin and 3mM IPTG. The standard concentration of cisplatin for comparative studies in adulthood was 500 μg/ml. The log-rank (Mantel-Cox) test (GraphPad Prism 5) was used to determine the significant differences between survival staircases. Each experiment was performed three independent times at least.

M.4.3. Analyses using *egl-1*, *gst-4* and *daf-16* reporters

To determine ectopic *egl-1* expression, a mixed population of P*egl-1*::GFP (WS1973) transgenic worms were grown in NGM plates containing fresh OP50 and 60 μg/ml cisplatin plates for 24 at 20°C. To *in vivo* observation, worms were recovered with M9 buffer, washed and mounted on a microscope slide containing 2% agar pad using a drop of 0.3mM of levamisole to anesthetize them. Using a Nikon ECLIPSE TI-s inverted microscope we analyzed the ectopic expression quantifying the number of L2 or L4 stage worms with altered GFP signal compared to untreated worms at the same developing time (n=50). Non-parametric Student's t-test (GraphPad Prism 5) was used to determine the significance of differences in the mean between untreated and cisplatin treated animals. These experiments were performed three independent times.

Same procedure as described above was performed to analyze the induced expression of P*gst-4::gfp* (CL2166). To quantify gst-4 induction, GFP fluorescence signals from the individual nematodes (n=25) at same developing time (L4) were measured using the image analyzer "ImageJ V.1.49". Non-parametric one-way ANOVA was used to determine the

significance of differences in the mean GFP signal values. These experiments were performed two independent times.

To observe DAF-16 cellular localization, a synchronized L2-stage population of worms carrying DAF-16::GFP transgene (TJ356) were transfer to M9 buffer containing 0-180 µg/ml of cisplatin for 5 hours at 20ºC. Then, worms were washed and mounted as described above. We quantified the DAF-16 intracellular localization by considering as "nuclear" worms showing a mainly nuclear GFP accumulation along the whole body. Non-parametric Student's t-test (GraphPad Prism 5) was used to determine the significance of differences in the mean between untreated and cisplatin treated animals. These experiments were performed three independent times.

M.4.4. Analysis of cisplatin effect in the germ line

To analyze the effect of cisplatin in the germ line, a synchronized population of L4 stage animals grown under normal conditions (39 hours at 20ºC) was transferred onto NGM plates containing 60µg/ml of cisplatin. After 24h of incubation at 20ºC worms were washed in PBS and germ lines were dissected anesthetizing worms with 3mM of levamisol in PBS, fixed with 4% paraformaldehyde and stained with DAPI (0,6µg/ml of mounting media). These stained gonads were photographed using a Nikon ECLIPSE TI-s inverted microscope. For germ cell quantification in the proliferative region the total number of cells in a single Z stack within 50 mm of the distal end of the gonad was counted. At least 15 germ lines were counted for each experiment. Non-parametric Student's t-test

(GraphPad Prism 5) was used to determine the significance of differences in the mean

M.4.5. Counting of progeny and unfertilized oocytes laid

For self-fertilization assays, a synchronized population of L3-stage worms was transferred to NGM plates with fresh OP50 and different doses of cisplatin for other 24 hours under same conditions. A total of twelve worms of each condition were singled out on fresh OP50 plates letting them to lay progeny. The whole progeny and the number of oocytes laid were scored three days later.

Similar procedure was performed for crossing assays. A N2 male-enriched population or *fog-2(oz40)* animals (that only is able to reproduce by mating) were treated with or without 60µg/ml of cisplatin. After 24 hours of exposure to cisplatin, a total of twelve crosses where performed for each condition. Crosses consisted of placing in fresh OP50 plates either one treated hermaphrodite at the fourth larval stage with four untreated males or untreated hermaphrodite with cisplatin treated males. A total of twelve crosses were performed for each condition. The whole progeny and the number of oocytes laid were scored three days later. Non-parametric Student's t-test (GraphPad Prism 5) was used to determine the significance of differences. The experiments were performed two independent times.

M.5. Generation of transgenic animals

M.5.1. F27C1.2 translational reporter

To generate a transgenic line expressing F27C1.2 fused to mCherry we used the MultiSite Gateway Three-Fragment Vector Construction Kit (Invitrogen). This technology allows obtaining a expression vector generating and combining three pENTRY clones (5', middle and 3') by a sequential series of recombination reactions. We combined three pENTRY vectors: pENTRY1, that contains the 551bp *F27C1.2* promoter; pENTRY2, containing the *F27C1.2* open reading frame and pENTRY3 that carries *mCherry* open reading frame fused to *unc-54* 3'UTR. All reactions performed to generate and combine these vectors to eventually obtain the P*F27C1.2::F27C1.2::mCherry::unc-54*3'UTR final construct were performed according to manufacturer's instructions (Invitrogen). This final vector was transformed in Library Efficiency DH5 competent bacteria (Invitrogen), purified and verified by sequencing using M13 primers. Transgenic animals were generated by microinjecting 20ng/µl of the purified DNA together with 10ng/µl of a vector containing P*myo-2::gfp*.

PCR amplification of F27C1.2 genomic fragments		
P*F27C1.2*	F	GGGGACAACTTTGTATAGAAAAGTTGCCGCCATTACCTGCAAAATTAAG
	R	GGGGACTGCTTTTTTGTACAAACTTGCGATCTGAAAATATATGACGTAAC
F27C1.2 ORF	F	GGGGACAATGTTGTACAAAAAAGCAGGCTCCATGGGTACACAATTGGCCAT
	R	GGGGACCACTTTGTACAAGAAAGCTGGGTCATGACACGCATCGGTTTGGA

Table 13. List of primerss used to create the pENTRY1 and pENTRY2 clones to generate F27C1.2 translational reporter.

Plasmisd	Backbone vector	Expressing	Source
pENTRY1	pDONR P4-P1R	*F27C1.2* promoter	This study
pENTRY2	pDONR221	F27C1.2 ORF	This study
pENTRY3	pDNOR P2R-P3	*mCherry* ORF + *unc-54*' 3UTR	JC
Final constuct	PCFJ150	P*F2C1.2::F27C1.2::mCherry::unc -54* 3'UTR	This study

Table 14. List of plasmids used to generate F27C1.2 translational reporter.

M.5.2. Transgenesis by CRISPR/Cas9 system

By using this methodology, we performed different strategies to generate the *F27C1.2(cer3)* mutant allele, and *trxr-1(cer4*[U666C]*) trxr-1(cer4*[U666STOP] point mutations. To create a null allele for *F27C1.2* we performed a big deletion targeting the gene with four sgRNAs: two at 5' limit and the other two at the 3' (Figure 48, Table 14). While for making *trxr-1* point mutations we only designed an sgRNA targeting at the 3' of the gene, close to selenocysteine and we generated a repair template containing the desired change in the selenocysteine codon (Figure 49).

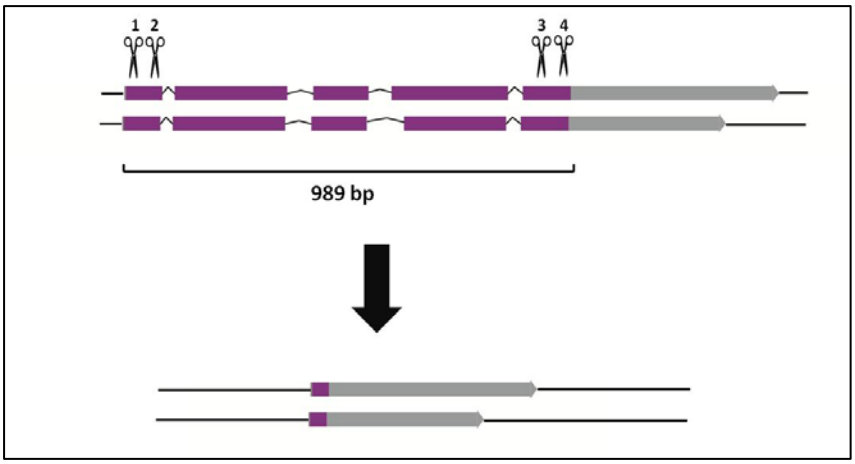

Figure 48. Strategy used to generate *F27C1.2(cer3)*.
Targeting the genome with four different sgRNAs, two in each side generates double strand breaks both at 5' and 3' of the gene. DNA repair by non homologous end joining can join both extremes generating an approximately 1Kb deletion.

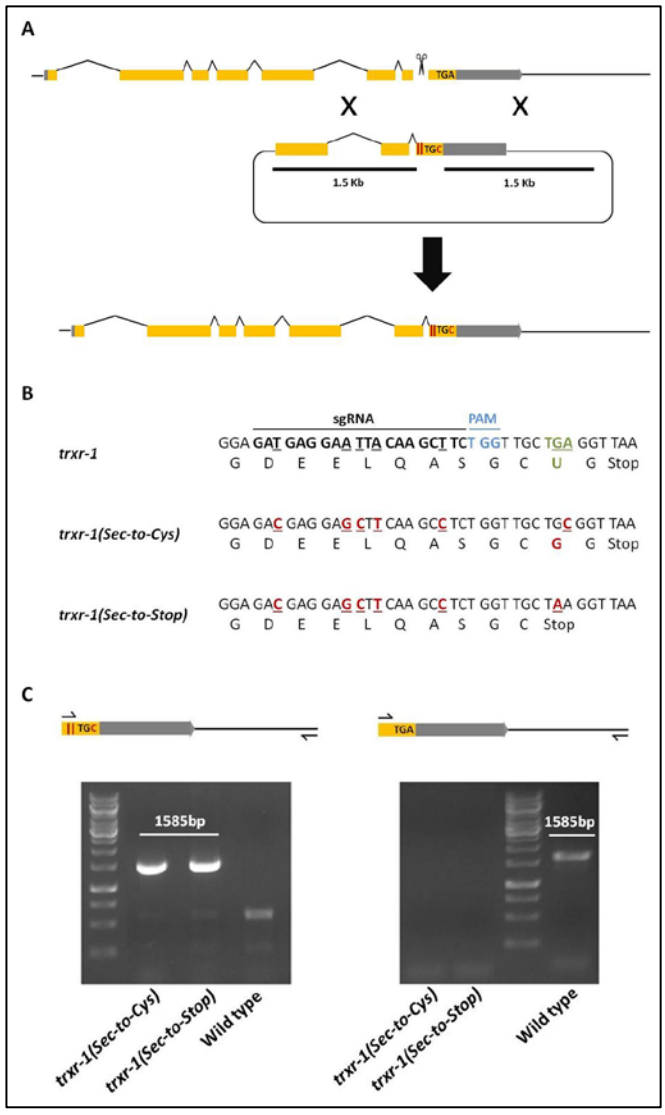

Figure 49. Generation of *trxr-1* point mutations.
(A) sgRNA targeted close to the end of the ORF produces a double strand break. DNA repair by homologous recombination using a designed repair template allows adding the desired point modifications. (B) Modifications carried by two designed different repair templates. A single modification in Sec codon allows changing Sec to Cys (TGA to TGC) and Sec for a stop codon (TGA to TAA). Other modifications that do not alter codon usage were included in the template to avoid Cas9 cut. (C) PCR strategy used to screen and genotype the new alleles. The modifications in the template allows to generate an specific forward primer for the new alleles that does not bind to the wild type sequence (left panel) while a primer without these changes only binds to wild type DNA (right panel).

For sgRNA selection and potential off-target sites prediction was used the CRISPR Design Tool (http://crispr.mit.edu). All sgRNAs were cloned into PMB70 vector (Waaijers et al. 2013). *trxr-1(cer4[U666C])* and *cer5[U666STOP]* repair templates were designed by Gibson Assembly Cloning Kit (New England BioLabs) and cloned into pBSK. Both sgRNAs and repair templates were verified by sequencing by T4 primer and M13 respectively. Mutant *F27C1.2* animals were generated by injecting to N2 worms 30ng/µl of each sgRNA, together with 50ng/µl of P*hsp16.48::*Cas9 plasmid and 2.5 ng/µl of P*myo-2::tdtomato* marker. These animals were then transferred to 35ºC for 1 hour. For generating *trxr-1* animals were injected 30ng/µl sgRNA, 100ng/µl repair template, 30ng/µl of *Peft-3*::Cas9 vector and 2.5ng/µl of P*myo-2::tdtomato* marker. PCR strategies and sequencing were performed to localize and verify the mutant animals (Table 15, Figure 49).

Plasmid	Expressing	Source
pMB70	sgRNAs	M.Boxem
pBSK	Repair template	Addgene
pUC57	P*eft-3::*Cas9	J.Calarco
pMB67	P*hsp16.48::*Cas9	M.Boxem
	*Pmyo-2::*tdtomato	M. Boxem

Table 15. List of plasmids used for transgenesis by CRISPR/Cas9 system.

F27C1.2 (cer3)		
sgRNA1	**F**	AATTGGTACACAATTGGCCATCCT
	R	AAACAGGATGGCCAATTGTGTACC
sgRNA2	**F**	AATTATGGTTGGCTGTGGCTTTGG
	R	AAACCCAAAGCCACAGCCAACCAT
sgRNA3	**F**	AATTAAATTGTGATGGAGAAGTGA
	R	AAACTCACTTCTCCATCACAATTT
sgRNA4	**F**	AATTATTAATGACACGCATCGGTT
	R	AAACAACCGATGCGTGTCATTAAT
***F27C1.2(cer-3)* external**	**F**	AGCGCATTTGGTGCTGCAAT
	R	TCATCGACCCGCAGGAGAGA
***F27C1.2(cer-3)* internal**	**F**	GTTGCGTATAAAAGGTCGCA
	R	CTAAGGTCGATTAGTGAGGA
trxr-1*(cer4*[U666C]*)* **and** ***trxr-****1(cer5*[U666STOP]*)*		
sgRNA	**F**	AATTGATGAGGAATTACAAGCTTC
	R	AAACGAAGCTTGTAATTCCTCATC
5' 1.5 Kb Overlaping fragment	**F**	CGGGCCCCCCCCTCGAGGTCGACGGTATCGATAAGCTT GATAGGTTATGGTTCGTTCTATTCTACTTCGTG
	R *(cer4*[U666C]*)*	CTTAACCGCAGCAACCAGAGGCTTGAAGCTCCTCGTCT CCTTCCTTCTTTTCAAGAG
	R*(cer5*[U666STOP]*)*	CTTAACCTTAGCAACCAGAGGCTTGAAGCTCCTCGTCT CCTTCCTTCTTTTCAAGAG
3' 1.5 Kb Overlaping fragment	**F *(cer4*[U666C]*)***	AAGGAGACGAGGAGCTTCAAGCCTCTGGTTGCTGCGG TTAAGAAGGGTCCAATTTG
	F *(cer5*[U666STOP]*)*	AAGGAGACGAGGAGCTTCAAGCCTCTGGTTGCTAAGG TTAAGAAGGGTCCAATTTG
	R	CTCTAGAACTAGTGGATCCCCCGGGCTGCAGGAATTC GATCCTGTTTTTTAGAGAGAGGTTGCGAGTAAGG
Mutant genotyping 1	**F**	GGAAGGAGACGAGGAGCTT
	R	AAACAGTGTGCAATTTCTATTTCG
Mutant genotyping 2	**F**	TGCTTCGTACGTCTCATTGG
	R	GCAACCAGAGGCTTGAAGC
Wild type genotyping 1	**F**	GATGAGGAATTACAAGCTTC
	R	AAACAGTGTGCAATTTCTATTTCG
Wild type genotyping 2	**F**	TGCTTCGTACGTCTCATTGG
	R	GAAGCTTGTAATTCCTCATC

Table 16. List of primers used to generate *F27C1.2(cer3)*, *trxr-1(cer4[U666C])* and *trxr-1(cer5[U666STOP])* strains. F: Forward primer. R: Reverse primer.

M.5.3. Generation of *cdr-1* translational reporters

CER177 and CER178 transgenic strains were generated by bombardment with gold particles (Biolistic Helium Gun, Caenotec). Wild type young adult worms were bombarded with a mix including 8µg of fosmid vector containing a GFP-tagged version of *cdr-1*, requested from the Transgeneome resource (Sarov et al. 2012), and 8µg of IR88 vector allowing the transgen selection by resistance to hygromycin B. Fosmid was purified using FosmidMAX™ DNA Purification Kit from Epicentre (FMAX046) and validated by sequencing.

M.6. Quantitative real-time PCR of engrafted tumors

Total RNA from tumors was extracted using Trizol reagent (Invitrogen) and cDNA obtained after a reverse transcription reaction (High Capacity cDNA Reverse Transcription Kit, Applied Biosystems) Real-time PCR of cDNA obtained from TGT17, TGT38, and TGT1 tumors was done with SYBR Green (Roche Molecular Biochemicals) and human specific primers for all genes showed in the table.

Real-time PCR was run on a LightCycler instrument (Roche Molecular Biochemicals). Forty cycles of amplification with denaturation at 95°C for 10 s followed by annealing at 60-65°C for 20 s and extension at 72°C for 13 s were done after an initial incubation at 95°C for 10 min. The fold change expression of the corresponding genes was based on the ddCT method and normalized after subtracting the mean Ct values of β-actin gene from the receptor gene mean Ct values.

Gene		Sequence
BAD	F	AGTGACGAGTTTGTGGAC
	R	CACCAGGACTGGAAGACT
COMTD1	F	CGGACAAGGAGAACTGCT
	R	TCGGAGGTTGCAGCACCTTC
CSMD1	F	CAAGAGCCGTCTGGACAC
	R	TCGTGGAAGGTCTTCGTC
DXO	F	CATCCACACAGCCCCCAA
	R	AAGCCAGCAACAACATTC
EPHX1	F	GTCTGGCTGCCTATATTC
	R	TGCTTCTGGGTCATCCAG
FAXC	F	TACCAGGGACAAGACCCGAA
	R	AAAAGCTAAAATCCAGCAGC
GSTP1	F	CTATGGGAAGGACCAGCA
	R	ATAGTCATCCTTGCCCGC
MCR1	F	AGCTTGTATAGGCTTTGG
	R	CCTGCTTCATTTGATGCA
PGC	F	AGCCAGGCCTGCACCAGT
	R	GTGGTGGCCTCATCCACG
RDH11	F	ATGAGATGGATGTGGTGG
	R	GCAGAGACCCATGCCACA
UGT3A2	F	AAGATGTCCACCTGGCTG
	R	GGCTGGTCTCCAAAGAGA
β-ACTIN	F	GGAGTGGGTGGAGGCAG
	R	AACTAAGGTGTGCACTTTTGTTC

Table 17. List of human specific primers used to analyze the corresponding gene tumoral expression. F: Forward primer. R: Reverse primer.

Bibliography

Abbas, M. et al., 2015. Glutathione S-Transferase Gene Polymorphisms and Treatment Outcome in Cervical Cancer Patients under Concomitant Chemoradiation. *PloS one*, 10(11), p.e0142501.

Aida, T. et al., 2005. Expression of copper-transporting P-type adenosine triphosphatase (ATP7B) as a prognostic factor in human endometrial carcinoma. *Gynecologic oncology*, 97(1), pp.41–5.

Al-Majed, A.A., 2007. Carnitine deficiency provokes cisplatin-induced hepatotoxicity in rats. *Basic & clinical pharmacology & toxicology*, 100(3), pp.145–50.

An, J.H. et al., 2005. Regulation of the Caenorhabditis elegans oxidative stress defense protein SKN-1 by glycogen synthase kinase-3. *Proceedings of the National Academy of Sciences of the United States of America*, 102(45), pp.16275–80.

An, J.H. & Blackwell, T.K., 2003. SKN-1 links C. elegans mesendodermal specification to a conserved oxidative stress response. *Genes & development*, 17(15), pp.1882–93.

Anestål, K. et al., 2008. Cell death by SecTRAPs: thioredoxin reductase as a prooxidant killer of cells. *PloS one*, 3(4), p.e1846.

Anon, 1998. Genome sequence of the nematode C. elegans: a platform for investigating biology. *Science (New York, N.Y.)*, 282(5396), pp.2012–8.

Apps, M.G., Choi, E.H.Y. & Wheate, N.J., 2015. The state-of-play and future of platinum drugs. *Endocrine-related cancer*, 22(4), pp.R219–33.

Aprison, E.Z. & Ruvinsky, I., 2014. Balanced trade-offs between alternative strategies shape the response of C. elegans reproduction to chronic heat stress. *PloS one*, 9(8), p.e105513.

Arantes-Oliveira, N. et al., 2002. Regulation of life-span by germ-line stem cells in Caenorhabditis elegans. *Science (New York, N.Y.)*, 295(5554), pp.502–5.

Aristizábal-Corrales, D., Schwartz, S. & Cerón, J., 2013. PAR-5 is a PARty hub in the germline: Multitask proteins in development and disease. *Worm*, 2(1), p.e21834.

Armstrong, D.K. et al., 2006. Intraperitoneal cisplatin and paclitaxel in ovarian cancer. *The New England journal of medicine*, 354(1), pp.34–43.

Arnér, E.S. & Holmgren, A., 2000. Physiological functions of thioredoxin and thioredoxin reductase. *European journal of biochemistry / FEBS*, 267(20), pp.6102–9.

Arnér, E.S.J., 2009. Focus on mammalian thioredoxin reductases--important selenoproteins with versatile functions. *Biochimica et biophysica acta*, 1790(6), pp.495–526.

Barsyte, D., Lovejoy, D. a & Lithgow, G.J., 2001. Longevity and heavy metal resistance in daf-2 and age-1 long-lived mutants of Caenorhabditis elegans. *The FASEB journal : official publication of the Federation of American Societies for Experimental Biology*, 15(3), pp.627–634.

Bartek, J. & Lukas, J., 2007. DNA damage checkpoints: from initiation to recovery or adaptation. *Current opinion in cell biology*, 19(2), pp.238–45.

Baugh, L.R. & Sternberg, P.W., 2006. DAF-16/FOXO regulates transcription of cki-1/Cip/Kip and repression of lin-4 during C. elegans L1 arrest. *Current biology : CB*, 16(8), pp.780–5.

Berdichevsky, A. & Guarente, L., 2006. A stress response pathway involving sirtuins, forkheads and 14-3-3 proteins. *Cell cycle (Georgetown, Tex.)*, 5(22), pp.2588–91.

Beyer, J. et al., 1996. High-dose chemotherapy as salvage treatment in germ cell tumors: a multivariate analysis of prognostic variables. *Journal of clinical oncology : official journal of the American Society of Clinical Oncology*, 14(10), pp.2638–45.

Blackwell, T.K. et al., 2015. SKN-1/Nrf, stress responses, and aging in Caenorhabditis elegans. *Free radical biology & medicine*, 88(Pt B), pp.290–301.

Blair, B.G. et al., 2009. Copper transporter 2 regulates the cellular accumulation and cytotoxicity of Cisplatin and Carboplatin. *Clinical cancer research : an official journal of the American Association for Cancer Research*, 15(13), pp.4312–21.

Bobylev, I. et al., 2015. [Chemotherapy-induced Peripheral Neuropathy]. *Fortschritte der Neurologie-Psychiatrie*, 83(8), pp.427–36.

Boyd, W.A. et al., 2010. Nucleotide excision repair genes are expressed at low levels and are not detectably inducible in Caenorhabditis elegans somatic tissues, but their function is required for normal adult life after UVC exposure. *Mutation research*, 683(1-2), pp.57–67.

Brenner, S., 1974. The genetics of Caenorhabditis elegans. *Genetics*, 77(1), pp.71–94.

Brozovic, A. et al., 2004. Long-term activation of SAPK/JNK, p38 kinase and fas-L expression by cisplatin is attenuated in human carcinoma cells that acquired drug resistance. *International journal of cancer. Journal international du cancer*, 112(6), pp.974–85.

Bujan, L. et al., 2013. Impact of chemotherapy and radiotherapy for testicular germ cell tumors on spermatogenesis and sperm DNA: a multicenter prospective study from the CECOS network. *Fertility and sterility*, 100(3), pp.673–80.

Burger, H. et al., 2011. Drug transporters of platinum-based anticancer agents and their clinical significance. *Drug Resistance Updates*, 14(1), pp.22–34.

Castedo, M. et al., 2006. Selective resistance of tetraploid cancer cells against DNA damage-induced apoptosis. *Annals of the New York Academy of Sciences*, 1090, pp.35–49.

Cebula, M., Schmidt, E.E. & Arnér, E.S.J., 2015. TrxR1 as a potent regulator of the Nrf2-Keap1 response system. *Antioxidants & redox signaling*, 23(10), pp.823–53.

Cepeda, V. et al., 2007. Biochemical mechanisms of cisplatin cytotoxicity. *Anti-cancer agents in medicinal chemistry*, 7(1), pp.3–18.

Chan, T.A. et al., 2000. Cooperative effects of genes controlling the G(2)/M checkpoint. *Genes & development*, 14(13), pp.1584–8.

Chang, E.M. et al., 2015. Cisplatin Induces Overactivation of the Dormant Primordial Follicle through PTEN/AKT/FOXO3a Pathway which Leads to Loss of Ovarian Reserve in Mice. *PloS one*, 10(12), p.e0144245.

Charão, M.F. et al., 2015. Caenorhabditis elegans as an alternative in vivo model to determine oral uptake, nanotoxicity, and efficacy of melatonin-loaded lipid-core nanocapsules on paraquat damage. *International journal of nanomedicine*, 10, pp.5093–106.

Chaurasia, B. & Summers, S.A., 2015. Ceramides - Lipotoxic Inducers of Metabolic Disorders. *Trends in endocrinology and metabolism: TEM*, 26(10), pp.538–50.

Chekhun, V.F. et al., 2013. In vitro modification of cisplatin cytotoxicity

with magnetic fluid. *Experimental oncology*, 35(1), pp.15–9.

Chen, H.H.W. & Kuo, M.T., 2010. Role of glutathione in the regulation of Cisplatin resistance in cancer chemotherapy. *Metal-based drugs*, 2010.

Chen, Y. et al., 2007. Collateral Damage in Cancer Chemotherapy: Oxidative Stress in Nontargeted Tissues. *Molecular Interventions*, 7(3), pp.147–156.

Choe, K.P., Przybysz, A.J. & Strange, K., 2009. The WD40 repeat protein WDR-23 functions with the CUL4/DDB1 ubiquitin ligase to regulate nuclear abundance and activity of SKN-1 in Caenorhabditis elegans. *Molecular and cellular biology*, 29(10), pp.2704–15.

Ciarimboli, G., 2012. Membrane transporters as mediators of Cisplatin effects and side effects. *Scientifica*, 2012, p.473829.

Collis, S.J. et al., 2006. C. elegans FANCD2 responds to replication stress and functions in interstrand cross-link repair. *DNA repair*, 5(11), pp.1398–406.

Conradt, B. & Horvitz, H.R., 1998. The C. elegans protein EGL-1 is required for programmed cell death and interacts with the Bcl-2-like protein CED-9. *Cell*, 93(4), pp.519–29.

Cornes, E. et al., 2014. Applying antibiotic selection markers for nematode genetics. *Methods (San Diego, Calif.)*, 68(3), pp.403–8.

Cortés, R. et al., 2014. A novel cyclometallated Pt(II)-ferrocene complex induces nuclear FOXO3a localization and apoptosis and synergizes with cisplatin to inhibit lung cancer cell proliferation. *Metallomics : integrated biometal science*, 6(3), pp.622–33. A

Craig, A.L. et al., 2012. Methods for studying the DNA damage response in the Caenorhabdatis elegans germ line. *Methods in cell biology*, 107, pp.321–52.

Di Cristofori, A. et al., 2015. The vacuolar H+ ATPase is a novel therapeutic target for glioblastoma. *Oncotarget*, 6(19), pp.17514–31.

Crone, B. et al., 2015. Elemental bioimaging of Cisplatin in Caenorhabditis elegans by LA-ICP-MS. *Metallomics : integrated biometal science*, 7(7), pp.1189–95.

Cui, Y. et al., 2007. Toxicogenomic analysis of Caenorhabditis elegans

reveals novel genes and pathways involved in the resistance to cadmium toxicity. *Genome biology*, 8(6), p.R122.

Dasari, S. & Bernard Tchounwou, P., 2014. Cisplatin in Cancer therapy: Molecular mechanisms of action. *European journal of pharmacology*, 740, pp.364–78.

Derry, W.B. et al., 2007. Regulation of developmental rate and germ cell proliferation in Caenorhabditis elegans by the p53 gene network. *Cell death and differentiation*, 14(4), pp.662–70.

Dittrich, C.M. et al., 2012. LEM-3 - A LEM domain containing nuclease involved in the DNA damage response in C. elegans. *PloS one*, 7(2), p.e24555.

Dong, J., Boyd, W.A. & Freedman, J.H., 2008. Molecular characterization of two homologs of the Caenorhabditis elegans cadmium-responsive gene cdr-1: cdr-4 and cdr-6. *Journal of molecular biology*, 376(3), pp.621–33.

Dong, J., Song, M.O. & Freedman, J.H., 2005. Identification and characterization of a family of Caenorhabditis elegans genes that is homologous to the cadmium-responsive gene cdr-1. *Biochimica et biophysica acta*, 1727(1), pp.16–26.

Ermolaeva, M. & Schumacher, B., 2013. The innate immune system as mediator of systemic DNA damage responses. *Communicative & integrative biology*, 6(6), p.e26926.

Ermolaeva, M.A. et al., 2013. DNA damage in germ cells induces an innate immune response that triggers systemic stress resistance. *Nature*, 501(7467), pp.416–20.

Fernández de Mattos, S. et al., 2008. FOXO3a mediates the cytotoxic effects of cisplatin in colon cancer cells. *Molecular cancer therapeutics*, 7(10), pp.3237–3246.

Fiebig, H.H., Maier, A. & Burger, A.M., 2004. Clonogenic assay with established human tumour xenografts: correlation of in vitro to in vivo activity as a basis for anticancer drug discovery. *European journal of cancer (Oxford, England : 1990)*, 40(6), pp.802–20.

Fire, A. et al., 1998. Potent and specific genetic interference by double-stranded RNA in Caenorhabditis elegans. *Nature*, 391(6669), pp.806–11.

Fraser, A.G. et al., 2000. Functional genomic analysis of C. elegans

chromosome I by systematic RNA interference. *Nature*, 408(6810), pp.325–30.

Frézal, L. & Félix, M.-A., 2015. C. elegans outside the Petri dish. *eLife*, 4.

Friedland, A.E. et al., 2013. Heritable genome editing in C. elegans via a CRISPR-Cas9 system. *Nature methods*, 10(8), pp.741–3.

Frøkjaer-Jensen, C. et al., 2008. Single-copy insertion of transgenes in Caenorhabditis elegans. *Nature genetics*, 40(11), pp.1375–83.

Galanski, M., 2006. Recent developments in the field of anticancer platinum complexes. *Recent patents on anti-cancer drug discovery*, 1(2), pp.285–95.

Galluzzi, L. et al., 2012. Molecular mechanisms of cisplatin resistance. *Oncogene*, 31(15), pp.1869–1883. Available at: http://dx.doi.org/10.1038/onc.2011.384.

Gañán-Gómez, I. et al., 2013. Oncogenic functions of the transcription factor Nrf2. *Free radical biology & medicine*, 65, pp.750–64.

Gartner, a et al., 2000. A conserved checkpoint pathway mediates DNA damage--induced apoptosis and cell cycle arrest in C. elegans. *Molecular cell*, 5(3), pp.435–443.

Gartner, A., MacQueen, A.J. & Villeneuve, A.M., 2004. Methods for analyzing checkpoint responses in Caenorhabditis elegans. *Methods in molecular biology (Clifton, N.J.)*, 280, pp.257–74.

Gasiunas, G. et al., 2012. Cas9-crRNA ribonucleoprotein complex mediates specific DNA cleavage for adaptive immunity in bacteria. *Proceedings of the National Academy of Sciences of the United States of America*, 109(39), pp.E2579–86.

Germà-Lluch, J.R. et al., 2002. Clinical pattern and therapeutic results achieved in 1490 patients with germ-cell tumours of the testis: the experience of the Spanish Germ-Cell Cancer Group (GG). *European urology*, 42(6), pp.553–62; discussion 562–3.

Giaccone, G., 2000. Clinical perspectives on platinum resistance. *Drugs*, 59 Suppl 4, pp.9–17; discussion 37–8.

Giordano-Santini, R. & Dupuy, D., 2011. Selectable genetic markers for nematode transgenesis. *Cellular and molecular life sciences : CMLS*, 68(11), pp.1917–27.

Girard, L.R. et al., 2007. WormBook: the online review of Caenorhabditis

elegans biology. *Nucleic acids research*, 35(Database issue), pp.D472–5.

Gladyshev, V.N. et al., 1999. Selenocysteine-containing thioredoxin reductase in C. elegans. *Biochemical and biophysical research communications*, 259(2), pp.244–9.

Glasauer, A. & Chandel, N.S., 2014. Targeting antioxidants for cancer therapy. *Biochemical pharmacology*, 92(1), pp.90–101.

Goldstein, D.A. et al., 2015. Metastatic Colorectal Cancer: A Systematic Review of the Value of Current Therapies. *Clinical colorectal cancer*.

Gönczy, P. et al., 2000. Functional genomic analysis of cell division in C. elegans using RNAi of genes on chromosome III. *Nature*, 408(6810), pp.331–6.

Goodsell, D.S., 2006. The molecular perspective: Cisplatin. *Stem cells (Dayton, Ohio)*, 24(3), pp.514–5.

Goto, S. et al., 1999. Overexpression of glutathione S-transferase pi enhances the adduct formation of cisplatin with glutathione in human cancer cells. *Free radical research*, 31(6), pp.549–58.

Goto, T. et al., 2008. The involvement of FOXO1 in cytotoxic stress and drug-resistance induced by paclitaxel in ovarian cancers. *British journal of cancer*, 98(6), pp.1068–75.

Gouazé, V. et al., 2005. Glucosylceramide synthase blockade down-regulates P-glycoprotein and resensitizes multidrug-resistant breast cancer cells to anticancer drugs. *Cancer research*, 65(9), pp.3861–7.

Greiss, S. et al., 2008. Transcriptional profiling in C. elegans suggests DNA damage dependent apoptosis as an ancient function of the p53 family. *BMC genomics*, 9, p.334.

Grishok, A., 2005. RNAi mechanisms in Caenorhabditis elegans. *FEBS letters*, 579(26), pp.5932–9.

Gromer, S., Urig, S. & Becker, K., 2004. The thioredoxin system--from science to clinic. *Medicinal research reviews*, 24(1), pp.40–89.

van Haaften, G. et al., 2006. Identification of Conserved Pathways of

DNA-Damage Response and Radiation Protection by Genome-Wide RNAi. *Current Biology*, 16(13), pp.1344–1350.

Hartmann, J.T. & Lipp, H.-P., 2003. Toxicity of platinum compounds. *Expert opinion on pharmacotherapy*, 4(6), pp.889–901.

Hasegawa, K. et al., 2008. Acrylamide-responsive genes in the nematode Caenorhabditis elegans. *Toxicological sciences : an official journal of the Society of Toxicology*, 101(2), pp.215–25.

Hayden, A. et al., 2014. The Nrf2 transcription factor contributes to resistance to cisplatin in bladder cancer. *Urologic oncology*, 32(6), pp.806–14.

Helmcke, K.J. et al., 2009. Characterization of the effects of methylmercury on Caenorhabditis elegans. *Toxicology and applied pharmacology*, 240(2), pp.265–72.

Hemmingsson, O. et al., 2010. ASNA-1 activity modulates sensitivity to cisplatin. *Cancer Research*, 70(24), pp.10321–10328.

Hidalgo, M. et al., 2014. Patient-derived xenograft models: an emerging platform for translational cancer research. *Cancer discovery*, 4(9), pp.998–1013.

Holzer, A.K., Manorek, G.H. & Howell, S.B., 2006. Contribution of the major copper influx transporter CTR1 to the cellular accumulation of cisplatin, carboplatin, and oxaliplatin. *Molecular pharmacology*, 70(4), pp.1390–4.

Honda, Y. & Honda, S., 1999. The daf-2 gene network for longevity regulates oxidative stress resistance and Mn-superoxide dismutase gene expression in Caenorhabditis elegans. *FASEB journal : official publication of the Federation of American Societies for Experimental Biology*, 13(11), pp.1385–93.

Horvitz, H.R. & Sulston, J.E., 1980. Isolation and genetic characterization of cell-lineage mutants of the nematode Caenorhabditis elegans. *Genetics*, 96(2), pp.435–54.

Huang, D.W., Sherman, B.T. & Lempicki, R.A., 2009a. Bioinformatics enrichment tools: paths toward the comprehensive functional analysis of large gene lists. *Nucleic acids research*, 37(1), pp.1–13.

Huang, D.W., Sherman, B.T. & Lempicki, R.A., 2009b. Systematic and integrative analysis of large gene lists using DAVID bioinformatics resources. *Nature protocols*, 4(1), pp.44–57.

Huang, W.-C. et al., 2011. Glucosylceramide synthase inhibitor PDMP sensitizes chronic myeloid leukemia T315I mutant to Bcr-Abl inhibitor and cooperatively induces glycogen synthase kinase-3-regulated apoptosis. *FASEB journal: official publication of the Federation of American Societies for Experimental Biology*, 25(10), pp.3661–73.

Hubbard, E.J. & Greenstein, D., 2000. The Caenorhabditis elegans gonad: a test tube for cell and developmental biology. *Developmental dynamics : an official publication of the American Association of Anatomists*, 218(1), pp.2–22.

Ichikawa, S. et al., 1996. Expression cloning of a cDNA for human ceramide glucosyltransferase that catalyzes the first glycosylation step of glycosphingolipid synthesis. *Proceedings of the National Academy of Sciences of the United States of America*, 93(22), p.12654.

Inoue, H. et al., 2005. The C. elegans p38 MAPK pathway regulates nuclear localization of the transcription factor SKN-1 in oxidative stress response. *Genes & development*, 19(19), pp.2278–83.

Ishida, S. et al., 2010. Enhancing tumor-specific uptake of the anticancer drug cisplatin with a copper chelator. *Cancer cell*, 17(6), pp.574–83.

Jain, H.V. & Meyer-Hermann, M., 2011. The molecular basis of synergism between carboplatin and ABT-737 therapy targeting ovarian carcinomas. *Cancer research*, 71(3), pp.705–15.

Jemal, A. et al., 2008. Cancer statistics, 2008. *CA: a cancer journal for clinicians*, 58(2), pp.71–96.

Jinek, M. et al., 2012. A programmable dual-RNA-guided DNA endonuclease in adaptive bacterial immunity. *Science (New York, N.Y.)*, 337(6096), pp.816–21.

de Jongh, F.E. et al., 2003. Weekly high-dose cisplatin is a feasible treatment option: analysis on prognostic factors for toxicity in 400 patients. *British journal of cancer*, 88(8), pp.1199–206.

Jorgensen, E.M. & Mango, S.E., 2002. The art and design of genetic screens: caenorhabditis elegans. *Nature reviews. Genetics*, 3(5), pp.356–69.

Juliachs, M. et al., 2013. Effectivity of pazopanib treatment in orthotopic models of human testicular germ cell tumors. *BMC cancer*, 13, p.382..

Juliachs, M. et al., 2014. The PDGFRβ-AKT pathway contributes to CDDP-acquired resistance in testicular germ cell tumors. *Clinical cancer research : an official journal of the American Association for Cancer Research*, 20(3), pp.658–67.

Kahn, N.W. et al., 2008. Proteasomal dysfunction activates the transcription factor SKN-1 and produces a selective oxidative-stress response in Caenorhabditis elegans. *The Biochemical journal*, 409(1), pp.205–13.

Kamal, N.S. et al., 2010. MutS homologue 2 and the long-term benefit of adjuvant chemotherapy in lung cancer. *Clinical cancer research : an official journal of the American Association for Cancer Research*, 16(4), pp.1206–15.

Kamath, R.S. & Ahringer, J., 2003. Genome-wide RNAi screening in Caenorhabditis elegans. *Methods (San Diego, Calif.)*, 30(4), pp.313–21.

Kang, T.-W. et al., 2011. Senescence surveillance of pre-malignant hepatocytes limits liver cancer development. *Nature*, 479(7374), pp.547–51.

Kanzok, S.M., 2001. Substitution of the Thioredoxin System for Glutathione Reductase in Drosophila melanogaster. *Science*, 291(5504), pp.643–646.

Kaspar, J.W., Niture, S.K. & Jaiswal, A.K., 2009. Nrf2:INrf2 (Keap1) signaling in oxidative stress. *Free radical biology & medicine*, 47(9), pp.1304–9.

Kelland, L., 2007. The resurgence of platinum-based cancer chemotherapy. *Nature reviews. Cancer*, 7(8), pp.573–84.

Kelland, L.R., 1993. New platinum antitumor complexes. *Critical reviews in oncology/hematology*, 15(3), pp.191–219. Available at: http://www.ncbi.nlm.nih.gov/pubmed/8142057 [

Kim, S., Park, D.-H. & Shim, J., 2008. Thymidylate synthase and dihydropyrimidine dehydrogenase levels are associated with response to 5-fluorouracil in Caenorhabditis elegans. *Molecules and cells*, 26(4), pp.344–349.

Kim, S.K., 2001. Http://C. elegans: mining the functional genomic landscape. *Nature reviews. Genetics*, 2(9), pp.681–9.

Kim, S.K. et al., 2008. Increased expression of Nrf2/ARE-dependent anti-

oxidant proteins in tamoxifen-resistant breast cancer cells. *Free radical biology & medicine*, 45(4), pp.537–46.

Kirsch, D.G. & Kastan, M.B., 1998. Tumor-suppressor p53: implications for tumor development and prognosis. *Journal of clinical oncology : official journal of the American Society of Clinical Oncology*, 16(9), pp.3158–68.

Köberle, B. et al., 2010. Cisplatin resistance: preclinical findings and clinical implications. *Biochimica et biophysica acta*, 1806(2), pp.172–82.

Kollmannsberger, C., Nichols, C. & Bokemeyer, C., 2006. Recent advances in management of patients with platinum-refractory testicular germ cell tumors. *Cancer*, 106(6), pp.1217–26.

Korkmaz, T., Seber, S. & Basaran, G., 2015. Review of the current role of targeted therapies as maintenance therapies in first and second line treatment of epithelial ovarian cancer; in the light of completed trials. *Critical Reviews in Oncology/Hematology*.

Kratz, K. et al., 2010. Deficiency of FANCD2-Associated Nuclease KIAA1018/FAN1 Sensitizes Cells to Interstrand Crosslinking Agents. *Cell*, 142(1), pp.77–88.

Kumar, S. et al., 2010. Anticancer drug 5-fluorouracil induces reproductive and developmental defects in Caenorhabditis elegans. *Reproductive toxicology (Elmsford, N.Y.)*, 29(4), pp.415–20. A

L'Hernault, S., 1997. Spermatogenesis - PubMed - NCBI.

Lackner, M.R. et al., 2005. Chemical genetics identifies Rab geranylgeranyl transferase as an apoptotic target of farnesyl transferase inhibitors. *Cancer cell*, 7(4), pp.325–36. ccessed December 15, 2015].

Larson, C.A. et al., 2009. The role of the mammalian copper transporter 1 in the cellular accumulation of platinum-based drugs. *Molecular pharmacology*, 75(2), pp.324–30.

Lee, S.R. et al., 2000. Mammalian thioredoxin reductase: oxidation of the C-terminal cysteine/selenocysteine active site forms a thioselenide, and replacement of selenium with sulfur markedly reduces catalytic

activity. *Proceedings of the National Academy of Sciences of the United States of America*, 97(6), pp.2521–6.

Lettre, G. & Hengartner, M.O., 2006. Developmental apoptosis in C. elegans: a complex CEDnario. *Nature reviews. Molecular cell biology*, 7(2), pp.97–108.

Li, J. et al., 2007. The 14-3-3 protein FTT-2 regulates DAF-16 in Caenorhabditis elegans. *Developmental biology*, 301(1), pp.82–91.

Li, W., Bandyopadhyay, J., Hwaang, H.S., Park, B.J., et al., 2012. Two thioredoxin reductases, trxr-1 and trxr-2, have differential physiological roles in caenorhabditis elegans. *Molecules and Cells*, 34(2), pp.209–218.

Li, W., Bandyopadhyay, J., Hwaang, H.S., Park, B.-J., et al., 2012. Two thioredoxin reductases, trxr-1 and trxr-2, have differential physiological roles in Caenorhabditis elegans. *Molecules and cells*, 34(2), pp.209–18.

Li, Z., Liu, J.-Y. & Zhang, J.-T., 2009. 14-3-3sigma, the double-edged sword of human cancers. *American journal of translational research*, 1(4), pp.326–40.

Liao, V.H.-C., Dong, J. & Freedman, J.H., 2002. Molecular characterization of a novel, cadmium-inducible gene from the nematode Caenorhabditis elegans. A new gene that contributes to the resistance to cadmium toxicity. *The Journal of biological chemistry*, 277(44), pp.42049–59.

Lin, K. et al., 2001. Regulation of the Caenorhabditis elegans longevity protein DAF-16 by insulin/IGF-1 and germline signaling. *Nature genetics*, 28(2), pp.139–45.

Link, C.D. & Johnson, C.J., 2002. Reporter transgenes for study of oxidant stress in Caenorhabditis elegans. *Methods in enzymology*, 353, pp.497–505.

Liu, T. et al., 2012. DNAJC25 is downregulated in hepatocellular carcinoma and is a novel tumor suppressor gene. *Oncology letters*, 4(6), pp.1274–1280.

Liu, Y. et al., 2012. Attenuation of cisplatin-induced renal injury by inhibition of soluble epoxide hydrolase involves nuclear factor κB signaling. *The Journal of pharmacology and experimental*

therapeutics, 341(3), pp.725–34.

Liu, Y.-Y. et al., 2011. Suppression of glucosylceramide synthase restores p53-dependent apoptosis in mutant p53 cancer cells. *Cancer research*, 71(6), pp.2276–85.

Liu, Y.Y. et al., 2001. Ceramide glycosylation potentiates cellular multidrug resistance. *FASEB journal: official publication of the Federation of American Societies for Experimental Biology*, 15(3), pp.719–30.

Lu, J. & Holmgren, A., 2014. The thioredoxin antioxidant system. *Free radical biology & medicine*, 66, pp.75–87.

Lu, Q. et al., 2013. The expression of V-ATPase is associated with drug resistance and pathology of non-small-cell lung cancer. *Diagnostic pathology*, 8, p.145.

Lüersen, K. et al., 2013. The Glutathione Reductase GSR-1 Determines Stress Tolerance and Longevity in Caenorhabditis elegans. *PLoS ONE*, 8(4), pp.1–16.

Maeda, I. et al., 2001. Large-scale analysis of gene function in Caenorhabditis elegans by high-throughput RNAi. *Current biology : CB*, 11(3), pp.171–6.

Maluccio, M., Einhorn, L.H. & Goulet, R.J., 2007. Surgical therapy for testicular cancer metastatic to the liver. *HPB : the official journal of the International Hepato Pancreato Biliary Association*, 9(3), pp.199–200.

Mandic, A. et al., 2003. Cisplatin induces endoplasmic reticulum stress and nucleus-independent apoptotic signaling. *The Journal of biological chemistry*, 278(11), pp.9100–6.

Marza, E. et al., 2009. Expression of ceramide glucosyltransferases, which are essential for glycosphingolipid synthesis, is only required in a small subset of C. elegans cells. *Journal of cell science*, 122(Pt 6), pp.822–833.

McColl, G. et al., 2010. Insulin-like signaling determines survival during stress via posttranscriptional mechanisms in C. elegans. *Cell metabolism*, 12(3), pp.260–72.

McKay, R.M. et al., 2007. Tripeptidyl peptidase II promotes fat formation in a conserved fashion. *EMBO reports*, 8(12), pp.1183–9.

Meier, B. et al., 2014. C. elegans whole-genome sequencing reveals mutational signatures related to carcinogens and DNA repair deficiency. *Genome research*, 24(10), pp.1624–36.

Mello, C.C. et al., 1991. Efficient gene transfer in C.elegans: extrachromosomal maintenance and integration of transforming sequences. *The EMBO journal*, 10(12), pp.3959–70.

Messner, M.C. & Cabot, M.C., 2010. Glucosylceramide in humans. *Advances in experimental medicine and biology*, 688, pp.156–64.

Miller, M.A. et al., 2001. A sperm cytoskeletal protein that signals oocyte meiotic maturation and ovulation. *Science (New York, N.Y.)*, 291(5511), pp.2144–7.

Miyako, E. et al., 2015. In Vivo Remote Control of Reactions in Caenorhabditis elegans by Using Supramolecular Nanohybrids of Carbon Nanotubes and Liposomes. *Angewandte Chemie (International ed. in English)*, 54(34), pp.9903–6.

Mukhopadhyay, A., Oh, S.W. & Tissenbaum, H.A., 2006. Worming pathways to and from DAF-16/FOXO. *Experimental gerontology*, 41(10), pp.928–34.

Muller, E.G., 1996. A glutathione reductase mutant of yeast accumulates high levels of oxidized glutathione and requires thioredoxin for growth. *Molecular biology of the cell*, 7(11), pp.1805–13.

Murphy, C.T. et al., 2003. Genes that act downstream of DAF-16 to influence the lifespan of Caenorhabditis elegans. *Nature*, 424(6946), pp.277–83.

Murphy, C.T. & Hu, P.J., 2013. Insulin/insulin-like growth factor signaling in C. elegans. *WormBook : the online review of C. elegans biology*, pp.1–43.

Muzzini, D.M. et al., 2008. Caenorhabditis elegans POLQ-1 and HEL-308 function in two distinct DNA interstrand cross-link repair pathways. *DNA repair*, 7(6), pp.941–50.

Myatt, S.S. & Lam, E.W.-F., 2007. The emerging roles of forkhead box (Fox) proteins in cancer. *Nature reviews. Cancer*, 7(11), pp.847–59.

Natarajan, B. et al., 2013. Depletion of the ER chaperone ENPL-1 sensitizes C. elegans to the anticancer drug cisplatin. *Worm*, 2(1),

p.e24059.

Neupane, D. & Korc, M., 2008. 14-3-3 Modulates Pancreatic Cancer Cell Survival and Invasiveness. *Clinical Cancer Research*, 14(23), pp.7614–7623.

Oing, C. et al., 2015. Pharmacotherapeutic treatment of germ cell tumors: standard of care and recent developments. *Expert opinion on pharmacotherapy*, pp.1–16.

Olaussen, K.A., 2009. A new step ahead for the consideration of ERCC1 as a candidate biomarker to select NSCLC patients for the treatment of cetuximab in combination with cisplatin. *Cancer biology & therapy*, 8(20), pp.1922–3.

Oliveira, R.P. et al., 2009. Condition-adapted stress and longevity gene regulation by Caenorhabditis elegans SKN-1/Nrf. *Aging cell*, 8(5), pp.524–41.

Ortiz, M.A. et al., 2014. A new dataset of spermatogenic vs. oogenic transcriptomes in the nematode Caenorhabditis elegans. *G3 (Bethesda, Md.)*, 4(9), pp.1765–72. A

Ozols, R.F., 1991. Ovarian cancer: new clinical approaches. *Cancer treatment reviews*, 18 Suppl A, pp.77–83.

Paix, A. et al., 2014. Scalable and Versatile Genome Editing Using Linear DNAs with Micro-Homology to Cas9 Sites in Caenorhabditis elegans. *Genetics*, 198(4), pp.1347–56.

Peng, X., Xu, J. & Arnér, E.S.J., 2012. Thiophosphate and selenite conversely modulate cell death induced by glutathione depletion or cisplatin: effects related to activity and Sec contents of thioredoxin reductase. *Biochemical Journal*, 447(1), pp.167–174.

Peng, X., Xu, J. & Arnér, E.S.J., 2012. Thiophosphate and selenite conversely modulate cell death induced by glutathione depletion or cisplatin: effects related to activity and Sec contents of thioredoxin reductase. *The Biochemical journal*, 447(1), pp.167–74.

Piano, F. et al., 2002. Gene clustering based on RNAi phenotypes of ovary-enriched genes in C. elegans. *Current biology: CB*, 12(22), pp.1959–64.

Piano, F. et al., RNAi analysis of genes expressed in the ovary of

Caenorhabditis elegans. *Current biology : CB*, 10(24), pp.1619–22.

de Plater, L. et al., 2010. Establishment and characterisation of a new breast cancer xenograft obtained from a woman carrying a germline BRCA2 mutation. *British journal of cancer*, 103(8), pp.1192–200.

Polimeni, M. & Gazzano, E., 2014. Is redox signaling a feasible target for overcoming multidrug resistance in cancer chemotherapy? *Frontiers in pharmacology*, 5, p.286.

Porta-de-la-Riva, M. et al., 2012. Basic Caenorhabditis elegans methods: synchronization and observation. *Journal of visualized experiments : JoVE*, (64), p.e4019.

Porter, G.W., Khuri, F.R. & Fu, H., 2006. Dynamic 14-3-3/client protein interactions integrate survival and apoptotic pathways. *Seminars in cancer biology*, 16(3), pp.193–202.

Praitis, V. et al., 2001. Creation of low-copy integrated transgenic lines in Caenorhabditis elegans. *Genetics*, 157(3), pp.1217–26.

Raffaghello, L. et al., 2008. Starvation-dependent differential stress resistance protects normal but not cancer cells against high-dose chemotherapy. *Proceedings of the National Academy of Sciences*, 105(24), pp.8215–8220.

Ramirez, P.T. et al., 2008. Phase I trial of the proteasome inhibitor bortezomib in combination with carboplatin in patients with platinum- and taxane-resistant ovarian cancer. *Gynecologic oncology*, 108(1), pp.68–71.

Reece-Hoyes, J.S. et al., 2007. Insight into transcription factor gene duplication from Caenorhabditis elegans Promoterome-driven expression patterns. *BMC genomics*, 8, p.27.

Richards, S. et al., 2012. Discovery and characterization of an inhibitor of glucosylceramide synthase. *Journal of medicinal chemistry*, 55(9), pp.4322–35.

Roberts, T.M. & Stewart, M., 2000. Acting like actin. The dynamics of the nematode major sperm protein (msp) cytoskeleton indicate a push-pull mechanism for amoeboid cell motility. *The Journal of cell biology*, 149(1), pp.7–12.

Roerink, S.F. et al., 2012. A broad requirement for TLS polymerases

and ??, and interacting sumoylation and nuclear pore proteins, in lesion bypass during C. elegans embryogenesis. *PLoS Genetics*, 8(6).

Roh, J.-Y., Lee, J. & Choi, J., 2006. Assessment of stress-related gene expression in the heavy metal-exposed nematode Caenorhabditis elegans: a potential biomarker for metal-induced toxicity monitoring and environmental risk assessment. *Environmental toxicology and chemistry / SETAC*, 25(11), pp.2946–56.

Rual, J.-F. et al., 2004. Toward improving Caenorhabditis elegans phenome mapping with an ORFeome-based RNAi library. *Genome research*, 14(10B), pp.2162–8.

Rubio-Peña, K. et al., 2015. Modeling of autosomal-dominant retinitis pigmentosa in Caenorhabditis elegans uncovers a nexus between global impaired functioning of certain splicing factors and cell type-specific apoptosis. *RNA (New York, N.Y.)*, 21(12), pp.2119–31.

Rubio-Viqueira, B. et al., 2006. An in vivo platform for translational drug development in pancreatic cancer. *Clinical cancer research : an official journal of the American Association for Cancer Research*, 12(15), pp.4652–61.

Ruggeri, B.A., Camp, F. & Miknyoczki, S., 2014. Animal models of disease: Pre-clinical animal models of cancer and their applications and utility in drug discovery. *Biochemical Pharmacology*, 87(1), pp.150–161.

Rybak, L.P. et al., 2009. Cisplatin ototoxicity and protection: clinical and experimental studies. *The Tohoku journal of experimental medicine*, 219(3), pp.177–86.

Salinas, L.S., Maldonado, E. & Navarro, R.E., 2006. Stress-induced germ cell apoptosis by a p53 independent pathway in Caenorhabditis elegans. *Cell death and differentiation*, 13(12), pp.2129–39.

Sarov, M. et al., 2012. A genome-scale resource for in vivo tag-based protein function exploration in C. elegans. *Cell*, 150(4), pp.855–66.

Sasazawa, Y. et al., 2009. Vacuolar H+-ATPase inhibitors overcome Bcl-xL-mediated chemoresistance through restoration of a caspase-independent apoptotic pathway. *Cancer science*, 100(8), pp.1460–7.

Sawers, L. et al., 2014. Glutathione S-transferase P1 (GSTP1) directly influences platinum drug chemosensitivity in ovarian tumour cell lines. *British journal of cancer*, 111(6), pp.1150–8.

Schumacher, B. et al., 2005. C. elegans ced-13 can promote apoptosis and is induced in response to DNA damage. *Cell death and differentiation*, 12(2), pp.153–61.

Schumacher, B. et al., 2001. The C. elegans homolog of the p53 tumor suppressor is required for DNA damage-induced apoptosis. *Current biology : CB*, 11(21), pp.1722–7.

Schwarz, T. & Schwarz, A., 2011. Molecular mechanisms of ultraviolet radiation-induced immunosuppression. *European journal of cell biology*, 90(6-7), pp.560–4.

Shachar, S. et al., 2009. Two-polymerase mechanisms dictate error-free and error-prone translesion DNA synthesis in mammals. *The EMBO journal*, 28(4), pp.383–93.

Shapira, M. et al., 2006. A conserved role for a GATA transcription factor in regulating epithelial innate immune responses. *Proceedings of the National Academy of Sciences of the United States of America*, 103(38), pp.14086–91.

She, Q.-B. et al., 2005. The BAD protein integrates survival signaling by EGFR/MAPK and PI3K/Akt kinase pathways in PTEN-deficient tumor cells. *Cancer cell*, 8(4), pp.287–97.

Shivers, R.P., Youngman, M.J. & Kim, D.H., 2008. Transcriptional responses to pathogens in Caenorhabditis elegans. *Current opinion in microbiology*, 11(3), pp.251–6.

Simmer, F. et al., 2003. Genome-wide RNAi of C. elegans using the hypersensitive rrf-3 strain reveals novel gene functions. *PLoS biology*, 1(1), p.E12.

Simonetta, S.H. & Golombek, D.A., 2007. An automated tracking system for Caenorhabditis elegans locomotor behavior and circadian studies application. *Journal of neuroscience methods*, 161(2), pp.273–80.

Singh, V. & Aballay, A., 2009. Regulation of DAF-16-mediated Innate Immunity in Caenorhabditis elegans. *The Journal of biological chemistry*, 284(51), pp.35580–7.

Stathopoulos, G.P. & Boulikas, T., 2012. Lipoplatin formulation review article. *Journal of drug delivery*, 2012, p.581363.

Stenvall, J. et al., 2011. Selenoprotein TRXR-1 and GSR-1 are essential for removal of old cuticle during molting in Caenorhabditis elegans. *Proceedings of the National Academy of Sciences of the United States of America*, 108(3), pp.1064–1069.

Stiernagle, T., 2006. Maintenance of C. elegans. *WormBook : the online review of C. elegans biology*, pp.1–11.

Stinchcomb, D.T. et al., 1985. Extrachromosomal DNA transformation of Caenorhabditis elegans. *Molecular and cellular biology*, 5(12), pp.3484–96.

Stope, M.B. et al., 2015. Jump in the fire - heat shock proteins and their impact on ovarian cancer therapy. *Critical reviews in oncology/hematology*.

Sulston, J.E. et al., 1983. The embryonic cell lineage of the nematode Caenorhabditis elegans. *Developmental biology*, 100(1), pp.64–119.

Sulston, J.E. & Horvitz, H.R., 1977. Post-embryonic cell lineages of the nematode, Caenorhabditis elegans. *Developmental biology*, 56(1), pp.110–56.

Tabara, H., Grishok, A. & Mello, C.C., 1998. RNAi in C. elegans: soaking in the genome sequence. *Science (New York, N.Y.)*, 282(5388), pp.430–1. Available at:

Tajeddine, N. et al., 2008. Hierarchical involvement of Bak, VDAC1 and Bax in cisplatin-induced cell death. *Oncogene*, 27(30), pp.4221–32.

Tatusov, R.L. et al., 2003. The COG database: an updated version includes eukaryotes. *BMC bioinformatics*, 4(1), p.41.

Tawe, W.N. et al., 1998. Identification of stress-responsive genes in Caenorhabditis elegans using RT-PCR differential display. *Nucleic acids research*, 26(7), pp.1621–7.

Teicher, B.A., 2006. Tumor models for efficacy determination. *Molecular Cancer Therapeutics*, 5(10), pp.2435–2443.

Tepper, R.G. et al., 2013. PQM-1 complements DAF-16 as a key transcriptional regulator of DAF-2-mediated development and longevity. *Cell*, 154(3), pp.676–690.

Timmons, L., Court, D.L. & Fire, A., 2001. Ingestion of bacterially expressed dsRNAs can produce specific and potent genetic interference in Caenorhabditis elegans. *Gene*, 263(1-2), pp.103–12.

Tischler, J., Lehner, B. & Fraser, A.G., 2008. Evolutionary plasticity of genetic interaction networks. *Nature genetics*, 40(4), pp.390–1.

Trapnell, C. et al., 2012. Differential gene and transcript expression analysis of RNA-seq experiments with TopHat and Cufflinks. *Nature protocols*, 7(3), pp.562–78.

Tullet, J.M.A. et al., 2008. Direct inhibition of the longevity-promoting factor SKN-1 by insulin-like signaling in C. elegans. *Cell*, 132(6), pp.1025–38.

Tzivion, G., Dobson, M. & Ramakrishnan, G., 2011. FoxO transcription factors; Regulation by AKT and 14-3-3 proteins. *Biochimica et Biophysica Acta - Molecular Cell Research*, 1813(11), pp.1938–1945.

Vanier, M.T., 2015. Complex lipid trafficking in Niemann-Pick disease type C. *Journal of inherited metabolic disease*, 38(1), pp.187–99.

Venier, R.E. & Igdoura, S.A., 2012. Miglustat as a therapeutic agent: prospects and caveats. *Journal of medical genetics*, 49(9), pp.591–7.

Vermezovic, J. et al., 2012. Differential regulation of DNA damage response activation between somatic and germline cells in Caenorhabditis elegans. *Cell death and differentiation*, 19(11), pp.1847–55.

Vidal, A. et al., 2012. Lurbinectedin (PM01183), a new DNA minor groove binder, inhibits growth of orthotopic primary graft of cisplatin-resistant epithelial ovarian cancer. *Clinical cancer research : an official journal of the American Association for Cancer Research*, 18(19), pp.5399–411.

Vidalain, P.-O. et al., 2004. Increasing specificity in high-throughput yeast two-hybrid experiments. *Methods (San Diego, Calif.)*, 32(4), pp.363–70.

Vitale, I. et al., 2007. Inhibition of Chk1 kills tetraploid tumor cells through a p53-dependent pathway. *PloS one*, 2(12), p.e1337.

Vousden, K.H. & Lane, D.P., 2007. p53 in health and disease. *Nature reviews. Molecular cell biology*, 8(4), pp.275–83.

Waaijers, S. et al., 2013. CRISPR/Cas9-targeted mutagenesis in Caenorhabditis elegans. *Genetics*, 195(3), pp.1187–91.

Waaijers, S. & Boxem, M., 2014. Engineering the Caenorhabditis elegans genome with CRISPR/Cas9. *Methods*, 68(3), pp.381–388.

Wang, D. & Lippard, S.J., 2005. Cellular processing of platinum anticancer drugs. *Nature reviews. Drug discovery*, 4(4), pp.307–20.

Wilm, T. et al., 1999. Ballistic transformation of Caenorhabditis elegans. *Gene*, 229(1-2), pp.31–5.

Yamasaki, M. et al., 2011. Role of multidrug resistance protein 2 (MRP2) in chemoresistance and clinical outcome in oesophageal squamous cell carcinoma. *British journal of cancer*, 104(4), pp.707–13.

Yang, J.-Y. & Hung, M.-C., 2009. A New Fork for Clinical Application: Targeting Forkhead Transcription Factors in Cancer. *Clinical Cancer Research*, 15(3), pp.752–757.

Yao, X. et al., 2007. Cisplatin nephrotoxicity: a review. *The American journal of the medical sciences*, 334(2), pp.115–24.

Yuan, J. et al., 1993. The C. elegans cell death gene ced-3 encodes a protein similar to mammalian interleukin-1 beta-converting enzyme. *Cell*, 75(4), pp.641–52.

Zalba, S. & Garrido, M.J., 2013. Liposomes, a promising strategy for clinical application of platinum derivatives. *Expert opinion on drug delivery*, 10(6), pp.829–44.

Zhong, L., Arnér, E.S. & Holmgren, A., 2000. Structure and mechanism of mammalian thioredoxin reductase: the active site is a redox-active selenolthiol/selenenylsulfide formed from the conserved cysteine-selenocysteine sequence. *Proceedings of the National Academy of Sciences of the United States of America*, 97(11), pp.5854–9.

Zhong, W. & Sternberg, P.W., 2006. Genome-wide prediction of C. elegans genetic interactions. *Science (New York, N.Y.)*, 311(5766), pp.1481–4.

Zhou, K.I., Pincus, Z. & Slack, F.J., 2011. Longevity and stress in Caenorhabditis elegans. *Aging*, 3(8), pp.733–753.

Zhu, H., 2014. Targeting forkhead box transcription factors FOXM1 and FOXO in leukemia (Review). *Oncology reports*, 32(4),pp.1327–34.

Publications

1. Rubio, K. Fontrodona, L. Aristizábal-Corrales, D. Torres, S. Cornes, E. **García-Rodríguez, FJ**. Serrat, X. Modeling of autosomal dominant Retinitis Pigmentosa in Caenorhabditis elegans uncovers a nexus between global impaired functioning of certain splicing factors and cell-type specific apoptosis. RNA 2015 Dec;21(12):2119-31.

2. Cornes, E. Porta-de-la-Riva, M. Aristizábal-Corrales, D. BrokateLlanos, AM. **García-Rodríguez, FJ.** Ertl, I. Díaz, M. Fontrodona, L. Reis, K. Johnsen, R. Baillie, D. Muñoz, MJ. Sarov, M. Dupuy, D. Cerón, J. Cytoplasmic LSM-1 protein regulates stress responses through the insulin/IGF-1 signaling pathway in C. elegans. RNA 21(9):1544-53 (2015).

3. Vidal A, Muñoz C, Guillén MJ, Moretó J, Puertas S, Martínez-Iniesta M, Figueras A, Padullés L, **García-Rodriguez FJ**, Berdiel-Acer M, Pujana MA, Salazar R, Gil-Martin M, Martí L, Ponce J, Molleví DG, Capella G, Condom E, Viñals F, Huertas D, Cuevas C, Esteller M, Avilés P, Villanueva A. Lurbinectedin (PM01183), a new DNA minor groove binder, inhibits growth of orthotopic primary graft of cisplatin-resistant epithelial ovarian cancer. Clinical Cancer Research. 2012 Oct 1;18(19):5399-411.

Modeling of autosomal-dominant retinitis pigmentosa in *Caenorhabditis elegans* uncovers a nexus between global impaired functioning of certain splicing factors and cell type-specific apoptosis

KARINNA RUBIO-PEÑA,[1,5] LAURA FONTRODONA,[1,5] DAVID ARISTIZÁBAL-CORRALES,[1,5] SILVIA TORRES,[1] ERIC CORNES,[1] FRANCISCO J. GARCÍA-RODRÍGUEZ,[1] XÈNIA SERRAT,[1] DAVID GONZÁLEZ-KNOWLES,[2] SYLVAIN FOISSAC,[3] MONTSERRAT PORTA-DE-LA-RIVA,[1,4] and JULIÁN CERÓN[1]

[1]Cancer and Human Molecular Genetics, Bellvitge Biomedical Research Institute-IDIBELL, Hospitalet de Llobregat, Barcelona 08908, Spain
[2]Integromics, Integromics SL, Parque Científico de Madrid, 28760, Tres Cantos, Madrid, Spain
[3]INRA, GenPhySE, F-31326 Castanet-Tolosan, France
[4]*C. elegans* Core Facility, Bellvitge Biomedical Research Institute-IDIBELL, Hospitalet de Llobregat, Barcelona 08908, Spain

ABSTRACT

Retinitis pigmentosa (RP) is a rare genetic disease that causes gradual blindness through retinal degeneration. Intriguingly, seven of the 24 genes identified as responsible for the autosomal-dominant form (adRP) are ubiquitous spliceosome components whose impairment causes disease only in the retina. The fact that these proteins are essential in all organisms hampers genetic, genomic, and physiological studies, but we addressed these difficulties by using RNAi in *Caenorhabditis elegans*. Our study of worm phenotypes produced by RNAi of splicing-related adRP (s-adRP) genes functionally distinguishes between components of U4 and U5 snRNP complexes, because knockdown of U5 proteins produces a stronger phenotype. RNA-seq analyses of worms where s-adRP genes were partially inactivated by RNAi, revealed mild intron retention in developing animals but not in adults, suggesting a positive correlation between intron retention and transcriptional activity. Interestingly, RNAi of s-adRP genes produces an increase in the expression of *atl-1* (homolog of human *ATR*), which is normally activated in response to replicative stress and certain DNA-damaging agents. The up-regulation of *atl-1* correlates with the ectopic expression of the pro-apoptotic gene *egl-1* and apoptosis in hypodermal cells, which produce the cuticle, but not in other cell types. Our model in *C. elegans* resembles s-adRP in two aspects: The phenotype caused by global knockdown of s-adRP genes is cell type-specific and associated with high transcriptional activity. Finally, along with a reduced production of mature transcripts, we propose a model in which the retina-specific cell death in s-adRP patients can be induced through genomic instability.

Keywords: *C. elegans*; retinitis pigmentosa; RNA-seq; spliceosome; intron retention

INTRODUCTION

Retinitis pigmentosa (RP) is a rare disease that affects approximately one out of 4000 individuals (more than 1.5 million people worldwide). RP causes a progressive loss of vision and ultimately blindness. Patients affected by this disease present defects in photoreceptors (rods and cones) and RPE (retinal pigment epithelium) cells that trigger cellular apoptosis and degeneration of the retina (Hartong et al. 2006; Ferrari et al. 2011). Although sporadic RP is not rare, most RP patients present inherited mutations, through diverse modes of genetic transmission, in any of the 50 genes that have been related to the disease (Daiger et al. 2013). Of all these RP familial cases, 30%–40% show autosomal-dominant genetic inheritance (Hartong et al. 2006). To date, mutations in 24 genes have been linked to autosomal-dominant RP (adRP) (Rossmiller et al. 2012). Among these genes, seven (*PRPF3*, *PRPF4*, *PRPF6*, *PRPF8*, *PRPF31*, *SNRNP200/BRR2*, and *RP9*) are coding for ubiquitous components of the spliceosome machinery and, when defective, cause disease only in the retina (Mordes et al. 2006; Zhao et al. 2009; Tanackovic et al. 2011b; Chen et al. 2014). All of them but *RP9/PAP-1*, which interacts at the protein level with PRPF3, are evolutionarily conserved (Supplemental Fig. S1; Maita et al. 2005).

[5]**These authors contributed equally to this work.**
Corresponding author: jceron@idibell.cat
Article published online ahead of print. Article and publication date are at http://www.rnajournal.org/cgi/doi/10.1261/rna.053397.115.

A better understanding of the mechanisms of action of these genes will provide a new insight into the disease that could help in the search of potential therapies for adRP patients. However, the essential function of s-adRP genes limits genetic and cellular studies. As a consequence, most of the knowledge that we have about how the spliceosome works comes from biochemical or in vitro studies. The multicellular organism *Caenorhabditis elegans*, thanks to the extraordinary conservation of these splicing-related proteins through evolution, offers a shortcut to understand why a mild reduction in the activity of genes required in all cells is critical only for a specific tissue.

The spliceosome is probably the most complex molecular machine of the cell and most of its components are evolutionarily conserved (Fabrizio et al. 2009). Moreover, splicing mechanisms are also similar from yeast to humans (Wahl et al. 2009; Will and Lührmann 2011). More than 200 proteins form this macromolecular complex that removes introns from eukaryotic pre-mRNAs. This is a highly dynamic process, with proteins going in and out of the complex depending on the splicing step that is taking place. The core of the spliceosome is composed of small nuclear ribonucleoproteins (snRNPs), which are complexes of proteins and uridine-rich small nuclear RNAs (named U1, U2, U4, U5, and U6 snRNAs). Particularly, the splicing-related genes linked with adRP encode proteins present in the U4/U6·U5 tri-snRNP complex, which is a main actor in the process of splicing. Among these proteins, PRP3, PRP4, and PRP31 are U4 snRNP components, whereas SNRNP200/BRR2, PRP6, and PRP8 are part of the U5 snRNP (Maita et al. 2005; Liu et al. 2006). For the sake of simplicity, we can place the s-adRP proteins within the process of splicing as follows: An intron flanked by two exons is recognized by the pre-spliceosome (U1 and U2 snRNPs complexes). Next, the U4/U6·U5 tri-snRNP remodels the spliceosome to later exclude U1 and U4 snRNPs, and keep U2, U5, and U6 snRNPs to form the activated spliceosome. Then, two catalytic steps occur to remove the intron and join the flanking exons.

In the present study, we use genetic and genomic tools to investigate in a multicellular organism how the alteration of a common and essential process such as pre-mRNA maturation can affect specific cells only.

RESULTS

A *C. elegans* toolkit to study splicing-related autosomal-dominant retinitis pigmentosa (s-adRP): RNAi, mutants, and transgenic animals

Despite the genetic nature of s-adRP, development of animal models to study this disorder has been hampered by the essential functions of the genes whose mutations are responsible of the disease. In multicellular organisms, complete depletion of s-adRP genes leads to lethality and, in consequence, described mutations in splicing-related genes causing adRP are either partial-loss-of-function mutations or deletion alleles that cause haploinsufficiency. To mimic and study the effect of this mild impairment of gene functions in *C. elegans* we took advantage of RNA interference (RNAi).

RNAi was first discovered and developed as a research tool in *C. elegans* (Fire et al. 1998). RNAi in this nematode is systemic, which implies that the effect of a specific dsRNA spreads through the whole organism. Because *C. elegans* feeds on bacteria, the feeding of worms with a clone producing a gene-specific RNAi results in the delivery of the specific dsRNA into the animal cells. As a complementary RNAi technique, dsRNA can also be administered by microinjection into the worm germline, which normally produces a stronger phenotype. RNAi clones corresponding to s-adRP genes were obtained, and validated by sequencing, from the two existing *C. elegans* RNAi libraries (Kamath et al. 2003; Rual et al. 2004), with the exception of the RNAi clone for *snrp-200*, which was generated in our laboratory by Gateway cloning (Fig. 1A). By quantitative PCR we investigated the effectiveness of the RNAi for some s-adRP genes and found that >50% of the targeted transcripts were depleted in our RNAi conditions (Fig. 1B).

Haploinsufficiency in s-adRP has been reported for human *PRPF31* but not for *PRPF8*, which does not allow the full loss of one copy of the gene (Abu-Safieh et al. 2006). We investigated haploinsufficiency in *C. elegans* by using deletion alleles for *prp-31* and *prp-8*. One copy of *prp-31 (gk1094)* or *prp-8(gk3511)* alleles (The *C. elegans* Deletion Mutant Consortium 2012), balanced with the translocation hT2 or with classic genetic markers, did not produce haploinsufficiency in terms of fertility or embryonic lethality (Supplemental Fig. S2A).

We further explored other evidences of haploinsufficiency in worms carrying the *prp-31* deletion by investigating different penetrance among individuals. We monitored the progeny of *prp-31(gk1094)* heterozygous individuals and observed no inter-individual variability in terms of brood size (Supplemental Fig. S2B). Moreover, the Mendelian proportions in the offspring of heterozygous animals were normal, with approximately one-quarter of arrested larvae (*prp-31 (gk1094)* homozygous) (Supplemental Fig. S2C).

In conclusion, *prp-31(gk1094)* and *prp-8(gk3511)* are haplosufficient in terms of somatic and germline development, although we cannot discard haploinsufficiency in any other specific cellular process. Strains carrying these mutations could be useful to screen for enhancers and therefore for potential modifiers of the disease.

Finally, we studied the expression of s-adRP genes using transgenic reporter strains. We analyzed the expression pattern of a *prp-8* transcriptional reporter (P*prp-8*::GFP) and observed an ubiquitous expression (Fig. 1C; Hunt-Newbury et al. 2007). This transgene, although informative, did not contain all the regulatory regions of the gene and moreover was not integrated in the worm genome, resulting in mosaicism in its expression. Thus, we made several

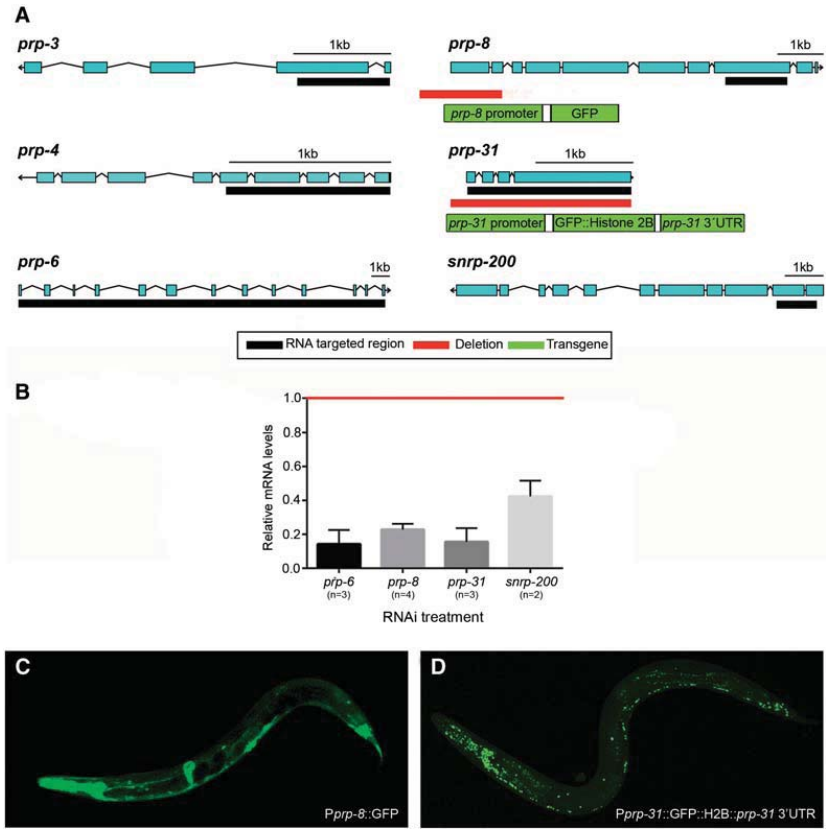

FIGURE 1. *C. elegans* toolkit to study s-adRP. (*A*) Scheme of s-adRP genes in *C. elegans* including the regions that are targeted by RNAi clones (black bars), the deleted fragment in the *prp-31(gk1094)* and *prp-8(gk3511)* alleles (red bars), and the elements of the *prp-8* and *prp-31* reporters generated in this study (green rectangles). The *prp-31(gk1094)* allele consists of a 5-bp insertion/1953-bp deletion. *prp-8(gk3511)* is a 1823-bp deletion. (*B*) Quantification of *prp* genes' expression levels after their respective inactivation by RNAi. mRNA levels of *prp* genes are represented relative to the expression in *gfp(RNAi)* control animals (arbitrary value of 1, indicated with a red line). Transcript levels are normalized against *tbb-2* levels in each case. RNA for analysis was obtained from up to four biological replicates (*n*). RNA from samples used for RNA-seq analyses were included. Error bars represent standard error of the mean. (*C*) Representative confocal image showing a transgenic worm expressing the transgene *sEx12486,* which consists of the GFP under the control of a promoter region for *prp-8*. (*D*) Representative confocal image showing a transgenic worm expressing the transgene *cerEx79*, which consists of the fusion protein GFP::H2B under the control of *prp-31* promoter and 3′UTR.

attempts to express s-adRP proteins tagged with green fluorescent protein (GFP), but we were not able to obtain transgenic animals by these means, suggesting that ectopic expression of these proteins could be toxic for animal development. Alternatively, we generated a transcriptional reporter containing the promoter region of *prp-31* in frame with the nuclear histone 2B, the *GFP* gene, and the 3′ UTR of *prp-31*. Animals were transformed by gene bombardment or microinjection, and we obtained several strains carrying this reporter either integrated in the genome or as an extrachromosomal array. All these strains broadly expressed the transgenes along the animal providing a useful genetic background to screen for other genes or small molecules capable of regulating the expression levels of *prp-31* (Fig. 1D).

In summary, RNAi clones for s-adRP genes, strains carrying deletion alleles for *prp-31* and *prp-8* in heterozygosity, and several GFP reporter strains for *prp-31* constitute the first version of a toolkit to investigate s-adRP genes in *C. elegans*.

RNAi phenotypes of s-adRP genes encoding U5 snRNP components are more dramatic than those corresponding to U4 snRNP proteins

To study the RNAi phenotypes of *prp-3*, *prp-4*, *prp-6*, *prp-8*, *prp-31*, and *snrp*-200, we performed RNAi by feeding in a synchronized population of worms at the first larval stage (L1) (Porta-de-la-Riva et al. 2012). We clearly distinguished

two phenotypic groups: Whereas *prp-6*, *prp-8* and *snrp-200* RNAi produced larval arrest, animals treated with RNAi for *prp-3*, *prp-4*, and *prp-31* produced adult animals that were sterile (Table 1; Fig. 2A).

As mentioned in the introduction, all six proteins are components of the U4/U6·U5 tri-snRNP, but only PRP-6, PRP-8 and SNRP-200 are present in the U5 snRNP and participate in the activated spliceosome (Fig. 2B). This functional difference could explain the stronger phenotype caused by their corresponding RNAi feeding clones.

To increase the efficiency of the RNAi, we synthesized and microinjected dsRNA for *prp-3*, *prp-4*, and *prp-31*. These RNAi by injection caused embryonic lethality for all three, confirming the phenotype observed for all the s-adRP genes in a previous large-scale RNAi by injection study (Sönnichsen et al. 2005).

Therefore, a strong RNAi inactivation of s-adRP genes produces a nonviable phenotype. However, RNAi by feeding of s-adRP genes produces milder defects, with *prp-6*, *prp-8*, and *snrp-200* displaying more dramatic RNAi phenotypes probably because of their functions in the activated or catalytic spliceosome.

The imprint of s-adRP genes on splicing catalysis

To study the molecular consequences of a partial inactivation of s-adRP genes, we analyzed the transcriptomes of animals treated with RNAi against *prp-6*, *prp-8*, and *prp-31*. L1 animals were fed with the corresponding RNAi clone and harvested after 24 h at 20°C, before developmental alterations due to RNAi became perceptible. In order to estimate the global levels of intron retention, we quantified the proportion of reads (read length 73 bp) mapping in intronic sequences in experimental and control samples. To ensure that our analysis was detecting intron retention and not stabilization of excised introns, we scored the proportion of reads mapping within introns and reads mapping in exon–intron junctions (Fig. 3A). Mild intron retention levels were observed in animals treated with RNAi against these three s-adRP genes. The strongest levels of intron retention were detected in *prp-8 (RNAi)* samples. More precisely, 6.49% and 4.07% of the reads mapped in exon–intron junctions in *prp-8(RNAi)* and *gfp(RNAi)* animals, respectively. These results indicate a basal level of unspliced transcripts in control animals, suggesting that the splicing machinery is not 100% efficient in the excision of introns in normal conditions. We corroborated the increase of intron retention events in *prp-8(RNAi)* animals by semiquantitative RT-PCR (Supplemental Fig. S3A) and by detecting reads crossing the exon–intron border of some pre-mRNAs (Supplemental Fig. S3B).

By considering only RNA-seq reads that mapped in annotated introns, we identified 69 statistically significant (*P*-value ≤ 0.01) common intron retention events in the whole genome of L3 animals treated with RNAi against s-adRP genes (Supplemental Table S1). We did not detect any common characteristic of the retained introns in terms of length (ranging from 114 to 4506 bp) or position within the gene (Supplemental Table S1).

The nonsense-mediated-decay (NMD) machinery prevents the expression of truncated proteins by degrading transcripts with premature termination codons (PTCs) (Hodgkin et al. 1989; Chang et al. 2007). Previous transcriptomic studies estimated that 20% of *C. elegans* genes produce transcripts that are degraded by the NMD pathway and many of those transcripts arise from splicing errors as retention of introns or wrong splice site selection (Ramani et al. 2009). Therefore, in our RNAi experiments the NMD system could be masking a stronger effect on intron retention. To address this concern we performed the same transcriptomic studies in the NMD defective strain *smg-1(r861)*. Although the proportion of reads on introns was slightly higher in all *smg-1(r861)* samples, results were comparable with those obtained in wild-type animals and we did not observe a more dramatic effect on intron retention in NMD mutants upon RNAi of s-adRP genes (Fig. 3A).

Interestingly, in adult animals without a germline (5-d-old *glp-4(bn2)* mutants) we did not observe the mild intron retention associated with *prp-8(RNAi)*, probably because of the much more reduced levels of transcriptional activity in adult animals compared with animals during development (Fig. 3B).

TABLE 1. Phenotypes observed after RNAi of s-adRP genes by two different methods

	RNAi by feeding	RNAi by injection
U4 protein coding genes		
prp-3	Sterility	Embryonic lethality
prp-4	Sterility	Embryonic lethality
prp-31	Sterility	Embryonic lethality
U5 protein coding genes		
prp-6	Larval arrest	Embryonic lethality[a]
prp-8	Larval arrest	Embryonic lethality[a]
snrp-200	Larval arrest	Embryonic lethality[a]

[a]Information obtained from the *C. elegans* PhenoBank (Sönnichsen et al. 2005).

RNAi of s-adRP genes induces the expression of the pro-apoptotic factor *egl-1* and apoptosis in a cell type-specific manner

The transcriptome of *prp-6(RNAi)*, *prp-8(RNAi)*, and *prp-31 (RNAi)* animals compared with those exposed to control RNAi brought to light a list of genes misregulated with distinct *P*-values derived from our bioinformatic analysis (Supplemental Table S2). There are different strategies to take benefit of this transcriptomic data but we followed a candidate-gene approach because among the genes with the lowest *P*-value (≤ 0.0001) we found the effector of apoptosis *egl-1*, which encodes a conserved BH3-only domain protein

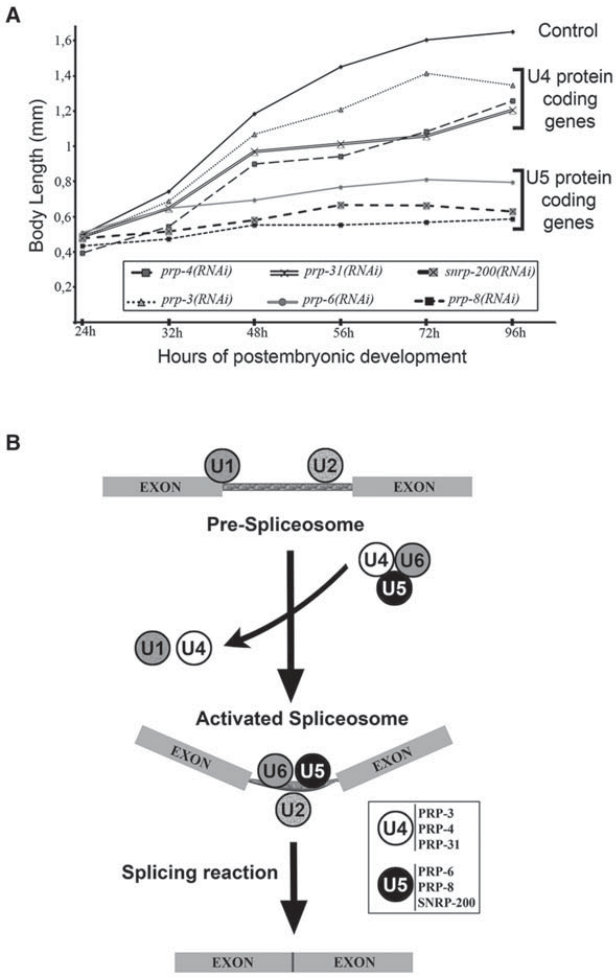

FIGURE 2. RNAi experiments classify s-adRP genes in two phenoclusters. (*A*) Developmental growth in animals treated with RNAi for s-adRP genes. Body length of wild-type worms with the indicated RNAi clones, starting from synchronized L1 and grown at 20°C. Mean body length of 50 worms per RNAi condition was scored at the indicated time points. Animal length was measured using the ImageJ software. Control worms were fed with the L4440 plasmid (empty vector). (*B*) Simplified scheme of the role of s-adRP genes in the splicing process. The six *C. elegans* s-adRP proteins are part of the tri-snRNP U4/U6·U5 complex. After the formation of the activated spliceosome, U5, but not U4, s-adRP proteins are required for subsequent splicing steps involving transesterification reactions. Exons are linked by thinner rectangles that represent an intron. White box: PRP-3, PRP-4, and PRP-31 are U4-specific, whereas PRP-6, PRP-8, and SNRNP-200 are U5-specific.

(Conradt and Horvitz 1998; Nehme and Conradt 2008). We validated this up-regulation by qPCR (Fig. 4A,B).

Because we analyzed the transcriptome of a multicellular organism, we wondered whether the over-expression of *egl-1* was global or cell type-specific. Hence, we treated EGL-1::GFP transgenic animals with *prp-8(RNAi)* and observed GFP expression in somatic cells that are not expected to suffer apoptosis in normal development (Sulston and Horvitz 1977). In wild-type worms, programmed cell death occurs in 18 cells at the L2 stage (Fig. 5A; Lettre and Hengartner 2006). However, *prp-8(RNAi)* animals displayed ectopic EGL-1::GFP expression that was particularly evident in hypodermal seam cells, which form a row from the head to the tail of the worm (Fig. 5B).

To confirm that ectopic *egl-1* expression results in apoptosis, we looked for apoptotic cell-corpses in larval cells using the mutant strain *ced-6(n2095)*, which is defective in the clearance of apoptotic cells. As expected, we detected apoptotic corpses in somatic hypodermal cells of animals treated with *prp-8(RNAi)* that were not present in wild-type worms (Fig. 5C,D). Moreover, using a GFP reporter for hypodermal seam cells, we observed a reduced number of seam cells in *prp-8(RNAi)* worms (Supplemental Fig. S4).

We further investigated this cell-specific phenotype by using strains where the RNAi effect was tissue-specific. These strains contain a mutation in the *rde-1* gene, which is essential for RNAi, and ectopically express *rde-1* either in muscle or hypodermal cells only. Strikingly, we observed the characteristic growth arrest of *prp-8(RNAi)* when the RNAi machinery was functional in hypodermal cells, but we did not detect such phenotype when the *prp-8(RNAi)* was effective in muscle cells (Fig. 6A,B). Interestingly, these hypodermal cells synthesize the proteins that form the cuticle and, similarly to retinal cells, require high transcriptional activity (Page and Johnstone 2007).

atl-1, the homolog of human *ATR*, is up-regulated after RNAi of s-adRP genes

Following the candidate gene approach, among the top up-regulated genes *atl-1*/*ATR* also called our attention (Fig. 4A,B). ATM and ATR are the primary sensors of DNA damage in humans. Whereas ATM mainly senses DNA double-strand breaks (DSBs), ATR responds to other DNA lesions such as those produced by replication fork stalling or UV damage, and it is recruited together with

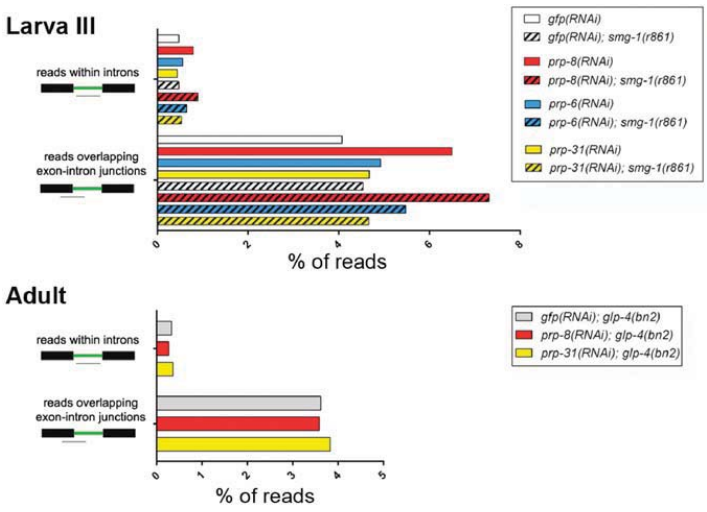

FIGURE 3. Intron retention caused by RNAi of s-adRP genes in different backgrounds and stages. Proportion of reads (73 bp) mapping within intron or in the intron–exon border in L3 N2 and *smg-1* mutants or in adult *glp-4* mutants, upon the indicated RNAis.

Replication protein A (RPA) to single-strand DNA regions originated by DNA damage (Kastan and Bartek 2004; Falck et al. 2005; Garcia-Muse and Boulton 2005).

Thus, we were persuaded to investigate whether a slight defect in the spliceosome activity could produce DNA lesions. It has been described that inactivation of various RNA processing factors induces the accumulation of DNA damage foci (Montecucco and Biamonti 2013). Therefore, we used the RPA-1::YFP reporter to study the effect of *prp-8(RNAi)* on the foci formation of the DNA damage sensing protein RPA-1. RPA-1::YFP is expressed in all worm cells, but the distribution of this tagged protein is diffuse and does not form visible foci (Vermezovic et al. 2012). We did not observe RPA-1::GFP foci after *prp-8(RNAi)* in normal growth conditions but the number of foci was higher in *prp-8(RNAi)* worms than in control animals upon UV exposure (Fig. 7). This result suggests that a partial depletion of *prp-8* activity may cause an alteration in the DNA that is not reported by our RPA-1::YFP transgenic in normal conditions, but it is uncovered upon UV exposure.

Another DNA insult that can increase the activity of *atl-1* is replicative stress. Replication forks can be collapsed by the presence of R-loops (DNA–RNA hybrids), whose formation can be promoted by alterations in the spliceosome (Aguilera and García-Muse 2012; Hamperl and Cimprich 2014). Such impact of R-loops on the replication machinery may induce replicative stress (Mazouzi et al. 2014). To induce replicative stress in *C. elegans* larvae, we exposed developing worms to hydroxyurea and observed, similarly to the effect of *prp-8 (RNAi)*, ectopic expression of *egl-1::GFP* and arrested development (Supplemental Fig. S5).

To confirm the impact of DNA damage or replicative stress in the expression of *egl-1* and *atl-1*, larvae were exposed to UV or treated with HU, respectively, and expression levels of these two genes were studied by qPCR 24 h after L1 (the same stage at which animals were harvested for RNA-seq experiments). These two DNA insults were capable of increasing the expression levels of *atl-1* and *egl-1* (Fig. 4C). Interestingly, we observed that the tissue-specific up-regulation of *atl-1* and *egl-1* occurred when *prp-8(RNAi)* was efficient in the hypodermis but did not happen when the RNAi worked in muscle cells only (Fig. 6C).

All together, these results suggest that larval arrest, cell type-specific apoptosis, and up-regulation of *egl-1* and *atl-1* could be consequences of DNA alterations driven by impaired functions of the spliceosome in a particular cell type.

DISCUSSION

Despite the publication of more than two hundred reports about the implication of spliceosome components in RP, the molecular mechanisms behind the role of ubiquitous proteins in a retinal-specific disease are still unclear. Similarly, *SMN1* and *SMN2* are widely expressed in human tissues but their mutations only produce defects in motor neurons. Such neuronal defects cause spinal muscular atrophy, a human disease that has also been investigated in *C. elegans* through the worm ortholog *smn-1* (Briese et al. 2009; Sleigh et al. 2011). This is just one example of the multiple human diseases (others are cancer or metabolic disorders) that have been studied and modeled in the multicellular organism *C. elegans* (Markaki and Tavernarakis 2010). Conveniently, s-adRP genes and the mechanisms of splicing in which they are implicated are very well conserved, which justifies the study of splicing-associated diseases in worms.

Alterations in U4 or U5 snRNP coding genes have a different impact on the organism

Based on the analysis of RNAi phenotypes, our study distinguishes between s-adRP genes coding for U4 or U5 components. All s-adRP proteins are required to activate the spliceosome, but U5 proteins remain in the activated complex whereas U4 proteins do not. This wider role of U5 snRNPs in splicing could explain why human genes coding for U5 snRNPs allow less harmful mutations than U4 snRNP coding genes. For example, most PRP8 adRP

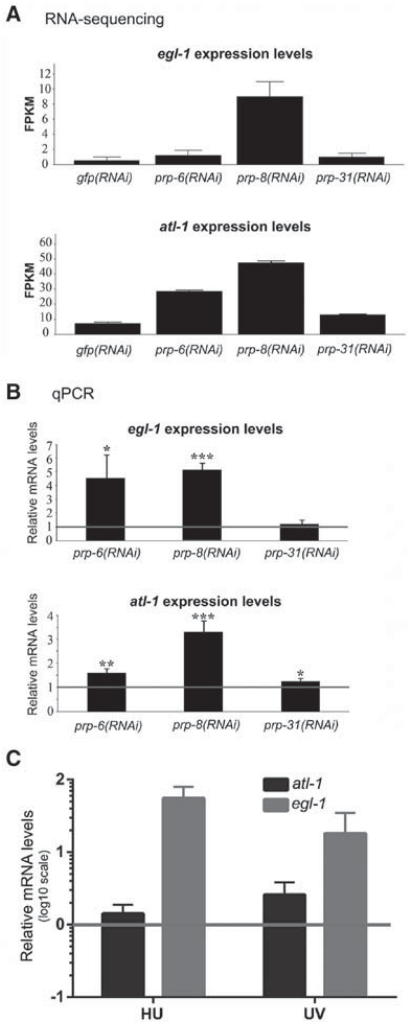

FIGURE 4. Up-regulation of *atl-1* and *egl-1* after RNAi of s-adRP genes follows a gradient from *prp-8(RNAi)* to *prp-31(RNAi)*. (*A*) RNA-seq data of *atl-1* and *egl-1* after RNAi in wild-type worms. FPKM represents the fragments per kilobase of transcript per million mapped reads. Bars indicate the average "confidence_high" and "confidence_low" values provided by Cufflinks (Trapnell et al. 2012) for each gene. (*B*) Validation of the RNA-seq data by qPCR. mRNA levels of *atl-1* and *egl-1* upon RNAi of some s-adRP genes are represented relative to their expression in *gfp(RNAi)* control animals (arbitrary value of 1, indicated with a gray line). qPCR expression data were normalized to transcript levels of *tbb-2*. Three separate experiments were analyzed. Error bars represent the standard deviation. Student's *t*-test for independent samples was used to analyze the statistical significance: One, two, and three asterisks indicate $P < 0.05$, $P < 0.01$, and $P < 0.001$, respectively. (*C*) Both DNA insults, UV and hydroxyurea, produce an increase in *atl-1* and *egl-1* expression. Quantification of expression levels of *atl-1* and *egl-1* in wild-type animals treated either with UV (100 J/m^2) or hydroxyurea (25 mM). Expression levels of these genes are represented relative to the ones in untreated worms.

mutations consist of a single amino acid change, caused by a point mutation in the last exon (exon 42) (Grainger and Beggs 2005; Towns et al. 2010), whereas genes coding U4 snRNP components such as *PRPF31* include null alleles that are able to be maintained in heterozygosis in adRP patients (Mordes et al. 2006; Rio Frio et al. 2008), and probably somatic loss of heterozygosity (Abu-Safieh et al. 2006). Accordingly, it is likely that human nonretinal cells can only handle the loss of a functional copy of the gene in s-adRP genes coding for U4 snRNPs components such as PRP31. Because there are still adRP patients whose disease-causing mutation has not been identified, other genes encoding proteins required for the tri-snRNP U4/U6·U5 formation, such as *SNU114* (U5 snRNP) or *SNU13* (U4 snRNP), are candidates to be screened for mutations responsible of adRP (de Sousa Dias et al. 2013).

Mutations in the U4 component PRP31 cause adRP with a variable penetrance that allows some carriers to stay asymptomatic. Recent studies focused on factors influencing the regulation of *PRPF31* expression and therefore the pathogenic effect of these mutations (Venturini et al. 2012; Rose et al. 2014). Our reporter strains carrying both the promoter and the 3′ UTR of *prp-31* can be used as a system to identify genes or conditions that could influence the expression of *prp-31*. Although we did not observe haploinsufficiency in worms heterozygous for a deletion in *prp-31*, these animals can serve as a sensitive background to search for factors capable of influencing *prp-31* functions.

Because all s-adRP proteins function in early splicing steps, future studies should focus on spliceosome assembly rather than on intron removal (catalysis) to unmask common mechanisms of action fueling the pathology.

Worms as a model for s-adRP

This study proposes the usage of *C. elegans* as a model to investigate the cellular mechanisms causing a subtype of the rare disease RP. Such a proposal is strongly supported by the following arguments: (i) Through RNAi we can mimic the partial loss of function of s-adRP genes occurring in RP patients (Longman et al. 2000). (ii) RNAi of s-adRP genes causes mild intron retention similar to what has been observed in other s-adRP models (Gamundi et al. 2008; Tanackovic et al. 2011b). (iii) Some retina cells of s-adRP patients suffer apoptotic cell death, whereas cells in other tissues are unaffected, and our model induces the ectopic expression of the pro-apoptotic gene *egl-1* and the onset of apoptotic cell corpses in developing hypodermal cells. (iv) RNAi by feeding of s-adRP genes supposes a constraint to developmental processes requiring high transcriptional activity (larval development for U5 genes and germline development for U4 genes), and s-adRP patients present disease only in the retina, a human tissue with very high transcriptional requirements (Derlig et al. 2015), whereas other tissues are asymptomatic.

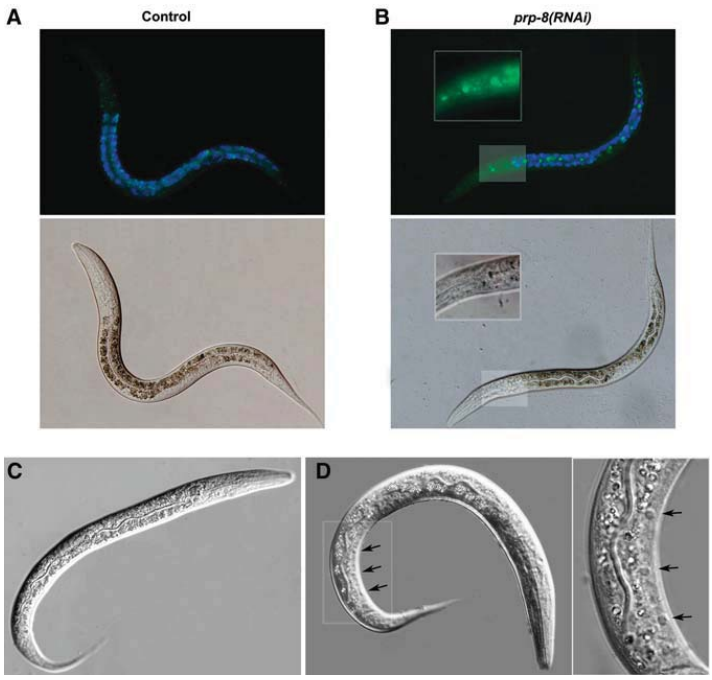

FIGURE 5. *egl-1*::GFP expression is ectopically induced in *prp-8(RNAi)* animals. Expression of the transgene *opIs56* [P*egl-1*::*2xNLS*::*GFP*] after 24 h at 20°C in (*A*) control RNAi (empty vector) and (*B*) *prp-8(RNAi)*. Size of the animals and the germline development stage indicate that in our experimental conditions *prp-8(RNAi)* worms develop to a similar stage as N2 during the first 24 h. *prp-8(RNAi)* worms ectopically express GFP in additional cells, including hypodermal seam cells (magnified area). Blue fluorescence is shown to label areas with autofluorescence. Images displayed are representative of three different experimental replicates. (*C*,*D*) Animals treated with *prp-8(RNAi)* display additional apoptotic cell corpses. The *ced-6* mutant larvae treated with (*C*) control RNAi and (*D*) *prp-8(RNAi)*. Black arrows indicate apoptotic cells (button-like refractile corpses) that were found in *prp-8(RNAi)* worms but not in control animals. The *right* panel shows a magnified image of the area highlighted with a white box.

Why do mutations in s-adRP genes have the ability to cause retina-specific diseases in humans?

Several hypotheses have been formulated to address this question and probably most of them are valid considering the complexity of the retina and the diversity of mutations leading to s-adRP. Taking into consideration the published data and our study, we find three compatible possibilities, which are defects in splicing reactions, lower transcriptional efficiency, and genome instability through the formation of R-loops (Fig. 8).

The most straightforward explanation is that splicing is inefficient in the retina, where cells present a high transcriptional activity, causing a reduction in the mRNA production and consequently a deficit in the amount of proteins. However, these defects in constitutive splicing are not general because studies in lymphoblastoid cell lines from s-adRP patients demonstrates that only five out of 57 introns tested presented unspliced products (Tanackovic et al. 2011b). Moreover, only three of these five intron retention events were common for all the PRPF mutations tested (Tanackovic et al. 2011a,b). Nevertheless, although a limited/mild intron retention has been observed in s-adRP models (Wilkie et al. 2008; Tanackovic et al. 2011b), a correlation between slight intron retention in certain genes and retinal degeneration has not been clearly established yet (Mordes et al. 2006).

In *C. elegans*, by RT-PCR and by observing intron retention events in a genome browser (i.e., a *fmo-5* intron [Supplemental Fig. S3]), we conclude that the likelihood of a partial depletion of s-adRP genes keeping transcripts unspliced is low, underscoring a high buffering capacity of spliceosomal proteins to maintain their essential functions despite an important reduction of their activity.

The alteration of these adRP splicing components may affect alternative splicing (AS) and thus the balance among isoforms. In fact, it has been shown that AS is affected in cell lines derived from patients carrying s-adRP mutations (Tanackovic et al. 2011b). The alterations in the levels of alternative transcripts do not seem to be similar in cell lines with different s-adRP mutations (Tanackovic et al. 2011b). On the contrary, a recent report based on siRNA in cell lines has uncovered a link between patterns of AS alterations and functionally related spliceosome components (Papasaikas et al. 2014). To explore the effect of our RNAi assays on AS we checked a panel of eight AS events occurring at L2 and L3 larval stages (Ramani et al. 2011) and did not find common AS alterations in s-adRP RNAi samples (Supplemental Table S3).

In any case, it is difficult to justify *C. elegans*' phenotypes, as well as the retinal degeneration in humans, just by slight intron retention or by a modest unbalance of alternative transcripts, which argues in favor of a more complex mechanism.

The second possible answer relies on co-transcriptional splicing. It is well established that splicing and transcription are coordinated processes and that alterations in the spliceosome can affect the transcriptional machinery (Das et al. 2007; Fong et al. 2013; Fontrodona et al. 2013; Montecucco and Biamonti 2013). As an example of such co-transcriptional splicing in a developing multicellular animal, our laboratory demonstrated that RSR-2 interacts with PRP-8 and the

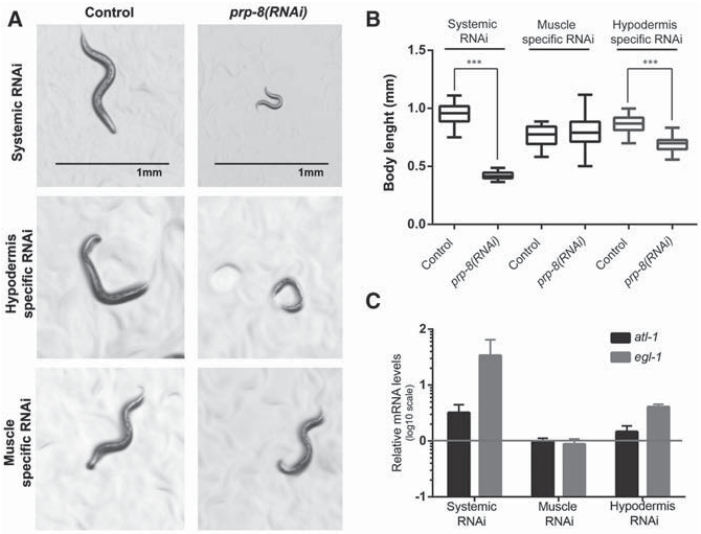

FIGURE 6. *prp-8(RNAi)* animals display tissue-specific phenotype. (*A*) Larval arrest phenotype was observed in wild-type- and hypodermis-specific RNAi animals (*rde-1 (ne219) V; KzIs9*), while no obvious phenotype was observed in muscle-specific RNAi worms (*rde-1 (ne219) V; KzIs20*). Representative images were taken under the stereoscope after 48 h at 20°C. Scale bar, 1 mm. (*B*) Body length measure of wild-type, and hypodermis- and muscle-specific RNAi animals fed with *prp-8(RNAi)* and control (empty vector) clones. Animals synchronized at L1 stage were treated with the corresponding RNAi clone and grown at 20°C. More than 25 worms were measured after 48 h of treatment in each condition. Animal length is showed in millimeters and was scored using the ImageJ software. Statistical significance was calculated using Student's *t*-test for independent samples. Three asterisks indicate statistical significance with $P < 0.001$. Whiskers were plotted by Tukey's test. (*C*) Up-regulation of *atl-1* and *egl-1* after *prp-8(RNAi)* is tissue specific. qPCR results for *atl-1* and *egl-1* expression in wild-type and hypodermis- and muscle-specific RNAi animals represented in a bar graph. mRNA levels of these genes after *prp-8(RNAi)* are relative to their expression in control animals. Results obtained from three independent biological replicates. mRNA transcript levels of *atl-1* and *egl-1* are normalized against *tbb-2* levels and represented in a log10 scale in both experiments. Error bars represent standard deviation.

RNA polymerase II (RNAPII) in *C. elegans*, and that the impairment of RSR-2 functions results in a lower transcriptional efficiency (Fontrodona et al. 2013). Consistent with this second hypothesis, the mutant allele *prp-8(rr40)*, which reduces the levels of wild-type PRP-8, diminishes the production of highly expressed germline transcripts, but it does not affect the splicing reaction (Hebeisen et al. 2008).

Finally, our results support a third hypothesis that can coexist with the previous ones: A reduction in the activity of s-adRP proteins produces genomic instability that, in cells with high transcriptional activity, can contribute to programmed cell death. The impairment of the splicing machinery can form R-loops (RNA/DNA duplex) that expose the single-strand DNA (ssDNA) to DNA-damaging agents such as UV light at active transcriptional regions (Aguilera and García-Muse 2012, 2013). This would explain the sensitivity of *prp-8(RNAi)* animals to UV exposure. Moreover, R-loops are also a source of transcriptional associated mutagenesis (TAM), which is elevated under high transcriptional activity (Kim et al. 2007) and can induce apoptosis (Hendriks et al. 2010).

In addition to the formation of these DNA damage-prone sites, R-loops can contribute to genome instability because replication and transcriptional machineries could meet and collide at these R-loop sites leading to replicative stress (Brambati et al. 2015). In *C. elegans* the collision with the replication machinery is feasible because hypodermal cells are actively dividing during larval stages and also suffer a round of endoreplication (Sulston and Horvitz 1977; Hedgecock and White 1985). In mammalian cells, the existence of a proliferative capacity in adult retinal cells has been reported (Tropepe et al. 2000; Kiilgaard et al. 2007; Al-Hussaini et al. 2008), providing a possible scenario for replicative stress in dividing cells.

However, in the process of understanding the pathogenesis of the disease, we should take into consideration that the retinal degeneration of adRP patients is a gradual process that may take many years. Here we present *C. elegans* as a promising model to investigate mechanisms of the disease and potential therapies in a short time frame.

Future prospects

In this study, we present a robust model to study s-adRP in *C. elegans*. We focused our attention in *atl-1* and *egl-1*, but we have identified other interesting genes in our data set (which is available at the Gene Expression Omnibus [GEO] repository) that are up-regulated in animals with reduced levels of spliceosomal proteins and that may have a role in compensating or repairing such deficiency. Among them, we identified genes coding for spliceosome components such as *mog-4*, *mog-5*, *prpf-4*, or *ddx-23* (Supplemental Table S1; Kerins et al. 2010).

Through an increased sensitivity to DNA insults and replicative stress we have opened a third way to explain the retina-specific apoptosis in s-adRP. This alternative way should be explored in terms of therapies that could alleviate the progressive loss of vision in s-adRP patients. To such aim, *C. elegans* can play a key role thanks to its amenability for high-throughput screening.

Our approach takes advantage of the RNAi but the new technologies for genome editing and the functional conservation of spliceosomal genes are making feasible the introduction of human s-adRP mutations in worms (Waaijers and

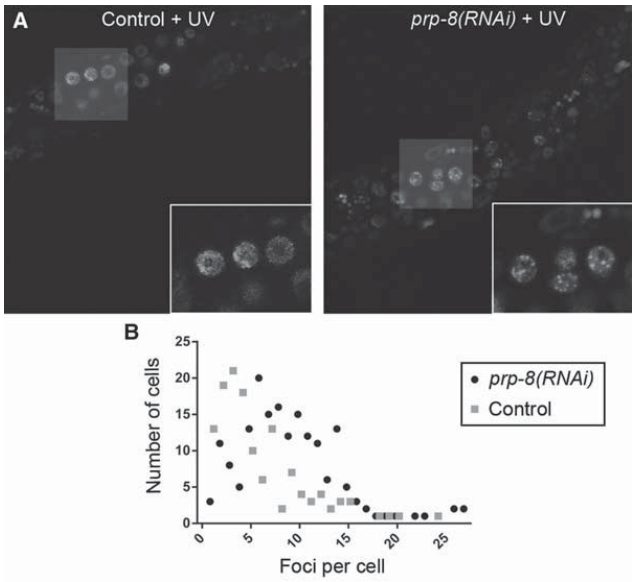

FIGURE 7. Higher sensitivity to UV damage observed in *prp-8(RNAi)*-treated animals. After UV exposure, foci formation evidenced by the transgene *opIs263 [Prpa-1::rpa-1::YFP+unc-119(+)]* is more abundant in animals with partial inactivation of *prp-8* compared with control worms (fed with empty vector clone). (*A*) Representative confocal images of transgenic worms carrying the RPA-1::YFP transgene under control and *prp-8(RNAi)* conditions. RNAi treatment started from L1 stage at 20°C. After 24 h, animals were exposed to a 100 J/m^2 dose of UV-C radiation, and 24 h later foci formation was assessed through confocal microscopy. *Foci* formation was observed in somatic and germline cells in both conditions. White squares show magnified images of germline cells with RPA-1::YFP foci. (*B*) Quantification of foci formation per cell represented in a dispersion graph. Each square (control) and dot (*prp-8(RNAi)*) represents the number of cells displaying the corresponding amount of foci. Only somatic and germline cells that displayed one or more foci were scored.

Boxem 2014). This approach could be an ideal platform to develop personalized medicine and drug discovery.

MATERIALS AND METHODS

Strains

Standard methods were used to culture and manipulate worms (Stiernagle 2006; Porta-de-la-Riva et al. 2012). In this study, we used the wild-type Bristol N2 and the strains TR1331: *smg-1 (r861)* I, SS104: *glp-4(bn2)* I, CER87: *unc-119(ed3)* III, *cerEx79* [P*prp-31::GFP::H2B::prp-31 3′ UTR* + pGH8 + *unc-119*(+)], CER148: *unc-119(ed3)* III; *cerIs05*[P*prp-31::GFP::H2B::prp-31* 3′ UTR +*unc-119*(+)], CER149: *unc-119(ed3)* III; *cerIs06*[P*prp-31::GFP::H2B::prp-31* 3′ UTR +*unc-119*(+)], VC2709: *prp-31 (gk1094) I/hT2*[*bli-4(e937) let-?(q782) qIs48*](I;III), CER100: *prp-31(gk1094)/unc-57(ad592) dpy-5(e61)* I, CER101: +/*unc-57 (ad592) dpy-5(e61)* I, VC3460: *prp-8(gk3511)* III/hT2 *[bli-4(e937) let-?(q782) qIs48]* (I;III), BC12486: *dpy-5(e907)* I; *sEx12486*[P*prp-8::GFP* + *pCeh361*], WS1973: *unc-119(ed3)* III; *opIs56*[P*egl-1::2xNLS::GFP* + *unc-119(+)*], MT4970: *ced-6(n2095)* III, NR222: *rde-1(ne219)* V; *kzIs9[pKK1260(lin-26p::nls::GFP)* + *pKK1253(lin-26p::rde-1)* + *pRF6(rol-6(su1006))*], NR350: *rde-1(ne219)* V;*kzIs20[pDM#715(hlh-1p::rde-1)* + *pTG95(sur-5p::NLS::GFP)]*, WS4581: *unc-119(ed3)* III; *opIs263[rpa-1p::rpa-1::YFP* + *unc-119(+)]*.

RNA-mediated interference

To induce RNA-mediated interference (RNAi) by feeding, nematode growth medium (NGM) plates were supplemented with 50 µg/mL ampicillin, 12.5 µg/mL tetracycline, and 1 mM IPTG. NGM-supplemented plates were seeded with the corresponding RNAi clone. All RNAi clones but the one corresponding to *snrp-200* were obtained either from the ORFeome library (Rual et al. 2004) or the Ahringer library (Kamath et al. 2003). From cDNA we generated an RNAi clone (pCUC24) for *snrp-200* by Gateway cloning (amplicon size 1091 bp), which includes the spliced sequence from 106 to 1197 bp (primers available under request). Each clone was validated by PCR and/or sequencing. To study the RNAi phenotypes of s-adRP genes, a synchronized population of N2 worms at L1 stage was fed with each clone and grown at 20°C. To induce RNAi by microinjection, dsRNA was synthesized from the RNAi feeding clone by using MEGAscript T7 kit (Ambion). Wild-type young adults were injected with 1 µg/µL of dsRNA.

RNA sequencing

RNA-seq analyses were performed using RNA of the following population sets: synchronized N2 and *smg-1(r861)* L1 larvae fed for 24 h at 20°C with the RNAi clones of *prp-6, prp-8, prp-31*, and *gfp*; and 5-d adult *glp-4(bn2)* worms grown at 25°C and fed first, for 72 h with OP50 and next, for 48 more hours with the RNAi clones of *prp-8, prp-31*, and *gfp*. RNA was isolated with TRI Reagent (MRC, Inc.) and purified by using the Purelink RNA Mini kit (Ambion) and Purelink DNAse (Ambion). RNA samples were subjected to quality and yield controls on the Agilent 2010 Bioanalyzer and Nanodrop Spectrophotometer, respectively. Poly(A)-enriched samples were multiplexed in libraries for paired-end RNA sequencing on Illumina Hiseq 2000 platform, through the CNAG (Centro Nacional de Análisis Genómico) sequencing facility. To generate BAM files, more than 50 million reads (length of 73 bp) for sample were mapped against the *C. elegans* worm version WS236 following the GEMTools pipeline (http://gemtools.github.io/). These BAM files were analyzed using the SeqSolve software, which use Cufflinks/Cuffdiff for differential gene/transcript expression analyses (Trapnell et al. 2012). A full 98.7% of the reads from the control *gfp(RNAi)* sample mapped in exons. The sequence data for the 11 transcriptomes analyzed in this study are available at the NCBI Gene Expression Omnibus (http://www.ncbi.nlm.nih.gov/geo/) under accession number GSE72952.

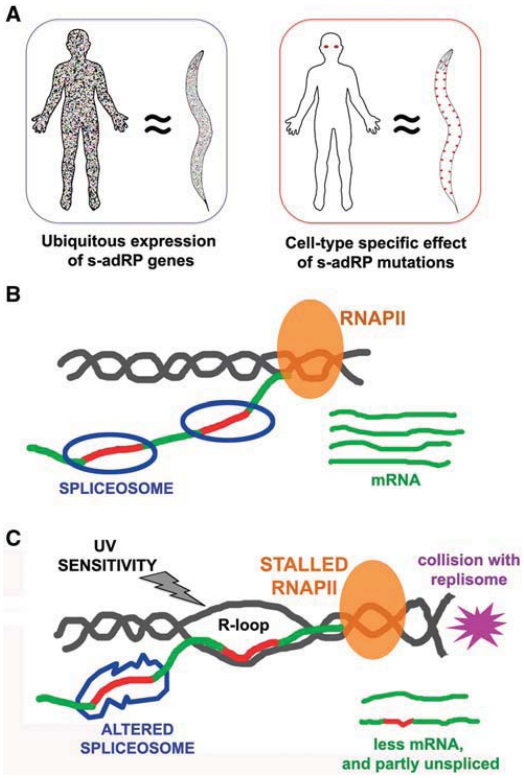

FIGURE 8. Model for the tissue-specific apoptosis in s-adRP. (*A*) Similarly to humans, s-adRP genes are expressed in all *C. elegans* cell types. Partial inactivation of s-adRP genes causes tissue-specific defects both in humans and worms. (*B*) In normal condition, splicing occurs cotranscriptionally. (*C*) When the functioning of the splicesome is altered, the activity of the RNAPII is affected and R-loops (DNA–RNA hybrids) are produced, creating single-strand DNA regions that are more sensitive to DNA insults. Moreover, R-loops may cause collisions between the transcriptional and the replicative machineries.

Real-time PCR

For gene expression analyses, synchronized worms were harvested, washed, and frozen in TRI Reagent to perform total RNA isolation. cDNA was synthesized with oligo(dT) primers using the RevertAid H Minus First Strand cDNA synthesis kit (ThermoScientific) following the manufacturer's instructions. To determine gene expression, the LightCycler 480 SYBR Green I Master kit (Roche) was used.

Generation of transgenic reporter strains

The molecular construct to study the expression and localization of *prp-31* (pCUC32) was made by the Gateway recombination cloning system (Invitrogen). The 5′ entry clone includes 664 bp of the promoter region, and 3′ entry clone contains the 77 bp of the 3′ UTR sequence (primer sequences available upon request). Plasmid pCM1.35 was used as the middle entry clone and pCFJ150 was the destination vector.

Microinjection

Transgenic animals were generated by microinjecting 2 ng/µL of pCUC32 [P*prp-31::GFP::H2B::prp-31 3′ UTR +unc-119(+)*] together with 20 ng/µL of the red neuronal marker pGH8 [P*rab-3::mCherry::unc-54utr*] into DP38 [*unc-119(ed3)*] young adult worms. 78 ng/µL of 1 Kb Plus DNA ladder (Invitrogen) were used as carrier. Wild-type animals were selected over uncoordinated (Unc) worms, and mCherry expression was checked under the dissecting microscope. GFP expression was observed at high magnification using an inverted fluorescence Nikon ECLIPSE Ti-S microscope.

Bombardment

One and a half milligrams of gold powder (Chempur, gold powder 0.3–3.0 micron 99.9%) was transferred to a low protein binding 1.5-mL tube, resuspended in 150 µL of 50 mM spermidine, and sonicated for 10 sec. Twenty-four micrograms of pCUC32 DNA was added to the mixture, deionized water was added up to 540 µL, and the mixture was incubated for 10 min. Next, we added 150 µL of 1 M $CaCl_2$. The mixture was incubated for another 10 min and centrifuged at maximum speed for 30 sec. After three washes with 96% ethanol, the pellet was resuspended in 300 µL PVP 0.1 mg/mL in EtOH. Shots with 20 µL of the suspension were performed using a Caenotec gene gun on pre-chilled 35-mm plates with 20–30 µL of DP38 [*unc-119(ed3)*] young adults. Then the NGM agar of each plate was sliced into six pieces, and each slice was placed on a 90-mm plate. These plates were incubated at 20°C for 2 wk and then screened for transgenic worms that rescued the *unc-119(ed3)* phenotype.

Replicative stress induction

To induce replicative stress we used hydroxyurea (HU) (Sigma-Aldrich, Cat# H8627). In all cases 25 mM HU plates were used and prepared adding 500 µL of 0.5 M HU to plates containing 10 mL of NGM medium and seeded with *E. coli* OP50. To observe *egl-1* expression, synchronized *Pegl-1*::GFP (WS1973) L1 worms were grown in either HU or standard plates for 24 and 48 h at 20°C. After each time point, worms were recovered with M9 buffer, washed, and mounted using 0.3 mM of levamisole for in vivo observation through an inverted fluorescence microscope. To quantify the expression levels of *atl-1* and *egl-1* in a replicative stress context, synchronized N2 L1 worms were grown at 20°C for 24 h in HU plates and then recovered with M9 buffer for total RNA isolation.

DNA damage induction through UV-C exposure

Synchronized worms were exposed to UV-C light (254 nm) at different time points depending on the experiment. A UV crosslinker (model 2400, Stratagene) was used to apply 100 J/m^2 in all the cases. Before the exposure to UV-C, worms were washed several times to get rid of bacteria and placed in a bacteria-free NGM plate.

To quantify the expression levels of *atl-1* and *egl-1* upon DNA damage induced by UV-C exposure, synchronized L1 N2 worms were grown in standard conditions at 20°C. UV-C exposure was performed 18 h post L1 and total RNA isolation 6 h later.

Foci quantification

For RPA-1 foci observation synchronized *Prpa::YFP* L1 worms were grown at 20°C for 24 h. Then, they were exposed to UV-C and later

placed again in control or *prp-8(RNAi)* plates for an additional 24 h. Worms were then mounted using 0.3 mM of levamisole and observed using a confocal fluorescence microscope. RPA-1::YFP foci formation was quantified by counting the number of bright foci present in germline and somatic cells.

SUPPLEMENTAL MATERIAL

Supplemental material is available for this article.

ACKNOWLEDGMENTS

We thank Dr. Juan Valcarcel and Dr. Ana Méndez for critical reading of the manuscript. Some strains were provided by the CGC (*Caenorhabditis* Genetics Center), which is funded by the National Institutes of Health Office of Research Infrastructure Programs (P40 OD010440). J.C. is a Miguel Servet Researcher (ISCIII). K.R.-P. has a FINCyT PhD fellowship from the government of Peru. This study was supported by La Marató de TV3 foundation (Ref. 100910) and by a grant from the Instituto de Salud Carlos III (ISCIII) (Exp. PI12/01554), which is cofunded by FEDER funds/European Regional Development Fund (ERDF)—a way to build Europe.

Received July 23, 2015; accepted September 19, 2015.

REFERENCES

Abu-Safieh L, Vithana EN, Mantel I, Holder GE, Pelosini L, Bird AC, Bhattacharya SS. 2006. A large deletion in the adRP gene PRPF31: evidence that haploinsufficiency is the cause of disease. *Mol Vis* **12:** 384–388.

Aguilera A, García-Muse T. 2012. R loops: from transcription byproducts to threats to genome stability. *Mol Cell* **46:** 115–124.

Aguilera A, García-Muse T. 2013. Causes of genome instability. *Annu Rev Genet* **47:** 1–32.

Al-Hussaini H, Kam JH, Vugler A, Semo M, Jeffery G. 2008. Mature retinal pigment epithelium cells are retained in the cell cycle and proliferate in vivo. *Mol Vis* **14:** 1784–1791.

Brambati A, Colosio A, Zardoni L, Galanti L, Liberi G. 2015. Replication and transcription on a collision course: eukaryotic regulation mechanisms and implications for DNA stability. *Front Genet* **6:** 166.

Briese M, Esmaeili B, Fraboulet S, Burt EC, Christodoulou S, Towers PR, Davies KE, Sattelle DB. 2009. Deletion of *smn-1*, the *Caenorhabditis elegans* ortholog of the spinal muscular atrophy gene, results in locomotor dysfunction and reduced lifespan. *Hum Mol Genet* **18:** 97–104.

Chang Y-F, Imam JS, Wilkinson MF. 2007. The nonsense-mediated decay RNA surveillance pathway. *Annu Rev Biochem* **76:** 51–74.

Chen X, Liu Y, Sheng X, Tam PO, Zhao K, Chen X, Rong W, Liu Y, Liu X, Pan X, et al. 2014. PRPF4 mutations cause autosomal dominant retinitis pigmentosa. *Hum Mol Genet* **23:** 2926–2939.

Conradt B, Horvitz HR. 1998. The *C. elegans* protein EGL-1 is required for programmed cell death and interacts with the Bcl-2-like protein CED-9. *Cell* **93:** 519–529.

Daiger SP, Sullivan LS, Bowne SJ. 2013. Genes and mutations causing retinitis pigmentosa. *Clin Genet* **84:** 132–141.

Das R, Yu J, Zhang Z, Gygi MP, Krainer AR, Gygi SP, Reed R. 2007. SR proteins function in coupling RNAP II transcription to pre-mRNA splicing. *Mol Cell* **26:** 867–881.

Derlig K, Gießl A, Brandstätter JH, Enz R, Dahlhaus R. 2015. Special characteristics of the transcription and splicing machinery in photoreceptor cells of the mammalian retina. *Cell Tissue Res* doi: 10.1007/s00441-015-2204-x.

De Sousa Dias M, Hernan I, Pascual B, Borràs E, Mañé B, Gamundi MJ, Carballo M. 2013. Detection of novel mutations that cause autosomal dominant retinitis pigmentosa in candidate genes by long-range PCR amplification and next-generation sequencing. *Mol Vis* **19:** 654–664.

Fabrizio P, Dannenberg J, Dube P, Kastner B, Stark H, Urlaub H, Lührmann R. 2009. The evolutionarily conserved core design of the catalytic activation step of the yeast spliceosome. *Mol Cell* **36:** 593–608.

Falck J, Coates J, Jackson SP. 2005. Conserved modes of recruitment of ATM, ATR and DNA-PKcs to sites of DNA damage. *Nature* **434:** 605–611.

Ferrari S, Di Iorio E, Barbaro V, Ponzin D, Sorrentino FS, Parmeggiani F. 2011. Retinitis pigmentosa: genes and disease mechanisms. *Curr Genomics* **12:** 238–249.

Fire A, Xu S, Montgomery MK, Kostas SA, Driver SE, Mello CC. 1998. Potent and specific genetic interference by double-stranded RNA in *Caenorhabditis elegans*. *Nature* **391:** 806–811.

Fong YW, Cattoglio C, Tjian R. 2013. The intertwined roles of transcription and repair proteins. *Mol Cell* **52:** 291–302.

Fontrodona L, Porta-de-la-Riva M, Morán T, Niu W, Díaz M, Aristizábal-Corrales D, Villanueva A, Schwartz S, Reinke V, Cerón J. 2013. RSR-2, the *Caenorhabditis elegans* ortholog of human spliceosomal component SRm300/SRRM2, regulates development by influencing the transcriptional machinery. ed. N. Maizels. *PLoS Genet* **9:** e1003543.

Gamundi MJ, Hernan I, Muntanyola M, Maseras M, López-Romero P, Alvarez R, Dopazo A, Borrego S, Carballo M. 2008. Transcriptional expression of cis-acting and trans-acting splicing mutations cause autosomal dominant retinitis pigmentosa. *Hum Mutat* **29:** 869–878.

Garcia-Muse T, Boulton SJ. 2005. Distinct modes of ATR activation after replication stress and DNA double-strand breaks in *Caenorhabditis elegans*. *EMBO J* **24:** 4345–4355.

Grainger RJ, Beggs JD. 2005. Prp8 protein: at the heart of the spliceosome. *RNA* **11:** 533–557.

Hamperl S, Cimprich KA. 2014. The contribution of co-transcriptional RNA:DNA hybrid structures to DNA damage and genome instability. *DNA Repair (Amst)* **19:** 84–94.

Hartong DT, Berson EL, Dryja TP. 2006. Retinitis pigmentosa. *Lancet* **368:** 1795–1809.

Hebeisen M, Drysdale J, Roy R. 2008. Suppressors of the *cdc-25.1(gf)*-associated intestinal hyperplasia reveal important maternal roles for *prp-8* and a subset of splicing factors in *C. elegans*. *RNA* **14:** 2618–2633.

Hedgecock EM, White JG. 1985. Polyploid tissues in the nematode *Caenorhabditis elegans*. *Dev Biol* **107:** 128–133.

Hendriks G, Jansen JG, Mullenders LHF, de Wind N. 2010. Transcription-coupled repair and apoptosis provide specific protection against transcription-associated mutagenesis by ultraviolet light. *Transcription* **1:** 95–98.

Hodgkin J, Papp A, Pulak R, Ambros V, Anderson P. 1989. A new kind of informational suppression in the nematode *Caenorhabditis elegans*. *Genetics* **123:** 301–313.

Hunt-Newbury R, Viveiros R, Johnsen R, Mah A, Anastas D, Fang L, Halfnight E, Lee D, Lin J, Lorch A, et al. 2007. High-throughput in vivo analysis of gene expression in *Caenorhabditis elegans*. *PLoS Biol* **5:** e237.

Kamath RS, Fraser AG, Dong Y, Poulin G, Durbin R, Gotta M, Kanapin A, Le Bot N, Moreno S, Sohrmann M, et al. 2003. Systematic functional analysis of the *Caenorhabditis elegans* genome using RNAi. *Nature* **421:** 231–237.

Kastan MB, Bartek J. 2004. Cell cycle checkpoints and cancer. *Nature* **432:** 316–323.

Kerins JA, Hanazawa M, Dorsett M, Schedl T. 2010. PRP-17 and the pre-mRNA splicing pathway are preferentially required for the proliferation versus meiotic development decision and germline sex determination in *Caenorhabditis elegans*. *Dev Dyn* **239:** 1555–1572.

Kiilgaard JF, Prause JU, Prause M, Scherfig E, Nissen MH, la Cour M. 2007. Subretinal posterior pole injury induces selective proliferation of RPE cells in the periphery in in vivo studies in pigs. *Invest Ophthalmol Vis Sci* **48:** 355–360.

Kim N, Abdulovic AL, Gealy R, Lippert MJ, Jinks-Robertson S. 2007. Transcription-associated mutagenesis in yeast is directly proportional to the level of gene expression and influenced by the direction of DNA replication. *DNA Repair (Amst)* **6:** 1285–1296.

Lettre G, Hengartner MO. 2006. Developmental apoptosis in *C. elegans*: a complex CEDnario. *Nat Rev Mol Cell Biol* **7:** 97–108.

Liu S, Rauhut R, Vornlocher H-P, Lührmann R. 2006. The network of protein–protein interactions within the human U4/U6.U5 tri-snRNP. *RNA* **12:** 1418–1430.

Longman D, Johnstone IL, Cáceres JF. 2000. Functional characterization of SR and SR-related genes in *Caenorhabditis elegans*. *EMBO J* **19:** 1625–1637.

Maita H, Kitaura H, Ariga H, Iguchi-Ariga SMM. 2005. Association of PAP-1 and Prp3p, the products of causative genes of dominant retinitis pigmentosa, in the tri-snRNP complex. *Exp Cell Res* **302:** 61–68.

Markaki M, Tavernarakis N. 2010. Modeling human diseases in *Caenorhabditis elegans*. *Biotechnol J* **5:** 1261–1276.

Mazouzi A, Velimezi G, Loizou JI. 2014. DNA replication stress: causes, resolution and disease. *Exp Cell Res* **329:** 85–93.

Montecucco A, Biamonti G. 2013. Pre-mRNA processing factors meet the DNA damage response. *Front Genet* **4:** 102.

Mordes D, Luo X, Kar A, Kuo D, Xu L, Fushimi K, Yu G, Sternberg P Jr, Wu JY. 2006. Pre-mRNA splicing and retinitis pigmentosa. *Mol Vis* **12:** 1259–1271.

Nehme R, Conradt B. 2008. egl-1: a key activator of apoptotic cell death in *C. elegans*. *Oncogene* **27**(Suppl 1): S30–S40.

Page AP, Johnstone IL. 2007. The cuticle. *wormbook*. www.wormbook.org.

Papasaikas P, Tejedor JR, Vigevani L, Valcárcel J. 2014. Functional splicing network reveals extensive regulatory potential of the core spliceosomal machinery. *Mol Cell* **57:** 7–22.

Porta-de-la-Riva M, Fontrodona L, Villanueva A, Cerón J. 2012. Basic *Caenorhabditis elegans* methods: synchronization and observation. *J Vis Exp* e4019.

Ramani AK, Nelson AC, Kapranov P, Bell I, Gingeras TR, Fraser AG. 2009. High resolution transcriptome maps for wild-type and nonsense-mediated decay-defective *Caenorhabditis elegans*. *Genome Biol* **10:** R101.

Ramani AK, Calarco JA, Pan Q, Mavandadi S, Wang Y, Nelson AC, Lee LJ, Morris Q, Blencowe BJ, Zhen M, et al. 2011. Genome-wide analysis of alternative splicing in *Caenorhabditis elegans*. *Genome Res* **21:** 342–348.

Rio Frio T, Wade NM, Ransijn A, Berson EL, Beckmann JS, Rivolta C. 2008. Premature termination codons in *PRPF31* cause retinitis pigmentosa via haploinsufficiency due to nonsense-mediated mRNA decay. *J Clin Invest* **118:** 1519–1531.

Rose AM, Shah AZ, Venturini G, Rivolta C, Rose GE, Bhattacharya SS. 2014. Dominant PRPF31 mutations are hypostatic to a recessive CNOT3 polymorphism in retinitis pigmentosa: a novel phenomenon of "linked trans-acting epistasis". *Ann Hum Genet* **78:** 62–71.

Rossmiller B, Mao H, Lewin AS. 2012. Gene therapy in animal models of autosomal dominant retinitis pigmentosa. *Mol Vis* **18:** 2479–2496.

Rual J-F, Ceron J, Koreth J, Hao T, Nicot A-S, Hirozane-Kishikawa T, Vandenhaute J, Orkin SH, Hill DE, van den Heuvel S, et al. 2004. Toward improving *Caenorhabditis elegans* phenome mapping with an ORFeome-based RNAi library. *Genome Res* **14:** 2162–2168.

Sleigh JN, Buckingham SD, Esmaeili B, Viswanathan M, Cuppen E, Westlund BM, Sattelle DB. 2011. A novel *Caenorhabditis elegans* allele, smn-1(cb131), mimicking a mild form of spinal muscular atrophy, provides a convenient drug screening platform highlighting new and pre-approved compounds. *Hum Mol Genet* **20:** 245–260.

Sönnichsen B, Koski LB, Walsh A, Marschall P, Neumann B, Brehm M, Alleaume A-M, Artelt J, Bettencourt P, Cassin E, et al. 2005. Full-genome RNAi profiling of early embryogenesis in *Caenorhabditis elegans*. *Nature* **434:** 462–469.

Stiernagle T. 2006. Maintenance of *C. elegans*. www.wormbook.org.

Sulston JE, Horvitz HR. 1977. Post-embryonic cell lineages of the nematode, *Caenorhabditis elegans*. *Dev Biol* **56:** 110–156.

Tanackovic G, Ransijn A, Ayuso C, Harper S, Berson EL, Rivolta C. 2011a. A missense mutation in *PRPF6* causes impairment of pre-mRNA splicing and autosomal-dominant retinitis pigmentosa. *A. m. J Hum Genet* **88:** 643–649.

Tanackovic G, Ransijn A, Thibault P, Abou Elela S, Klinck R, Berson EL, Chabot B, Rivolta C. 2011b. PRPF mutations are associated with generalized defects in spliceosome formation and pre-mRNA splicing in patients with retinitis pigmentosa. *Hum Mol Genet* **20:** 2116–2130.

The *C. elegans* Deletion Mutant Consortium. 2012. large-scale screening for targeted knockouts in the *Caenorhabditis elegans* genome. *G3 (Bethesda)* **2:** 1415–1425.

Towns KV, Kipioti A, Long V, McKibbin M, Maubaret C, Vaclavik V, Ehsani P, Springell K, Kamal M, Ramesar RS, et al. 2010. Prognosis for splicing factor PRPF8 retinitis pigmentosa, novel mutations and correlation between human and yeast phenotypes. *Hum Mutat* **31:** E1361–E1376.

Trapnell C, Roberts A, Goff L, Pertea G, Kim D, Kelley DR, Pimentel H, Salzberg SL, Rinn JL, Pachter L. 2012. Differential gene and transcript expression analysis of RNA-seq experiments with TopHat and Cufflinks. *Nat Protoc* **7:** 562–578.

Tropepe V, Coles BL, Chiasson BJ, Horsford DJ, Elia AJ, McInnes RR, van der Kooy D. 2000. Retinal stem cells in the adult mammalian eye. *Science* **287:** 2032–2036.

Venturini G, Rose AM, Shah AZ, Bhattacharya SS, Rivolta C. 2012. CNOT3 is a modifier of PRPF31 mutations in retinitis pigmentosa with incomplete penetrance. *PLoS Genet* **8:** e1003040.

Vermezovic J, Stergiou L, Hengartner MO, d'Adda di Fagagna F. 2012. Differential regulation of DNA damage response activation between somatic and germline cells in *Caenorhabditis elegans*. *Cell Death Differ* **19:** 1847–1855.

Waaijers S, Boxem M. 2014. Engineering the *Caenorhabditis elegans* genome with CRISPR/Cas9. *Methods* **68:** 381–388.

Wahl MC, Will CL, Lührmann R. 2009. The spliceosome: design principles of a dynamic RNP machine. *Cell* **136:** 701–718.

Wilkie SE, Vaclavik V, Wu H, Bujakowska K, Chakarova CF, Bhattacharya SS, Warren MJ, Hunt DM. 2008. Disease mechanism for retinitis pigmentosa (RP11) caused by missense mutations in the splicing factor gene *PRPF31*. *Mol Vis* **14:** 683–690.

Will CL, Lührmann R. 2011. Spliceosome structure and function. *Cold Spring Harb Perspect Biol* **3:** a003707.

Zhao C, Bellur DL, Lu S, Zhao F, Grassi MA, Bowne SJ, Sullivan LS, Daiger SP, Chen LJ, Pang CP, et al. 2009. Autosomal-dominant retinitis pigmentosa caused by a mutation in SNRNP200, a gene required for unwinding of U4/U6 snRNAs. *Am J Hum Genet* **85:** 617–627.

RNA
A PUBLICATION OF THE RNA SOCIETY

Modeling of autosomal-dominant retinitis pigmentosa in *Caenorhabditis elegans* uncovers a nexus between global impaired functioning of certain splicing factors and cell type-specific apoptosis

Karinna Rubio-Peña, Laura Fontrodona, David Aristizábal-Corrales, et al.

RNA 2015 21: 2119-2131 originally published online October 21, 2015
Access the most recent version at doi:10.1261/rna.053397.115

REPORT

Cytoplasmic LSM-1 protein regulates stress responses through the insulin/IGF-1 signaling pathway in *Caenorhabditis elegans*

ERIC CORNES,[1,7,8] MONTSERRAT PORTA-DE-LA-RIVA,[1,2] DAVID ARISTIZÁBAL-CORRALES,[1] ANA MARÍA BROKATE-LLANOS,[3] FRANCISCO JAVIER GARCÍA-RODRÍGUEZ,[1] IRIS ERTL,[1] MÒNICA DÍAZ,[4] LAURA FONTRODONA,[1] KADRI REIS,[1] ROBERT JOHNSEN,[5] DAVID BAILLIE,[5] MANUEL J. MUÑOZ,[3] MIHAIL SAROV,[6] DENIS DUPUY,[7,8] and JULIÁN CERÓN[1]

[1]Cancer and Human Molecular Genetics, [2]*C. elegans* Core Facility, Bellvitge Biomedical Research Institute—IDIBELL, L'Hospitalet de Llobregat, Barcelona 08908, Spain
[3]Centro Andaluz de Biología del Desarrollo (CABD), CSIC – UPO – Junta de Andalucía, Sevilla 41013, Spain
[4]Drug Delivery and Targeting, CIBBIM-Nanomedicine, Vall d'Hebron Research Institute, Universidad Autónoma de Barcelona, Barcelona 08035, Spain
[5]Department of Molecular Biology and Biochemistry, Simon Fraser University, Burnaby, British Columbia V5A 1S6, Canada
[6]TransgeneOmics Unit, Max Planck Institute of Molecular Cell Biology and Genetics, Dresden 01307, Germany
[7]Université Bordeaux, IECB, Laboratoire ARNA, F-33600 Pessac, France
[8]INSERM, U869, Laboratoire ARNA, F-33000 Bordeaux, France

ABSTRACT

Genes coding for members of the Sm-like (LSm) protein family are conserved through evolution from prokaryotes to humans. These proteins have been described as forming homo- or heterocomplexes implicated in a broad range of RNA-related functions. To date, the nuclear LSm2-8 and the cytoplasmic LSm1-7 heteroheptamers are the best characterized complexes in eukaryotes. Through a comprehensive functional study of the LSm family members, we found that *lsm-1* and *lsm-3* are not essential for *C. elegans* viability, but their perturbation, by RNAi or mutations, produces defects in development, reproduction, and motility. We further investigated the function of *lsm-1*, which encodes the distinctive protein of the cytoplasmic complex. RNA-seq analysis of *lsm-1* mutants suggests that they have impaired Insulin/IGF-1 signaling (IIS), which is conserved in metazoans and involved in the response to various types of stress through the action of the FOXO transcription factor DAF-16. Further analysis using a DAF-16::GFP reporter indicated that heat stress-induced translocation of DAF-16 to the nuclei is dependent on *lsm-1*. Consistent with this, we observed that *lsm-1* mutants display heightened sensitivity to thermal stress and starvation, while overexpression of *lsm-1* has the opposite effect. We also observed that under stress, cytoplasmic LSm proteins aggregate into granules in an LSM-1-dependent manner. Moreover, we found that *lsm-1* and *lsm-3* are required for other processes regulated by the IIS pathway, such as aging and pathogen resistance.

Keywords: *Caenorhabditis elegans*; stress response; LSM, *daf-16*; P bodies; stress granules

INTRODUCTION

The presence of a domain forming a tertiary structure known as "Sm-fold" is the common signature of the large Sm/LSm (Sm-like) protein family. Genes encoding Sm/LSm proteins exist in Archaea, Bacteria, and Eukaryotes (Mura et al. 2013; Weichenrieder 2014). The Sm-fold mediates the interaction between Sm/LSm proteins in order to make multimeric complexes involved in many aspects of RNA metabolism (Wilusz and Wilusz 2013). While eukaryotic members of the Sm family form protein complexes that are components of different snRNPs in the spliceosome (U1, U2, U4, U5, U11, and U12), the LSm proteins have expanded specialized RNA-related functions including splicing, nuclear RNA processing, and messenger RNA decay (Tharun 2009; Veretnik et al. 2009).

Eukaryotic LSm proteins are distributed in two distinct LSm complexes, the nuclear LSm2-8 and the cytoplasmic LSm1-7 (Tharun 2009). Therefore, LSm2 to LSm7 are common subunits of the two complexes, while Lsm8 and Lsm1

Corresponding author: jceron@idibell.cat, jceronmadrigal@gmail.com
Article published online ahead of print. Article and publication date are at http://www.rnajournal.org/cgi/doi/10.1261/rna.052324.115.

are specific for nuclear and cytoplasmic compartments, respectively. The nuclear complex binds to U6 snRNA in the U6 snRNP and is involved in splicing, whereas the cytoplasmic complex has been described as an activator of the decapping step in the 5′–3′ mRNA decay pathway in P bodies (Tharun et al. 2000; Parker and Sheth 2007).

Besides the above-mentioned canonical LSm complexes, other heteromeric rings have been characterized in yeast and vertebrate cells pointing toward an expanded catalog of LSm functions in the modulation of RNA–RNA and RNA–protein interactions (Tomasevic and Peculis 2002; Pillai et al. 2003; Fernandez et al. 2004). Moreover, by doing RNAi against *lsm* genes in diverse genetic backgrounds, we and others have observed a greater functional complexity than expected from the two described heteroheptameric complexes (Ceron et al. 2007). The goal of the present study is to explore the functions of LSm proteins in *Caenorhabditis elegans* and therefore provide insights into their roles in the physiology and development of multicellular animals.

A phylogenetic analysis based on protein sequences revealed that the *C. elegans* genome contains all eight genes (*lsm-1, lsm-2, lsm-3, lsm-4, lsm-5, lsm-6, lsm-7*, and *lsm-8*) coding for small proteins (77–125 amino acids) of the canonical eukaryotic complexes, and three other genes (Y48G1C.9, K07A1.15, and C49H3.4) coding for small proteins with only Sm domains (Supplemental Fig. S1A). In addition to this set of *lsm* genes, other well-characterized and conserved Sm-like genes including *edc-3* and *car-1* encode larger proteins containing other functional domains (Supplemental Fig. S1A; Squirrell et al. 2006; Tritschler et al. 2007).

The study of LSm proteins in multicellular organisms has biomedical relevance since the overexpression of LSm1/CaSm (cancer-associated Sm-like) has been associated with malignant development in diverse types of human cancers (Streicher et al. 2007; Watson et al. 2008), although the causal oncogenic mechanism of LSm1 in tumor cells is unknown.

RESULTS AND DISCUSSION

LSM-1 and LSM-3 are not essential for *C. elegans* viability but contribute to the regulation of development, reproduction, and motility

To shed light on the roles of the LSm complexes in *C. elegans*, we initiated functional studies of the components of the two canonical complexes as well as for Y48G1C.9, K07A1.15, and C49H3.4. First, we performed RNAi using both feeding and injection methods (Table 1). These experiments showed that (i) the three genes encoding LSm proteins that are not present in the canonical complexes are not required for the viability of the animals; and (ii) there is a heterogeneous phenotypic signature for the core *lsm* genes: *lsm-2*, *lsm-4*, *lsm-5*, *lsm-6*, *lsm-7*, and *lsm-8* are essential, while *lsm-1* and *lsm-3* are not. These phenotypes are consistent with genetic data in yeast with the exceptions of *lsm6* and *lsm7*, which are not essential in yeast (Supplemental Table S1); and *lsm3*, which is essential (Mayes et al. 1999; Salgado-Garrido et al. 1999). Therefore, *lsm1*/*lsm-1* is the only nonessential member in both organisms.

We validated our RNAi results by analyzing mutants for *lsm-1* and *lsm-3*. Both these mutants contain deletions that lack almost half of their transcripts, disrupting the Sm-like domain of the proteins (Fig. 1A). Both deletions are putatively functional null alleles since the corresponding dsRNAs delivered by microinjection did not further modify the mutant phenotype (Supplemental Fig. S1B). *lsm-1(tm3585)* and *lsm-3(tm5166)* mutant strains are viable but display pleiotropic phenotypes. Both mutations cause a low incidence of larval arrest, adult lethality, and embryonic lethality (Table 2). Moreover, *lsm-1(tm3585)* and *lsm-3(tm5166)* both exhibit reduced locomotor activity (Fig. 1B), are small compared with wild-type worms (Fig. 1C) and result in reduced brood sizes (Rbs) at 15°C. This Rbs phenotype is more pronounced at higher temperatures (Fig. 1D). We detected a reduction in the number of germ cells in adult *lsm-1* worms compared with wild-type worms (Supplemental Fig. S1C), which is the possible cause of the reduced fertility. Low brood size was also observed for worms with mutations in other P body components such as homologs of the decapping enzyme DCAP-2/Dcp2 and the translation repression related protein CGH-1/Dhh1 (Supplemental Fig. S1D).

We generated a transgenic strain containing integrated copies of a LSM-1::GFP reporter with the *lsm-1(tm3585)*. The reporter rescued the developmental and Rbs phenotypes

TABLE 1. Phenotypic analysis classifies *lsm* genes in distinct functional categories

Gene targeted	Canonical complex	RNAi by feeding		RNAi by injection
		P0	F1	F1
lsm-1[a]	Cytoplasmic	Rbs	Rbs, Gro	Rbs, Gro, low% Emb
lsm-2	Cytoplasmic/nuclear	Rbs, Ste	—	100% Emb
lsm-3[a]	Cytoplasmic/nuclear	Rbs	Rbs, Gro	Rbs, Gro, low % Emb
lsm-4	Cytoplasmic/nuclear	Rbs	Ste, Lva	100% Emb
lsm-5	Cytoplasmic/nuclear	Rbs	Ste	100% Emb
lsm-6	Cytoplasmic/nuclear	Rbs	Ste, Lva	100% Emb
lsm-7	Cytoplasmic/nuclear	Rbs	Ste, Lva	100% Emb
lsm-8	Nuclear	Rbs	Ste, Lva	100% Emb
Y48G1C.9[a]	Not applicable	WT	WT	WT
K07A1.15[a]	Not applicable	WT	WT	WT
C49H3.4[a]	Not applicable	WT	WT	WT

The table summarizes the RNAi phenotypes of the 11 *lsm* genes tested relative to control animals (treated with an empty-vector clone). Phenotypes are abbreviated as follows: (Rbs) Reduced brood size, (Gro) slow growth, (Lva) larval arrest, (Ste) sterile, (Emb) embryonic lethal, and (WT) wild type.
[a]*lsm* genes whose RNAi knockdown produces viable phenotypes.

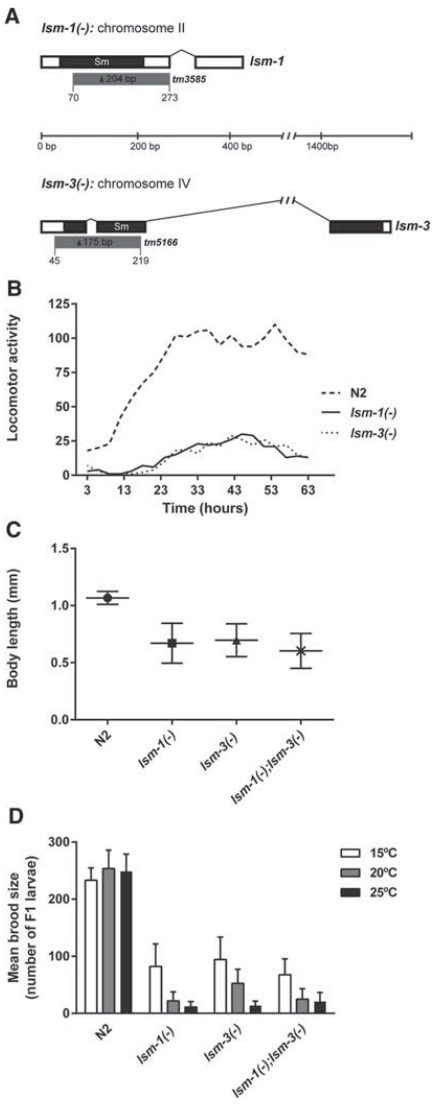

FIGURE 1. Characterization of *lsm-1* and *lsm-3* mutants. (*A*) Gene structures of *lsm-1* and *lsm-3*. White boxes represent exons. Connecting lines represent introns. Black areas indicate the regions encoding the conserved Sm domain. Gray boxes represent regions deleted by *lsm-1(tm3585)* and *lsm-3(tm5166)* alleles; (bp) base pair scale. (*B*) Measure of animal motility using an automated locomotor tracking system (Simonetta and Golombek 2007). Locomotor activity plots showing the activity of L4 worms at 20°C (1 worm/well in a 96-well microplate, eight wells per genotype were analyzed). Each dot corresponds to the mean activity (measured in bins/hour) of 3 h intervals. (*C*) Graph representing the body length of young adults (grown for 48 h at 25°C from L1 stage). Mean and standard deviations are plotted ($n \geq 100$ worms per genotype tested). (*D*) Brood sizes of wild type (N2) and the indicated mutant strains. Bars represent the standard deviation among individuals ($n \geq 20$).

(Supplemental Fig. S1E), indicating that the *lsm-1* deletion is directly responsible for the observed phenotypes and demonstrated that our integrated LSM-1::GFP reporter is functional.

In yeast, *lsm3* is essential for viability and necessary for correct splicing (Mayes et al. 1999). Since spliceosome core components are expected to be essential in *C. elegans* (Kamath et al. 2003; Rual et al. 2004; Kerins et al. 2010), the viability of *lsm-3* mutants argues against a central role for LSM-3 in splicing. To test for any relevance of *lsm-3* in this process, we generated a strain carrying a GFP reporter for constitutive splicing and the *lsm-3* deletion. These animals displayed normal GFP expression in the intestinal nuclei, indicating that LSM-3 is not required for constitutive splicing (Supplemental Fig. S2A).

Given that neither *lsm-1* nor *lsm-3* are necessary for the survival of the animal, we tested to see if these genes have redundant functions by making a double homozygous mutant strain. The lack of a synthetic phenotype (Fig. 1C,D) and the fact that *lsm-3* and *lsm-1* mutants phenocopy each other indicate that these genes are not redundant but might participate in the same cellular processes during reproduction and development.

We also tested for additional synthetic interactions between the nonessential *lsm* genes in *C. elegans* by microinjecting combinations of diverse dsRNAs (Supplemental Fig. S1F). Since we did not observe any synthetic interaction, we concluded that *C. elegans*' LSm family does not function as in *Arabidopsis*, where functional redundancies among Lsm proteins are evident (Perea-Resa et al. 2012).

In summary, our analysis showed that *lsm-1* and *lsm-3* are the only nonessential genes coding for members of the canonical LSm complexes, nevertheless, they are required for normal *C. elegans* development and health.

Expression of *lsm* genes in *C. elegans*

In addition to the apparent functional diversity of the *lsm* genes in *C. elegans*, we wanted to know if differences also exist at the regulatory level. The features of *lsm* genes in the *C. elegans* genome indicate heterogeneity in terms of regulatory regions because *lsm* genes present distinct UTR sequences and four out of the eleven genes are located in predicted operons (Supplemental Fig. S3A). We produced reporter constructs by PCR fusion (Hobert 2002) to generate promoter::GFP::*unc-54*_3′-UTR transgenic lines for the 11 *lsm* genes studied in this report (Supplemental Table S3). All promoters reported expression except for K07A1.15. We analyzed fluorescence intensities for several identifiers in *C. elegans*' anatomy and observed overlapping but distinct gene expression patterns across family members (Supplemental Fig. S3B). However, these transcriptional reporters provide insufficient information to draw major conclusions because they do not contain all the regulatory sequences. As an example of the importance of other regulatory regions, a translational reporter for *lsm-4* in a fosmid context (including UTRs and introns)

TABLE 2. Phenotypes caused by mutations in *lsm-1* and *lsm-3*

Strains	%Emb	%Lva	%Let
lsm-1(-)	19.1 ± 19.8 (*n* = 511)	9.4 ± 1.5 (*n* = 2035)	8.1 ± 0.9 (*n* = 1340)
lsm-3(-)	8.4 ± 5.8 (*n* = 845)	12.5 ± 0 (*n* = 1912)	5.7 ± 1.6 (*n* = 1911)

Synchronized L1 worms were seeded on NGM plates and phenotypes scored after 48 h at 20°C. (Emb) Embryonic lethality, (Lva) larval arrest, and (Let) adult lethality. Mean values and ± standard deviations are shown. (*n*) The total number of eggs or individuals scored for each phenotype.

was ubiquitously expressed although with apparent varying levels depending on the cell type (Supplemental Fig. S3C).

However, this localizome study showed that internal promoters can drive the expression of *lsm* genes located within different purported operons (as *lsm-3* and *lsm-8*). Since both SL1 and SL2 splice leaders have been detected upstream of their messenger RNA (Allen et al. 2011), the activity of these internal promoters may not fully capture the endogenous expression pattern.

lsm-1 and lsm-3 are required for various stress responses

To gain insight into LSM-1 functions, the LSm protein with the highest biomedical relevance, we compared the transcriptomes of L3 (where the germline is not yet fully developed) *lsm-1(tm3585)* and wild-type animals (Supplemental Table S4). RNA-seq data suggest that genes related to the Insulin/IGF-1 signaling (IIS) pathway are mis-regulated in *lsm-1 (tm3585)* mutants (Supplemental Table S4; McElwee et al. 2003; Murphy et al. 2003; Liu et al. 2004; Halaschek-Wiener et al. 2005; Oh et al. 2006; Pinkston-Gosse and Kenyon 2007; Lee et al. 2009; Schuster et al. 2010). The IIS pathway has been associated with immune response and stress protection, processes interconnected and regulated by DAF-2, which is the *C. elegans* ortholog of the insulin-like growth factor-1 (IGF-1) receptor (Troemel et al. 2006; Singh and Aballay 2009; Murphy and Hu 2013). In *C. elegans,* DAF-2 activity keeps the FOXO transcription factor DAF-16 in the cytoplasm. However, inactivation of DAF-2 signaling allows DAF-16 to translocate to the nucleus, thus inducing stress response at the transcriptional level (Yen et al. 2011).

Remarkably, among the top 24 up-regulated genes (fold change >3, Supplemental Table S4) in *lsm-1(tm3585)* mutants, we found four genes that are normally down-regulated by the IIS effector DAF-16 (C32H11.4, C32H11.9, *dod-21*, and *dod-24*) (Murphy et al. 2003). Moreover, *pud-1.1* and *pud-2.2*, which are up-regulated in *daf-2* mutants (Dong et al. 2007), are among the top 17 down-regulated genes (fold change < −3, Supplemental Table S4) in *lsm-1 (tm3585)* mutants. Therefore, our transcriptome data point toward a DAF-16 deficiency in *lsm-1(tm3585)* mutants under normal conditions.

To further investigate the functional relationship between LSM-1 and the IIS pathway, we studied the stress-induced nuclear translocation dynamics of DAF-16 in the *lsm-1(tm3585)* mutant background. Interestingly, we observed that upon heat stress the translocation of DAF-16 to the nucleus is impaired in *lsm-1(tm3585)* mutants (Fig. 2A,B), a defect previously associated with diminished stress resistance (Lin et al. 2001). We observed a delay in the DAF-16 nuclear translocation although most of DAF-16 is eventually relocated to the nuclei. Such an effect is a hallmark of mutations that affect the correct function of the IIS pathway (Chiang et al. 2012). The DAF-16::GFP reporter that we used and *lsm-3* are located in the same chromosome, making the generation of a genetic hybrid difficult. Thus to test the impact of *lsm-3* on DAF-16 nuclear relocalization kinetics, we injected *lsm-3* dsRNA and *lsm-1* dsRNA as positive controls in a DAF-16::GFP strain. In both cases, we observed a defect in DAF-16 nuclear translocation upon heat shock (Supplemental Fig. S2B).

Consistent with our previous observations, we found that *lsm-1(tm3585)* and *lsm-3(tm5166)* mutants were sensitive to heat stress (Fig. 2C), while strains overexpressing *lsm-1* displayed a significant thermoresistance, similar to that reported for *daf-2(e1370)* mutants where DAF-16 is constitutively nuclear and transcriptionally active (Fig. 2D; McColl et al. 2010). Furthermore, we also observed that *lsm-1(tm3585)* and *lsm-3(tm5166)* mutant L1 larvae were more sensitive to starvation than wild-type animals, whereas larvae with extra copies of *lsm-1* had a higher survival rate than wild-type worms (Fig. 2E). All these results support the idea that *lsm-1* and *lsm-3* contribute to stress responses through the IIS pathway in *C. elegans* and that *lsm-1* levels influence the robustness of these responses.

The IIS pathway also regulates resistance to bacterial infection and longevity (Evans et al. 2008). We observed that mutations in *lsm-1* and *lsm-3* cause heightened sensitivity to infection by certain pathogens (Fig. 3A) and have negative effects on lifespan (Fig. 3B). However, ectopic *lsm-1* expression does not protect *C. elegans* from pathogens or extend its lifespan (Fig. 3). Moreover, the *daf-2(m577)* extended lifespan requires *lsm-1* and *lsm-3*, and the short lifespan of *daf-16(mu86)* mutants is shortened by *lsm-1(tm3585)*, suggesting that the harmful effect of the *lsm-1* mutation on longevity is independent of the regulation of DAF-16 nuclear location.

Redistribution of cytoplasmic LSm proteins in stress conditions

We generated integrated transgenic reporter lines for LSM-1 and LSM-4, which allowed the tracking of nuclear and cytoplasmic LSm complexes in the germline and early embryo. As previously observed in other systems (Ingelfinger et al. 2002; Spiller et al. 2007), LSM-1 was located exclusively in the

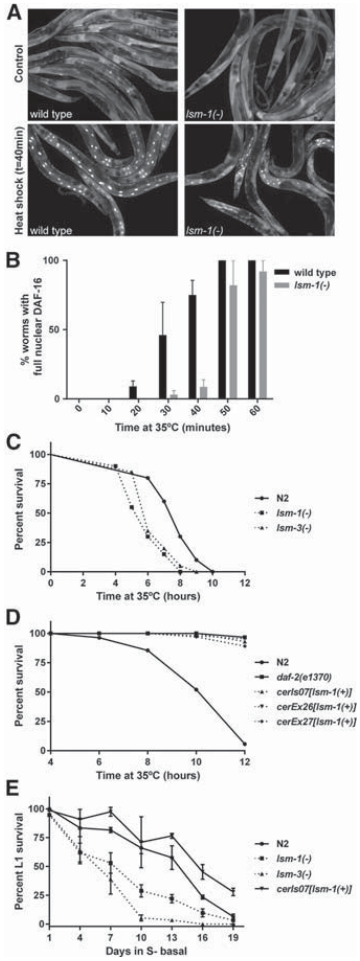

FIGURE 2. *lsm-1* promotes DAF-16 nuclear localization upon stress and influences stress responses. (*A*) *lsm-1* is required for proper stress-induced DAF-16 nuclear translocation. Fluorescence images of DAF-16::GFP in wild-type (N2) and *lsm-1* mutant animals grown at 25°C, and after a 40 min heat shock at 35°C. (*B*) Time-course analysis of DAF-16::GFP nuclear accumulation in response to heat stress. The histogram represents the average of percentages of worms with full nuclear DAF-16::GFP in three independent experiments ($n \geq 50$ for each strain and time point). Error bars, SEM. (*C*) Representative graph of experiments (see Supplemental Fig. S4A) showing the significant reduced resistance to heat stress caused by mutations in *lsm-1* and *lsm-3* (P-value < 0.001). Young adult worms were incubated at 35°C and survival was scored every hour. (*D*) Representative graph of experiments (see Supplemental Fig. S4A) showing the significant resistance to heat stress caused by three distinct strains overexpressing *lsm-1* (P-value < 0.001). *daf-2(e1370)* were used as positive control for heat stress resistance. Young adult worms were incubated at 35°C and survival was scored every 2 h. (*E*) *lsm-1* and *lsm-3* mutations reduce the survival of L1 larvae during starvation at 20°C. Ectopic expression of *lsm-1* through the integrated reporter LSM-1::GFP displayed a significant survival to starvation compared with wild-type (N2) animals after 19 d (P-value < 0.001). Graph represents the mean percentage of survival and standard deviations from three experimental replicates ($n \geq 100$ for each replicate and time point).

cytoplasm whereas LSM-4 was expressed both in the nucleus and cytoplasm (Fig. 4A).

As previously reported in *C. elegans*, we observed constitutive cytoplasmic LSm granules in the early embryo in somatic blastomeres (Fig. 4A; Gallo et al. 2008). However, we found that in young adult animals the distribution of cytoplasmic LSm proteins was diffuse rather than located in aggregates (Fig. 4B). However, under heat stress, adult animals expressing LSM-1::GFP or LSM-4::GFP showed cytoplasmic GFP granules (Fig. 4B). Microscopic analysis of the LSM-4::GFP reporter in *lsm-1* mutants indicated that the formation of cytoplasmic LSm granules after stress was dependent on the presence of LSM-1 (Fig. 4B).

In summary, while the formation of cytoplasmic LSM granules is constitutive in some embryonic cells, the accumulation of visible LSm granules in larvae and adults may occur upon stress only, in an LSM-1-dependent manner.

The described competition of LSm8 and LSm1 for the common components of the LSm complexes (LSm2-7) implies that nuclear and cytoplasmic functions are somehow interconnected, and such co-regulation should be carefully studied in multicellular organisms (Spiller et al. 2007; Novotny et al. 2012).

Cytoplasmic LSm granules: P-bodies or stress granules?

In yeast and humans, the LSm1-7 complex has been associated with P bodies (PBs) (Kedersha and Anderson 2007). PBs are dynamic cytoplasmic aggregates of proteins and RNA molecules that participate in diverse processes related to RNA metabolism such as translational repression and mRNA degradation (Sheth and Parker 2006; Parker and Sheth 2007; Buchan et al. 2010). In particular, the LSm1-7 complex has been implicated in the 5′–3′ mRNA decay machinery as a decapping activator of oligoadenilated mRNAs in P-bodies (Tharun 2009).

Stress granules (SGs) are another type of cytoplasmic aggregate, composed of nontranslating mRNAs and diverse proteins related to mRNA processing that form when translational initiation is impaired (for example, when cells are exposed to environmental stresses) (Buchan and Parker 2009).

PBs and SGs are dynamic structures that share some protein components and can physically interact (Kedersha and Anderson 2007; Buchan et al. 2010); however, the physiological roles of these aggregates are not well understood and the classification of proteins within one or another is mostly based on protein co-localization experiments with previously characterized proteins.

In the *C. elegans* embryo, it has been shown that LSM-1::GFP co-localizes with other PB components, but the presence of visible LSM-1::GFP granules is not required for mRNA degradation (Gallo et al. 2008). Comparing the localization of LSM-1 to the known P bodies component DCAP-

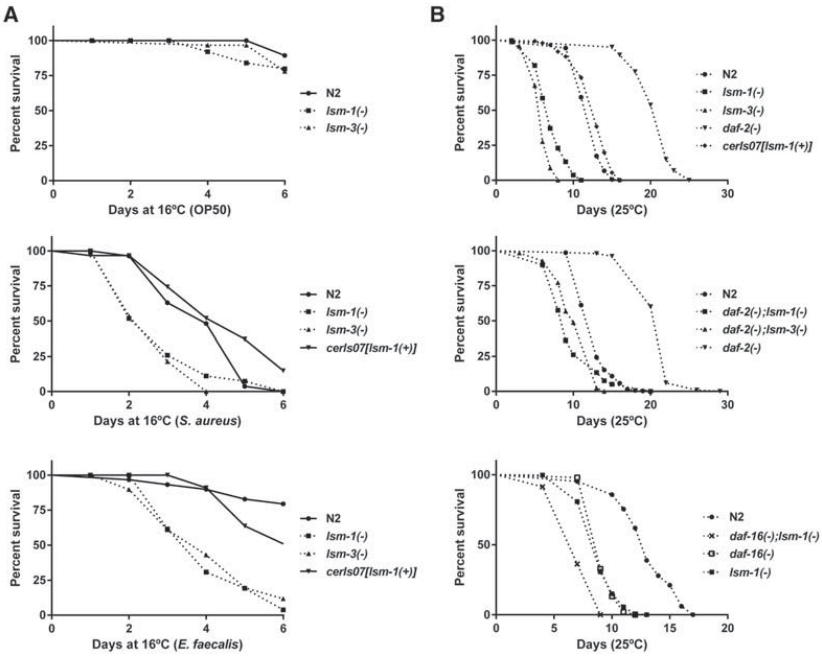

FIGURE 3. Mutations in *lsm-1* and *lsm-3* cause hypersensitivity to pathogen infection and affect IIS-induced longevity. (*A*) Representative graph of survival experiments (see Supplemental Fig. S4B) of wild-type (N2) and mutant strains on *Escherichia coli* OP50, *Staphylococcus aureus*, and *Enterococcus faecalis* ($n = 30$). No significant differences were observed after 6 d on OP50 between *lsm*-1 and *lsm*-3 mutants compared with wild-type (N2) animals. Differences between *lsm-1* and *lsm-3* mutants were significant compared with wild-type (N2) after pathogen infection ($0.01 < P$-value < 0.001 in all cases). (*B*) Representative graphs showing lifespan analysis (see Supplemental Fig. S4C) of wild-type (N2) and different mutant and transgenic strains. *daf-2(m577)* and *daf-16(mu86)* mutants were used as control for extended and shortened lifespans, respectively.

2, which is the catalytic enzyme of the 5′–3′ decapping step in PBs, shows they are different. In developing *C. elegans* embryos, LSM-1 is present only in somatic blastomeres, whereas DCAP-2 localizes in P granules in germline blastomeres (Lall et al. 2005). Another PB component, the decapping enzyme DCAP-1, localizes in granules that are only weakly reduced upon *lsm-1* RNAi inactivation (Sun et al. 2011). Moreover, in adult animals, although DCAP-1-positive granules have been described to increase in size with age (Sun et al. 2011), we did not observe this effect in LSM-1::GFP worms (not shown).

Distinct cytoplasmic aggregates can share many RNA-binding proteins and depending on cellular conditions, these factors can relocalize from one type of granule to another (Buchan 2014). Since LSM-1::GFP aggregates in stress conditions, LSM-1 may shuttle between PBs and SGs depending on physiological or environmental conditions. To confirm the aggregation of LSM-1 in SGs, we used an RFP-tagged TIAR-1 (TIA-1-related), which is a RNA-binding protein described as a SG component (Kedersha et al. 1999). We observed the co-localization of LSM-1::GFP and TIAR-1::RFP under heat stress (Fig. 4C), suggesting that LSM-1 can also accumulate in SG under specific conditions. In mammalian cells, LSm1 is mostly P body-specific in the absence of stress, although it has been observed associated with some types of stress granules (Kedersha and Anderson 2007).

Since the single bacterial LSm protein homolog Hfq is also required for stress responses in bacteria (Wilusz and Wilusz 2013), the capability of LSm proteins to chaperone RNA–protein and RNA–RNA interactions seems to be conserved through evolution as an adaptive response, distributing RNA molecules and regulating protein synthesis, to cope with adverse environmental conditions. Interestingly, such a response in *C. elegans* seems to be linked to the IIS pathway, also evolutionary conserved in Metazoa.

Concluding remarks

Through a comprehensive phenotypic analysis of the *lsm* family in *C. elegans*, we have uncovered the role of cytoplasmic LSm proteins in *C. elegans* stress response. We found that LSM-1 is required to establish a primary response to stress through two known mechanisms: (i) the translocation of DAF-16 to the nucleus, and (ii) the formation of cytoplasmic

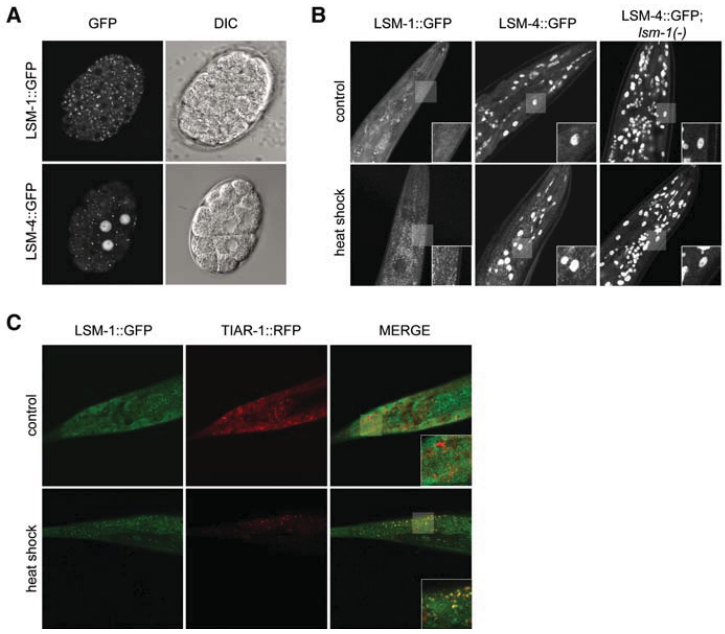

FIGURE 4. LSM proteins accumulate in cytoplasmic foci in specific stages and conditions. (*A*) LSM proteins accumulate in cytoplasmic granules during embryogenesis. Confocal images of embryos expressing LSM-1::GFP in the cytoplasm and LSM-4::GFP in the nucleus and the cytoplasm. *Right* panels show the same embryos visualized under differential interference contrast (DIC). (*B*) LSm accumulation in cytoplasmic granules in adult cells is induced by heat stress (1 h at 35°C) (additional images in Supplemental Fig. S5) and is dependent on *lsm-1*. Confocal images (Z hyperstack) of the head of young adult worms expressing LSM-1::GFP and LSM-4::GFP in control (20°C) and after heat-shock. (*C*) LSM-1 granules colocalize with TIAR-1 granules under heat-stress conditions (1 h at 35°C). Confocal images of the tail of L4 worms coexpressing LSM-1::GFP and RFP::TIAR-1.

granules. To the best of our knowledge, this is the first time that a functional link has been observed between these two mechanisms in the stress response.

Regarding the link between LSm1 and cancer, it is tempting to establish a parallel between cancer cells and the conditions required in *C. elegans* for LSM-1 cytoplasmic aggregation, namely, rapid cell division in the embryo and environmental stress. Thus, we present *C. elegans* as an excellent model to further investigate the impact of cytoplasmic Lsm proteins in cellular metabolism and cancer.

MATERIALS AND METHODS

Strains

Caenorhabditis elegans strains were cultured and maintained using standard procedures (Stiernagle 2006; Porta-de-la-Riva et al. 2012). Bristol N2 was the wild-type strain, and the following alleles and transgenic strains were used: CER60: *lsm-1(tm3585)*II, CER59: *lsm-3(tm5166)*IV, CER36: *lsm-1(tm3585)*II, *lsm-3(tm5166)*IV, CB1370: *daf-2(e1370)*III, CF1038: *daf-16(mu86)*I, BL3466: *inIs173 [PNvitgfp]*, TJ356: *zIs356[Pdaf-16::daf-16::gfp,rol-6(su1006)]*IV, DR1567: *daf-2(m577)*III, CER154: *lsm-1(tm3585)*II;*daf-2(m577)* III, CER158: *lsm-1(tm3585)*II;*daf-16(mu86)*I, CER159: *lsm-3 (tm5166)*IV;*daf-2(m577)*III, DG1701: *cgh-1(tn691)*III and RB1641: *dcap-2(ok2023)*IV.

We also generated the following transgenic strains: CER26: *unc-119(ed3)*III; *cerEx26[*P*lsm-1*::*lsm-1*::*gfp*::*lsm*-1_3′UTR, *unc-119(+)]*, CER27: *unc-119(ed3)*III; *cerEx27*[P*lsm-1*::*lsm-1*::*gfp*::*lsm*-1_3′UTR, *unc-119(+)]*, CER41: *unc-119(ed3)*III; *cerIs02*[P*lsm*-4::*lsm-4*::*gfp*:: *lsm*-4_3′UTR, *unc-119(+)]*, CER157: *unc-119(ed3)*III; *cerIs07* [P*lsm-1*::*lsm-1*::*gfp*::*lsm*-1_3′UTR, *unc-119(+)]*, CER152: *cerIs02*; *lsm-1(tm3585)*II, CER155: *zIs356*IV;*lsm-1(tm3585)*II, CER129: *inIs173[PNvitgfp];lsm-3(tm5166)*IV, CER162: *cerIs07*;*lsm-1(tm3585)* II, CER166: *cerIs07;cerEx42[*P*tiar-1::RFP::tiar-1ORF::tiar-1 3′UTR +rol-6(+)]*.

Generation of transgenic animals

For the generation of *lsm-1* and *lsm-4* translational reporters, fosmid vectors containing a GFP-tagged version of these genes were requested from the Transgeneome resource (Sarov et al. 2012) and transformation was performed by bombardment with gold particles (Biolistic Helium Gun, Caenotec). *unc-119(ed3)* young adults were shot with 16 µg of the purified DNA of interest (Praitis et al. 2001).

For the co-localization experiments, CER157 animals expressing integrated copies of LSM-1::GFP were injected with a mix containing 80 ng/µL of a RFP::TIAR-1 construct (Rousakis et al. 2014) and 20 ng/µL of the linearized roller marker pRF4 [*rol-6(su1006)*].

Transcriptional reporters, described in the Supplemental Material, were constructed by PCR fusion (Hobert 2002).

RNAi

The RNAi clones used in this study were obtained from the ORFeome library (Rual et al. 2004) (*lsm-1, lsm-3, lsm-5, lsm-7,* C49H3.4) or the Ahringer library (Kamath et al. 2003) (*lsm-2, lsm-4, lsm-6*). We completed the *lsm* family RNAi clone collection by amplifying the cDNAs of *lsm-8,* Y48G1C.9, and K07A1.15, and cloning them into a L4440 vector by ligation after digestion with restriction enzymes. All RNAi clones were verified by sequencing. RNA-mediated interference (RNAi) by feeding was performed following standard conditions (Fontrodona et al. 2013), using a concentration of 3 mM IPTG on the RNAi plates. To induce RNAi by microinjection, specific dsRNAs were synthesized by using the MEGAscript T7 kit (Ambion). Young adult animals were injected with 1 µg/µL of the dsRNA of interest.

RNA-seq analyses

N2 wild-type and *lsm-1(tm3585)* L1 synchronized worms were grown and harvested at L3 stage (26 h at 25°C). Animals were washed with M9 buffer to remove bacteria, and pellet frozen in TRIzol. Total RNA purification was performed using the *mirVana* miRNA isolation kit (Ambion) followed by Ribosomal RNA depletion with the RiboMinus Eukaryote Kit (Invitrogen). RNA quality was verified in the *Experion Bioanalyzer* (Bio-Rad). We used an *Illumina* kit to make libraries that were run through a Genome Analyzer IIX Ultrasequencer (*Illumina*). Each sample produced ~10 million reads that were processed using TopHat (Trapnell et al. 2009) to be mapped against the *C. elegans* genome (WS225). BAM files were analyzed with the SeqSolve NGS software (Integromics, S.L.) using a false discovery rate of 0.05, and filtering reads displaying multiple mapping sites. SeqSolve uses Cufflinks (Trapnell et al. 2010) and Cuffdiff (Trapnell et al. 2013) programs to perform differential gene expression analyses between samples (P-value < 0.005). Expression values were normalized in FPKM (fragments per kilobase of exon per million fragments mapped).

Stress assays

For thermotolerance assays, L4 animals grown at 16°C were transferred to plates seeded with OP50 bacteria and grown to day 1 of adulthood. Next, worms ($n = 40$) were transferred to two 6 cm plates without any food and incubated at 35°C. Viability was scored at several time points; death was determined by the lack of movement and/or pharyngeal pumping after prodding.

To quantify DAF-16::GFP subcellular localization, L4 worms grown at 16°C were shifted to 25°C until they reached day 1 adult stage. GFP was analyzed using an Axio Imager Z1 Zeiss microscope at 40× magnification before and after heat shock at 35°C. For heat shock time-course analyses, worms were scored for the presence or absence of GFP accumulation in the nuclei of somatic cells along the body every 10 min at 35°C. Animals were scored as having full nuclear GFP if DAF-16::GFP was observed in the nucleus of somatic cells homogeneously from head to tail.

L1 starvation assay was performed as previously described by Zhang et al. (2011). Briefly, adult worms were bleached and the resulting eggs were resuspended in 4–6 mL S-basal without cholesterol in 15-mL tubes. Egg prep was filtered using a 40 µm nylon cell strainer (BD Falcon) in order to remove debris and larger clumps of unhatched eggs derived from the bleaching. Tubes were incubated rotating at 20°C. To determine larval viability, 20-µL aliquots (~100 worms) were placed every 3 d onto three 6-cm nematode growth medium (NGM) plates and survival rates were calculated.

For bacterial pathogen assays, L4 worms grown at 16°C ($n = 10$ for each genotype) were cultured in the presence of pathogenic bacteria as the sole food source, and the number of survivors was counted every day. *Enterococcus faecalis* OG1RF was grown in BHI with 40 µg/mL of gentamycin. *Staphylococcus aureus* NTCT8325 was grown in TSB with 10 µg/mL of nalidixic acid.

For all the stress assays, graphical representation of survival curves and Kaplan-Meier statistical analyses were made using GraphPad Prism 4.0 software (GraphPad Software Inc.) P-values were obtained applying the Mantel-Cox logrank test.

Lifespan experiments

A synchronized population of L1 larvae was grown at 15°C for 72 h until they reached L4 stage. At that point, worms were washed from the plate using sterile M9 buffer and transferred (at least 100 animals per experiment) onto NGM plates seeded with OP50 and 0.1 mg/mL 5-fluoro-2′-deoxyuridine (FUDR) to chemically inhibit reproduction and to eliminate any effects reproduction might have on longevity. The viability of the worms, cultured at 25°C was scored every two or three days. Animals that failed to respond to stimulation by touch were considered dead. Day 0 of adulthood was defined as the day that mid-to-late L4s were transferred to NGM-FUDR plates and maintained at 25°C. Survival curves were made with GraphPad Prism 4.0 software.

SUPPLEMENTAL MATERIAL

Supplemental material is available for this article.

ACKNOWLEDGMENTS

We thank the CGC (Caenorhabditis Genetics Center) and the Japanese *C. elegans* knockout consortium (National BioResource Project, NBRP) for providing strains; Dr. Popi Syntichaki for providing us with constructs; and Dr. Anne Royou and members from the Royou laboratory for confocal microscopy technical advice. This work was supported by a grant from the Instituto de Salud Carlos III (ISCIII) (Exp. PI12/01554). R.J. and D.B. were supported by a Natural Sciences and Engineering Research Council (NSERC) Canada grant. D.B. holds a Canada Research Chair. J.C. is a Miguel Servet Researcher (ISCIII). E.C. was supported with a CTP-AIRE fellowship from AGAUR (Generalitat de Catalunya) and a TRANSBIO SUDOE collaborative project.

Author contributions: E.C., D.D., and J.C. conceived and designed the experiments. E.C., D.A., M.P., A.B., I.E., M.S., L.F, F.J., K.R., and J.C. performed the experiments. E.C., D.D., and J.C. analyzed the data. R.J., D.B., M.M., and M.D. contributed reagents/materials/analysis tools. E.C., D.D., and J.C. wrote the paper.

Received April 27, 2015; accepted June 6, 2015.

REFERENCES

Allen MA, Hillier LW, Waterston RH, Blumenthal T. 2011. A global analysis of *C. elegans* trans-splicing. *Genome Res* **21:** 255–264.

Buchan JR. 2014. mRNP granules: assembly, function, and connections with disease. *RNA Biol* **11:** 1019–1030.

Buchan JR, Parker R. 2009. Eukaryotic stress granules: the ins and outs of translation. *Mol Cell* **36:** 932–941.

Buchan JR, Nissan T, Parker R. 2010. Analyzing P-bodies and stress granules in *Saccharomyces cerevisiae*. *Methods Enzymol* **470:** 619–640.

Ceron J, Rual J-F, Chandra A, Dupuy D, Vidal M, Van Den Heuvel S. 2007. Large-scale RNAi screens identify novel genes that interact with the *C. elegans* retinoblastoma pathway as well as splicing-related components with synMuv B activity. *BMC Dev Biol* **7:** 30.

Chiang W-C, Tishkoff DX, Yang B, Wilson-Grady J, Yu X, Mazer T, Eckersdorff M, Gygi SP, Lombard DB, Hsu A-L. 2012. *C. elegans* SIRT6/7 homolog SIR-2.4 promotes DAF-16 relocalization and function during stress. *PLoS Genet* **8:** e1002948.

Dong M-Q, Venable JD, Au N, Xu T, Park SK, Cociorva D, Johnson JR, Dillin A, Yates JR. 2007. Quantitative mass spectrometry identifies insulin signaling targets in *C. elegans*. *Science* **317:** 660–663.

Evans E, Chen WC, Tan M-W. 2008. The DAF-2 insulin-like signaling pathway independently regulates aging and immunity in *C. elegans*. *Aging Cell* **7:** 879–893.

Fernandez CF, Pannone BK, Chen X, Fuchs G, Wolin SL. 2004. An Lsm2-Lsm7 complex in *Saccharomyces cerevisiae* associates with the small nucleolar RNA snR5. *Mol Biol Cell* **15:** 2842–2852.

Fontrodona L, Porta-de-la-Riva M, Morán T, Niu W, Díaz M, Aristizábal-Corrales D, Villanueva A, Schwartz S Jr, Reinke V, Cerón J. 2013. RSR-2, the *Caenorhabditis elegans* ortholog of human spliceosomal component SRm300/SRRM2, regulates development by influencing the transcriptional machinery. *PLoS Genet* **9:** e1003543.

Gallo CM, Munro E, Rasoloson D, Merritt C, Seydoux G. 2008. Processing bodies and germ granules are distinct RNA granules that interact in *C. elegans* embryos. *Dev Biol* **323:** 76–87.

Halaschek-Wiener J, Khattra JS, McKay S, Pouzyrev A, Stott JM, Yang GS, Holt RA, Jones SJM, Marra MA, Brooks-Wilson AR, et al. 2005. Analysis of long-lived *C. elegans* daf-2 mutants using serial analysis of gene expression. *Genome Res* **15:** 603–615.

Hobert O. 2002. BioTechniques—PCR fusion-based approach to create reporter gene constructs for expression analysis in transgenic *C. elegans*. *Biotechniques* **32:** 728–730.

Ingelfinger D, Arndt-Jovin DJ, Lührmann R, Achsel T. 2002. The human LSm1-7 proteins colocalize with the mRNA-degrading enzymes Dcp1/2 and Xrnl in distinct cytoplasmic foci. *RNA* **8:** 1489–1501.

Kamath RS, Fraser AG, Dong Y, Poulin G, Durbin R, Gotta M, Kanapin A, Le Bot N, Moreno S, Sohrmann M, et al. 2003. Systematic functional analysis of the *Caenorhabditis elegans* genome using RNAi. *Nature* **421:** 231–237.

Kedersha N, Anderson P. 2007. Mammalian stress granules and processing bodies. *Methods Enzymol* **431:** 61–81.

Kedersha NL, Gupta M, Li W, Miller I, Anderson P. 1999. RNA-binding proteins TIA-1 and TIAR link the phosphorylation of eIF-2 α to the assembly of mammalian stress granules. *J Cell Biol* **147:** 1431–1442.

Kerins JA, Hanazawa M, Dorsett M, Schedl T. 2010. PRP-17 and the pre-mRNA splicing pathway are preferentially required for the proliferation versus meiotic development decision and germline sex determination in *Caenorhabditis elegans*. *Dev Dyn* **239:** 1555–1572.

Lall S, Piano F, Davis RE. 2005. *Caenorhabditis elegans* decapping proteins: localization and functional analysis of Dcp1, Dcp2, and DcpS during embryogenesis. *Mol Biol Cell* **16:** 5880–5890.

Lee S-J, Murphy CT, Kenyon C. 2009. Glucose shortens the life span of *C. elegans* by downregulating DAF-16/FOXO activity and aquaporin gene expression. *Cell Metab* **10:** 379–391.

Lin K, Hsin H, Libina N, Kenyon C. 2001. Regulation of the *Caenorhabditis elegans* longevity protein DAF-16 by insulin/IGF-1 and germline signaling. *Nat Genet* **28:** 139–145.

Liu T, Zimmerman KK, Patterson GI. 2004. Regulation of signaling genes by TGFβ during entry into dauer diapause in *C. elegans*. *BMC Dev Biol* **4:** 11.

Mayes AE, Verdone L, Legrain P, Beggs JD. 1999. Characterization of Sm-like proteins in yeast and their association with U6 snRNA. *EMBO J* **18:** 4321–4331.

McColl G, Rogers AN, Alavez S, Hubbard AE, Melov S, Link CD, Bush AI, Kapahi P, Lithgow GJ. 2010. Insulin-like signaling determines survival during stress via posttranscriptional mechanisms in *C. elegans*. *Cell Metab* **12:** 260–272.

McElwee J, Bubb K, Thomas JH. 2003. Transcriptional outputs of the *Caenorhabditis elegans* forkhead protein DAF-16. *Aging Cell* **2:** 111–121.

Mura C, Randolph PS, Patterson J, Cozen AE. 2013. A structural and evolutionary perspective on Sm function Archaeal and eukaryotic homologs of Hfq. *RNA Biol* **10:** 636–651.

Murphy CT, Hu PJ. 2013. Insulin/insulin-like growth factor signaling in *C. elegans*. In *WormBook* (ed. The *C. elegans* Research Community). http://www.wormbook.org.

Murphy CT, McCarroll SA, Bargmann CI, Fraser A, Kamath RS, Ahringer J, Li H, Kenyon C. 2003. Genes that act downstream of DAF-16 to influence the lifespan of *Caenorhabditis elegans*. *Nature* **424:** 277–283.

Novotny I, Podolská K, Blazíková M, Valásek LS, Svoboda P, Stanek D. 2012. Nuclear LSm8 affects number of cytoplasmic processing bodies via controlling cellular distribution of Like-Sm proteins. *Mol Biol Cell* **23:** 3776–3785.

Oh SW, Mukhopadhyay A, Dixit BL, Raha T, Green MR, Tissenbaum HA. 2006. Identification of direct DAF-16 targets controlling longevity, metabolism and diapause by chromatin immunoprecipitation. *Nat Genet* **38:** 251–257.

Parker R, Sheth U. 2007. P bodies and the control of mRNA translation and degradation. *Mol Cell* **25:** 635–646.

Perea-Resa C, Hernández-Verdeja T, López-Cobollo R, del Mar Castellano M, Salinas J. 2012. LSM proteins provide accurate splicing and decay of selected transcripts to ensure normal *Arabidopsis* development. *Plant Cell* **24:** 4930–4947.

Pillai RS, Grimmler M, Meister G, Will CL, Lührmann R, Fischer U, Schümperli D. 2003. Unique Sm core structure of U7 snRNPs: assembly by a specialized SMN complex and the role of a new component, Lsm11, in histone RNA processing. *Genes Dev* **17:** 2321–2333.

Pinkston-Gosse J, Kenyon C. 2007. DAF-16/FOXO targets genes that regulate tumor growth in *Caenorhabditis elegans*. *Nat Genet* **39:** 1403–1409.

Porta-de-la-Riva M, Fontrodona L, Villanueva A, Cerón J. 2012. Basic *Caenorhabditis elegans* methods: synchronization and observation. *J Vis Exp* e4019.

Praitis V, Casey E, Collar D, Austin J. 2001. Creation of low-copy integrated transgenic lines in *Caenorhabditis elegans*. *Genetics* **157:** 1217–1226.

Rousakis A, Vlanti A, Borbolis F, Roumelioti F, Kapetanou M, Syntichaki P. 2014. Diverse functions of mRNA metabolism factors in stress defense and aging of *Caenorhabditis elegans*. *PLoS One* **9:** e103365.

Rual J-F, Ceron J, Koreth J, Hao T, Nicot A-S, Hirozane-Kishikawa T, Vandenhaute J, Orkin SH, Hill DE, van den Heuvel S, et al. 2004. Toward improving *Caenorhabditis elegans* phenome mapping with an ORFeome-based RNAi library. *Genome Res* **14:** 2162–2168.

Salgado-Garrido J, Bragado-Nilsson E, Kandels-Lewis S, Séraphin B. 1999. Sm and Sm-like proteins assemble in two related complexes of deep evolutionary origin. *EMBO J* **18:** 3451–3462.

Sarov M, Murray JI, Schanze K, Pozniakovski A, Niu W, Angermann K, Hasse S, Rupprecht M, Vinis E, Tinney M, et al. 2012. A genome-scale resource for in vivo tag-based protein function exploration in *C. elegans*. *Cell* **150:** 855–866.

Schuster E, McElwee JJ, Tullet JMA, Doonan R, Matthijssens F, Reece-Hoyes JS, Hope IA, Vanfleteren JR, Thornton JM, Gems D. 2010. DamID in *C. elegans* reveals longevity-associated targets of DAF-16/FoxO. *Mol Syst Biol* **6:** 399.

Sheth U, Parker R. 2006. Targeting of aberrant mRNAs to cytoplasmic processing bodies. *Cell* **125:** 1095–1109.

Simonetta SH, Golombek DA. 2007. An automated tracking system for *Caenorhabditis elegans* locomotor behavior and circadian studies application. *J Neurosci Methods* **161:** 273–280.

Singh V, Aballay A. 2009. Regulation of DAF-16-mediated innate immunity in *Caenorhabditis elegans*. *J Biol Chem* **284:** 35580–35587.

Spiller MP, Reijns MAM, Beggs JD. 2007. Requirements for nuclear localization of the Lsm2-8p complex and competition between nuclear and cytoplasmic Lsm complexes. *J Cell Sci* **120:** 4310–4320.

Squirrell JM, Eggers ZT, Luedke N, Saari B, Grimson A, Lyons GE, Anderson P, White JG. 2006. CAR-1, a protein that localizes with the mRNA decapping component DCAP-1, is required for cytokinesis and ER organization in *Caenorhabditis elegans* embryos. *Mol Biol Cell* **17:** 336–344.

Stiernagle T. 2006. Maintenance of *C. elegans*. In *WormBook* (ed. The *C. elegans* Research Community). http://www.wormbook.org.

Streicher KL, Yang ZQ, Draghici S, Ethier SP. 2007. Transforming function of the LSM1 oncogene in human breast cancers with the 8p11-12 amplicon. *Oncogene* **26:** 2104–2114.

Sun Y, Yang P, Zhang Y, Bao X, Li J, Hou W, Yao X, Han J, Zhang H. 2011. A genome-wide RNAi screen identifies genes regulating the formation of P bodies in *C. elegans* and their functions in NMD and RNAi. *Protein Cell* **2:** 918–939.

Tharun S. 2009. Roles of eukaryotic Lsm proteins in the regulation of mRNA function. *Int Rev Cell Mol Biol* **272:** 149–189.

Tharun S, He W, Mayes AE, Lennertz P, Beggs JD, Parker R. 2000. Yeast Sm-like proteins function in mRNA decapping and decay. *Nature* **404:** 515–518.

Tomasevic N, Peculis BA. 2002. Xenopus LSm proteins bind U8 snoRNA via an internal evolutionarily conserved octamer sequence. *Mol Cell Biol* **22:** 4101–4112.

Trapnell C, Pachter L, Salzberg SL. 2009. TopHat: discovering splice junctions with RNA-Seq. *Bioinformatics* **25:** 1105–1111.

Trapnell C, Williams BA, Pertea G, Mortazavi A, Kwan G, van Baren MJ, Salzberg SL, Wold BJ, Pachter L. 2010. Transcript assembly and quantification by RNA-Seq reveals unannotated transcripts and isoform switching during cell differentiation. *Nat Biotechnol* **28:** 511–515.

Trapnell C, Hendrickson DG, Sauvageau M, Goff L, Rinn JL, Pachter L. 2013. Differential analysis of gene regulation at transcript resolution with RNA-seq. *Nat Biotechnol* **31:** 46–53.

Tritschler F, Eulalio A, Truffault V, Hartmann MD, Helms S, Schmidt S, Coles M, Izaurralde E, Weichenrieder O. 2007. A divergent Sm fold in EDC3 proteins mediates DCP1 binding and P-body targeting. *Mol Cell Biol* **27:** 8600–8611.

Troemel ER, Chu SW, Reinke V, Lee SS, Ausubel FM, Kim DH. 2006. p38 MAPK regulates expression of immune response genes and contributes to longevity in *C. elegans* ed. S. Kim. *PLoS Genet* **2:** e183.

Veretnik S, Wills C, Youkharibache P, Valas RE, Bourne PE. 2009. Sm/Lsm genes provide a glimpse into the early evolution of the spliceosome. *PLoS Comput Biol* **5:** e1000315.

Watson PM, Miller SW, Fraig M, Cole DJ, Watson DK, Boylan AM. 2008. CaSm (LSm-1) overexpression in lung cancer and mesothelioma is required for transformed phenotypes. *Am J Respir Cell Mol Biol* **38:** 671–678.

Weichenrieder O. 2014. RNA binding by Hfq and ring-forming (L)Sm proteins: a trade-off between optimal sequence readout and RNA backbone conformation. *RNA Biol* **11:** 537–549.

Wilusz CJ, Wilusz J. 2013. Lsm proteins and Hfq: life at the 3′ end. *RNA Biol* **10:** 592–601.

Yen K, Narasimhan SD, Tissenbaum HA. 2011. DAF-16/Forkhead box O transcription factor: many paths to a single Fork(head) in the road. *Antioxid Redox Signal* **14:** 623–634.

Zhang X, Zabinsky R, Teng Y, Cui M, Han M. 2011. microRNAs play critical roles in the survival and recovery of *Caenorhabditis elegans* from starvation-induced L1 diapause. *Proc Natl Acad Sci* **108:** 17997–18002.

RNA
A PUBLICATION OF THE RNA SOCIETY

Cytoplasmic LSM-1 protein regulates stress responses through the insulin/IGF-1 signaling pathway in *Caenorhabditis elegans*

Eric Cornes, Montserrat Porta-De-La-Riva, David Aristizábal-Corrales, et al.

RNA 2015 21: 1544-1553

Published OnlineFirst August 15, 2012; DOI: 10.1158/1078-0432.CCR-12-1513

Clinical Cancer Research

Cancer Therapy: Preclinical

Lurbinectedin (PM01183), a New DNA Minor Groove Binder, Inhibits Growth of Orthotopic Primary Graft of Cisplatin-Resistant Epithelial Ovarian Cancer

August Vidal[3], Clara Muñoz[1], María-José Guillén[6], Jemina Moretó[2], Sara Puertas[1], María Martínez-Iniesta[1], Agnés Figueras[1], Laura Padullés[1], Francisco J. García-Rodriguez[1], Mireia Berdiel-Acer[1], Miguel A. Pujana[1], Ramón Salazar[4], Marta Gil-Martin[4], Lola Martí[5], Jordi Ponce[5], David G. Molleví[1], Gabriel Capella[1], Enric Condom[3], Francesc Viñals[1], Dori Huertas[2], Carmen Cuevas[6], Manel Esteller[2], Pablo Avilés[6], and Alberto Villanueva[1]

Abstract

Purpose: Epithelial ovarian cancer (EOC) is the fifth leading cause of death in women diagnosed with gynecologic malignancies. The low survival rate is because of its advanced-stage diagnosis and either intrinsic or acquired resistance to standard platinum-based chemotherapy. So, the development of effective innovative therapeutic strategies to overcome cisplatin resistance remains a high priority.

Experimental Design: To investigate new treatments in *in vivo* models reproducing EOCs tumor growth, we generated a preclinical model of ovarian cancer after orthotopic implantation of a primary serous tumor in nude mice. Further, matched model of acquired cisplatin-resistant tumor version was successfully derived in mice. Effectiveness of lurbinectedin (PM01183) treatment, a novel marine-derived DNA minor groove covalent binder, was assessed in both preclinical models as a single and a combined-cisplatin agent.

Results: Orthotopically perpetuated tumor grafts mimic the histopathological characteristics of primary patients' tumors and they also recapitulate in mice characteristic features of tumor response to cisplatin treatments. We showed that single lurbinectedin or cisplatin-combined therapies were effective in treating *cisplatin-sensitive* and *cisplatin-resistant* preclinical ovarian tumor models. Furthermore, the strongest *in vivo* synergistic effect was observed for combined treatments, especially in cisplatin-resistant tumors. Lurbinectedin tumor growth inhibition was associated with reduced proliferation, increased rate of aberrant mitosis, and subsequent induced apoptosis.

Conclusions: Taken together, preclinical orthotopic ovarian tumor grafts are useful tools for drug development, providing hard evidence that lurbinectedin might be a useful therapy in the treatment of EOC by overcoming cisplatin resistance. *Clin Cancer Res; 18(19); 5399–411. ©2012 AACR.*

Authors' Affiliations: [1]Translational Research Laboratory, Catalan Institute of Oncology - Bellvitge Biomedical Research Institute (IDIBELL); [2]Cancer Epigenetics and Biology Program (PEBC); [3]Department of Pathology, Hospital Universitari de Bellvitge; [4]Department of Medical Oncology, Catalan Institute of Oncology; [5]Department of Gynecology, Hospital Universitari de Bellvitge, Barcelona; and [6]Department of Research and Development (R&D), PharmaMar S.A, Madrid, Spain

Note: Supplementary data for this article are available at Clinical Cancer Research Online (http://clincancerres.aacrjournals.org/).

August Vidal and Clara Muñoz contributed equally to this work.

Corresponding Authors: Alberto Villanueva, Laboratory of Translational Research, Catalan Institute of Oncology - Bellvitge Biomedical Research Institute (IDIBELL), Hospital Duran i Reynals, Avda Gran Via s/n km 2.7, L'Hospitalet de Llobregat, 08907 Barcelona, Spain. Phone: 34-93-260-7952; Fax: 34-93-260-7466; E-mail: avillanueva@iconcologia.net; and Pablo Aviles, Department of Research and Development (R&D), PharmaMar S.A, Avda de los Reyes 1, Polígono Industrial La Mina, Colmenar Viejo, 28770 Madrid, Spain. Phone: 34-91-823 4514. E-mail: paviles@pharmamar.com.

doi: 10.1158/1078-0432.CCR-12-1513

Introduction

Ovarian cancer is the fifth leading cause of death among women, and is the most common cause arising from gynecologic malignancies (1). Although progress has been made in the treatment of epithelial ovarian cancer (EOC) by improved surgical debulking and the introduction of platinum-taxane regimens, overall 5-year survival rate is only 29% in advanced-stage disease (2–6). This low survival rate is because of its frequent diagnosis at an advanced stage and by intrinsic and acquired resistance to platinum-based chemotherapy. In the recurrent disease setting, those patients who experience progression through first-line, platinum-based therapy (*platinum refractory*), or those who experience relapse within 6 months of receiving platinum therapy (*platinum resistant*) are typically treated with a second-line non–platinum-based regimen, such as single-agent doxorubicin (7) gemcitabine (8), paclitaxel,

Published OnlineFirst August 15, 2012; DOI: 10.1158/1078-0432.CCR-12-1513

Translational Relevance

The efficacy of conventional platinum-based chemotherapy for EOCs is limited; most patients show an initial response to treatment but upon relapse, the platinum response rates progressively diminish and they ultimately die. So, the development of effective innovative therapeutic strategies to overcome cisplatin resistance remains a high priority. On the way to identifying novel therapeutic targets and for drug testing, we have developed two paired (*cisplatin-sensitive* and *cisplatin-resistant*) preclinical models of serous carcinoma phenocopying patients' primary tumor features including chemotherapy response behavior. In this study, we show that single lurbinectedin (PM01183), a novel marine-derived DNA minor groove covalent binder, or cisplatin-combined therapies were effective in treating *cisplatin-sensitive* and *cisplatin-resistant* preclinical models. Thus, we present hard evidences that lurbinectedin might be a useful therapy in epithelial ovarian cancer overcoming acquired cisplatin resistance providing a rationale for future trials.

topotecan (9), vinorelbine (10), or trabectedin plus pegylated liposomal doxorubicin (11). Agents yielding responses in the range of 15% to 20% that last a median of approximately 4 months, emphasize the great need for novel effective therapeutic strategies for its management (12–15).

DNA structure features 2 well-defined clefts known as the major and minor grooves, and DNA-binding proteins and drugs usually make contacts with the sides of the bases exposed in both grooves (16, 17). The DNA major groove is a site of attack for cisplatin and many alkylating agents, and when cisplatin binds to DNA 3 types of lesions can be formed on purine bases: monoadducts, and intra- and interstrand crosslinks. On the other hand, other antitumor drugs including mitomycin C, chromomycin A_3, and ecteinascidins, bind to the minor groove (18). One of the best examples is trabectedin (Yondelis), which reacts with certain guanines in the minor groove of DNA to form a covalent bond (19–21). The adduct is stabilized by van der Waals interactions with nucleotides in the opposite DNA strand, creating the equivalent of a functional interstrand crosslink (22). Lurbinectedin (PM01183) is a new synthetic alkaloid that is structurally related to ecteinascidins (23), which, with the exception of a module addition (ring C), confer important pharmacokinetic and pharmacodynamics properties benefits as well intrinsic activity (24–26).

Establishment of preclinical models phenocopying patients' primary tumor features, which accurately reflect phenotypic, genotypic, and tumor chemotherapy response behavior, is a basic step on the way to identifying novel therapeutic targets and for testing novel treatments (27, 28). Several lines of evidence indicate that engrafting primary tumor tissues orthotopically into immune-deficient mice (termed "tumor grafts") may be outstandingly valuable preclinical models for new drug development, and for reducing the high failure rate that exists in translating preclinical results to patients (29–33).

Here, we report the establishment and characterization of a serially transplantable, orthotopic, subject-derived epithelial ovarian tumor graft that retains crucial characteristics of the original primary tumor specimen, and its further development as an *in vivo* cisplatin-resistance tumor model. We show in engrafted preclinical models that lurbinectedin, a new minor groove DNA binder, is effective in the treatment of experimental ovarian tumors as a single or a combined-cisplatin agent. Overall, we present evidence of the efficacy of a therapeutic strategy based on the idea that a combination of 2 drugs that bind differentially to each DNA groove could overcome frequent cisplatin resistance in advanced-stage ovarian cancer.

Materials and Methods

Drugs and cell lines

Lyophilized lurbinectedin (PM01183) vials (1 mg/mL) were obtained from PharmaMar (Colmenar Viejo) and cisplatin (1 mg/mL) from Ferrer-Farma. The A2780 human ovarian carcinoma cell line was obtained from the European Collection of Cell Cultures. Cell cultures were grown *in vitro* at 37°C in a humidified atmosphere of 5% CO_2 in RPMI-1640 (Sigma-Aldrich Co.) supplemented with 10% FBS.

Animals

Female athymic *nu/nu* mice (Harlan) between 4 to 6 weeks of age were housed in individually ventilated cages on a 12-hour light-dark cycle at 21 to 23°C and 40% to 60% humidity. Mice were allowed free access to an irradiated diet and sterilized water. All animal protocols were reviewed and approved according to regional Institutional Animal Care and Use Committees.

Primary sample and orthotopic tumor engrafted in mice

The primary tumor specimen was obtained at Hospital Universitari de Bellvitge (L'Hospitalet de Llobregat, Barcelona, Spain). The study was approved by the Institutional Review Board. Written informed consent was collected from a patient who had not received cisplatin-based chemotherapy. Nonnecrotic tissue pieces (*ca.* 2–3 mm^3) from resected serous human epithelial ovarian tumor were selected and placed in DMEM (BioWhittaker) supplemented with 10% FBS and penicillin/streptomycin at room temperature. Under isofluorane-induced anesthesia, animals were subjected to a lateral laparotomy, their ovaries exposed and tumor pieces anchored to the ovary surface with prolene 7.0 sutures. Tumor growth was monitored 2 to 3 times per week and when the tumor grew, it was harvested, cut into small fragments, and transplanted into 2 to 5 new animals. Engrafted tumors at early mouse passages were cut in 6 to 8 mm^3 pieces and stored in liquid nitrogen in a solution of

Published OnlineFirst August 15, 2012; DOI: 10.1158/1078-0432.CCR-12-1513

90% FBS and 10% dimethyl sulfoxide for subsequent implantation.

Histology and immunohistochemical tumor characterization

The morphology of the primary patient's tumor and of the both engrafted tumors (OVA1X and OVA1XR) was compared by H&E staining in paraffin-embedded sections. Determination of cytokeratin (CK) 7, Ki67, WT1, alpha estrogen, and progesterone receptors status by immunohistochemistry, in accordance with the standard clinical protocols of the Department of Pathology (see Fig. 1 legend).

In vivo establishment of cisplatin-resistant xenografted tumor

Cisplatin-resistant tumor (named OVA1XR) was developed by iterative cycles of *in vivo* exposure to cisplatin of OVA1X. Briefly, orthotopically engrafted OVA1X tumors (at mouse passage #3) were allowed to grow until intra-abdominal palpable masses were noted. Then, animals were intravenously (i.v.) administered with cisplatin at a dose of 2 mg/kg for 3 consecutive weeks (Days 0, 7 and 14; cycle#1 of treatment). Post-cisplatin tumor relapse were harvested, prepared as previously described, and engrafted in new animals. This process was repeated up to five times by treating tumor-bearing mice with stepwise increasing doses of cisplatin: cycle#2, 3 mg/kg; cycle#3, 3.5 mg/kg; cycle#4, 4 mg/kg; and cycle#5, 5 mg/kg (see Fig. 1C). Cisplatin-resistant tumors were obtained in three independent experiments (OVA1XR-L1, -L2 and -L3). At doses higher than 3.5 mg/kg, signs of cisplatin-induced toxicity were ameliorated by 2 days administration of saline containing 5% glucose.

Drug treatment of engrafted cisplatin-sensitive and cisplatin-resistant tumor models

Mice were transplanted with fragments of OVAX1 and OVAX1R tumors, and when tumors reached a homogeneous palpable size were randomly allocated into the treatment groups (n = 8–12/group): i) Placebo; ii) Lurbinectedin (0.18 mg/kg); iii) Cisplatin (3.5 mg/kg); and iv) Lurbinectedin plus cisplatin (0.18 + 3.5 mg/kg). Drugs were i.v. administered once per week for 3 consecutive weeks (days 0, 7, and 14). Seven days after the final dose (day 21), animals were sacrificed, their ovaries dissected out, and weighed. Representative fragments were either frozen in nitrogen or fixed and then processed for paraffin embedding.

Evaluation of histologic response after chemotherapeutic treatment

Regressive histopathological features were evaluated (34–37), and 3 histologic response categories were established (38): (i) *NHR*, no histopathological response ($\leq$1 regression criterion [3+] present); (ii) *MHR*, moderate (2 regression criteria [3+] present); and (iii) *GHR*, good histopathological response ($\geq$3 regression criteria [3+] present).

In vivo evaluation of synergism among lurbinectedin and cisplatin treatments

Female mice were subcutaneously implanted with 10^7 A2780 cells suspended in a 1:1 solution of RPMI-1640: Matrigel (Becton, Dickinson & Co.). Mice bearing tumors (*ca.* 150 mm^3) were randomly allocated to 13 treatment groups (see Fig. 3 legend). All treatments were intravenously administered once per week for 2 consecutive weeks (days 0 and 7). Tumor growth was recorded 2 to 3 times per week starting from the first day of treatment (day 0) and tumor volume (in mm^3), estimated according to the formula $V = (a \cdot b^2)/2$, (a: length or biggest diameter; b: width or smallest diameter). Antitumor drug activity was measured with respect to the T/C index, and the fraction affected (F_a) by treatment was calculated ($F_a = 1 - T/C$). A CI was determined by the CI-isobol method (39).

Determination of tumor proliferation, apoptosis, and angiogenesis

Proliferation was assessed by quantifying the anti-phospo-Histone H3 (S10; Millipore) mitosis marker as described (40). Aberrant mitotic figures were identified by double immunostaining with α-tubulin (1:200) and anti-phospo-Histone H3 (S10; ref. 40). Apoptotic cells were quantified with two approaches: (i) immunostaining in paraffin-embedded samples with anti-Cleaved Caspase-3 (Asp175) antibody (Cell Signaling) at 1:200; and (ii) by terminal deoxynucleotidyl transferase-mediated biotin-dUTP nick end labeling (TUNEL) staining kit (Promega) in frozen OCT tissues (41).

Statistical analysis

Postchemotherapy tumor weight data were analyzed using a 2-tailed Mann–Whitney *U* test. The data are presented as medians and interquartile ranges (IQR) or means ± SD. Statistical analyses were done and graphs plotted using GraphPad Prism, version 5.02 (GraphPad Software Inc.). Synergism analyses were done by CompuSyn, version 1.0 (ComboSyn Inc.).

Results

Orthotopic model of epithelial ovarian cancer mimics the histopathological characteristics of primary patients' tumors

Primary tumors engrafted in the ovarian surface of athymic female mice (named OVA1X) grew as large solid masses. Ovarian infiltration and neighboring organ invasion were not seen in any of the implanted animals (Fig. 1A). The engrafted rate was close to 95% in all mouse-to-mouse passages, with a mean time of *ca.* 1,000 to 1,500 mm^3 during the first 6 passages of 84 ± 8 days. As shown in Fig. 1A, a very high histologic correlation was found between primary and engrafted tumors. Indeed, OVA1X had a typical serous adenocarcinoma appearance showing high cellularity, cellular papillae formation, and irregular slit-like spaces, and it remained stable throughout multiple rounds of serial mouse-to-mouse transplantation.

Published OnlineFirst August 15, 2012; DOI: 10.1158/1078-0432.CCR-12-1513

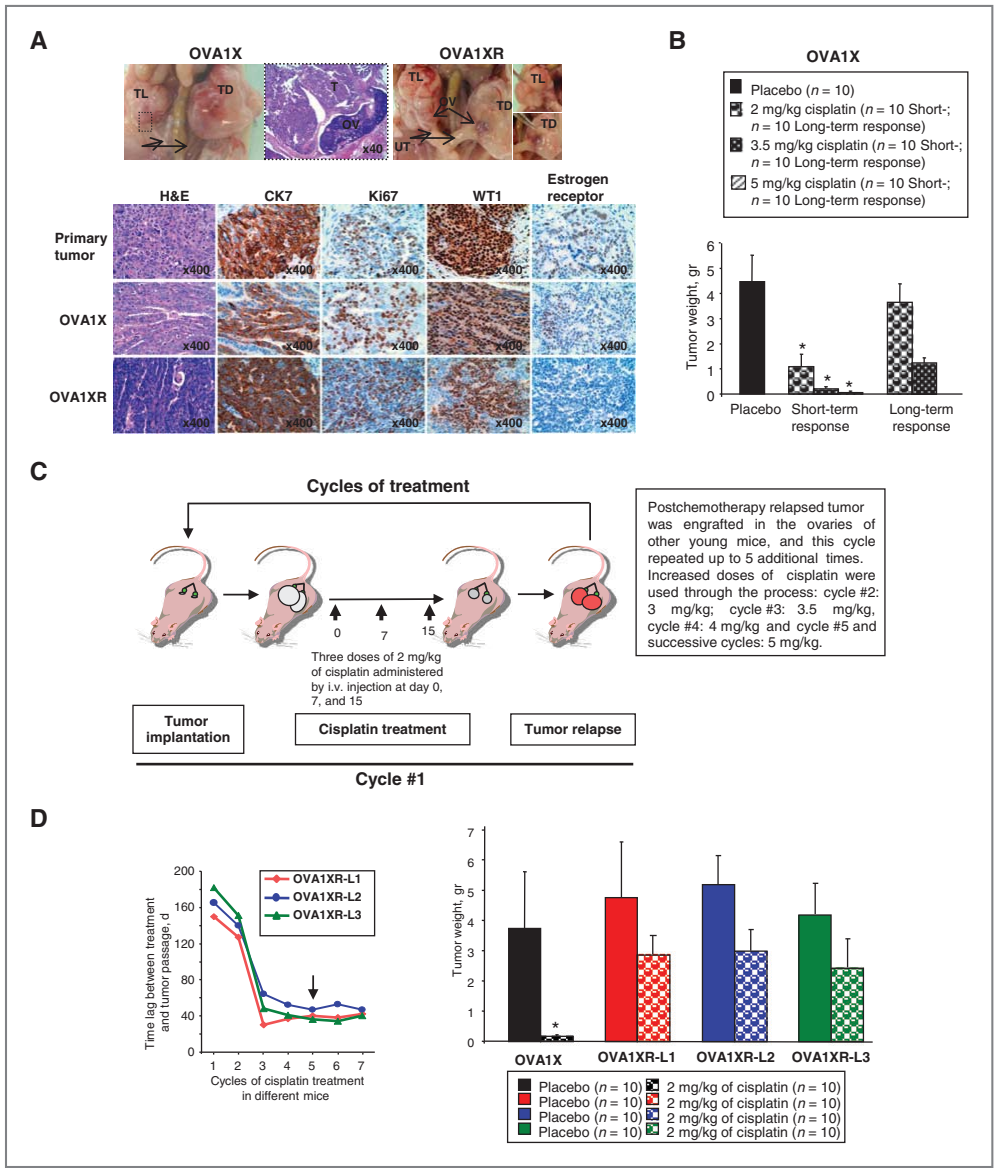

Figure 1. Establishment, and comparative histopathological characterization of primary and engrafted OVA1X and its paired developed cisplatin-resistant OVA1XR tumor. A, top, lateral laparatomy was conducted in isofluorane-anesthetized mice, the ovary mobilized and small tumor pieces of primary tumor anchored on the ovarian mouse surface with prolene 7.0 sutures. Engrafted tumors grew as large solid masses (usually 1,000–1,500 mm^3) in diameter at the time of sacrifice, and ovarian infiltration/invasion or ascitis were not seen. Bottom, representative H&E and immunohistochemical staining reveals a high correlation between primary and paired engrafted tumors. Primary antibodies were monoclonal antibodies: CK7 (clone OV-TL 12/30, Dako); Ki67 (clone MIB-1, Dako); WT1 (clone 6F-H2, Dako) and estrogen receptor alpha (clone SP1, Dako) OV, ovary; TL, tumor engrafted in the left ovarian; TD, engrafted in the right ovarian; UT, uterus. B, mice engrafted with OVA1X tumor were treated intravenously with low (2 mg/kg), intermediate (3.5 mg/kg), and high (5 mg/kg) cisplatin doses, and either short- or long-term responses were

Published OnlineFirst August 15, 2012; DOI: 10.1158/1078-0432.CCR-12-1513

Ki-67 immunostaining revealed a similar proliferative rate in primary and engrafted tumors, and they both preserved the same cytokeratin 7 (CK7) and Wilm's tumor susceptibility gene 1 (WT1) immunostaining pattern. Engrafted OVA1X tumor also retained their levels of positive immunostaining for estrogen receptor through mouse-to-mouse passages. Ascitis or synchronic peritoneal implants arising through tumor perpetuation were rarely identified in mice (data not shown).

Cisplatin treatment of engrafted tumor recapitulates characteristic features of primary tumor response in mice

OVA1X-implanted mice were treated with low (2 mg/kg), intermediate (3.5 mg/kg), and high (5 mg/kg) doses of cisplatin, and short- and long-term responses were evaluated (Fig. 1B). Low or intermediate doses of cisplatin were associated with a good short-term response, characterized by significant tumor weight reduction relative to the control group, whereas there was a complete response at high doses. Long-term response was investigated in a subgroup of mice ($n = 4$–6 mice/treatment/dose) that were kept alive for a postchemotherapy follow-up of 6 to 12 months. Tumors relapsed in 5 of 10 (50%) mice treated with 2 mg/kg and in 3 of 10 (30%) treated with 3.5 mg/kg at 6 months, whereas all animals treated with 5 mg/kg were disease-free after a 12-month follow-up. Postchemotherapy, histologic and immunohistochemical analysis of relapsed masses exhibited a viable serous adenocarcinoma that preserved the morphology and the main immunophenotypical characteristics of untreated engrafted tumors.

***In vivo* development of a cisplatin-resistant engrafted tumor model that recapitulates cisplatin primary tumor behavior response is a feasible model for pharmacologic drug evaluations**

The general approach use to obtain the cisplatin-resistant engrafted tumor model is illustrated in Fig. 1C. OVA1X-implanted mice were initially treated with low doses (2 mg/kg) of cisplatin. When tumors relapsed, they were harvested and implanted in new animals (mouse-to-mouse passage). The process was repeated up to 5 times by treating tumor-bearing mice with stepwise increasing doses of cisplatin (Fig. 1C). A progressively shortened time lag between treatment and tumor relapse was noted for the 3 independent tumor lines (named OVA1XR-L1, -L2, and -L3) generated after iterative cycles of treatment. Indeed, a shortened time lag was mainly noted after the third or fourth cycle, and became stabilized (41 ± 6.1 days) subsequently for successive cycles of cisplatin treatment (Fig. 1D, left). Next, we evaluated the levels of cisplatin tumor resistance by comparative assays of OVA1X and each of the 3 independent lines of resistant tumors and homogeneous resistance was reproduced with each individual OVA1XR tumors (Fig. 1D, right). Thus, we selected OVA1XR-L2 for all further experiments, hereafter referred to as OVA1XR. Figure 1A shows that OVA1X and OVA1XR both recapitulated the histologic and immunohistochemical patterns found in the original patient-derived tumor. Interestingly, a consistent loss of estrogen expression was observed among resistant OVA1XR tumor respect to primary and OVA1X.

Lurbinectedin is effective in the treatment of cisplatin-sensitive and cisplatin-resistant ovarian tumor models

OVA1X and OVA1XR were orthotopically implanted in mice and when homogeneous tumor sizes (300–500 mm^3) were identified at palpation (on days 60 and 64 for OVA1X and OVA1XR, respectively) animals bearing tumors were randomized to the following groups ($n = 8$–12 mice/group): (i) placebo; (ii) cisplatin (3.5 mg/kg); (iii) lurbinectedin (0.180 mg/kg); and (iv) lurbinectedin + cisplatin (0.180 + 3.5 mg/kg). On day 21, cisplatin-sensitive tumor OVA1X experienced reductions of 95.3%, 88.3%, and 87.2% following the treatment with cisplatin, lurbinectedin, and lurbinectedin + cisplatin, respectively (Fig. 2A, left). Although, as single agents both cisplatin and lurbinectedin had a significant response with respect to the placebo-treated animals, nonsignificant differences were observed between both individual treatments. Likewise, combined lurbinectedin + cisplatin treatment had no additional significant benefit with respect to each individual treatment (lurbinectedin + cisplatin vs. cisplatin, $P = 0.15$; lurbinectedin + cisplatin vs. lurbinectedin, $P = 0.85$).

Figure 2B summarizes the results obtained for treatments of cisplatin-resistant tumor (OVA1XR), showing important differences between both tumors for lurbinectedin-based treatments. Thus, 48.2%, 93.6%, and 96.7% reductions in tumor weight were recorded following cisplatin, lurbinectedin, or lurbinectedin + cisplatin treatments, respectively. Lurbinectedin, as a single therapy was a significantly better response than with cisplatin ($P = 0.003$). Notably, the combined lurbinectedin + cisplatin treatment proved to be more active than either drug separately, suggesting a synergistic drug effect (lurbinectedin + cisplatin vs. lurbinectedin, $P = 0.022$; or vs. cisplatin, $P = 0.002$).

Histopathological changes were assessed for the different treatments within the tumor as surrounding stromal tissue in both cisplatin-sensitive (Fig. 2A, right, and Supplementary Table S1) and cisplatin-resistant tumors (Fig. 2B, right, and Table 1). Thus, enlargement of tumor cells, presence of

analyzed for each treatment. For short-term response studies, all dose-response mice were sacrificed on day 21 after treatment, whereas for long-term studies they were sacrificed after 6 months. C, experimental approach used for cisplatin-resistant tumor generation combines: (i) iterative cycles of cisplatin treatment (3 doses of cisplatin administered by i.v. injection on days 0, 7, and 15); and (ii) successive increase of administered doses through the process. D, left, illustrates a short time lag between successive cycles of treatment for 3 independent OVA1XR-L1, -L2, and -L3 tumor lines. For each line, tumors at cycle #5 of cisplatin treatment (arrow), were selected for further cisplatin assays. Right, shows comparative short-time cisplatin response between untreated OVA1X tumor versus each independent cisplatin-resistant OVA1XR-L1, -L2, and -L3 tumors. All mice were treated with 2 mg/kg of cisplatin administered by i.v. injection on days 0, 7, and 15 and sacrificed on day 21. *, $P < 0.05$.

Published OnlineFirst August 15, 2012; DOI: 10.1158/1078-0432.CCR-12-1513

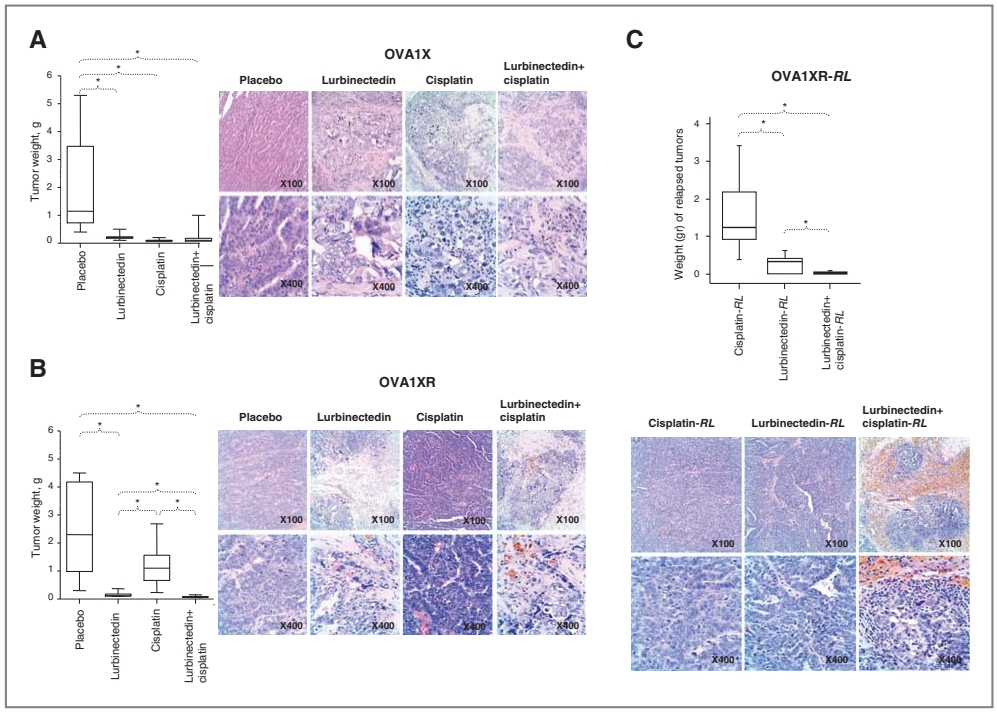

Figure 2. Response of engrafted OVA1X and OVA1XR tumors after lurbinectedin-based chemotherapy treatments. Animals were treated with placebo, cisplatin (3.5 mg/kg), or lurbinectedin (0.180 mg/kg) administered following the same schedule in three doses by i.v. tail vein injection on Days 0, 7, and 15 and sacrificed on day 21 ($n = 8$ placebo; $n = 10$ cisplatin; $n = 12$ lurbinectedin; and $n = 12$ combined lurbinectedin + cisplatin treatments). The doses of the combination (0.180 mg/kg + 3.5 mg/kg; lurbinectedin plus cisplatin) were selected on the basis of the optimal treatment tolerability in mice bearing tumors (data not shown). A and B, graphs illustrate responses of cisplatin-sensitive OVA1X and cisplatin-resistant OV1XR tumors on day 21 of treatment. Histopathological characterization of residual tumor masses postchemotherapy of cisplatin-sensitive OVA1X and cisplatin-resistant OVA1XR tumors, respectively. Sections were stained with H&E and an extensive study of tumor regression characteristics done, as an indicator of chemotherapeutic response (see Supplementary Table S1 and Table 1). C, characterization of the long-term response of cisplatin-resistant OVA1XR tumor. A subgroup of mice ($n = 5$) for each treatment was kept alive postchemotherapy, and was simultaneously sacrificed upon tumor relapse of the cisplatin-treated group. The graph illustrates differences in the weight of relapsed tumor masses for the different treatments. Histopathological characterization of relapsed tumor masses (*-RL*) from mice treated with cisplatin, lurbinectedin, and lurbinectedin + cisplatin. Sections were stained with H&E and an extensive study of tumor regression characteristics done, as an indicator of chemotherapeutic response (see Supplementary Table S1 and Table 1). Cisplatin-*RL*, lurbinectedin-*RL*, lurbinectedin + cisplatin-*RL*, tumor relapsed after cisplatin, lurbinectedin, or combined treatments, respectively. *, $P < 0.05$.

multinucleated giant cells, lymphocytic and histiocytic infiltrates with the presence of hemosiderin and fibrosis, and the scarring of tumoral stroma were observed associated with treatments. Interestingly, cisplatin treatment did not induce morphologic changes in the cisplatin-resistant OVA1XR tumors (Fig. 2B).

To investigate the long-term response a subgroup of treated mice ($n = 4$–6 mice/group) were kept alive postchemotherapy. Thus, OVA1XR tumor relapse took place more than a period of 42 days in all cisplatin-treated mice, whereas in cisplatin-sensitive OVA1X regrowth was found in only 1 cisplatin-treated mouse after eight months follow-up. At sacrifice of OVA1XR, significant differences were found in the weight and histology of relapsed masses (*-RL*) for lurbinectedin-based treatments compared with the cisplatin-*RL* group (lurbinectedin-*RL* vs. cisplatin-*RL*, $P = 0.0020$; or lurbinectedin + cisplatin-*RL* vs. cisplatin-*RL*, $P = 0.0008$; Fig. 2C, top). Furthermore, combined lurbinectedin + cisplatin treatment was more active than lurbinectedin monotherapy ($P = 0.046$), suggesting a long-term synergistic antitumor response for combined therapy. This finding is reinforced by the histology of lurbinectedin + cisplatin-*RL* masses (Fig. 2C, bottom). Together, although our results showed the efficacy of lurbinectedin treatment in the treatment of cisplatin-sensitive and cisplatin-resistant orthotopic engrafted tumor models, it is of note that they also suggest a synergistic effect with cisplatin in cisplatin-resistant OVA1XR.

Table 1. Extensive histopathological tumor regression criteria analyses in postchemotherapy engrafted OVA1XR tumor

	Mice	Fibrosis	Necrosis	Inflammation	Foamy macrophages	Calcification	Hemosiderin	Foreign-body giant cells	Giant tumor cells	Pattern of tumor infiltration[b]	Chemotherapy response based on histopathological features[e]
Short-term response[a]											
Placebo	1	0	1+	0	0	0	0	0	1+	1+	*NHR*
	2	0	1+	1+	0	0	0	0	1+	1+	*NHR*
	3	1+	1+	0	0	CD[c]	0	0	1+	1+	*NHR*
	4	1+	0	1+	0	0	0	0	1+	1+	*NHR*
	5	1+	1+	0	0	0	0	0	1+	1+	*NHR*
Cisplatin	6	2+	0	0	0	0	0	0	0	1+	*NHR*
	7	2+	0	0	0	0	1+	0	1+	1+	*NHR*
	8	1+	0	0	0	0	1+	0	1+	1+	*NHR*
	9	1+	0	0	0	0	0	0	1+	1+	*NHR*
	10	1+	1+	0	0	0	0	0	1+	1+	*NHR*
Lurbinectedin	11	2+	1+	1+	0	0	2+	0	2+	2+	*NHR*
	12	2+	0	1+	0	CD	2+	0	2+	2+	*NHR*
	13	2+	0	2+	0	0	2+	0	2+	2+	*NHR*
	14	1+	0	1+	0	0	1+	0	1+	1+	*NHR*
	15	2+		1+	0	0	2+	0	2+	1+	*NHR*
Lurbinectedin + cisplatin	16	3+	0	2+	0	0	2+	0	3+	2+	*MHR*
	17	3+	0	1+	0	0	2+	0	3+	3+	*GHR*
	18	3+	0	2+	0	CD	2+	0	3+	3+	*GHR*
	19	1+	0	2+	0	0	1+	0	3+	3+	*MHR*
	20	3+	0	1+	1+	CD	2+	0	3+	3+	*GHR*
Long-term response[a]											
Cisplatin-RL	21	1+	1+	0	0	0	0	0	1+	1+	*NHR*
	22	1+	2+	1+	0	0	0	0	1+	1+	*NHR*
	23	1+	0	0	0	0	0	0	1+	1+	*NHR*
Lurbinectedin-RL	24	1+	0	1+	0	0	1+	0	1+	1+	*NHR*
	25	1+	0	1+	0	0	0	0	1+	1+	*NHR*
	26	3+	0	1+	0	0	2+	0	3+	2+	*MHR*
	27	NV[d]	NV	NV	NV	NV	NV	NV	NV	NV	*GHR*
Lurbinectedin + cisplatin-RL	28	3+	0	2+	0	0	2+	0	3+	3+	*GHR*
	29	3+	0	1+	0	0	0	0	3+	3+	*GHR*
	30	NV	NV	NV	NV	NV	NV	NV	NV	NV	*GHR*
	31	NV	NV	NV	NV	NV	NV	NV	NV	NV	*GHR*

[a]For short-term response studies, animals were sacrificed on day 21 of treatment, whereas for long-term-response studies, mice were sacrificed 42 days after the end of treatment when the tumor had relapsed.

[b]Pattern and extent of tumor infiltration was classified as follows: 1+, macroscopic large confluent tumor mass(es); 2+, multiple small tumor foci; 3+, scattered solitary tumor cells or complete absence of residual tumor. The remaining regression criteria were graded as follows: 0/1+, no or only minimally presence of the regression criterion within the specimen; 2+, focal occurrence of the respective regression criterion; 3+, widespread occurrence of the respective regression criterion.

[c]CD, dystrophic calcification.

[d]NV, not evaluated by complete tumor regression. Characterized by the absence of macro- and microscopic lesions.

[e]Three histopathological response categories were defined based on the number of regression criteria: *NHR*, no histopathological response (≤1 regression criteria [3+] present); *MHR*, moderate (2 regression criteria [3+] present), and *GHR*, good histopathological response (≥3 regression criteria [3+] present).

Published OnlineFirst August 15, 2012; DOI: 10.1158/1078-0432.CCR-12-1513

Histopathological tumor regression criteria are associated with treatment response in cisplatin-sensitive OVA1X and cisplatin-resistant OVA1XR tumors

Cytotoxic therapy leads to morphologic and histopathological changes within tumor tissue as well in the involved stroma. Next, we evaluated histopathological tumor regression, which has been established as the gold standard for the assessment of treatment response in several types of solid tumors (42–45). Supplementary Table S1 and Table 1 show extensive analysis of regression criteria for both OVA1X and OVA1XR, to establish whether they are suitable indicators of treatment response, as described for primary neoadjuvant EOC (38). On the basis of these criteria, a moderate histopathological response was observed in OVA1X for single cisplatin and lurbinectedin treatments, whereas a good response with respect to regression criteria was found for the combined treatment (Supplementary Table S1). Taken together, the tumor response and the histopathological regression criteria were evidence of the relevance of the combined treatment in cisplatin-sensitive OVA1X. In this context, in cisplatin-resistant OVA1XR tumor a good histopathological response was confirmed for the combined lurbinectedin + cisplatin treatment (Table 1). Moreover, the relevance of combined treatments was reinforced by the observation that the histopathological response was maintained in relapsed masses (Table 1).

Lurbinectedin and cisplatin treatments are synergistic *in vivo* in A2780-derived tumor xenografts

The synergism of the combined lurbinectedin + cisplatin treatment was further investigated in mice bearing A2780 xenografted tumors. Figure 3A shows the *T*/*C* values,

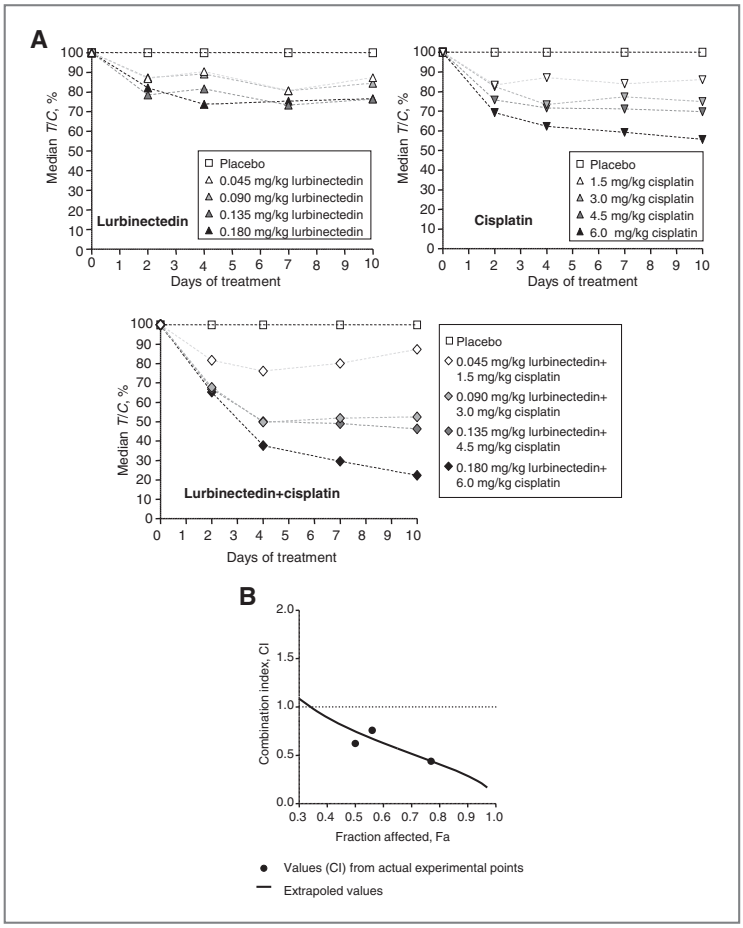

Figure 3. *In vivo* characterization of the synergistic effect among lurbinectedin and cisplatin treatments. Xenografted s.c. tumors were generated in nude mice after injection of 10^7 cells of the A2780 ovarian cancer cell line, and mice bearing tumors (*ca.* 150 mm^3) were randomly allocated to 13 treatment groups ($n = 8$–10/group): (i) placebo; (ii) lurbinectedin at 4 dose levels, namely MTD (0.180 mg/kg), 0.75 MTD (0.135 mg/kg), 0.5 MTD (0.09 mg/kg), and 0.25 MTD (0.045 mg/kg); (iii) cisplatin, at 4 dose levels MTD (6 mg/kg), 0.75 MTD (4.5 mg/kg), 0.5 MTD (3.0 mg/kg), and 0.25 MTD (1.5 mg/kg); and (iv) lurbinectedin plus cisplatin, administered with the combination at (1 + 1), (0.75 + 0.75), (0.50 + 0.50), and (0.25 + 0.25) of MTD ratios. A, graphs show antitumor activity of each single or combined treatment followed by *T*/*C* values, defined as the change in tumor volume for each treated (*T*) and placebo (*C*) group during the placebo-treated survival period. B, determination of tumor fraction affected (F_a) by treatment, calculated according to the formula $F_a = 1 - T/C$ and CI determined by the CI-isobol method using CompuSyn software, version 1.0 (ComboSyn, Inc. Paramus).

Published OnlineFirst August 15, 2012; DOI: 10.1158/1078-0432.CCR-12-1513

Table 2. Dose-response treatment effect of s.c. xenografts of A2780-derived cell line

			Dose-effect parameters[b]		
Treatment	**Dose, mg/kg**	**Fraction affected[a], F_a**	***m* (SD)**	**D_m**	***r***
Lurbinectedin	0.180	0.29			
	0.135	0.26	1.04 (0.16)	2.12	0.978
	0.090	0.22			
	0.045	0.09			
Cisplatin	6.0	0.45			
	4.5	0.31	1.24 (0.12)	1.29	0.990
	3.0	0.23			
	1.5	0.12			
Lurbinectedin + cisplatin	0.180 + 6.0	0.77			
	0.135 + 4.5	0.56	2.34 (0.36)	1.20	0.977
	0.090 + 3.0	0.50			
	0.045 + 1.5	0.10			

[a]Fraction affected ($F_a = 1-T/C$), defined as the change in tumor volume for each treated (*T*) and placebo (*C*) groups during placebo-treated survival period.

[b]Derived from the median-effect plot: [log*F*a/(1-Fa)] versus log(Dose), where *m* is the slope (as mean ± SD), D_m is the intercept of the plot, and *r* is the linear regression coefficient.

defined as the change in tumor volume for each treated (*T*) and placebo (*C*) group during the placebo-treated survival period, for mice treated with lurbinectedin, cisplatin or combined lurbinectedin + cisplatin. Animals treated with high cisplatin doses showed the lowest *T*/*C* of 55.2% on day 10, whereas there was no antitumor effect induced by the lurbinectedin single-agent treatment (minimal *T*/*C*, 70.8% on day 4). The combined lurbinectedin + cisplatin treatment produced lower *T*/*C* values than the more active agent in this experiment (cisplatin at 6.0 mg/kg). The antitumor effect seen on day 4 (*T*/*C*, 39.8%) for the highest dose of the combination (0.180 + 6.0 mg/kg; lurbinectedin + cisplatin) increased on subsequent days (*T*/*C*, 23.4% on day 10). On day 10, lurbinectedin + cisplatin treatment displayed a dose-dependent antitumor effect with median tumor volumes (mm^3) of 572.8, 1,074, 1,233, and 2,199 for animals treated with lurbinectedin + cisplatin at 0.180 + 6.0, 0.135 + 4.5, 0.09 + 3.0, and 0.045 + 1.5 mg/kg levels, respectively. Applying the median-effect principle to the data gave a Combination Index (CI) of 0.17 (at Fa = 0.97), suggesting a synergistic effect of the combination lurbinectedin + cisplatin in ovarian (A2780) xenografted tumors (Fig. 3B and Table 2).

Lurbinectedin-induced tumor response is mediated by antiproliferative and proapoptotic features and causes mitotic catastrophe

Next, we investigated whether tumor response mechanisms were induced by lurbinectedin associated with antiproliferative and proapoptotic features. Two experimental approaches were used: (i) in A2780-derived subcutaneous (s.c.) tumor xenografts treated with cisplatin, lurbinectedin or combined drugs for 24 or 72 hours; and (ii) in cisplatin-sensitive OVA1X and cisplatin-resistant OVA1XR tumors.

We found that 24 hours after treatments of the A2780 xenografts, the anti-phospo-Histone H3 (S10; H3S10ph) mitosis marker significantly decreased in cisplatin ($P = 0.007$), lurbinectedin ($P = 0.002$), or combined ($P < 0.001$) treatments compared with placebo-treated tumors (Fig. 4A). In fact, the decrease was significantly greater for the combined treatment than for each single therapy (lurbinectedin + cisplatin vs. lurbinectedin, $P = 0.005$; or vs. cisplatin, $P = 0.015$). In addition, a proapoptotic effect was associated with lurbinectedin treatments. Thus, a 6.7-fold increase in the number of apoptotic cells (by TUNEL assay) was observed in combined lurbinectedin + cisplatin ($P = 0.013$) treatment compared with the placebo group, and 3.0-fold and 3.7-fold increases with respect to cisplatin and lurbinectedin, respectively (Fig. 4C, left).

Likewise, antiproliferative and proapoptotic effects were confirmed in both engrafted orthotopic models. In OVA1XR (Fig. 4B), all treatments showed a significant decrease in the number of mitoses determined by H3S10ph (cisplatin, $P = 0.007$; lurbinectedin, $P = 0.003$; lurbinectedin + cisplatin, $P < 0.001$). As a single treatment, lurbinectedin was more effective than cisplatin ($P = 0.044$). Combined lurbinectedin + cisplatin treatment significantly diminished the number of mitoses with respect to single lurbinectedin ($P = 0.016$) or cisplatin ($P = 0.003$) treatment (Fig. 4B). This effect was also maintained in relapsed tumor masses (lurbinectedin + cisplatin-*RL* vs. cisplatin-*RL*, $P = 0.005$; or vs. lurbinectedin, $P = 0.012$). Apoptotic drug-induction was assessed in OVA1X and OVA1XR by immunodetection in paraffin-embedded tissues of caspase-3, an early and specific apoptotic marker. In cisplatin-sensitive

Published OnlineFirst August 15, 2012; DOI: 10.1158/1078-0432.CCR-12-1513

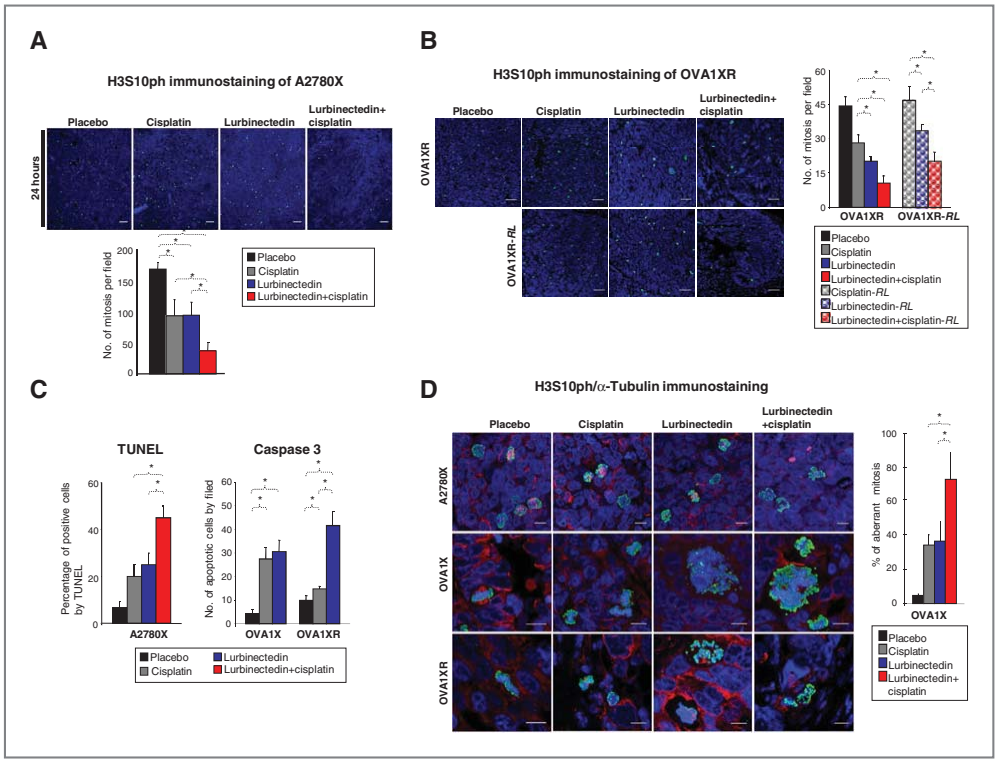

Figure 4. Tumor proliferation was determined after immunostaining mitotic figures with antiphosphorylated histone H3 (S10) antibody (H3S10ph; green staining), and mitotic spindles with anti α-tubulin (red staining). Chromosomes were labeled with 4′, 6-diamidino-2-phenylindole in the blue channel. Treatment doses were: (i) lurbinectedin (0.18 mg/kg); (ii) cisplatin (3.5 mg/kg); and (iii) lurbinectedin plus cisplatin (0.18 + 3.5 mg/kg). A, in A2780-derived s.c. tumors (A2780X) and (B) in residual tumor masses of cisplatin-resistant OVA1XR tumor or in long-term relapsed masses (-RL; 36 days after the sacrifice of the short-term response group). Stained cells were counted in 6 nonoverlapping representative fields. Images were taken with a Leica TCS LP5 spectral confocal microscope (Leica Microsystems) with ×20 and ×63 objectives and 405 Diode, Argon and DPSS 561 lasers, acquiring stacks every 1 mm. Stacks were projected and processed using ImageJ software (MacBiophotonics). Hotspot fields in viable comparable tissues zones at ×400 magnification were captured for each tumor and quantified, also taking the stromal component into consideration. C, apoptosis was evaluated by TUNEL and immunostaining of Caspase 3. Left, TUNEL assay in A2780X s.c. tumors treated with lurbinectedin, cisplatin, or combined lurbinectedin + cisplatin, and mice sacrificed 72-hour posttreatment. Right, cleaved Caspase 3 was analyzed in paraffin sections of residual tumor masses on day 21 of single cisplatin and lurbinectedin treatments of OVA1X and OVA1XR tumors. D, the presence of aberrant mitotic figures was determined by coimmunostaining with anti-H3S10ph and anti-α-tubulin (40) in A2780X s.c. tumors 72-hour posttreatment as in residual masses of OVA1X and OVA1XR tumors on day 21 of treatment. Graphs show the percentage of aberrant mitosis in OVA1X tumor. Scale bar is 10 μm. *, $P < 0.05$.

OVA1X, nonsignificant differences for the proapoptotic-induced effect were observed for the single treatments (cisplatin, 6.3-fold; lurbinectedin, 7.1-fold; $P = 0.45$; Fig. 4C, right). Whereas in cisplatin-resistant OVA1XR tumor the strong proapoptotic effect was noted for lurbinectedin (4.2-fold induction relative to the placebo, $P = 0.014$; and 2.8-fold with respect to cisplatin, $P = 0.007$), cisplatin retaining a moderate capability of inducing apoptosis in OVA1XR tumors (1.5-fold induction relative to placebo, $P = 0.036$; Fig. 4C, right). We did not analyze apoptosis induction in the combined treatment because the extensive histopathological regression prevents the reliable interpretation of the caspase cleaved apoptosis assay (data not shown).

Finally, we investigated whether lurbinectedin treatments affected the morphology of the mitotic spindle by double immunofluorescence staining with α-tubulin (red staining), a protein localized in the spindle, combined with staining with the mitosis marker histone H3S10ph (green staining; Fig. 4D and Supplementary Fig. 1). Thus, in mitotic cells identified by H3S10ph with vehicle-treated tumors, α-tubulin shows that control cells display

Published OnlineFirst August 15, 2012; DOI: 10.1158/1078-0432.CCR-12-1513

normal bipolar mitotic spindles with chromosomes correctly aligned on the metaphase plate. On the other hand, lurbinectedin-treated cells exhibited abnormal mitotic figures, with seriously defective chromosome alignment, and the cells displaying aberrant figures failed to progress through mitosis. The presence of cells displaying aberrant figures was particularly manifested for combined lurbinectedin + cisplatin treatment, in A2780-derived xenografts and both engrafted orthotopic models (Fig. 4D).

Discussion

In this work, we report the generation and characterization of a serous ovarian cancer model based on orthotopic tumor implantation in nude mice, and its further *in vivo* development as a tumor model of cisplatin resistance. Next, as preclinical models, we show that lurbinectedin, a new synthetic alkaloid binder to the DNA minor groove, is effective either in the treatment of *cisplatin-sensitive* and *cisplatin-resistant* ovarian tumors. So, our results show that the combination of 2 compounds that differentially bind the DNA major and minor grooves should be a useful treatment strategy for EOC patients, and suggest its importance for overcoming cisplatin resistance.

Recent data suggest an overall success rate of 10% for oncology products in clinical development, being one of the reasons attributed to this failure the fact that preclinical models used frequently do not predict clinical results (31). Currently, preclinical *in vivo* drug development is mainly realized in s.c. tumor xenografts generated after cell line injection, or in some cases after s.c. engraftment of primary tumor (29, 32, 33), and pure primary orthotopic tumor-based models have rarely been used. Few such tumor models are available: because surgery is often complex, small numbers of mice are used per study, and the models are more expensive (28). Here, we show that these orthotopic-based preclinical ovarian tumor models, which reproduce primary tumor properties, are outstanding resources for the development of new drug therapies. They would also be very valuable for exploring new therapeutic applications for drugs that are currently approved for use in humans, as we recently reported in microsatellite instability (MSI) + colorectal tumors with enoxacin (46). Thus, assessed chemotherapy responses in cisplatin-sensitive and cisplatin-resistant tumor models that maintain the morphologic, histologic, and genetic characteristics of patients' tumors, including the behavior of the stromal component and the tissue architecture, may improve preclinical drug translation to patients.

To overcome cisplatin resistance and reduce the side effects, new agents should have different mechanisms of action and should be non–cross-resistant with platinum (47). Structurally, the DNA duplex gives rise to two well-defined clefts known as the major and minor grooves (25). While the DNA major groove represents a site of attack for cisplatin and many alkylating agents, other antitumor drugs such as ecteinascidins, mitomycin C and chromomycin A3 bind to the minor groove (16, 17). Our work with the new synthetic alkaloid lurbirnectedin strongly suggests that strategies based on dual major and minor DNA groove-targeted therapies should be useful for treating cisplatin-resistant/refractory cases of ovarian carcinomas. Further studies in these models will allow a deeper insight into the cooperative mechanism of action among cisplatin and lubirnectedin, and enable their combined properties with other drugs such olaparib, temozolamide, doxorrubicine, etc. to be evaluated. Although, lurbinectedin is structurally similar to trabectedin (Yondelis), their important different pharmacokinetics properties identified may lead to novel and/or increased antitumor activity compared with original trabectedin (25, 26).

Our preclinical findings in cisplatin-sensitive OVA1X tumor indicate that lurbinectedin monotherapy treatment could be an active first-line drug on the basis of its similar cisplatin response rates and the related long-term behavior response. However, from the clinical standpoint, certainly, the most relevant preclinical result was the capability of lurbinectedin, either on its own or in combination with cisplatin, to overcome the cisplatin resistance of OVA1XR tumor. Its relevance was underlined by the better response and by the histopathological regression found in OVA1XR treated with lurbinectedin alone or combined with cisplatin, both in short- and long-term experiments. All together, our results indicate that combined lurbinectedin treatment should overcome cisplatin resistance, it being an effective second-line treatment for platinum responder patients as a first-line agent for refractory tumors.

In agreement with previously described *in vitro* results (25), we showed that the tumor response produced *in vivo* by lurbinectedin was mediated by an antiproliferative and proapoptotic induction and causes mitotic catastrophe. Previous reports showed common PM01183 (lurbinectedin) effectiveness in the nanomolar range in a panel of representative cell lines of different tumor types, and described that PM01183 (lurbinectedin) and cisplatin acted synergistically when tested *in vitro* on platinum-resistant cells lines (26). In this work, we showed that lurbinectedin synergizes *in vivo* with cisplatin treatments, an effect that is mainly observed in cisplatin-resistant OVA1XR tumors. It has been reported that although DNA lesions generated by lurbinectedin are not repaired by nucleotide excision repair (NER), it can interfere with NER, thereby attenuating the repair of specific NER substrates. Thus, lurbinectedin has enhanced activity in cisplatin-resistant cell lines with higher NER activity (26).

Dissemination in EOCs characteristically involves local invasion of pelvic and abdominal organs, and unlike many epithelial cancers, initial dissemination rarely requires the vasculature, although this is often involved in the advanced stages of disease (48). The tumor model presented here, as happens in their original patient, rarely disseminate in mice. Nevertheless, the generation of other orthotopic-based EOCs tumor models reproducing human dissemination patterns should be very useful for investigating drug action in malignant ascitis formation, the characteristic feature of advanced ovarian cancer at diagnosis. In fact, we have

Published OnlineFirst August 15, 2012; DOI: 10.1158/1078-0432.CCR-12-1513

developed other engrafted primary EOCs models that mimic in mice human local and distal dissemination behaviors (A. Vidal and A. Villanueva, personal communication).

After neoadjuvant chemotherapy, the residual tumor size in ovarian specimens was the only histopathological criterion that was significantly associated with treatment and subsequent overall survival. Histopathological responders defined by the absence of residual tumor, scattered solitary tumor cells, or a residual tumor of 5 mm or less had a significantly longer survival (38). The size of the residual tumor remaining after debulking surgery is known to be an important prognostic factor (49). Likewise, we show in both tumor models that the size of the residual masses and the abundance of regressive criteria correlate with response. The strong correlation between our preclinical tumor models and clinical settings in terms of tumor progression and response to chemotherapy, strongly argues in favor of conducting clinical lurbinectedin trials in resistant/refractory EOC.

In conclusion, we have shown that lurbinectedin, a drug targeting the minor DNA groove, is active and *in vivo* synergizes with cisplatin, which targets the major DNA groove, in the treatment of orthotopic cisplatin-sensitive and cisplatin-resistant patient-derived preclinical tumor models. Overall, our results provide solid evidence supporting clinical trials with lurbinectedin alone or in combination with cisplatin in advanced EOCs.

Disclosure of Potential Conflicts of Interest

M.J. Guillén, C. Cuevas, and P. Avilés are employees and shareholders of PharmaMar, SA (Madrid, Spain). No potential conflicts of interest were disclosed by the other authors.

Grant Support

This work was supported in part by grants FIS PI10-0222 A. Villanueva and Centro para el Desarrollo Tecnológico e Industrial (CDTI) IDI-20101640 (A. Villanueva). A. Vidal received a BAE grant (BAE/00073) from the Instituto de Salud Carlos III. D. Huertas is a Ramon y Cajal Researcher; C. Muñoz is an AGAUR Fellow and F.J. García–Rodriguez was supported by FIS. A. Villanueva has received a Research Grant from PharmaMar, SA.

The costs of publication of this article were defrayed in part by the payment of page charges. This article must therefore be hereby marked *advertisement* in accordance with 18 U.S.C. Section 1734 solely to indicate this fact.

Received May 7, 2012; revised July 31, 2012; accepted August 2, 2012; published OnlineFirst August 15, 2012.

References

1. Jemal A, Siegel R, Ward E, Murray T, Xu J, Thun MJ. Cancer statistics, 2007. CA Cancer J Clin 2007;57:43–66.
2. Alberts DS, Liu PY, Hannigan EV, O'Toole R, Williams SD, Young JA, et al. Intraperitoneal cisplatin plus intravenous cyclophosphamide versus intravenous cisplatin plus intravenous cyclophosphamide for stage III ovarian cancer. N Engl J Med 1996;335:1950–5.
3. Armstrong DK, Bundy B, Wenzel L, Huang HQ, Baergen R, Lele S, et al. Intraperitoneal cisplatin and paclitaxel in ovarian cancer. N Engl J Med 2006;354:34–43.
4. Berkenblit A, Cannistra SA. Advances in the management of epithelial ovarian cancer. J Reprod Med 2005;50:426–38.
5. Bhoola S, Hoskins WJ. Diagnosis and management of epithelial ovarian cancer. Obstet Gynecol 2006;107:1399–410.
6. Hoskins WJ, Bundy BN, Thigpen JT, Omura GA. The influence of cytoreductive surgery on recurrence-free interval and survival in small-volume stage III epithelial ovarian cancer: a Gynecologic Oncology Group study. Gynecol Oncol 1992;47:159–66.
7. Muggia FM, Hainsworth JD, Jeffers S, Miller P, Groshen S, Tan M, et al. J. Phase II study of liposomal doxorubicin in refractory ovarian cancer: antitumor activity and toxicity modification by liposomal encapsulation. J Clin Oncol 1997;15:987–93.
8. Lund B, Hansen OP, Theilade K, Hansen M, Neijt JP. Phase II study of gemcitabine (2′,2′-difluorodeoxycytidine) in previously treated ovarian cancer patients. J Natl Cancer Inst 1994;86:1530–3.
9. ten Bokkel Huinink W, Gore M, Carmichael J, Gordon A, Malfetano J, Hudson I, et al. Topotecan versus paclitaxel for the treatment of recurrent epithelial ovarian cancer. J Clin Oncol 1997;15:2183–93.
10. Rothenberg ML, Liu PY, Wilczynski S, Nahhas WA, Winakur GL, Jiang CS, et al. Phase II trial of vinorelbine for relapsed ovarian cancer: a Southwest Oncology Group study. Gynecol Oncol 2004;95:506–12.
11. Poveda A. Introduction. Trabectedin treatment in GYN cancers. Int J Gynecol Cancer 2011;21 Suppl 1:S1–2.
12. Gonzalez-Martin AJ, Calvo E, Bover I, Rubio MJ, Arcusa A, Casado A, et al. Randomized phase II trial of carboplatin versus paclitaxel and carboplatin in platinum-sensitive recurrent advanced ovarian carcinoma: a GEICO (Grupo Español de Investigación en Cáncer de Ovario) study. Ann Oncol 2005;16:749–55.
13. Pujade-Lauraine E, Wagner U, Aavall-Lundqvist E, Gebski V, Heywood M, Vasey PA, et al. Pegylated liposomal Doxorubicin and Carboplatin compared with Paclitaxel and Carboplatin for patients with platinum-sensitive ovarian cancer in late relapse. J Clin Oncol 2010;28:3323–9.
14. Alberts DS, Liu PY, Wilczynski SP, Clouser MC, Lopez AM, Michelin DP, et al. Randomized trial of pegylated liposomal doxorubicin (PLD) plus carboplatin versus carboplatin in platinum-sensitive (PS) patients with recurrent epithelial ovarian or peritoneal carcinoma after failure of initial platinum-based chemotherapy (Southwest Oncology Group Protocol S0200). Gynecol Oncol 2008;108:90–4.
15. Ushijima K. Treatment for recurrent ovarian cancer-at first relapse. J Oncol 2010;2010:497429.
16. Pabo CO, Sauer RT. Protein-DNA recognition. Annu Rev Biochem 1984;53:293–321.
17. Rohs R, West SM, Sosinsky A, Liu P, Mann RS, Honig B. The role of DNA shape in protein-DNA recognition. Nature 2009;461:1248–53.
18. Susbielle G, Blattes R, Brevet V, Monod C, Kas E. Target practice: aiming at satellite repeats with DNA minor groove binders. Curr Med Chem Anticancer Agents 2005;5:409–20.
19. Guan Y, Sakai R, Rinehart KL, Wang AH. Molecular and crystal structures of ecteinascidins: potent antitumor compounds from the Caribbean tunicate Ecteinascidia turbinata. J Biomol Struct Dyn 1993;10:793–818.
20. Kishi K, Yazawa K, Takahashi K, Mikami Y, Arai T. Structure-activity relationships of saframycins. J Antibiot (Tokyo) 1984;37:847–52.
21. Pommier Y, Kohlhagen G, Bailly C, Waring M, Mazumder A, Kohn KW. DNA sequence- and structure-selective alkylation of guanine N2 in the DNA minor groove by ecteinascidin 743, a potent antitumor compound from the Caribbean tunicate Ecteinascidia turbinata. Biochemistry 1996;35:13303–9.
22. Casado JA, Rio P, Marco E, Garcia-Hernandez V, Domingo A, Perez L, et al. Relevance of the Fanconi anemia pathway in the response of human cells to trabectedin. Mol Cancer Ther 2008;7:1309–18.
23. Manzanares I, Cuevas C, Garcia-Nieto R, Marco E, Gago F. Advances in the chemistry and pharmacology of ecteinascidins, a promising new class of anti-cancer agents. Curr Med Chem Anticancer Agents 2001;1:257–76.
24. Bueren-Calabuig JA, Giraudon C, Galmarini CM, Egly JM, Gago F. Temperature-induced melting of double-stranded DNA in the absence and presence of covalently bonded antitumour drugs: insight from molecular dynamics simulations. Nucleic Acids Res 2011;39:8248–57.

Published OnlineFirst August 15, 2012; DOI: 10.1158/1078-0432.CCR-12-1513

25. Leal JF, Martinez-Diez M, Garcia-Hernandez V, Moneo V, Domingo A, Bueren-Calabuig, et al. PM01183, a new DNA minor groove covalent binder with potent *in vitro* and *in vivo* anti-tumour activity. Br J Pharmacol 2010;161:1099–110.
26. Soares DG, Machado MS, Rocca CJ, Poindessous V, Ouaret D, Sarasin A, et al. Trabectedin and its C subunit modified analogue PM01183 attenuate nucleotide excision repair and show activity toward platinum-resistant cells. Mol Cancer Ther 2010;10:1481–9.
27. de Plater L, Lauge A, Guyader C, Poupon MF, Assayag F, de Cremoux P, et al. Establishment and characterisation of a new breast cancer xenograft obtained from a woman carrying a germline BRCA2 mutation. Br J Cancer 2010;103:1192–200.
28. Teicher BA. Tumor models for efficacy determination. Mol Cancer Ther 2006;5:2435–43.
29. Bibby MC. Orthotopic models of cancer for preclinical drug evaluation: advantages and disadvantages. Eur J Cancer 2004;40:852–7.
30. Derose YS, Wang G, Lin YC, Bernard PS, Buys SS, Ebbert MT, et al. Tumor grafts derived from women with breast cancer authentically reflect tumor pathology, growth, metastasis and disease outcomes. Nat Med 2011;17:1514–20.
31. Hait WN. Anticancer drug development: the grand challenges. Nat Rev Drug Discov 2010;9:253–4.
32. Kerbel RS. Human tumor xenografts as predictive preclinical models for anticancer drug activity in humans: better than commonly perceived-but they can be improved. Cancer Biol Ther 2003;2:S134–9.
33. Teicher BA, Herman TS, Holden SA, Wang YY, Pfeffer MR, Crawford JW, et al. Tumor resistance to alkylating agents conferred by mechanisms operative only *in vivo*. Science 1990;247:1457–61.
34. Becker K, Mueller JD, Schulmacher C, Ott K, Fink U, Busch R, et al. Histomorphology and grading of regression in gastric carcinoma treated with neoadjuvant chemotherapy. Cancer 2003;98:1521–30.
35. Fisher ER, Wang J, Bryant J, Fisher B, Mamounas E, Wolmark N. Pathobiology of preoperative chemotherapy: findings from the National Surgical Adjuvant Breast and Bowel (NSABP) protocol B-18. Cancer 2002;95:681–95.
36. McCluggage WG, Lyness RW, Atkinson RJ, Dobbs SP, Harley I, McClelland HR, et al. Morphological effects of chemotherapy on ovarian carcinoma. J Clin Pathol 2002;55:27–31.
37. Moreno A, Escobedo A, Benito E, Serra JM, Guma A, Riu F. Pathologic changes related to CMF primary chemotherapy in breast cancer. Pathological evaluation of response predicts clinical outcome. Breast Cancer Res Treat 2002;75:119–25.
38. Sassen S, Schmalfeldt B, Avril N, Kuhn W, Busch R, Hofler H, et al. Histopathologic assessment of tumor regression after neoadjuvant chemotherapy in advanced-stage ovarian cancer. Hum Pathol 2007;38:926–34.
39. Chou TC, Talalay P. Quantitative analysis of dose-effect relationships: the combined effects of multiple drugs or enzyme inhibitors. Adv Enzyme Regul 1984;22:27–55.
40. Huertas D, Soler M, Moreto J, Villanueva A, Martinez A, Vidal A, et al. Antitumor activity of a small-molecule inhibitor of the histone kinase Haspin. Oncogene 2012;31:1408–18.
41. Castillo-Avila W, Piulats JM, Garcia Del Muro X, Vidal A, Condom E, Casanovas O, et al. Sunitinib inhibits tumor growth and synergizes with cisplatin in orthotopic models of cisplatin-sensitive and cisplatin-resistant human testicular germ cell tumors. Clin Cancer Res 2009;15:3384–95.
42. Evans DB, Rich TA, Byrd DR, Cleary KR, Connelly JH, Levin B, et al. Preoperative chemoradiation and pancreaticoduodenectomy for adenocarcinoma of the pancreas. Arch Surg 1992;127:1335–9.
43. Honkoop AH, Pinedo HM, De Jong JS, Verheul HM, Linn SC, Hoekman K, et al. Effects of chemotherapy on pathologic and biologic characteristics of locally advanced breast cancer. Am J Clin Pathol 1997;107:211–8.
44. Junker K, Thomas M, Schulmann K, Klinke F, Bosse U, Muller KM. Tumour regression in non-small-cell lung cancer following neoadjuvant therapy. Histological assessment. J Cancer Res Clin Oncol 1997;123:469–77.
45. Mandard AM, Dalibard F, Mandard JC, Marnay J, Henry-Amar M, Petiot JF, et al. Pathologic assessment of tumor regression after preoperative chemoradiotherapy of esophageal carcinoma. Clinicopathologic correlations. Cancer 1994;73:2680–6.
46. Melo S, Villanueva A, Moutinho C, Davalos V, Spizzo R, Ivan C, et al. Small molecule enoxacin is a cancer-specific growth inhibitor that acts by enhancing TAR RNA-binding protein 2-mediated microRNA processing. Proc Natl Acad Sci U S A 2011;108:4394–9.
47. Dunton CJ. New options for the treatment of advanced ovarian cancer. Semin Oncol 1997;24:S5-2–S5-11.
48. Shield K, Ackland ML, Ahmed N, cRice GE. Multicellular spheroids in ovarian cancer metastases: biology and pathology. Gynecol Oncol 2009;113:143–8.
49. Cannistra SA. Cancer of the ovary. N Engl J Med 2004;351:2519–29.

Published OnlineFirst August 15, 2012; DOI: 10.1158/1078-0432.CCR-12-1513

AACR American Association for Cancer Research

Clinical Cancer Research

Lurbinectedin (PM01183), a New DNA Minor Groove Binder, Inhibits Growth of Orthotopic Primary Graft of Cisplatin-Resistant Epithelial Ovarian Cancer

August Vidal, Clara Muñoz, María-José Guillén, et al.

Clin Cancer Res 2012;18:5399-5411. Published OnlineFirst August 15, 2012.